AN INTRODUCTION TO RAMAN SPECTROSCOPY

Boris A. Kolesov

An Introduction to Raman Spectroscopy

An Introduction to Raman Spectroscopy

By

Boris A. Kolesov

Cambridge Scholars Publishing

An Introduction to Raman Spectroscopy

By Boris A. Kolesov

This book first published 2022

Cambridge Scholars Publishing

Lady Stephenson Library, Newcastle upon Tyne, NE6 2PA, UK

British Library Cataloguing in Publication Data
A catalogue record for this book is available from the British Library

ISBN (10): 1-5275-8377-5
ISBN (13): 978-1-5275-8377-1

CONTENTS

PREFACE

Vibrational spectroscopy, which includes infrared absorption (IR) and Raman scattering, is a powerful physical method for the study of chemical compounds – solid, liquid, and gaseous. In this, IR spectroscopy is to a greater extent an analytical method, and Raman spectroscopy is a research method.

The book is addressed, first of all, to students and scientists whose interests lie in the field of research of chemical, mineralogical, biological systems. This requires from a specialist both professional knowledge in each of the named areas and a deep understanding of the processes occurring in the medium during the scattering or absorption of electromagnetic radiation. For this reason, in the book, in addition to general information from the field of solid-state physics, much attention is paid to the description of those physical phenomena that have long been worked out in detail and are considered as if they do not require additional explanations. These include the concepts of a harmonic oscillator, vibration symmetry, anharmonicity, etc. These phenomena, however, underlie vibrational spectroscopy, are implicitly present in every vibrational spectrum, and their clear understanding is necessary at any level of work with vibrational spectra. The presentation is conducted at an extremely simple level that provides an understanding of the essence of the phenomenon, sometimes at the expense of a rigorous theoretical description. A small exception is only the first two chapters, where the theory of light scattering and the theory of vibrations are presented. But here, too, a general outline of the theory is given and many details are omitted. This is done in part to prevent the reader from wanting to close the book on the second page.

The text contains a large number of Raman spectra of compounds – organic and inorganic. All of them were obtained in the course of the author's work.

The author will be grateful for the comments and feedback sent to the address: kolesov@niic.nsc.ru

CHAPTER 1

RAMAN SCATTERING: BASIC CONCEPTS AND BRIEF THEORETICAL DESCRIPTION

1.1. Elastic and inelastic light scattering

Vibrational spectroscopy is actually the only physical method representing information on the pair potential of interactions between atoms. This information is embedded in the vibrational frequencies of the system. The vibrational spectrum of a compound can be obtained by infrared absorption spectroscopy or Raman scattering[1]. These experiments are characterized by different selection rules and therefore perfectly complement each other.

Let us briefly consider the processes yielding to the occurrence of both effects. Let there be a polar two-atomic molecule and an electromagnetic wave $\boldsymbol{E} = \boldsymbol{E}_0\cos(\omega_L t)$ with the variable frequency ω_L.

The electric field of the incident radiation interacts with the charged atoms of the molecule. When the radiation energy is small enough and is comparable to the energy of the fundamental mechanical vibrations of the molecule, a quantum of light is absorbed, and a quantum of vibration arises in the system (Fig. 1.1). More complex examples than diatomic molecules, such as systems of vibrating atoms, usually have a set of different fundamental vibrations, and in this case one can observe an infrared absorption spectrum consisting of several absorption bands.

When the energy of the incident radiation is high and approaches the energy of the allowed optical dipole transition between different electronic states of a molecule or crystal, we observe an absorption spectrum in the UV and visible regions.

---

[1] Raman scattering was discovered almost simultaneously by C.V. Raman and K.S. Krishnan [1] in India and G.S. Landsberg and L.I. Mandelstam [2] in Russia in 1928.

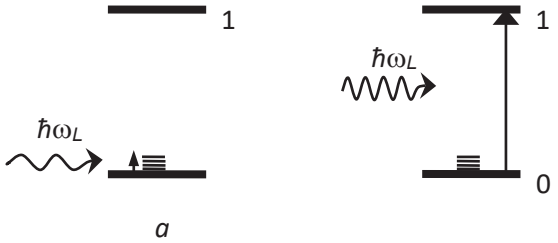

Fig. 1.1. The emergence of an absorption spectrum on vibrations (a) and electronic transitions (b)

And what happens when the energy of the electromagnetic wave is greater than the energy of atomic vibrations and less than the energy of the dipole electronic transition? In this case, the electronic subsystem is able to respond to changes in the electric field, while the atomic one is not. Under the action of an external field, the electron cloud of the molecule is displaced, forming a dipole oscillating with the frequency of the incident radiation. This process can be described as absorption of the incident wave energy by an electron and its transition to a state that is often called virtual for convenience, i.e. not a stationary state of this system[2].

It follows from the Heisenberg uncertainty relation $\Delta E \Delta t \approx \hbar$ that the lifetime of an electron in a virtual state is very small, on the order of half of the oscillation period of the electric field of the incident wave, i.e. 10^{-15} - 10^{-16} s, after which the electron is forced to leave it, emitting a quantum of light with the same energy as the energy of the incident wave, producing Rayleigh scattering (Fig. 1.2, a).

However, even in that short time that the electron is in a virtual state, due to the electron-vibrational (electron-phonon in the crystal) interaction in the system, a quantum of mechanical vibrations can arise, after which the electron returns to its initial state with the emission of a quantum of light with an energy lower than the energy of an incident photon on the energy of the emitted vibration. This process is depicted in Fig. 1.2, b. In this case, in the spectrum of scattered light, we will observe the main (i.e., upshifted Rayleigh) line ω_L and one more accompanying line with a lower frequency that differs from frequency ω_L to the frequency of the emitted quantum of the mechanical vibration.

[2] As will be shown below, neither the classical nor the quantum mechanical description of the process of Raman scattering require the presence of a virtual state. However, its inclusion simplifies the diagram of the scattering process and makes it extremely clear.

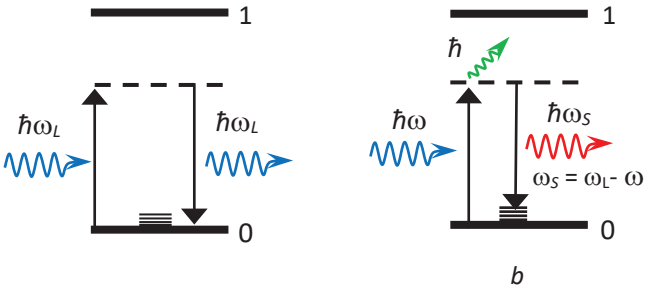

Fig. 1.2. Diagram of the appearance of elastic Rayleigh (a) and inelastic Raman (b) scattering. The emitted mechanical vibration (phonon) is marked in green $\hbar\omega$

This is spontaneous Raman scattering, or, more precisely, Stokes Raman scattering. Why Stokes? The fact is that the scattering process can be characterized not only by the generation of a vibrational quantum, but also by the elimination of a vibrational quantum already existing in the system (Fig. 1.3). In this case, the spectrum contains a line with energy higher than the energy of an incident photon on the energy of the eliminated vibration.

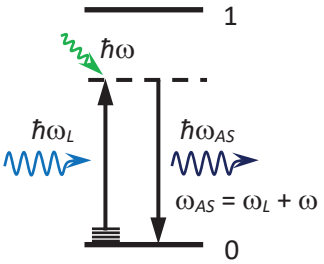

Fig. 1.3. Anti-Stokes Raman scattering

The main difference between IR absorption and Raman scattering is that the incident radiation interacts with the vibrating atoms in the first case and with their electronic subsystem in the second.

1.2. Elementary theory of Raman scattering

To elucidate the reasons for the appearance of inelastic Raman scattering on vibrations, it is necessary to consider the question of the interaction of radiation with an atomic system. The electric field of an incident electromagnetic wave

$$\boldsymbol{E} = \boldsymbol{E}_0 \cos(\omega_L t) \tag{1.1}$$

yields to the appearance in the atomic system of an induced dipole moment

$$\boldsymbol{P} = \alpha \boldsymbol{E}. \tag{1.2}$$

If the polarizability[3] α is a time-independent constant, $\alpha = \alpha_0$, we get

$$\boldsymbol{P} = \alpha_0 \boldsymbol{E}_0 \cos(\omega_L t). \tag{1.3}$$

In other words, a dipole moment, vibrating harmonically with the same frequency ω_L arises. Such a dipole moment (Hertzian dipole) emits radiation, and the radiation energy in all directions of space per unit of time is

$$W_S = \frac{2}{3c^3}\left|\frac{d^2P}{dt^2}\right|^2 = \frac{2\omega_L^4}{3c^3}|\alpha_0|^2 E_0^2 cos^2 \omega_L t \tag{1.4}$$

The dipole radiation creates coherent scattered light with constant frequency and phase. Time averaging gives

$$\overline{W_S} = \frac{2\omega_L^4}{3c^3}|\alpha_0|^2 E_0^2 \overline{cos^2 \omega_L t} = \frac{\omega_L^4}{3c^3}|\alpha_0|^2 E_0^2. \tag{1.5}$$

This is the so-called Rayleigh scattering. If the scattering particles are ordered in the system, like atoms in a crystal, then the scattered light interferes in a single direction, coinciding with the direction of the incident beam in the crystal, and we observe the light passing through the crystal. Rayleigh scattering in all directions occurs precisely because of the violation of the ordered distribution of the scattering particles. For example, fluctuations in the density of a gas in the atmosphere are responsible for the sunlight scattering, and the blue color of the sky is

[3] The term "polarizability" is used for atoms and molecules. To describe the response in solids and liquids, it is preferred to use the concept of "polarization", which is the sum of the induced dipole moments from all the particles that make up the medium. In this case, the polarization is $\boldsymbol{P} = \chi \boldsymbol{E}$, where χ is the dielectric (or simply electrical) susceptibility. The latter value is related to the molecular polarizability α by a simple relationship: $\chi = N\alpha$ (N is the number of particles per unit volume). For this reason, one can find in the literature a description of the theory of the Raman effect using the dielectric susceptibility; however, neither the essence of the effect nor the basic relations change in this case.

explained by the fourth power of the frequency in the expression for the scattering energy.

We must consider, however, what happens when the polarizability of the system (molecule, crystal) changes over time during the vibration. (The polarizability is a tensor quantity and is usually determined by the second-rank tensor. For more details, see Chapter 6.) Indeed, for a hypothetical square molecule (Fig. 1.4, a) the α_{xx} and α_{yy} components of the polarizability tensor along the x and y directions are respectively equal to each other. It is intuitively clear, however, that they become different when the molecule changes its shape during vibration (Fig. 1.4, b).

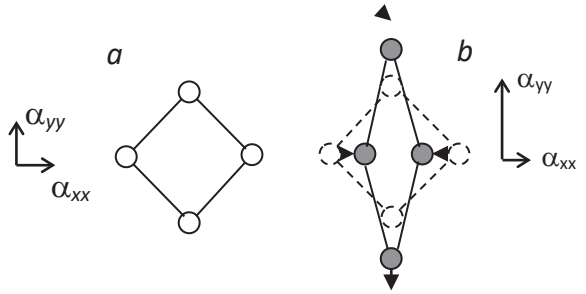

Fig. 1.4.

Polarizability of a hypothetical square molecule during rest (a) and vibration (b)

Vibrations of the system are not random, but are determined by a set of so-called normal vibrations ω_i with the corresponding normal coordinates ξ_i (definition of normal vibrations and coordinates will be given in Ch. 2). Expanding the components of the polarizability tensor in a Taylor series in normal coordinates, we obtain:

$$\alpha_{\rho\sigma} = (\alpha_{\rho\sigma})_0 + \sum_k \left(\frac{\partial \alpha_{\rho\sigma}}{\partial \xi_k}\right)_0 \xi_k + \frac{1}{2}\sum_{k,l}\left(\frac{\partial^2 \alpha_{\rho\sigma}}{\partial \xi_k \partial \xi_l}\right)_0 \xi_k \xi_l \ldots, \quad (1.6)$$

where ξ_k and ξ_l… are the normal coordinates of vibrational modes with ω_k, ω_l, etc. frequencies, and ρ, $\sigma = x, y, z$. The subscript 0 in the derivative indicates that its value is determined at the equilibrium position. In the harmonic approximation, neglecting terms with a degree ξ higher than 1, one can write

$$(\alpha_{\rho\sigma})_k = (\alpha_{\varrho\sigma})_0 + (\alpha'_{\varrho\sigma})_k \xi_k, \quad (1.7)$$

where

$$\left(\alpha'_{\varrho\sigma}\right)_k = \left(\frac{\partial \alpha_{\varrho\sigma}}{\partial \xi_k}\right)_0 \tag{1.8}$$

is the derivative of the polarizability with respect to the normal coordinate. Since relations (1.7) and (1.8) hold for all components of the polarizability tensor and the polarizability derivative, we rewrite (1.7) in a simpler form:

$$\alpha_k = \alpha_0 + \alpha'_k \xi_k. \tag{1.9}$$

Assuming a simple harmonic motion of atoms during vibrations, the dependence of ξ_k on time can be expressed as

$$\xi_k = \xi_{k0} \cos(\omega_k t + \delta_k) \tag{1.10}$$

(ξ_{k0} is the amplitude of the normal coordinate, and δ is the phase of vibration). Now we can rewrite expression (1.2) for the dipole moment in the form:

$$\boldsymbol{P} = \alpha \boldsymbol{E} = \alpha_0 \boldsymbol{E}_0 \cos(\omega_L t) + \alpha'_k \xi_{k0} \cos(\omega_k t + \delta_k) \boldsymbol{E}_0 \cos(\omega_L t). \tag{1.11}$$

Using the well-known trigonometric relation for products of cosines, we get:

$$\boldsymbol{P} = \alpha_0 \boldsymbol{E}_0 \cos(\omega_L t) + \frac{1}{2} \alpha'_k \xi_{k0} \boldsymbol{E}_0 \cos[(\omega_L - \omega_k)t \pm \delta_k] +$$

$$+ \frac{1}{2} \alpha'_k \xi_{k0} \boldsymbol{E}_0 \cos[(\omega_L + \omega_k)t \pm \delta_k]. \tag{1.12}$$

It can be seen that, in addition to the first term, which is responsible for coherent Rayleigh scattering, two additional terms appear in expression (1.12) that describe the incoherent (phase δ is random for each vibration) Raman scattering with frequencies $\omega_L - \omega_k$ (Stokes part) and $\omega_L + \omega_k$ (anti-Stokes part). As before, the Raman scattering intensity is

$$\overline{W_S} = A(\omega_L - \omega_k)^4 |\alpha'_k|^2 \boldsymbol{E}_0^2 \qquad \text{(Stokes scattering)} \tag{1.13}$$

and

$$\overline{W_S} = A(\omega_L + \omega_k)^4 |\alpha'_k|^2 \boldsymbol{E}_0^2 \quad \text{(anti-Stokes scattering)} \tag{1.14}$$

where A is constant. In both cases, the scattering intensity is proportional to the square of the amplitude of the electric field of the incident light, the square of the amplitude of the derivative of the polarizability of the system, and the fourth power of the frequency of the scattered radiation.

In conclusion, it should be noted that the simplified scheme proposed here is not a scattering theory in the full sense, and the results obtained are devoid of many important details. The only important result obtained above is the appearance of two scattering components, Stokes and anti-Stokes. However, the physics of the process of Raman scattering is much richer and it is necessary, therefore, to go to the next, higher level of the theoretical description of this phenomenon.

1.3. Semi-classic and quantum-mechanical approaches[4]

The dipole moment $\boldsymbol{P}$ induced in the system (atom, molecule, crystal) by the electric field $\boldsymbol{E}_L = \boldsymbol{e}_L^{\sigma} E_L$ ($\boldsymbol{e}_L^{\sigma}$ – the unit vector of polarization of the incident electromagnetic wave) is

$$\boldsymbol{P} = \alpha \boldsymbol{e}_L^{\sigma} E_L. \tag{1.15}$$

Let us rewrite expression (1.4) for the energy emitted by an oscillating electric dipole $\boldsymbol{P}$ per unit time in the form:

$$\frac{dW_S}{d\Omega} = \frac{\omega_L^4}{(4\pi)^2 \varepsilon_0 c^3} \left| \boldsymbol{e}_S^{\rho} \cdot \boldsymbol{P} \right|^2 = \frac{\omega_L^4}{(4\pi)^2 \varepsilon_0 c^3} \left| \boldsymbol{e}_S^{\rho} \cdot \boldsymbol{\alpha} \cdot \boldsymbol{e}_L^{\sigma} \right|^2 E_L^2, \tag{1.16}$$

where $d\Omega$ is the element spatial angle, ε_0 is the dielectric constant of the medium, $\boldsymbol{e}_S^{\rho}$ is the unit vector of polarization of the scattered radiation, and $\rho, \sigma = x, y, z$.

The scattering process is usually characterized by the differential cross section $d\sigma/d\Omega$, which can be obtained by dividing (1.16) by the energy $W_L = \varepsilon_0 c E_L^2$, falling per unit area per unit time:

$$\frac{d\sigma}{d\Omega} = \frac{\omega_L^4}{(4\pi\varepsilon_0)^2 c^4} \left| \boldsymbol{e}_S^{\rho} \cdot \boldsymbol{\alpha} \cdot \boldsymbol{e}_L^{\sigma} \right|^2 \tag{1.17}$$

In the last expression, the unknown quantity is the polarizability of the system. To find it, it is usually assumed that the scattering medium consists of a set of N electron oscillators per unit volume. Each oscillator can be represented as an electron of mass m and charge e, bonded to the

[4] It is stated in accordance with [3].

nucleus, and this bonding is characterized by a force constant *f*. The equation of motion for such a harmonic oscillator is written in the usual way:

$$\frac{d^2x}{dt^2} + \omega_r^2 x = 0, \tag{1.18}$$

where $\omega_r^2 = f/m$ is the vibrational frequency of the oscillator (in quantum mechanics, ω_r is interpreted as the frequency at which an atom absorbs a quantum of light, i.e., the frequency of an electronic transition). For an oscillator in an external field E_L, we introduce the force $F = eE_L/m$ into expression (1.18):

$$\frac{d^2x}{dt^2} + \omega_r^2 x = F. \tag{1.19}$$

In addition, a real physical system is characterized by a finite lifetime (damping of the oscillator), which adds one more term to the equation of motion (1.19):

$$\frac{d^2x}{dt^2} + \gamma_r \frac{dx}{dt} + \omega_r^2 x = F. \tag{1.20}$$

The solution of the equation (1.20) for an electronic oscillator with a fundamental frequency ω_r and a damping coefficient γ_r, being in the electric field of an incident wave of frequency ω_L, is as follows:

$$x = \frac{(\frac{e}{m})E_L}{\omega_r^2 - \omega_L^2 - i\omega_L\gamma_r}. \tag{1.21}$$

Since $\boldsymbol{P} = \alpha\boldsymbol{E} = ex$, we get:

$$\alpha = \frac{e^2/m}{\omega_r^2 - \omega_L^2 - i\omega_L\gamma_r}. \tag{1.22}$$

Substituting (1.22) into (1.17), we obtain an expression for the scattering cross section:

$$\frac{d\sigma}{d\Omega} = \frac{r_e^2\omega_L^4}{(\omega_r^2 - \omega_L^2)^2 + \omega_L^2\gamma_r^2}\left|e_L^\sigma \cdot e_S^\rho\right|^2, \tag{1.23}$$

where $r_e = e^2/4\pi\varepsilon_0 mc^2$ is the classical radius of the electron. Far from resonance, i.e. for $\omega_L << \omega_r$, expression (1.23) can be rewritten as:

$$\frac{d\sigma}{d\Omega} = r_e^2 \frac{\omega_L^4}{\omega_r^4} \left| e_L^\sigma \cdot e_S^\rho \right|^2. \tag{1.24}$$

Formula (1.24) describes elastic scattering of an isotropic medium. As before, in order to obtain inelastic scattering, it is necessary to consider how the polarizability of the system changes during vibration. Each vibrational mode ω_j is characterized by the displacement of N atoms in the molecule dependent on time as $\exp(\pm i\omega_j t)$. The displacements of the k-atom in the molecule (k = 1,2, ..., N) $q_k^{(j)}$ can be expressed in terms of the normal coordinates ξ as will be done in Chapter 2, Eq. (2.40), but only in complex form:

$$q_k^{(j)}\left(\pm\omega_j t\right) = \boldsymbol{e}_k \xi e^{-i\omega_j t} + \boldsymbol{e}_k^* \xi^* e^{i\omega_j t}, \tag{1.25}$$

where $\boldsymbol{e}_k$ is the unit vector of displacement of the k-atom. From here, decomposing polarizability in a series in the normal coordinate ξ, we obtain a relation similar to (1.6):

$$\boldsymbol{\alpha}(\omega_L, \xi) = \boldsymbol{\alpha}(\omega_L) + \frac{\partial \boldsymbol{\alpha}}{\partial \xi} \xi e^{-i\omega_j t} + \frac{\partial \boldsymbol{\alpha}}{\partial \xi^*} \xi^* e^{i\omega_j t} + \frac{1}{2} \frac{\partial^2 \boldsymbol{\alpha}}{\partial \xi^2} \xi^2 e^{-2i\omega_j t} + \frac{1}{2} \frac{\partial^2 \boldsymbol{\alpha}}{\partial \xi^{*2}} \xi^{*2} e^{2i\omega_j t} + \cdots \tag{1.26}$$

Substituting (1.26) into (1.17) and restricting ourselves to the linear terms of expansion (1.26), we obtain scattering without changing the frequency ω_L (Rayleigh) and with frequency $\omega_L \pm \omega_j$ (Stokes and anti-Stokes scattering). For the last two, the differential cross-section is written as:

$$\frac{d\sigma_S}{d\Omega} = \frac{\left(\omega_L - \omega_j\right)^4}{(4\pi\varepsilon_0)^2 c^4} \left| \boldsymbol{e}_S \cdot \frac{\partial \boldsymbol{\alpha}}{\partial \xi} \cdot \boldsymbol{e}_L \right|^2 \langle \xi \xi^* \rangle \quad \text{(Stokes scattering)}, \tag{1.27}$$

$$\frac{d\sigma_{AS}}{d\Omega} = \frac{\left(\omega_L + \omega_j\right)^4}{(4\pi\varepsilon_0)^2 c^4} \left| \boldsymbol{e}_S \cdot \frac{\partial \boldsymbol{\alpha}}{\partial \xi} \cdot \boldsymbol{e}_L \right|^2 \langle \xi^* \xi \rangle \quad \text{(anti-Stokes scattering)}. \tag{1.28}$$

The factors $\langle \xi \xi^* \rangle$ and $\langle \xi^* \xi \rangle$, where the brackets denote averaging over the ground state of a molecule, are derived in quantum mechanics by replacing the displacements ξ and ξ^* with the corresponding operators ξ and ξ †, called the creation and annihilation operators. Omitting rather complicated quantum-mechanical calculations (see, for example, Ref. [4]), we present the final result of the calculation of the Stokes and anti-Stokes factors:

$$\langle \xi \xi^\dagger \rangle = \frac{\hbar}{2\omega_j}(n+1) \qquad \text{Stokes component}, \tag{1.29}$$

$$\langle \xi^{\dagger}\xi \rangle = \frac{\hbar}{2\omega_j} n \qquad \text{anti-Stokes component,} \tag{1.30}$$

where n determines the statistical (Maxwell-Boltzmann) population of the vibrational state

$$n = \frac{1}{exp(\hbar\omega_j/kT)-1}. \tag{1.31}$$

Substituting the last expressions in (1.27) and (1.28), we obtain:

$$\frac{d\sigma_S}{d\Omega} = \frac{\hbar(\omega_L-\omega_j)^4}{2\omega_j(4\pi\varepsilon_0)^2c^4}\left|\boldsymbol{e}_S \cdot \frac{\partial \boldsymbol{\alpha}}{\partial \xi} \cdot \boldsymbol{e}_L\right|^2 (n+1) \quad \text{(Stokes scattering),} \tag{1.32}$$

$$\frac{d\sigma_{AS}}{d\Omega} = \frac{\hbar(\omega_L+\omega_j)^4}{2\omega_j(4\pi\varepsilon_0)^2c^4}\left|\boldsymbol{e}_S \cdot \frac{\partial \boldsymbol{\alpha}}{\partial \xi} \cdot \boldsymbol{e}_L\right|^2 n \quad \text{(anti-Stokes scattering)} \tag{1.33}$$

The fact that the anti-Stokes scattering is proportional to the number of phonons with a given energy follows from the definition of the anti-Stokes process: in order for a scattering act to occur with absorption of a phonon, this phonon must be presented in the system. But the fact that the Stokes scattering's intensity consists of two components, one of which is also proportional to the number of phonons in the system with exactly the same frequency as the scattered phonon, seems unexpected at first glance. Strange as it may seem, the well-known experiment with two identical pendulums fixed on one thread helps to understand this complex phenomenon. If an oscillation is excited in one of the pendulums, then due to the connection between them, this oscillation will be completely transferred to the second pendulum for some time, while the oscillations of the first will cease. Then the process starts in the opposite direction. Such transfer of energy from one oscillator to another and back becomes possible due to the identity of their fundamental vibrational frequencies. Now, returning to the process of light scattering by a vibration, it is easy to understand that the emitting of a phonon ω during scattering becomes much more probable if the system already has a vibration with the same frequency, which, as it were, "shakes" the system and, due to the kinematic interaction between phonons, helps the occurring of another such vibration. In the process of scattering, there is no need to transfer energy from one oscillator to another, since in this case the energy is taken from the photon. The temperature-independent part of the Stokes scattering arises due to the existence of zero-point vibrations, which provide the necessary perturbations of the system. The proportionality of the number of excitations to the number of the same excitations already

presented in the system is characteristic of all particles with integer spin, i.e. bosons. From this point of view, Stokes Raman scattering is completely analogous to the well-known phenomenon of the spontaneous and stimulated emission of light. Indeed, if an atom passes into an excited electronic state, which is usually stationary, i.e. allowed, then the lifetime of this state is, nevertheless, finite, and the electron returns to the ground state with the emission of a quantum of light either under the action of zero-point oscillations of the electromagnetic field (spontaneous emission) or a quantum of an external field with the same energy (stimulated emission).

From expressions (1.32) and (1.33) we find for the ratio of the intensities of anti-Stokes I_A and Stokes I_S scattering

$$\frac{I_A}{I_S} = \frac{(\omega_L+\omega_j)^4}{(\omega_L-\omega_j)^4} exp\left(-\frac{\hbar\omega_j}{kT}\right). \tag{1.34}$$

Eq. (1.34) makes it possible to estimate the real temperature in the scattering volume of the sample (far from resonance). And since this volume is very often represented simply by a local point on the surface of a crystal or powder, the proposed method for temperature measuring is actually the only one in this case.

Returning to relations (1.27) and (1.28), it is necessary to note that their meaning is the same as that of relations (1.13) and (1.14). But, receiving both, we did not consider the dependence of the polarizability of the system (1.22) on the frequency of the incident radiation. In expression (1.22), the polarizability is represented by the scalar quantity. To preserve its tensor character, we need to multiply polarizability (1.22) by the unit tensor of the force of the electron oscillator $\boldsymbol{f_e}$ as follows:

$$\boldsymbol{\alpha} = \frac{(e^2/m)\boldsymbol{f_e}}{\omega_r^2-\omega_L^2-i\omega_L\gamma} + const. \tag{1.35}$$

Now the derivative of the polarizability with respect to the normal coordinate in (1.27) and (1.28) will consist of two contributions:

$$\frac{d\boldsymbol{\alpha}}{d\xi} = -\frac{2\omega_r\left(\frac{e^2}{m}\right)\boldsymbol{f_e}}{\left[\omega_r^2-\omega_L^2-i\omega_L\gamma\right]^2}\frac{d\omega_r}{d\xi} + \frac{\left(\frac{e^2}{m}\right)}{\omega_r^2-\omega_L^2-i\omega_L\gamma}\frac{d\boldsymbol{f_e}}{d\xi}. \tag{1.36}$$

The first term on the right-hand side of (1.36) expresses the dependence of the frequency of the electronic oscillator (energy of electronic transition) ω_r on the shift of atoms during vibration and is determined by the electron-phonon interaction. The second term represents the dependence of the

oscillator strength (the intensity of the electronic transition) on the displacement of atoms. The analysis of both terms is not an easy task, and therefore we restrict ourselves here to only stating the fact that a resonance factor appears in the expression for the scattering cross section, which, after some simplifications, may look like

$$\frac{d\sigma}{d\Omega} \propto \frac{1}{\left(\omega_L^2-\omega_r^2\right)^2+\omega_L^2\gamma^2}. \tag{1.37}$$

1.4. Quantum mechanical description

In the quantum mechanical description, the induced electric dipole of the classical theory is replaced by the dipole moment $(\boldsymbol{p})_{fi}$ of the transition from the initial state *i* to the final state *f*. But, as can be seen in Fig. 1.2, in the process of Raman scattering, both states, initial and final, are the ground electronic state of the system (i.e., $(\boldsymbol{p})_{fi} = 0$) with the only difference that the state *f* is vibrationally excited. At the same time, the frequency of the incident electromagnetic wave ω_L is much higher than $\omega_{if} = E_{if}/\hbar$, where E_{if} is the difference between the energies of the initial and final states. Therefore, to calculate the dipole moment of electronic transition in quantum mechanics, an intermediate state *r* is used, which is a real (stationary) excited electronic state of the system. In this case, the energy E_r of the excited state can be any, but it is usually assumed that ω_L is less than $\omega_r = E_r/\hbar$. The term "less" means in this case that the laser excitation frequency ω_L is spaced from the resonance frequency ω_r by many frequencies of the system ω_{if}. Under this condition, the absorption coefficient of the system (i.e., the probability of transition from the ground state to the excited electronic state) practically does not depend on the vibration of the system. At this the vibration itself can be considered as its static deformation, and the molecule can be characterized at each moment of time by the definite polarizability. The quantum mechanical scattering scheme and the designation of states are shown in Fig. 1.5.

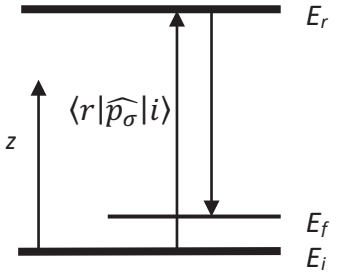

Fig. 1.5. Designation of states used in quantum mechanical calculation

Following this scheme, the dipole moment of the transition $(\boldsymbol{p}^{(1)})_{fi}$ from the initial state to the final state in the framework of approximation theory – when only the terms linear in the field $\boldsymbol{E}$ are taken into account in the intermediate expansions (as indicated by the superscript in the designation of the dipole moment) – should be proportional to both the matrix element of the transition from the initial state i to the intermediate state r and the matrix element of the transition from the state r to the final state f. G. Placek [5] showed that the ρ-component of $(\boldsymbol{p}^{(1)})_{fi}$ can be written as

$$\left(\boldsymbol{p}_{\varrho}^{(1)}\right)_{fi} = \frac{1}{2\hbar}\sum_{r\neq i,f}\left\{\frac{\langle f|\hat{p}_\rho|r\rangle\langle r|\hat{p}_\sigma|i\rangle}{\omega_{ri}-\omega_L-i\Gamma_r}+\frac{\langle f|\hat{p}_\sigma|r\rangle\langle r|\hat{p}_\varrho|i\rangle}{\omega_{ri}+\omega_L+i\Gamma_r}\right\}\tilde{E}_{\sigma 0}exp(-i\omega_S t)$$

$$+ \text{ complex conjugated,} \qquad (1.38)$$

where the summation is carried out over all formally possible intermediate states r (for simplicity, the entire sum can be replaced by just one state). In this expression $\hat{p}$ is the operator of the dipole moment (operator of electronic coordinate), and Γ_r is the half-width of the state r of the system, $\omega_s = \omega_L - \omega_{fi}$.

The numerator of expression (1.38) contains the matrix elements of transitions between states and, thus, describes the probabilities of system excitation and interaction with a phonon. The denominator $\omega_{ri} \pm (\omega_L + i\Gamma_r)$ is the resonance factor presented above.

Let us introduce a general expression for the ρσ-components of the polarizability $(\alpha_{\rho\sigma})_{fi}$:

$$\left(\boldsymbol{\alpha}_{\sigma\varrho}\right)_{fi} = \frac{1}{\hbar}\sum_{r\neq i,f}\left\{\frac{\langle f|\hat{p}_\rho|r\rangle\langle r|\hat{p}_\sigma|i\rangle}{\omega_{ri}-\omega_L-i\Gamma_r}+\frac{\langle f|\hat{p}_\sigma|r\rangle\langle r|\hat{p}_\varrho|i\rangle}{\omega_{ri}+\omega_L+i\Gamma_r}\right\}. \qquad (1.39)$$

Far from resonance $(\omega_L << \omega_{ri})$, the term $i\Gamma_r$ can be neglected, therefore

$$\left(\alpha_{\sigma\varrho}\right)_{fi} = \frac{1}{\hbar}\sum_{r\neq i,f}\left\{\frac{\langle f|\hat{p}_{\varrho}|r\rangle\langle r|\hat{p}_{\sigma}|i\rangle}{\omega_{ri}-\omega_L} + \frac{\langle f|\hat{p}_{\sigma}|r\rangle\langle r|\hat{p}_{\varrho}|i\rangle}{\omega_{ri}+\omega_L}\right\}. \quad (1.40)$$

The first term in brackets is usually significantly larger than the second due to the resonant denominator, so the second term is often neglected for simplicity. Now it is necessary to substitute expression (1.40) for the polarizability into the series expansion (1.26) and, confining ourselves, as before, to the harmonic approximation, obtain the intensity of Raman scattering using relations (1.32) and (1.33). However, the transition from theoretical expressions to numerical values of intensities for molecules and crystals is still a difficult task.

The analysis presented here differs from the simplified classical scheme (§ 1.2) by the appearance of a resonance factor, which very often makes the dependence of the scattering intensity on the wavelength of the exciting radiation much stronger than the fourth power of the frequency in expressions (1.13) and (1.14). When the energy of the laser line approaches the energy of the electronic transition, the scattering intensity can increase hundreds and thousands of times (see Chapter 8). In addition, the scattering intensity turned out to depend on the thermal population of the vibrational state, which primarily affects the ratio of the intensities of the Stokes and anti-Stokes scatterings.

CHAPTER 2

VIBRATIONS OF MOLECULES

2.1. Harmonic oscillator in classical mechanics

The harmonic oscillator is an approximation that is used in physics to describe the free vibrations of various systems – mechanical, electrical, and electromagnetic. The approximation is that the restoring force acting on the system when it deviates from the equilibrium position is assumed to be linearly dependent on the magnitude of the deviation, i.e. $F = -f$x, where f is the proportionality coefficient (rigidity of spring, force constant of chemical bond). And although the last condition is satisfied only for small deviations in mechanical systems and weak fields in electromagnetic oscillations, the theory of a harmonic oscillator is fundamental in vibrational processes.

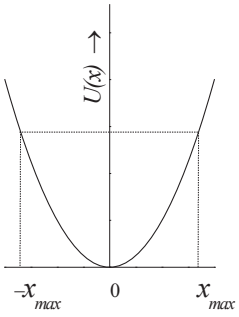

Fig. 2.1. Potential energy of a one-dimensional harmonic oscillator

We will consider a one-dimensional harmonic oscillator, in which, by definition, the potential energy $U(x)$ of one particle of mass m quadratically changes with the coordinate x (Fig. 2.1) according to the law

$$U(x) = \frac{1}{2} f x^2 , \qquad (2.1)$$

and the kinetic energy takes the form

$$T(x) = \frac{1}{2}m\left(\frac{dx}{dt}\right)^2 = \frac{1}{2}m\dot{x}^2 = \frac{p^2}{2m}. \quad (2.2)$$

Let us write the equation of motion of a harmonic oscillator:

$$m\ddot{x} = -\frac{dU}{dx} = -fx, \qquad \ddot{x} + \frac{f}{m}x = \ddot{x} + \omega^2 x = 0, \quad (2.3)$$

where $\omega = \sqrt{\frac{f}{m}}$. Solution (2.3) is either of the following two:

$$x = x_{max}\sin(\omega t + \varphi), \qquad x = x_1\cos\omega t + x_2\sin\omega t, \quad (2.4)$$

where the arbitrary constants x_{max}, φ, x_1, and x_2 are related as

$$x_{max} = \sqrt{x_1^2 + x_2^2}, \qquad \operatorname{tg}\varphi = -\frac{x_2}{x_1}. \quad (2.5)$$

(Equalities (2.5) follow from the trigonometric equation $\sin(\omega t + \varphi) = \sin\omega t \cdot \cos\varphi + \cos\omega t \cdot \sin\varphi$.) This solution describes harmonic oscillations with the frequency ω, amplitude x_{max} and initial phase φ. Angular frequency ω refers to spectroscopic frequency ν and period of vibrations T as

$$\omega = 2\pi\nu = \frac{2\pi}{T} = \sqrt{\frac{f}{m}}. \quad (2.6)$$

For definiteness, we choose one of two solutions for the harmonic oscillator (2.4), namely

$$x = x_{max}\sin(\omega t + \varphi). \quad (2.7)$$

$$p = m\dot{x} = m\omega x_{max}\cos(\omega t + \varphi) = p_{max}\cos(\omega t + \varphi). \quad (2.7a)$$

From (2.1) and (2.2) we have

$$U(x) = \frac{1}{2}fx^2 = \frac{1}{2}m\omega^2 x_{max}^2\sin^2(\omega t + \varphi), \quad (2.8)$$

$$T(x) = \frac{1}{2}m\dot{x}^2 = \frac{1}{2}m\omega^2 x_{max}^2\cos^2(\omega t + \varphi). \quad (2.9)$$

The total energy, equal to the sum of the potential and kinetic energies, remains constant during oscillation:

$$E = T + U = \frac{1}{2}m\omega^2 x_{max}^2 \cos^2(\omega t + \varphi) + \frac{1}{2}m\omega^2 x_{max}^2 \sin^2(\omega t + \varphi) == \frac{1}{2}m\omega^2 x_{max.}^2 \quad (2.10)$$

The potential energy U becomes equal to the total E at $x = \pm x_{max}$, therefore, the kinetic energy should vanish at these points, which are turning points for the classical oscillator. For $x = 0$, i.e. in the equilibrium position, the potential energy vanishes, and the kinetic energy reaches its maximum value. The probability of detecting an oscillating particle in a state with a coordinate x is maximum at the turning points $x = \pm x_{max}$, where the velocity of the atoms becomes equal to zero, and is minimum at the equilibrium position. The mean values of the coordinate and momentum are equal to zero because

$$\overline{x} = x_{max}\frac{1}{2\pi}\int_0^{2\pi} \sin(\omega t + \varphi)d\varphi = 0$$

$$\overline{p} = p_{max}\frac{1}{2\pi}\int_0^{2\pi} \cos(\omega t + \varphi)d\varphi = 0\,. \quad (2.11)$$

However, the mean values of the squares of the coordinate and momentum are nonzero:

$$\overline{x^2} = x_{max}^2\frac{1}{2\pi}\int_0^{2\pi} \sin^2(\omega t + \varphi)d\varphi = \frac{x_{max}^2}{2}$$

$$\overline{p^2} = p_{max}^2\frac{1}{2\pi}\int_0^{2\pi} \cos^2(\omega t + \varphi)d\varphi = \frac{p_{max}^2}{2}. \quad (2.12)$$

Hence, the standard deviations are:

$$\delta x = \sqrt{\overline{x^2} - (\overline{x})^2} = \frac{x_{max}}{\sqrt{2}}$$

$$\delta p = \sqrt{\overline{p^2} - (\overline{p})^2} = \frac{p_{max}}{\sqrt{2}} \quad (2.13)$$

2.2. Quantum mechanical harmonic oscillator

The solution to the problem of a quantum harmonic oscillator is directly related to the appearance of quantum mechanics. This phenomenon itself is much more complex than that of a classical oscillator. For this reason, we will first obtain a formal solution, as it is usually presented in textbooks on quantum mechanics, and then we will try to clarify the main features inherent in a quantum oscillator.

For the quantum mechanical solution of the harmonic oscillator problem, it is necessary to find the eigenvalues and eigenfunctions of the energy operator $\widehat{H}$. Introducing the generalized momentum $p = \frac{\partial T}{\partial \dot{q}} = m\dot{q}$ (q – coordinate) and taking into account expressions (2.1) and (2.2) for the kinetic and potential energies of the oscillator, we write the Hamilton function

$$\widehat{H} = \frac{1}{2m}\hat{p}^2 + \frac{1}{2}fq^2 = -\frac{\hbar^2}{2m}\frac{d^2}{dq^2} + \frac{1}{2}fq^2. \qquad (2.14)$$

Replacing the classical momentum p with the momentum operator $\hat{p} = \frac{\hbar}{i}\frac{d}{dq}$ (i.e., replacing the momentum with a mathematical operation that, acting on the function, reveals the determination of the momentum of the system), we obtain for the energy operator of the harmonic oscillator

$$\widehat{H} = \frac{1}{2m}\hat{p}^2 + \frac{1}{2}fq^2 = -\frac{\hbar^2}{2m}\frac{d^2}{dq^2} + \frac{1}{2}fq^2. \qquad (2.15)$$

The solution of an eigenvalue problem for the Schrödinger operator (stationary Schrödinger equation)

$$\widehat{H}\psi_n(q) = \left\{-\frac{\hbar^2}{2m}\frac{d^2}{dq^2} + \frac{1}{2}fq^2\right\}\psi_n(q) = E_n\psi_n(q) \qquad (2.16)$$

determines the energy spectrum

$$E_n = \hbar\omega\left(n + \frac{1}{2}\right) \qquad (2.17)$$

(where $\omega = \sqrt{\frac{f}{m}}$, as in the classical oscillator, and n is the vibrational quantum number taking integer values n = 0, 1, 2, ...) and the eigenfunctions

$$\psi_n(q) = \frac{1}{N_n} H_n(\beta q) e^{-\frac{\beta^2 q^2}{2}} = \frac{1}{N_n} H_n(\xi) e^{-\frac{\xi^2}{2}}; \qquad (2.18)$$

here N_n is the normalization factor, $\beta = \frac{1}{q_{max(0)}}$, $\xi = \beta q$. The functions $H(\xi)$ are Hermite polynomials of degree n ($n = 0, 1, 2 \ldots$), written as

$$\begin{aligned} H_0(\xi) &= 1 \\ H_1(\xi) &= 2\xi \\ H_2(\xi) &= 4\xi^2 + 2 \\ H_3(\xi) &= 8\xi^3 - 12\xi \\ H_4(\xi) &= 16\xi^4 - 48\xi^2 + 12. \end{aligned} \qquad (2.19)$$

Wave functions (2.18) and their squares, which determine the probability distribution of coordinate values, are shown in Fig. 2.2. It can be seen that the functions ψ_0 and ψ_2 are even with respect to the change in the sign of the coordinate, and the functions ψ_1 and ψ_3 are odd. The distribution probability is maximal at the center (i.e., in the classical equilibrium position) for the function ψ_0 and shifts towards the turning points for the remaining functions. Unlike the classical oscillator, the probability outside the classical movement is not zero, but falls off exponentially, and, in addition, it can have several maxima within the oscillator.

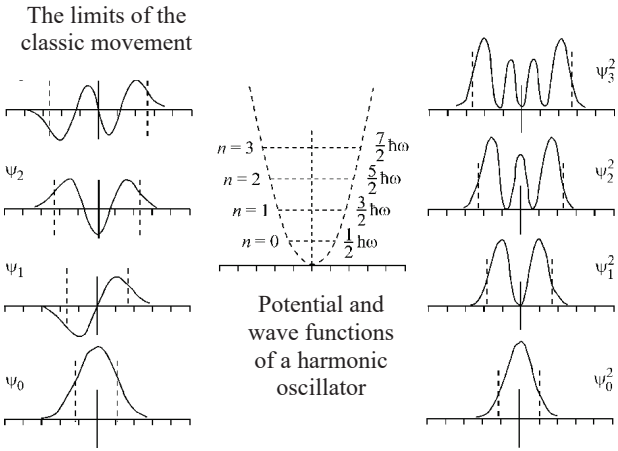

Fig. 2.2. Wave functions of a harmonic oscillator. The divisions of the abscissa scale are in units of ξ

The probability of a transition between states n and n' under the action of an electromagnetic field in the main order is determined by the dipole approximation. In this case, the disturbance potential can be considered in the form $\varphi = d \cdot E$, where d is the dipole moment equal to eq, and E is the amplitude of the electromagnetic field. Thus, in this case, the perturbation energy can be considered a linear function of q; accordingly, the transition probability will be determined by the square of the matrix element of the q coordinate between the states $|n>$ and $|n'>$

$$\langle n|q|n'\rangle = \int \psi_n q \psi_{n'} dq. \tag{2.20}$$

Using the wave functions (2.18) and (2.19), we find that, for example, the probability of the $0 \rightarrow 1$ transition will be proportional to the integral of an even function q_2 and therefore finite, and the probability of the $0 \rightarrow 2$ transition is proportional to the integral of the odd function q_3 and is equal to zero, since the integration is carried out in symmetric limits. These observations constitute a special case of the general selection rule, according to which only transitions between neighboring quantum states are allowed, i.e. with a change in the quantum number n by one

$$\Delta n = \pm 1. \tag{2.21}$$

The proof of the selection rules (2.21) is based on the fact that radiative transitions with high accuracy can be considered as dipole, in which the angular momentum of the photon is equal to $\hbar$. Consequently, the angular momentum of the oscillation during the emission or absorption of a quantum of light can change only by one, which satisfies condition (2.21).

The average values of the coordinate and momentum of stationary states of a harmonic quantum oscillator are determined by the integrals

$$\langle \psi_n|q|\psi_n\rangle = 0$$

$$\langle \psi_n|p|\psi_n\rangle = 0 \tag{2.22}$$

and are equal to zero, since the integration is carried out within symmetric limits.

In a quantum oscillator, the instantaneous values of the coordinate and momentum of a particle are not determined (these physical quantities are not observable); instead, the mean values of the squares of the coordinate and momentum are usually found. We can, however, express the amplitude of a quantum oscillator in terms of the observed parameters.

In classical mechanics, the vibrational energy is determined by expression (2.10), and in the quantum case, by expression (2.17). Equating both quantities, we obtain for the amplitude of the quantum oscillator:

$$q_{\max}(n) = \sqrt{\frac{2\hbar\left(n+\frac{1}{2}\right)}{m\omega}}. \tag{2.23}$$

In this notation, the quantity $q_{\max}(n)$ for a quantum oscillator is analogous to the turning points of the classical one. Based on the equality of the kinetic and potential energies of the oscillator, the maximum value of the momentum is expressed in terms of the coordinate as

$$p_{max}(n) = m\omega q_{max}(n) = \sqrt{2\hbar m\omega\left(n+\frac{1}{2}\right)}. \tag{2.24}$$

The mean value of the squares of the coordinate and momentum of the quantum oscillator are determined by the expressions

$$\overline{x^2} = \langle\psi_n|q^2|\psi_n\rangle = \left(n+\frac{1}{2}\right)\frac{\hbar}{m\omega} = \frac{q_{max}^2(n)}{2}$$

$$\overline{p^2} = \langle\psi_n|p^2|\psi_n\rangle = \left(n+\frac{1}{2}\right)\hbar m\omega = \frac{p_{max}^2(n)}{2} \tag{2.25}$$

and the standard deviations:

$$\delta q(n) = \sqrt{\frac{\hbar\left(n+\frac{1}{2}\right)}{m\omega}} = \frac{q_{max}(n)}{\sqrt{2}}$$

$$\delta p(n) = \sqrt{\hbar m\omega\left(n+\frac{1}{2}\right)} = \frac{p_{max}(n)}{\sqrt{2}} \tag{2.26}$$

We see that the root-mean-square deviations of the coordinate and momentum for the classical (2.13) and quantum (2.26) oscillators, expressed in terms of their amplitudes, coincide.

The results obtained can be interpreted as follows. A quantum particle, according to de Broglie, is not only a particle, but also a wave, the length of which in the case of rectilinear motion is determined by its momentum p:

$$\lambda = \frac{h}{p} \tag{2.27}$$

Since when we consider the oscillation of a particle inside the limited space of the oscillator and outside the oscillator there is no solution, then the particle-wave must "fit into its size", i.e. fit on the segment ($-x_{max}$, x_{max}) in such a way that its amplitude decays when approaching the turning points. This condition can be satisfied by a wave consisting of half a period, one period, one and a half periods, etc., since only in this case does the wave amplitude drop to zero at both boundaries of the oscillator. However, if waves with a different number of half-periods are placed on the same section ($-x_1$, x_1), then their lengths will be different. The energies of these waves, determined by the ratio

$$E = \frac{p^2}{2m} = \frac{h^2}{2m\lambda^2}, \tag{2.28}$$

will also be different. In other words, each possible energy state of a particle in a quantum oscillator corresponds to a single de Broglie wave with one or another length, determined by the size of the oscillator at a given energy and the number of half-periods in this section. Since the number of half-periods of the de Broglie wave inscribed in the oscillator can change only discretely during the transition from one vibrational state to another, then the particle energy also changes discretely. The resulting energy states are called stationary, and the corresponding de Broglie waves are called the wave functions of stationary states. They are shown in Fig. 2.2. This implies a very important difference between the classical and quantum oscillators: if in a classical oscillator the amplitude and total energy of oscillations can vary continuously (see 2.10), then in a quantum oscillator they can only vary discretely and in accordance with (2.17). Taking into account relations (2.23) - (2.26), one can see that the kinematic parameters of a particle in a quantum oscillator also change discretely.

Relation (2.17) and the location of the wave functions of stationary states (Fig. 2.2) can be mistakenly interpreted as changes in the oscillation frequency in the series ω, 2ω, 3ω, etc. But the actual vibration frequency of a quantum oscillator is constant and equal to $\omega = \sqrt{\frac{f}{m}}$.

In quantum mechanics, the vibrational energy of a harmonic oscillator, defined by expression 2.17, is a system of successive equidistant levels

$$E_{n+1} - E_n = \hbar\omega \tag{2.29}$$

where the frequency of the transition between the levels

$$\omega = \frac{E_{n+1} - E_n}{\hbar} \tag{2.30}$$

is exactly equal to the vibrational frequency of the classical harmonic oscillator, which is an important agreement between the results of both theories. However, the minimum energy of a quantum oscillator is not zero, as in a classical one, but

$$E_0 = \frac{\hbar\omega}{2}. \tag{2.31}$$

These are the so-called zero-point quantum motions, which exist even at temperatures close to absolute zero (see also Chapter 9). The existence of zero-point motions at absolute zero is a consequence of the wave nature of the particle and can be confirmed by the Heisenberg uncertainty relation:

$$\Delta p \Delta x \sim \hbar, \tag{2.32}$$

in which, if we put $\Delta p = 0$ (no vibrations), Δx should become infinitely large (a particle at rest exists in all space!), which is unrealistic for our case.

The amplitude of zero-point motions, as follows from (2.23), is equal to

$$q_{max}(0) = \sqrt{\frac{\hbar}{m\omega}}, \tag{2.33}$$

and the standard deviation

$$\delta q(0) = \sqrt{\frac{\hbar}{2m\omega}}. \tag{2.34}$$

Expression (2.17) for the energy of a quantum oscillator can be rewritten using (2.23):

$$E_n = \hbar\omega\left(n + \frac{1}{2}\right) = \frac{1}{2}m\omega^2 q_{max}^2(n). \tag{2.35}$$

In (2.33), the quantum number n determines the amplitude of the oscillation. In this notation, the energies of the quantum and classical oscillators change with the oscillation amplitude in the same way (see (2.10) for the total energy of the classical oscillator). The only difference

is that in a classical oscillator the energy is a continuous function of the amplitude of vibrations, while in a quantum oscillator the increase in energy (and amplitude) occurs discretely, each time changing by the value $\hbar\omega$.

Stationary states are states with a certain energy and constant mean values of the coordinate and momentum. They have no analogue in classical mechanics. The solutions obtained above determine the energies of stationary states and the form of wave functions, but they do not contain vibrations in the classical sense, i.e. they do not contain the factor cos (ωt). To create a semblance of a classical oscillator, it is necessary to solve the Schrödinger equation for wave functions that depend not only on coordinates, but also on time [1]. Omitting all mathematical calculations, we present only the final result. At $t = 0$, the harmonic oscillator can be described as the sum of all its stationary states, taken with some coefficients c_n:

$$|\phi(0)\rangle = \sum_{n=0}^{\infty} c_n(0)\,|\psi_n\rangle \tag{2.36}$$

Then the time-dependent wave function $\phi(t)$ is written as

$$|\phi(t)\rangle = \sum_{n=0}^{\infty} c_n(0)\, e^{-\frac{iE_n t}{\hbar}}|\psi_n\rangle \sum_{n=0}^{\infty} c_n(0)\, e^{-i\left(n+\frac{1}{2}\right)\omega t}|\psi_n \tag{2.37}$$

The last expression contains the factors $e^{\pm i\omega t}$, which are sinusoidal functions of time and angular frequency ω. It suggests that the time-dependent wave function of a harmonic oscillator is a wave packet formed from stationary states, i.e. from those waves that a particle represents in each of the stationary states.

As already mentioned above, a quantum oscillator is characterized by only one frequency ω. However, the question arises: what is an overtone of the vibration? An overtone is a vibration with a doubled frequency, and in an ideal harmonic oscillator, overtones and combination tones are forbidden, i.e. absent. But they can be observed in an anharmonic (i.e. real) oscillator. As will be shown in Chapter 9, in an anharmonic oscillator, due to the excess of the repulsive forces over the restoring forces, any oscillations cause an increase in the distance between the atoms and, therefore, to a decrease in the vibrational frequency. This means that the phonon arising from the scattering lowers its own vibrational frequency. In other words, in a short time, on the order of the half-period of the vibration, the phonon frequency should decrease from the value ω_0 (the frequency of the "bare" phonon) to the value $\omega_0 + \Delta_{ph}$,

where Δ_{ph} is the negative anharmonic contribution from the phonon itself. The time dependence of the phonon frequency makes it possible to expand the function $\omega(t)$ in a Fourier series in harmonics, i.e. in a series whose terms are proportional to both sin (ωt) and sin ($2\omega t$), sin ($3\omega t$), etc. It is this effect, i.e. a change in the vibration frequency in a short time interval in an anharmonic oscillator, that is responsible for the appearance of overtones and combination tones in the spectrum.

In conclusion, it should be noted that in quantum mechanics the problem of a harmonic oscillator has an exact solution only in the case of oscillations of **one** particle in the parabolic potential well shown in Fig. 2.1. The simplest object of vibrational spectroscopy is a diatomic molecule. However, the problem of determining stationary states for a diatomic molecule is already too complicated. The fact is that the vibrations of molecules consist of displacements of both the nuclei and the electronic component. It is impossible to take into account both types of displacements simultaneously in a general form even for a diatomic molecule. (Particular problems, taking into account the motion of both nuclei and electrons, are currently being solved with the use of modern programs and computers.) The latter circumstance, however, affects the shape of the potential curve of interaction between atoms in a molecule. The main results obtained above when solving the problem of a quantum harmonic oscillator, i.e. discreteness of the energy spectrum, vibration amplitudes, the presence of zero-point motions, etc., remain valid for molecular systems of any complexity. The question of the nature of the interatomic interaction potential will be considered in more detail in Chapter 9.

2.3. Vibrations of polyatomic molecules. The secular equation

The equation of motion for a system of particles, i.e. molecules, can be written in the form of Newton's equation:

$$\frac{d}{dt}\frac{\partial T}{\partial \dot{q}_j} + \frac{\partial U}{\partial q_j} = 0,\ j = 1,2,3 \ldots ,3N, \tag{2.38}$$

where the kinetic energy T depends only on the velocities, and the potential U depends on the coordinates. For a one-dimensional harmonic oscillator, this expression is transformed into the differential equation (2.3).

From the theory of small-amplitude vibrations it follows that the kinetic and potential energies can be represented as

$$T = \frac{1}{2}\sum_{i,j=1}^{3N} m_{ij}\dot{q}_i\dot{q}_j\,, \qquad U = \frac{1}{2}\sum_{i,j=1}^{3N} f_{ij}q_iq_j. \tag{2.39}$$

Each of these expressions is a square matrix 3N×3N, in which the elements characterizing a separate vibrational coordinate (i.e., the reduced mass in the kinetic energy matrix and its force constant in the potential energy matrix) are located diagonally. The natural coordinates of the molecule, i.e. bond lengths, bond angles, and dihedral angles, are usually chosen as vibrational coordinates. The off-diagonal terms in the expression for the kinetic energy determine the effect of a change in the geometry of the molecule during vibration on the reduced mass of a given *i*-th coordinate, and in the expression for the potential energy, the effect of a change in the *j*-th vibrational coordinates on the force constant of the *i*-coordinate. Separating the diagonal and off-diagonal terms in expressions (2.39), we obtain:

$$T = \tfrac{1}{2}\textstyle\sum_i m_{ii}\dot{q}_i^2 + \sum_{ij(i>j)} m_{ij}\dot{q}_i\dot{q}_j\,, \quad U = \tfrac{1}{2}\textstyle\sum_i f_{ii}q_i^2 + \sum_{ij(i>j)} f_{ij}q_iq_j. \tag{2.40}$$

If we neglect the off-diagonal interactions, we obtain a set of independent harmonic oscillators, where the coordinate changes according to the law

$$q_i = q_{i0}\sin\omega_i t = q_{i0}\sin 2\pi\nu_i t \tag{2.41}$$

with frequency

$$\omega_i = 2\pi\nu_i = \sqrt{\frac{f_{ii}}{m_{ii}}}. \tag{2.42}$$

If off-diagonal interactions cannot be neglected, which, as a rule, takes place, expressions (2.39) can be reduced to a diagonal form if the initial coordinates q_i are rewritten as linear combinations:

$$\xi_\lambda = \textstyle\sum_i C_{\lambda i}q_i. \tag{2.43}$$

The new coordinates ξ_λ are the so-called *normal coordinates*, in which *T* and *U* take the diagonal form:

$$T = \frac{1}{2}\sum_{\lambda} m_\lambda \dot{\xi}_\lambda^2 \ , \qquad U = \frac{1}{2}\sum_{\lambda} f_\lambda \xi_\lambda^2 \ , \tag{2.44}$$

where m_λ and f_λ are new constants depending on the previous and transformation coefficients $C_{\lambda i}$. A wonderful property of normal coordinates is that, when using them, we again get a set of independent oscillators, but now each oscillator includes the vibrations of all the original vibrational coordinates of the molecule, united by off-diagonal interactions, and not the vibrations of individual bonds or angles, as it was in (2.41). The total energy of vibrations is again equal to the sum of the energies of harmonic oscillators with the frequencies of *normal vibrations*

$$\omega_\lambda = \sqrt{\frac{f_\lambda}{m_\lambda}}. \tag{2.45}$$

However, now the force constants f_λ and reduced masses m_λ are determined by both diagonal and off-diagonal interactions.

The original q_k coordinates can be expressed in terms of normal coordinates using the inverse transformation

$$q_k = \sum_\lambda d_{k\lambda}\, \xi_\lambda \ . \tag{2.46}$$

Moreover, for one definite normal vibration ξ_j, the inverse transformation gives

$$q_k^{(j)} = d_{kj}\xi_j = d_{kj}\xi_{j0} \sin \omega_j t \ . \tag{2.47}$$

Using the concept of kinematic and potential interaction of coordinates, the equation of motion can be written as

$$\ddot{q}_j + \sum_{i=1}^{3N} W_{ij} q_j = 0 \ , \tag{2.48}$$

where W_{ij} are the coefficients of total interaction, including force constant of bonds, mass of atoms, as well as kinematic and potential interaction of bonds (i.e. off-diagonal elements) simultaneously. Expression (2.48) is a system of joint linear differential equations of second order. Solutions (2.48) are harmonic oscillations with as yet unknown frequency ω and phase ε

$$q_i = q_{0i} \sin(\omega t + \varepsilon). \tag{2.49}$$

From (2.49) it follows that each atom vibrates about an equilibrium position with the same frequency ω and phase ε. That is, all atoms pass the positions of equilibrium and maximum deviation at the same time, but their displacements are characterized by different amplitudes. Vibration with such characteristics is called normal, and frequency is called the normal (or fundamental) vibrational frequency. The experimental vibrational spectrum (IR and/or Raman) of a compound is the spectrum of its normal vibrations. Moreover, each normal vibration (each experimental vibrational mode) includes the displacement of all atoms of the molecule, i.e. the vibration of all bonds and angles of a molecule; however, the relative participation of different pairs of atoms in any normal vibration is different. The determination of the degree of participation of individual vibrational coordinates in experimentally observed modes (i.e., assignment of lines in the spectrum) is the main subject of experimental vibrational spectroscopy.

If expression (2.49) is substituted into (2.48), we obtain the system of equations

$$\sum_{i=0}^{3N}\left(W_{ij} - \delta_{ij}\omega^2\right)q_{0i} = 0, \tag{2.50}$$

for amplitude of vibrations, where δ_{ij} is the Kronecker symbol. The condition for solving the system is the equality to zero of the determinant of the 3*N*th order

$$\begin{vmatrix} W_{11} - \omega^2 & W_{12} & \dots & W_{1,3N} \\ W_{21} & W_{22} - \omega^2 & \dots & W_{2,3N} \\ \dots & \dots & \dots & \dots \\ W_{3N,1} & W_{3N,2} & W_{3N,3N} - \omega^2 \end{vmatrix} = 0 \tag{2.51}$$

In matrix form, relation (2.51) can be written as

$$|\boldsymbol{W} - \lambda \boldsymbol{E}| = 0, \tag{2.52}$$

where $W = T^{-1}U$, T is a matrix of kinematic coefficients, with U - matrix of force constants, E - unit matrix, and λ - eigenvalue (square of the frequency of normal vibration of the molecule). This is the famous secular equation. The solution to the secular equation has $3N - 6$ roots $\lambda^{(i)}$, where $3N$ is the number of degrees of freedom. All matrices in the secular equation are of the order of $3N$, so solving it for large molecules is a difficult task. Dividing vibrational coordinates into groups of equivalent ones and constructing symmetry coordinates within each group (this

procedure will be discussed in detail in Chapter 4) allows us to reduce the matrix W to a block form, consisting of submatrices of an order not higher than three, and to find the frequency and eigen vector of vibrations to use as solutions for linear, quadratic or cubic equations. But even these equations are still too cumbersome and their solution is carried out with the help of appropriate computer programs. Typically, programs are designed in such a way that they require only input data from the user, and most of the calculations are performed without his/her participation. For this reason, there is no need to consider in detail the procedure for solving the secular equation and all the steps associated with it (making of symmetry coordinates, matrices T, U, etc.).

The solution to the secular equation is the frequency of normal vibrations. It is assumed that the matrices of the kinematic coefficients and force constants are known, and the determination of the vibrational frequencies is the result of solving the *direct spectral problem*. In practice, however, the opposite case is realized, i.e. what is known from the experiment is just the vibrational frequencies, and the unknown is the set of force constants, diagonal and off-diagonal. Finding the force constants of bonds from a known set of frequencies of normal vibrations is the subject of an *inverse spectral problem*. Since the number of force constants in a molecule, as a rule, greatly exceeds the number of experimentally determined frequencies of the vibrational spectrum, the formal solution of the inverse spectral problem is always mathematically incorrect. However, modern programs for the quantum-chemical calculation of molecules use a different algorithm for calculating the force constants, and the vibrational spectrum calculated using such programs, as a rule, does not differ from the experimental one within the limits of insignificant and quite acceptable deviations.

2.4. Rotational states of two atomic molecules

Finally, we will very briefly consider one more important spectroscopic problem using diatomic molecules as an example. If the molecules are in the gas phase, then, along with vibrational ones, they also have rotational states. The rotation of molecules is characterized by the angular momentum $\boldsymbol{M_p}$, the square of which in quantum mechanics is defined as

$$\boldsymbol{M}_p^2 = \hbar^2 J(J+1), \tag{2.53}$$

where J is the rotational quantum number taking the value J = 0, 1, 2, 3, ... The rotational energy is

$$E = \frac{\boldsymbol{M}_p^2}{2J}, \tag{2.54}$$

where $I = \sum_{i=1}^{N} m_i r_i^2$ is the moment of inertia about the axis of rotation, and r is the distance of the nuclei from the center of gravity of the molecule. From here

$$E_j = \frac{\hbar^2}{2I} J(J+1) = BJ(J+1), \tag{2.55}$$

where the rotational constant B is

$$B = \frac{\hbar^2}{2I} = \frac{2.8 \cdot 10^{-39}}{I} cm^{-1} \tag{2.56}$$

When J takes consecutive values of 0, 1, 2, 3, ..., the rotational energy runs through the values of $2B$, $6B$, $12B$, etc.

For a nitrogen molecule N_2 with a distance between the nuclei ρ ~ 1.1 Å and an atomic mass of 14 amu we have

$$I = \frac{m_N \rho^2}{2} = \frac{14 \cdot 1.66 \cdot 1.2 \cdot 10^{-24} \cdot 10^{-16}}{2} = 13.9 \cdot 10^{-40}\ g \cdot cm^2,$$

$$B = \frac{2.8 \cdot 10^{-39}}{13.9 \cdot 10^{-40}} = 2.0\ \ cm^{-1}.$$

We see that the frequencies of rotation of molecules are very small (and the lower, the heavier the molecule), and at room temperature, rotational states with large quantum numbers are already populated. For this reason, the registration of rotational spectra for a large part of molecules is a difficult task. More often, the rotational structure is observed in the spectrum of combination tones, i.e. in the form of combinations of any stretching mode (for example, stretching vibration C–C or C–N, etc.) with the rotational states of the entire molecule. In this case, the corresponding vibrational mode in the spectrum is accompanied by wide wings of rotational states, Stokes (R-branches), and anti-Stokes (P-branches).

The rotational spectra of polyatomic molecules are usually studied to obtain accurate values of the moments of inertia, centrifugal distortion constants, coefficients of Coriolis interaction, and anharmonicity constants for various vibrational modes.

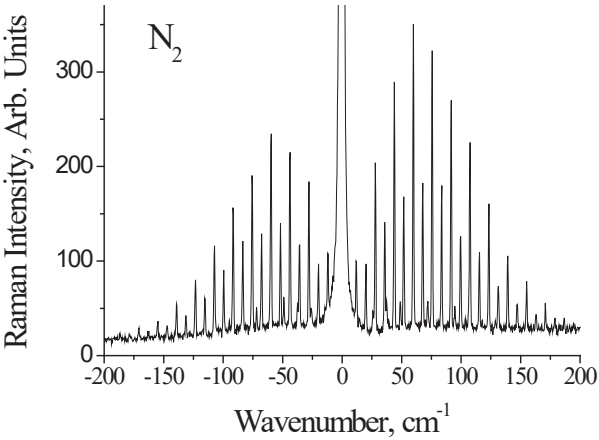

Fig. 2.3. The spectrum of rotational states of molecular nitrogen in gas phase.

Rotational spectra of molecules are recorded using specially designed high-resolution IR spectrometers. In routine spectroscopy used to obtain Raman spectra of crystalline inorganic or organic compounds, rotational spectra are generally not observed. However, with the development of spectral equipment, it has become possible to record spectra from very low frequencies, that is, from 4 cm^{-1}. (For example, a Raman spectrometer LabRAM HR Evolution, Horiba with a set of notch and Bragg filters allows you to obtain spectra from 4 cm^{-1} with excitation at 633 nm and from 10 cm^{-1} with excitation at 488 nm.) Fig. 2.3 shows the spectrum of rotational states of N_2 molecules in the gas phase, obtained with this spectrometer.

CHAPTER 3

VIBRATIONS OF CRYSTALS

3.1. Types of phonons in crystals

Until now, speaking of the vibrational system, we have meant a molecular system. Next, we will consider the features of crystal vibrations.

Any direction in the crystal can be represented as a chain of potential wells with common walls. For electrons, a well is an atom in a lattice site, for an excited vibration – a chemical bond between atoms. If all the wells are the same, which is always observed in the crystal due to translational symmetry, then, according to quantum mechanical concepts, the excitation that appears in one well after some time will be observed with equal probability in any of them. In other words, the excited vibration of any bond in a crystal cannot remain localized, as in a molecule, but must propagate in a lattice with a certain direction and momentum (more correctly, a quasi-momentum). A vibrational quantum in a crystal acquires the properties of a particle (quasi-particle) and is
called a phonon.

Fig. 3.1, *a* shows a one-dimensional chain at rest, the unit cell of which contains two atoms of different types, and in Fig. 3.1, *b* - the same chain, but with a vibration excited in it. The depicted vibration can be characterized by a frequency ω, a wavelength λ, and a wave vector $\boldsymbol{k} = 2\pi/\lambda$ (i.e., the number of wavelengths that fit in the segment 2π). The phonon wave vector indicates the direction of phonon propagation (in a one-dimensional chain, a phonon can propagate, naturally, only along the chain, but for a three-dimensional crystal this can be in any direction). The displacements of atoms shown in Fig. 3.1, *b* occur along the direction of phonon propagation. This vibration is called longitudinal. Figs. 3.1, *c* and *d* depict transverse phonons (displacements of atoms that occur in the direction perpendicular to $\boldsymbol{k}$), and one of the phonons (Fig. 3.1, *c*) is polarized along the *x* axis, and the other (Fig. 3.1, *d*) along *y*. The direction of the displacement determines the polarization of the phonon. The phonons shown in Figs. 3.1, *b*, *c* and *d*, have one common property: the center of gravity of each elementary cell does not shift during vibration,

i.e. the displacements of atoms in the cell occur in opposite directions and balance each other. These are the so-
called optical phonons. Their frequency is comparable to the frequency of vibrations of electromagnetic radiation in the infrared region. For this

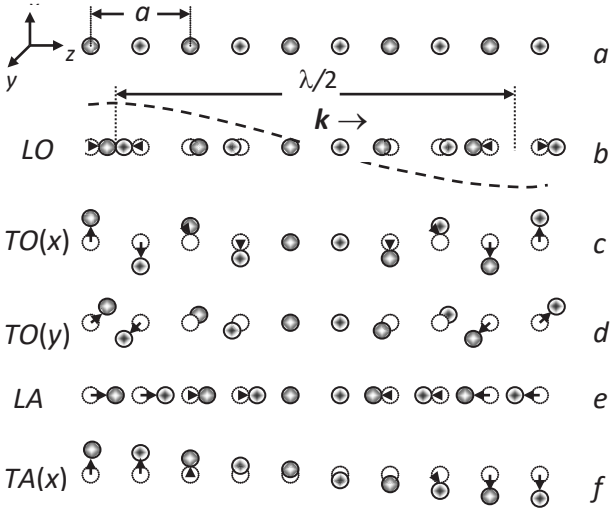

Fig. 3.1. Vibrations of a one-dimensional diatomic lattice. *LO* – longitudinal optical, *TO* – transverse optical, LA – longitudinal acoustic, TA – transverse acoustic phonons (phonon *TA*(*y*) with displacement of atoms along *y*-axis is not shown in the figure).

reason, if the atoms of the cell have charges of different signs (as, for example, in NaCl), then the optical vibration can be excited by the absorption of an IR photon by the lattice (hence the name of the phonon). Vibrations of the chain shown in Figs. 3.1, *e* and *f* refer to longitudinal and transverse acoustic phonons. In them, both atoms are displaced in the same direction and set the displacement of the entire cell. These phonons are responsible for the propagation of sound waves in the crystal.

3.2. Dispersion of phonons

It is possible to calculate the vibration frequencies of a one-dimensional chain consisting of atoms of mass m_1 and m_2, the bonding between which is characterized by the force constant f (Fig. 3.2) [1].

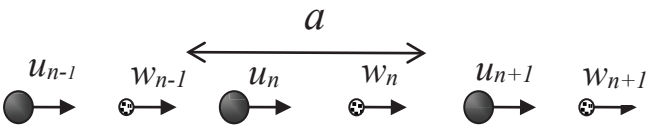

Fig. 3.2. One-dimensional chain of atoms with masses m_1 and m_2 ($m_1 > m_2$) and parameter a of unit cell. u and w are the displacements of atoms from the equilibrium position.

An atom with mass m_1, when displaced along the chain, will experience the action of interatomic forces on the right, proportional to the difference in coordinates ($w_n - u_n$), and on the left, proportional to the difference ($u_n - w_{n-1}$), i.e.

$$F = f(w_n - u_n) - f(u_n - w_{n+1}) = f(w_n + w_{n+1} - 2u_n). \tag{3.1}$$

Therefore, the equation of motion for it will be written as

$$m_1 \frac{d^2 u_n}{dt^2} = f(w_n + w_{n-1} - 2u_n). \tag{3.2}$$

Similarly, for an atom with mass m_2

$$m_2 \frac{d^2 w_n}{dt^2} = f(u_{n+1} + u_n - 2w_n). \tag{3.3}$$

We are looking for a solution in the form of running waves with amplitudes u and w for different atoms:

$$u_n = ue^{inka}e^{-i\omega t}, \quad w_n = we^{inka}e^{-i\omega t}. \tag{3.4}$$

Substituting these expressions into (3.2, 3.3) and solving a system of two homogeneous linear equations, we obtain the following quadratic equation for ω^2:

$$m_1 m_2 \omega^4 - 2f(m_1 + m_2)\omega^2 + 2f^2(1 - \cos ka) = 0. \tag{3.5}$$

The solution to the equation is a periodic function with respect to the value of k, varying within the limits determined by the values $\cos(ka) = +1$ (center of the Brillouin zone, see Appendix ***A***) and $\cos(ka) = -1$ (edge of

the Brillouin zone). In the case of small values of $ka \approx 0$ (i.e., at the center of the Brillouin zone), we obtain two roots of equation (3.5):

$$\omega_{op}^2 \approx 2f\left(\frac{1}{m_1}+\frac{1}{m_2}\right) \quad \text{(optical branch)}, \tag{3.6}$$

$$\omega_{ac}^2 = \frac{\frac{1}{2}f}{m_1+m_2}k^2a^2 \quad \text{(acoustical branch)}. \tag{3.7}$$

At $k = \pi/a$ (i.e., at the boundary of the Brillouin zone) we have:

$$\omega_{op}^2 = \frac{2f}{m_2}, \qquad \omega_{ac}^2 = \frac{2f}{m_1}. \tag{3.8}$$

The infinite phonon wavelength ($\lambda = \square$, $k = 0$) means for an optical phonon that all unit cells of the chain (crystal) vibrate in phase, i.e. with the same displacement at the same time (Fig. 3.3, *b*). The frequency of such a vibration is finite and usually has a maximum for

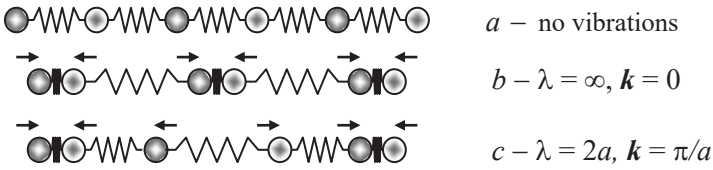

Fig. 3.3. Longitudinal optical phonons related to the center (*b*) and edge (*c*) of the Brillouin zone

any given type of phonon. For an acoustic phonon, the same simultaneous displacement in all unit cells means a displacement of the crystal as a whole - this is a vibration with zero frequency. The shortest wave in a crystal can be the one in which atoms in neighboring cells are displaced in antiphase and with a maximum amplitude, with $\lambda = 2a$, $k = \pi/a$ (Fig. 3.3, *c*). In an optical vibration with $k = 0$, both bonds (springs) between atoms belonging to the same cell and bonds between atoms of neighboring cells are involved, while in vibrations with $k = \pi/a$, the force constants of bonds between atoms of neighboring cells do not take part in the oscillatory process (Fig. 3.3, *b*,*c*). This means that the vibration frequency of an optical phonon with $k = \pi/a$ is lower than that of the same phonon with $k = 0$, and there is a dependence of the vibration frequency of phonons on their wave vector.

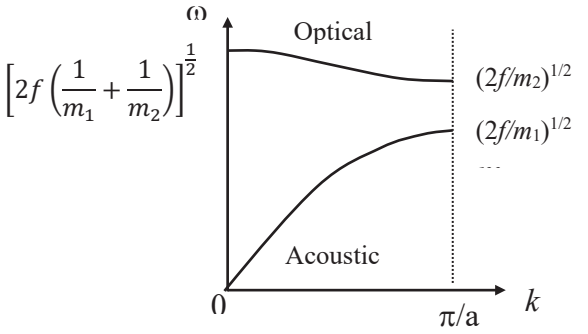

Fig. 3.4. Dispersion curves of phonons of a diatomic linear chain.

Such dependences are called dispersion curves (branches) and are schematically shown in Fig. 3.4 for a diatomic linear chain. Despite the extreme simplification of the considered model of a one-dimensional crystal, the shape of the dispersion curves in many real cases is very close to that shown in Fig. 3.4.

As a rule, only optical phonon modes related to the center of the Brillouin zone are available in Raman spectra and phonon combinations (i.e., their sum or difference) – at highly symmetric points (see Appendix A). Full dispersion branches in the direction of highly symmetric points could be obtained in a neutron scattering experiment. Fig. 3.5 shows the dispersion branches for two crystallographic directions in a diamond crystal (O_h group).

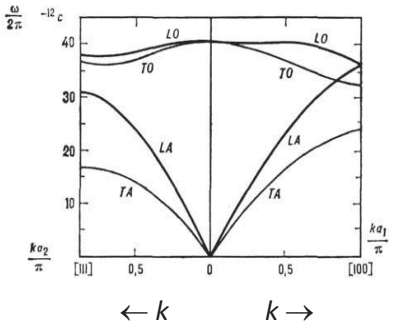

Fig. 3.5. Dispersion curves of optical and acoustic phonons of a diamond crystal (point symmetry group O_h) in the direction [111] (left side) and [100] (right side).

In the one-dimensional chain considered above, one acoustic and one optical branch appear. In the three-dimensional case, if a unit cell contains two atoms (as, for example, in crystals of zinc blende ZnS, silicon, diamond), three acoustic (one longitudinal and two transverse) and three optical (also one longitudinal and two transverse) branches arise. If a unit crystal cell contains p atoms, then such a crystal has $3p$ phonon branches: 3 acoustic and $3p$ - 3 optical.

As already mentioned, a phonon in a crystal is represented in the form of a running wave, where the displacements of each atom are characterized by expression (3.4). Replace the wave vector $\boldsymbol{k}$ in this expression with $\boldsymbol{k}' = \boldsymbol{k} + \frac{2\pi g}{a}$, where g is any positive or negative integer, and the new displacement of the atom, for example, u_n, will be written as

$$u_n' = ue^{ink'a}e^{-i\omega t} = ue^{inka}e^{-i\omega t}e^{i2\pi gn} = u_n, \qquad (3.9)$$

since g and n are integers and $e^{i2\pi gn} = 1$. This means that the new wave is completely identical to the old one and we can consider the dispersion branches of phonons at the values of the wave vector bounded by the region $-\frac{\pi}{a} \le k \le \frac{\pi}{a}$, i.e. the first Brillouin zone. A change in the wave vector to an arbitrary *reciprocal lattice vector* $G = \frac{2\pi g}{a}$ will mean the transfer of a state from one Brillouin zone to exactly the same state of another zone, as a change in any position in a unit cell of direct space by the lattice translation vector means its transfer to exactly the same position of the other cell. In addition, the change in the sign of the wave vector, i.e. the transition from $+k$ to $-k$, means only a change in the direction of phonon propagation in the lattice to the opposite and the dispersion branch in the region $-\frac{\pi}{a} \le k \le 0$ turns out to be a mirror reflection of the branch in the region $0 \le k \le \frac{\pi}{a}$. Thus, the interval $0 \le k \le \frac{\pi}{a}$ of the first Brillouin zone of phonon frequency values, as a function of the wave vector, as shown in Fig. 3.4, fully characterizes its dispersion in the crystal in a given direction.

The slope of the dispersion curves towards the abscissa axis, shown in Fig. 3.4 and 3.5, vanishes (or is close to zero) for optical phonons at the center of the Brillouin zone and for both types of phonons at the edge of the Brillouin zone. Indeed, the solution to equation (3.4) for the vibrational frequency is a function of cos(ka). The slope of the $\omega(k)$ dependences to the wave vector axis should vanish at $k = 0$ and $k = \pi/a$, since the derivatives of such functions are proportional to sin(ka).

3.3. Density of phonon states

Atomic chains, considered as a one-dimensional analogue of a crystal, consist of a very large number of atoms. Nevertheless, the main difference between vibrations of an atomic chain and vibrations of a string is that the wave vectors of phonons must take discrete values and the number of possible phonon states is finite. The total number of states in each branch of the first Brillouin zone is equal to N, where N is the number of unit cells in the crystal. Since the frequency of phonon vibration and its wave vector are related by a complex nonlinear dependence, we can introduce the concept of the density of phonon states $\rho(k)$ as the number of possible vibrations with different k, falling into the interval $\Delta\omega$ in the space of wave vectors $\rho(\omega) = dk/d\omega$. It is convenient, however, to express $\rho(\omega)$ not as $dk/d\omega$, but as $\rho(\omega) = (d\omega/dk)^{-1}$. The point is that $d\omega/dk$ is already a well-known physical quantity, namely, the group velocity of the wave packet of phonons. For example, as can be seen from Figs. 3.4 and 3.5, for acoustic phonons the derivative $d\omega/dk$ in most of the Brillouin zone is practically constant; in this case, the group velocity of the wave packet is equal to the speed of sound in the crystal. However, at the boundary of the Brillouin zone, the derivative $d\omega/dk$ of the acoustic phonons (i.e., the slope of the dispersion curve) becomes zero, and phonons in this region become standing waves, as required by the periodic boundary conditions. Indeed, in an acoustic phonon with $\boldsymbol{k} = \pi/a$, the vibration phase of each pair of neighboring unit cells remains constant throughout the crystal, which turns the phonon into a standing wave. The slope of the dispersion branch of the optical phonons becomes zero at the center and at the boundary of the Brillouin zone (Figs. 3.4, 3.6). Since the slope ($d\omega/dk$) vanishes at $k = 0$ and $k = \pi/a$ for optical vibrations and at $k = \pi/a$ for acoustic vibrations, the value $(d\omega/dk)^{-1} \to \infty$ at these points, and the density of the phonon states are characterized by a sharp maximum. These features of the density of states function are called van Hoof singularities. The dispersion curves shown in Figs. 3.4 and 3.5 refer to the relatively simple cases of a linear chain (Fig. 3.4) and a monatomic diamond crystal (Fig. 3.5). But already in diamond one of the optical branches, a weak maximum in the [100] direction and a minimum in the [111] direction in the region $0 < k < \pi/a$ (Fig. 3.5) is exhibited. In inorganic crystals of complex composition, the number of dispersion branches is much larger and they can have singular points (minima, maxima, and saddle points) not only at the boundaries of the Brillouin zone, but also in intermediate regions, and each time the singular point will be characterized by the van Hoof singularity of the density function phonon states.

The maxima of the density function of phonon states, especially at the center and at the boundary of the Brillouin zone, are of great importance for Raman scattering in crystals. We will return to them when discussing the selection rules.

3.4. Wave vector selection rules

The description of vibrations in crystals by phonons, i.e. excitations propagating through the crystal and characterized by a wave vector, forces us to take into account in the process of Raman scattering not only the law of conservation of energy, but also the law of conservation of the wave vector, which requires that the wave vector of the exciting radiation before scattering should be equal to the total wave vector of all particles after scattering (Fig. 3.6).

In other words, the wave vector of the scattered phonon k_{ph} is the vector difference of the wave vectors of the incident $\boldsymbol{k}_i$ photons and the scattered $\boldsymbol{k}_s$ photons and is equal in order of magnitude to both of them. From here it follows that the phonon wavelength should be several hundreds of nanometers (to excite the Raman spectrum, coherent radiation with a wavelength in the region of 400-700 nm is usually used), i.e. several hundred or even thousands of lattice periods. A phonon with such a wavelength is characterized by a wave vector close to zero (on the scale of phonon wave vectors) and, therefore, only phonons belonging to the center of the Brillouin zone take part in the scattering. The frequency and energy of acoustic phonons at the center of the Brillouin zone is equal to zero; therefore, only optical phonons are observed in the experiment. (Measurement of the spectrum of acoustic phonons is the subject of Mandelstam-Brillouin scattering spectroscopy).

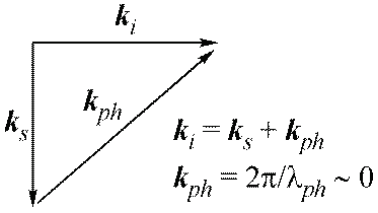

Fig. 3.6. Illustration of the selection rule for wave vector

Thus, optical phonons in the center of the Brillouin zone of a crystal are characterized by the maximum density of states and activity in scattering according to the selection rules. This makes scattering by optical phonons with $k = 0$ much more efficient than scattering by all other phonons of the Brillouin zone.

3.5. Interaction effects in polar crystals

If a dipole moment arises in a longitudinal optical phonon at the displacement of atoms in a unit cell relative to each other, then at $k = 0$ this will lead to the appearance of a macroscopic electric field in the crystal due to the addition of dipole moments from all unit cells.

For simplicity, consider the polar vibration of a chain (Fig. 3.7, a), consisting of two kinds of atoms with different charges. At rest, the dipole moment directed from atom A to atom B (neighbor to the right) along the $+x$ axis is exactly equal to the dipole moment from A to B (neighbor to the left) directed along $–x$, and the total dipole moment of the entire chain is zero. In the case of longitudinal optical vibration with $k = 0$ (the displacement of atoms along the chain is the same for all unit cells that make it up), the distance between atoms A and B in the $+x$ direction becomes different from the distance from A to B along the $–x$ direction, the neighboring dipole moments turn out to be different in magnitude, and the total dipole moment of the chain is nonzero (Fig. 3.7, b). In such a vibration, a situation arises in which the sublattice of ions of one sign is displaced relative to the sublattice of ions of the other sign, as if an external electric field were applied to the crystal. When the vibration phase changes, i.e. when the atoms are displaced in the opposite direction, the arising macrofield also changes its direction (Fig. 3.7, c). Thus, at each moment of time, both types of ions turn out to be moving in the direction of the macrofield created by them, which yields to an increase in the vibration frequency of this longitudinal phonon. (In a transverse optical vibration, where the ions are displaced in a direction perpendicular to the direction of the linear chain, the values of the dipole moments in neighboring pairs of atoms remain equal in magnitude and a macroscopic field does not arise). In crystals of low symmetry, the frequencies of the longitudinal and transverse phonons are different in magnitude, and the discussed effect will most likely be unnoticed, since it is not known in advance what the frequency of the longitudinal phonon should be. In cubic crystals, the optical and acoustic vibrations must be threefold degenerated due to the physical equivalence of all three crystallographic directions. However, in those of them where there is no inversion center, and optical modes that are active in the IR and Raman scattering exist simultaneously (this is the condition for the polarity of the vibration), there is a longitudinal-transverse splitting of the threefold degenerated mode at the center of the Brillouin zone into *LO* and *TO* components. (It should be noted that the symmetry of the modes does not change in this case, i.e., it remains equal to F_2). One of the most striking examples of the effect is the

longitudinal-transverse splitting of the optical mode in III–V – semiconductor compounds (GaAs, GaP, etc.). Fig. 3.8 shows the spectrum of GaAs, where a threefold degenerated optical vibration is split into transverse (*TO*, 269 cm^{-1}) and longitudinal (*LO*, 291 cm^{-1}) modes.

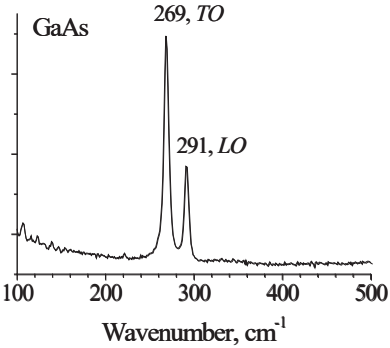

Fig. 3.8. Raman spectrum of an undoped GaAs single crystal. The threefold degenerated optical vibration is split into transverse (*TO*, 269 cm^{-1}) and longitudinal (*LO*, 291 cm^{-1}) modes.

The numerical value of the frequencies of longitudinal and transverse optical phonons arising as a result of splitting obey the Liddane-Sachs-Teller relation:

$$\frac{\omega_T^2}{\omega_L^2} = \frac{\varepsilon_\infty}{\varepsilon_0}, \tag{3.10}$$

where ε_0 and ε_∞ are low and high frequency dielectric constants, respectively.

Semiconductor crystals, where longitudinal-transverse splitting of optical modes exists, often have intrinsic or impurity conductivity, i.e. some concentration of free carriers. The macrofield arising in longitudinal optical modes interacts with free carriers, giving rise to a specific electron-phonon interaction (only for *LO* phonons in noncentrosymmetric crystals!), called the *Frohlich interaction*.

In addition, in doped semiconductors, plasma oscillations (plasmons) of free carriers, electrons or holes, can be observed, the frequency of which is determined by the expression

$$\omega_p^2 = \frac{4\pi e^2 n}{m^* \varepsilon} \tag{3.11}$$

where n is the concentration of carriers and m^* is the effective mass. Fig. 3.9 shows the spectrum of doped GaAs with $n = 2 \cdot 10^{18}$ cm^{-3}, in which

scattering by plasmons is represented by a broad weak band in the region of 300 cm^{-1} (dashed line).

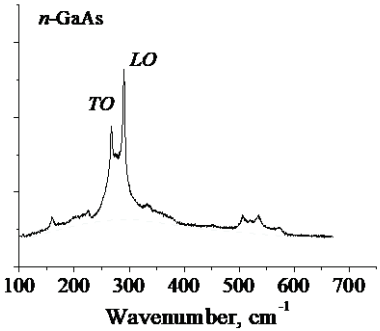

Fig. 3.9. Spectrum of doped *n*-GaAs ($n = 2 \cdot 10^{18}$ cm^{-3}). The dashed line is scattering by plasma oscillations of the electron gas.

The manifestation of polar vibrations in IR spectra is somewhat more complicated. The incident electromagnetic wave is always transverse, i.e. the electric field vector in it is perpendicular to the direction of wave propagation. Therefore, the incident wave does not interact with a longitudinal optical phonon propagating in the same direction, i.e. for $\boldsymbol{k_i} = \boldsymbol{k_{ph}}$. Transverse optical phonons are another matter. In IR spectra, the wavelengths of the incident light and the excited

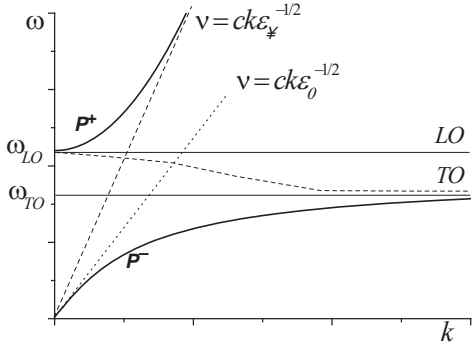

Fig. 3.10. Polariton states in ionic (polar) crystals. Solid curves represent bound polariton states, P^+ and P^-. Thin straight lines in the figure denote the dispersion dependence for photons ($v = ck\varepsilon_0^{-1/2}$ at low frequencies, $v = ck\varepsilon_\infty^{-1/2}$ at high frequencies) and transverse optical phonons ($\omega = \omega_{TO}$) in a crystal in if they did not interact with each other [1].

phonon coincide, just as the direction of the electric field of the incident wave and the dipole moment in the transverse phonon coincide. That is, two waves, electromagnetic and mechanical, are precisely superimposed on each other. This leads not only to a strong interaction between a photon

and a phonon, but to the appearance of certain states in the crystal, which are no longer either a photon or a phonon. These states are called polaritons. The solutions of the equations for the photon-phonon system in the crystal are two dispersion branches P^+ and P^- (Fig. 3.10, solid curves), one of which asymptotically tends from zero at $k = 0$ to the phonon frequency *TO*. The other, from the *LO* phonon frequency at $k = 0$, also asymptotically tends to an inclined straight line characterizing the dispersion of a "bare", non-interacting photon in the crystal. (If the two waves, electromagnetic and elastic, did not interact with each other, then the dispersion of the first of them would be described by an inclined straight line $\omega = ck\varepsilon_\infty^{-1/2}$, where c – the speed of light, ε_∞ – high-frequency dielectric constant, and k – the wave vector of the photon, and the dispersion of the second of them would be a straight line $\omega = \omega_{TO}$. Both of these straight lines are plotted in Fig. 3.9 by thin lines). Thus, for each value of the wave vector of a photon and phonon, there are two polaritons in the crystal - a low-frequency P^- and a high-frequency P^+. At small k, the low-frequency polariton is more like a photon, and the high-frequency polariton is more like a phonon. For large k, it is vice versa. Acoustic and longitudinal optical phonons do not interact with incident radiation.

What is observed in the IR spectra of crystals? First of all, there is no solution for the photon-phonon system in the frequency range between the values of *TO* and *LO* phonons (Fig. 3.10). In other words, the incident wave does not pass into the crystal, which will be recorded in the IR absorption spectrum as 100% absorption in this entire region. In this case, all electromagnetic radiation will be reflected from the crystal and give the so-called residual rays. A typical IR reflectance spectrum is shown in Fig. 3.11. The width of the IR reflection band, or rather the shelf, where the reflection is maximum and approximately constant, corresponds to the region of large values of the imaginary wave vector (see Fig. 3.10, dashed line) near ω_{TO}.

The mathematical procedure for processing such spectra, called the Kramers - Kronig analysis, makes it possible to find, with a certain degree of accuracy, the values of the frequencies of transverse and longitudinal optical phonons. It is only necessary to remember that neither one nor the other is recorded directly in the IR reflection spectra, since the latter are a consequence of the existence of polaritons, but not purely elastic waves in polar crystals. However, as we remember, "pure" *TO* and *LO* modes are observed in the Raman spectra, which at one time served was a powerful impetus for the development of the Raman method as a tool for studying the physics and chemistry of solids.

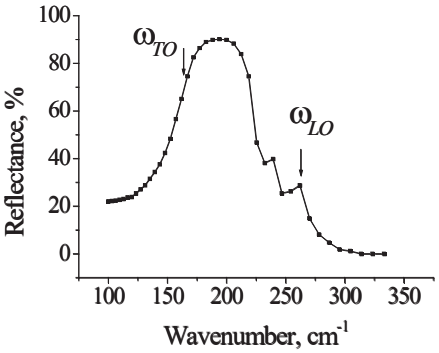

Fig. 3.11. Reflectance spectrum of NaCl crystal at room temperature [1].

The rather complicated theoretically problem of the appearance of polariton states in the IR spectrum of polar crystals is actually a special case of the general quantum-mechanical problem of the interaction of two states of the same or different symmetry, considered in [2], where it was shown that only terms of different symmetry can intersect.

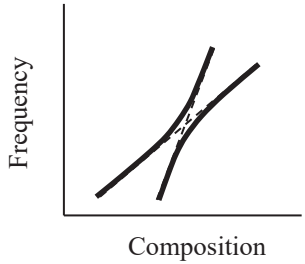

Fig. 3.12. Real behavior of two intersecting modes of the same symmetry (solid curves).

The states of the same symmetry do not intersect, leaving always a gap between themselves, as happens with photons and TO phonons in Fig. 3.10. Vibrational modes of the same symmetry behave in a similar way in a series of compounds (for example, solid solutions), in which their frequencies shift at different rates and, according to the experimental conditions, should intersect. In this case, the true frequency trajectory looks like that shown in Fig. 3.12.

CHAPTER 4

SYMMETRY OF VIBRATIONS OF MOLECULES AND CRYSTALS

4.1. Symmetry of molecular vibrations, symmetry coordinates and equivalent coordinates

Symmetry of vibrations is a central concept in vibrational spectroscopy. Internal vibrations of molecules and optical vibrations of crystals should occur in such a way that the center of gravity of the molecule (unit cell) does not shift. Consequently, the topology of the arrangement of atoms in a molecule, which determines its symmetry, imposes restrictions on the possible modes of vibrations, or, in other words, the displacement of atoms during vibrations must be closely related to the symmetry of the molecules. For example, consider the vibrations of the H_2O molecule. The symmetry group of the molecule is C_{2v} (Fig. 4.1). (See Appendix B).

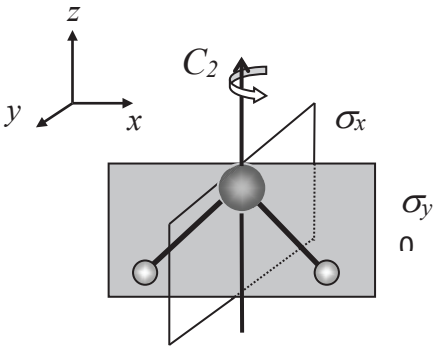

Fig. 4.1. Symmetry elements of the H_2O molecule

Let us choose natural internal coordinates, i.e. changes in bond lengths O–H, $q_{1,2}$, and angle H–O–H, q_α as vibrational coordinates (Fig. 4.2). Moreover, the stretching of the bond and the increase in the angle will be considered as positive changes in coordinates, and the shortening as a negative change.

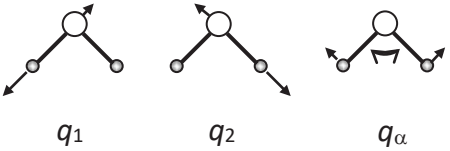

Fig. 4.2. Vibrational coordinates of the H_2O molecule

If we apply symmetry operations to the vibrational coordinates shown in Fig. 4.2, then when the molecule rotates by 180° about the z axis or is reflected in the σ_x plane, it is necessary to somehow describe the transition of the coordinate q_1 to q_2 and vice versa. For the H_2O molecule, this is possible, for example, by using second-order matrices. However, for molecules with the number of atoms N, where N can amount to several tens, the number of vibrational coordinates is also large and it is necessary to use rotation matrices of the order of $N \times N$, which will make the task difficult to fulfill. Therefore, they usually act in a different way.

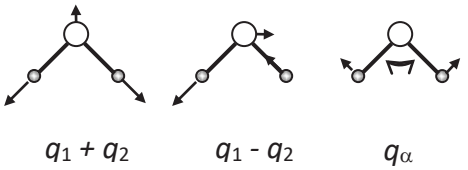

Fig. 4.3. Stretching vibrations of H_2O in the phase ($q_1 + q_2$), in antiphase ($q_1 - q_2$) and bending vibrations (q_α).

Since the O–H bonds are equivalent, the amplitude of the q_1 and q_2 vibrational coordinates are also equivalent. It is easy to imagine three possible vibrations of a water molecule: 1) both bonds are lengthened simultaneously, i.e. both bond lengths change in phase, and the total oscillation is $q_1 + q_2$; 2) one bond is lengthened, and the other is shortened (vibration of bonds in antiphase), $q_1 - q_2$; 3) changing the angle q_α (Fig. 4.3). These last combinations, i.e. ($q_1 + q_2$), ($q_1 - q_2$) and q_α, *can also be viewed as a set of vibrational coordinates along with the original set of* q_1, q_2 *and* q_α.

Consider the action of the symmetry operations of the C_{2v} group on each vibration (Table 4.1). When the molecule is rotated by 180° about the z axis (operation C_2), the oxygen atom remains in place, while the hydrogen atoms are swapped. But in this case, the behavior of the vectors of atomic displacement is of interest. In the ($q_1 + q_2$) vibration, the displacement vector of the oxygen atom is directed along the z axis and does not change upon rotation. The displacements of hydrogen atoms

change places, but at the same time they pass into each other in such a way that the overall picture of displacements does not change. In other words, if, in the case of using separate coordinates q_1 and q_2, it is necessary to find a way to describe the procedure for the transition from q_1 to q_2 and back under the action of a symmetry element, then when using the combination $(q_1 + q_2)$ this need disappears.

Table 4.1. The effect of symmetry operations of the C_{2v} group on atomic displacements in different vibrations

Symmetry Operations of C_{2v} group	$q_1 + q_2$	$q_1 - q_2$	q_α
$E \rightarrow$			
$C_2 \rightarrow$			
σ_y			
σ_x			
	A_1	B_1	A_1

The same thing happens with the vibration $(q_1 + q_2)$ and when using the operations σ_y, σ_x – the pattern of displacements remains unchanged. Thus, all symmetry operations of the C_{2v} group, including the identity E, do not change the vibration modes $(q_1 + q_2)$, and the coordinate $(q_1 + q_2)$ itself is called the *coordinate of symmetry*. They say that this vibration is *totally symmetric* and in the C_{2v} group it is denoted as A_1. A similar behavior is demonstrated by the bending vibration of H_2O with a vibrational coordinate q_α (Table 4.1) - it does not change for all symmetry operations and, therefore, is also totally symmetric. However, the

displacements of all atoms in vibration with the coordinate $(q_1 - q_2)$ change sign to the opposite under the action of C_2 and reflection in the σ_x plane, perpendicular to the plane of the molecule, and do not change sign under the action of the identity operation E and reflection in the σ_y plane, which coincides with the plane molecules (see Table 4.1). Otherwise,

$$(q_1 - q_2) \xrightarrow{E,\sigma_y} (q_1 - q_2) \text{ and } (q_1 - q_2) \xrightarrow{C_2,\sigma_x} -(q_1 - q_2).$$

This vibration is nonsymmetrical and is designated in the C_{2v} group as B_1. The property of vibrations to react differently to symmetry operations is fixed in the concept of *symmetry of vibrations*.

Thus, the symmetry of the vibration does not mean its normal coordinate, although it is directly related to the normal coordinate, but the transformation law (response) of atomic displacements during symmetry operations in a given point group.

It is important to note the following.

1. The initial internal coordinates of a molecule form groups of equivalent vibrational coordinates if they are transformed into each other under the action of symmetry operations. Thus, the q_1 and q_2 coordinates of the H_2O molecule form one group of equivalent vibrational coordinates and the only coordinate q_α – another. In low-symmetry objects, even among the coordinates of the same type, for example, angle deformations, it is possible to distinguish separate groups consisting of one or more coordinates, which also never transform into each other under the action of all symmetry operations in a given point group. So, in the molecule shown in Fig. 4.4, the coordinates (q_1, q_2), (q_3), (q_α) and $(q_{\beta1}, q_{\beta2})$ form different groups of equivalent vibrational coordinates.
2. In polyatomic molecules, when considering the action of symmetry operations, it is necessary to use not individual displacements of atoms, but their combinations that form the coordinates of symmetry. In our case, these are coordinates $(q_1 + q_2)$, $(q_1 - q_2)$ and q_α. The transition from natural internal coordinates to coordinates of symmetry is in fact fundamentally important, representing the possibility of analyzing vibrations based on the symmetry of molecules of any complexity. Coordinates of symmetry are constructed within each separate group of equivalent vibrational coordinates.

3. Under the action of the symmetry operations of the C_{2v} group, all three symmetry coordinates introduced for the H_2O molecule transform into themselves, with or without sign change, and do not transform into each other. As we will see below, this is an essential sign of nondegeneracy of vibrations.

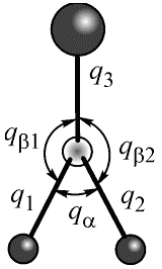

Fig. 4.4. Vibrational coordinates of a molecule with C_{2v} symmetry. Out-of-plane vibrational coordinates are not shown.

Looking ahead, we note that this circumstance greatly facilitates finding the frequencies of the normal vibrations of a molecule or crystal, since it allows us to reduce the matrices of dynamic and potential interactions in the secular equation (Chapter 3) to a block form.

4.2. Transformation matrixes of vibrational coordinates

The simplest actions that we performed with the coordinates of the H_2O molecule can be given a mathematical formulation, which is trivial, perhaps at this stage, but necessary in more complex cases. We will consider the sum $(q_1 + q_2)$ as the vibrational coordinate $Q(1)$. The invariability of the vibrational coordinate under the action of symmetry operations means that the transformation of this coordinate in all cases is reduced to its multiplication by the unit matrix of the first order:

$$Q'(1) \xrightarrow{E,C_2,\sigma_y,\sigma_x} (+1)\cdot Q(1) \qquad (4.1)$$

Matrices are usually characterized by their trace, or character, i.e. the sum of the diagonal elements. In our case, the characters of all transformation matrices of the coordinate $Q(1)$ under the action of the symmetry operations of the group C_{2v} are the same and equal +1. Let us denote the coordinate q_α as $Q(2)$, and $(q_1 - q_2)$ as $Q(3)$. Obviously, the characters of the transformation matrices $Q(2)$ are the same as the characters of $Q(1)$, and in the case of the coordinates $Q(3)$ the characters

of the operations E and σ_y are +1, and the characters of the operations C_2 and σ_x are equal to (–1). We can compile a table of the characters of the transformation matrices of the vibrational coordinates $Q(1)$, $Q(2)$, and $Q(3)$ of the water molecule (Table 4.2).

Table 4.2. Characters of transformation matrices for vibrational coordinates of H_2O

Coordinate	E	C_2	σ_y	Symmetry type
$Q(1)$	1	1	1	A_1
$Q(2)$	1	1	1	A_1
Q(3)	1	–1	1	B_1

4.3. Degenerate and nondegenerate vibrations

Let us now turn to another example, namely, the vibration of a flat square molecule AB_4 (Fig. 4.5).

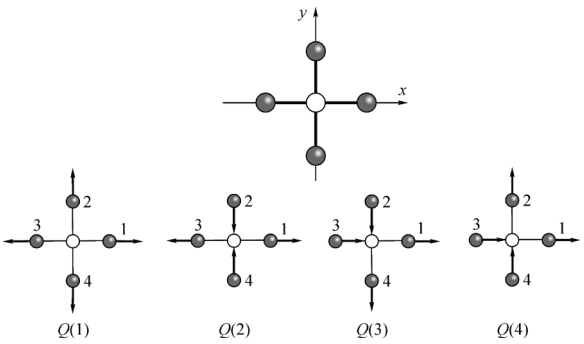

Fig. 4.5. Stretching vibrations of a square AB_4 molecule

The symmetry group of the molecule is D_{4h}. We will consider only stretching vibrations and neglect the displacement of the central atom so as not to complicate the picture. To describe the stretching of four bonds q_i, create the following symmetry coordinates (the order of construction symmetry coordinates is described in Appendix B):

$$\begin{aligned} Q(1) &= q_1 + q_2 + q_3 + q_4 \\ Q(2) &= q_1 - q_2 + q_3 - q_4 \\ Q(3) &= q_1 - q_2 - q_3 + q_4 \\ Q(4) &= q_1 + q_2 - q_3 - q_4 \end{aligned} \qquad (4.2)$$

If we do not do this, then the description of the response of the molecule to the action of symmetry operations would turn out to be too complicated even for such a small system, namely, we would have to determine how each of the coordinates q_1, q_2, q_3, q_4 transforms into each other for all operations symmetry. Introducing symmetry coordinates greatly simplifies this task. Thus, the coordinate $Q(1)$ goes over into itself and does not change sign for all symmetry operations of the group D_{4h}. Its transformation is thus described in all cases by the identity matrix with a trace +1. This is a fully symmetric vibration and is designated as A_{1g} in the D_{4h} group. The $Q(2)$ coordinate also goes into itself, but changes sign during the operations C_4, C_2'', S_4, and σ_d. This corresponds to vibration B_{1g}. Coordinate $Q(3)$ after rotation by 90° goes to coordinate $Q(4)$, and Q(4) – to [–Q(3)]. This transformation will be written in matrix form as

$$\begin{pmatrix} Q(3)' \\ Q(4)' \end{pmatrix} \overset{C_4}{\rightarrow} \begin{pmatrix} 0 & 1 \\ -1 & 0 \end{pmatrix} \begin{pmatrix} Q(3) \\ Q(4) \end{pmatrix}. \qquad (4.3)$$

This means the transformation matrix is a second-order matrix with a trace equal to 0. In other words, if Q(1) and Q(2) are transformed independently of others, then the coordinates Q(3) and Q(4) are transformed together under all symmetry operations of the group D_{4h} (Fig. 4.6).

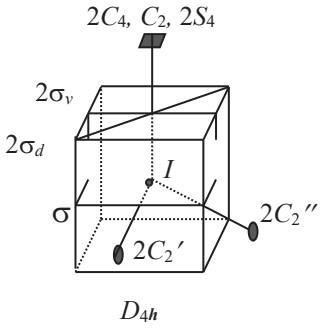

Fig. 4.6. Symmetry elements of the D_{4h} group

Due to the equivalence of the molecular coordinates x and y, the displacements $Q(3)$ and $Q(4)$ are physically equivalent, and the frequencies

of the corresponding vibrations are equal. The resulting vibration is called doubly degenerate, and the displacements $Q(3)$, $Q(4)$ are the components of one *twofold degenerate vibration*. Obviously, doubly degenerate vibrations appear only in systems where there are two equivalent molecular (crystallographic) directions, i.e. if there is an axis of rotation of the order of 3 or more. In cubic systems, where there are several C_3 axes and three equivalent directions, *threefold degenerate vibration* appears. In this case, there will always be at least one triple of vibrational coordinates that transform together, and the matrix of their transformation will be a matrix of the third order. An example of the components of a threefold degenerate vibration is shown in Fig. 4.7 for a molecule with point symmetry O_h.

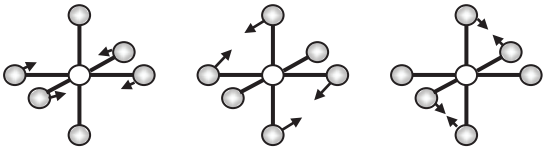

Fig. 4.7. Components of one threefold degenerate bending vibration of an octahedral molecule (point group O_h)

When the symmetry operation from the O_h group is applied to any of the depicted components of the triple degenerate vibration, the corresponding symmetry coordinate will go over to the neighboring one with or without a sign change. For example, when rotated by 120° about the axis, one component goes into the other without changing the sign and the transformation matrix is a matrix of the type

$$F_2 \quad \begin{pmatrix} 0 & 0 & 1 \\ 1 & 0 & 0 \\ 0 & 1 & 0 \end{pmatrix} \tag{4.4}$$

with a character equal to zero.

The degenerate vibration is observed in the spectrum as one line, and the real displacement of atoms in the degenerate vibration is the sum of the displacements in each component.

Thus, applying the concept of equivalent coordinates and constructing symmetry coordinates from them, we were able to describe their response to the action of symmetry operations in a very simple way, namely, by transformation using matrices of the first, second or third order, which for

non-degenerate vibrations is reduced to multiplying the symmetry coordinate by ±1.

4.4. Symmetry groups of molecules and crystals

Each molecule or crystal has a set of symmetry elements that characterize it as a symmetric object. Symmetry elements (or symmetry operations) are the *identity E*, *rotary axes of order n (turn of the first kind)*, *mirror-rotary axes S_n (turn of the second kind)*, *planes of symmetry*, *and center of symmetry (inversion)*. (For more details on the properties of symmetry of molecules, see Appendix B).

All elements of symmetry are linked by rules of multiplication, i.e. the sequence of any two operations is equivalent to the third. For example, multiplication (sequential application) of operations C_2 and σ is equivalent to inversion, i.e.

$$I = C_2^z \sigma_z = \sigma_z C_2^z. \tag{4.5}$$

An obvious consequence of the rules of multiplication is that the existence of some elements of symmetry in an object entails the presence of others. It also follows from this that from the entire sequence of symmetry elements applicable to a given figure, it is always possible to choose several *generating elements*, the successive application of which makes it possible to obtain all the remaining elements.

A complete set of symmetry elements that characterize an object forms a group, the mathematical properties of which are described by the properties of algebraic groups. These include:

1. The existence of the *composition law*, in which any two elements *A* and *B* from the set match the third element *C* of the same set, i.e. $AB = C$, where *C* is called product of *A* and *B*.
2. *Associativity*, i.e. $(AB)C = A(BC)$.
3. The existence of an *identity element E* (*a unit element, identity*) defined as $AE = EA = A$.
4. For each element *A* from the set, there is an inverse element A^{-1} such that $AA^{-1} = A^{-1}A = E$. Moreover, $(AB)^{-1} = B^{-1}A^{-1}$.

Depending on the number of elements forming the group, it can be finite or infinite. The number of operations in a finite group is called its order. If the elements of the group commute with each other, i.e. $AB = BA$, then the group is called *Abelian group*. The symmetry groups of crystals and molecules, where this rule is satisfied, are Abelian. Usually, all

symmetry operations of a molecule leave one point fixed, which would be the center of gravity of the molecule if atoms of the same mass are placed at its vertices. Therefore, the symmetry groups of molecules are often called *point groups*. In crystals, we are dealing with a *factor group*, where partial translations are added to the usual symmetry operations of point groups.

4.5. Incredible representations

As noted above, the set of symmetry operations that characterize a group has the properties of algebraic groups. It turns out that a set of transformation matrices of vibrational coordinates and their characters must also follow certain group rules. To describe these rules, the concept of irreducible representations is introduced, which belongs to the theory of representations of algebraic groups. It applies to all physical systems with symmetry properties, be they electronic, magnetic or vibrational states in molecules or crystals.

We assign to each symmetry element R of the point group $\Im$ a square regular matrix $\boldsymbol{M}(R)$, but in such a way that for any pair of elements

$$AB = C$$

the equality was fulfilled

$$\boldsymbol{M}(A)\boldsymbol{M}(B) = \boldsymbol{M}(C).$$

If we add properties such as associativity of multiplication to the above law of composition of matrices, i.e. $[\boldsymbol{M}(A)\boldsymbol{M}(B)]\boldsymbol{M}(C)=\boldsymbol{M}(A)[\boldsymbol{M}(B)\boldsymbol{M}(C)]$, and the existence of inverse matrices, then the totality of matrices $\boldsymbol{M}(R)$ is a *representation* of this point group. The order of the matrices $\boldsymbol{M}(R)$ is the *representation dimension*.

Let there be a molecule consisting of N atoms. Each atom performs thermal vibrations, and its displacement from the equilibrium position can be specified by three components of the polar vector. We can create matrices $\boldsymbol{M}(R)$ of transformations of these components under the action of the operations of the point symmetry group of the molecule, but now these will be square matrices ($3N \times 3N$). The dimension of this representation is $3N$, and the components of the atomic displacement vectors form its *basis*. Moving on to the internal coordinates of the molecule, i.e. bond lengths and angles, we can create another representation with dimension m (m is the total number of internal coordinates). Both of these representations are *reducible*. Their

reducibility lies in the fact that both the Cartesian and the internal coordinates of the molecule can be divided into groups of equivalent ones and the symmetry coordinates can be constructed from them. This, as we have seen, leads to the transformation under the action of the symmetry operations of the given point group using the transformation matrices of the first, second, or third order. The representations formed by these last matrices are called *irreducible*.

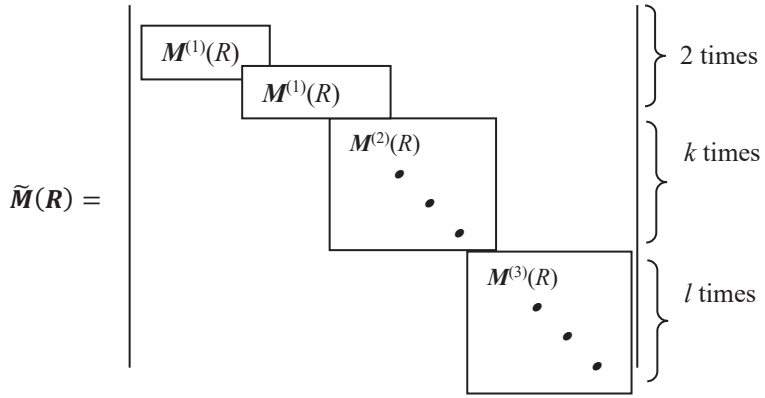

Fig. 4.8. Block view of the transformation matrix of the internal coordinates of a molecule, resulting from the transition to the symmetry coordinates

When passing from internal coordinates to symmetry coordinates, the original matrices $\boldsymbol{M}^{(m)}(R)$ of order m, generated on the basis of internal coordinates, are transformed to block form (Fig. 4.8), where $\boldsymbol{M}^{(1)}(R)$, $\boldsymbol{M}^{(2)}(\mathrm{R})$, and $\boldsymbol{M}^{(3)}(R)$ are matrices of order 1, 2, or 3 (but not higher, in any case, for molecules and crystals belonging to one of 32 crystal classes). In this case, the set of matrices $\boldsymbol{M}^{(i)}(R)$ for all symmetry operations R of this group constitutes one irreducible representation Γ_i of the group, which can occur in the general representation n_i times.

Irreducible representations of a group have the remarkable property that their characters do not depend on the method of obtaining and on what variables are their basis: be it the normal coordinates of a molecule, a crystal, or atomic wave functions forming molecular orbitals, etc.

Let's turn again to the example with a square molecule (see Fig. 4.5), whose symmetry group is D_{4h}. We saw how the coordinates $Q(1)$, $Q(2)$, $Q(3)$ and $Q(4)$ (the last two together) are transformed under the action of the operation C_4. Now consider the action of the rest of the symmetry elements of the D_{4h} group on these coordinates (Table 4.3).

Table 4.3. Coordinate transformation matrices $Q(1)$, $Q(2)$, $Q(3)$ and $Q(4)$ under the action of the symmetry operation of the group D_{4h}

$\boldsymbol{D_{4h}}$	E	$2C_4$	C_2	$2C_2'$	$2C_2''$	I	$2S_4$	σ_h	$2\sigma_v$	$2\sigma_d$
$\boldsymbol{M}_{Q(1)}$	(1)	(1)	(1)	(1)	(1)	(1)	(1)	(1)	(1)	(1)
$\boldsymbol{M}_{Q(2)}$	(1)	(–1)	(1)	(1)	(–1)	(1)	(–1)	(1)	(1)	(–1)
$\boldsymbol{M}_{Q(3),Q(4)}$	$\begin{pmatrix}1&0\\0&1\end{pmatrix}$	$\begin{pmatrix}0&1\\-1&0\end{pmatrix}$	$\begin{pmatrix}-1&0\\0&-1\end{pmatrix}$	$\begin{pmatrix}0&-1\\-1&0\end{pmatrix}$	$\begin{pmatrix}1&0\\0&-1\end{pmatrix}$	$\begin{pmatrix}-1&0\\0&-1\end{pmatrix}$	$\begin{pmatrix}0&1\\-1&0\end{pmatrix}$	$\begin{pmatrix}1&0\\0&1\end{pmatrix}$	$\begin{pmatrix}0&-1\\1&0\end{pmatrix}$	$\begin{pmatrix}1&0\\0&-1\end{pmatrix}$
Character	2	0	–2	0	0	–2	0	2	0	0

The last line of Table 4.3 shows the characters of the matrices $\boldsymbol{M}_{Q(3),Q(4)}$, but for the matrices $\boldsymbol{M}_{Q(1)}$ and $\boldsymbol{M}_{Q(2)}$ the characters coincide with the matrix elements themselves and therefore are not shown.

Some of the symmetry elements (the first row of the table) are presented with integer indices indicating the number of elements in this *class*. For example, $2C_4$ represents C_4 and C_4^3, $2C_2'$ represents C_2^x and C_2^y, and so on. The characters corresponding to the symmetry operations of one class (for a given representation) are the same, so they are combined with an indication of the number of elements. The structure and symmetry elements of the finite groups of 32 crystal classes are presented in Appendix B.

One can conclude from Table 4.3 that the sets of transformation matrices of Q_1, Q_2, etc. coordinates form various irreducible representations of the group D_{4h}.

In general, each point symmetry group has several different *types of irreducible representations*, differing from each other in how they react to symmetry operations in the given group. The types of irreducible representations that make up a point group, as well as the characters of the transformation matrices that make up the irreducible representations, are well known for each point group. Together they form the table of characters of the groups. Tables of characters of all point symmetry groups are given in Appendix D.

The sets of matrices presented in Table 4.3, constitute two one-dimensional and one two-dimensional irreducible representations of the group D_{4h}. The basis for the representation $\boldsymbol{M}_{Q(1)}(R)$ is $Q(1)$, $\boldsymbol{M}_{Q(2)}(R)$ – $Q(2)$, and for $\boldsymbol{M}_{Q(3),Q(4)}(R)$ – the pair $Q(3)$ and $Q(4)$. If we compare the sequences of characters $\chi(R)$ of each of the matrices with the sequences given in the table of characters for representations of the group D_{4h} (Table 4.4), then we can make sure that the set $\chi(R)$ for the matrices $\boldsymbol{M}_{Q(1)}$ coincides with the set of characters representation A_{1g}, $\chi(R)$ for matrices $\boldsymbol{M}_{Q(2)}$ coincides with the string of characters representation B_{1g}, and $\chi(R)$ for matrices $\boldsymbol{M}_{Q(3),Q(4)}$ coincides with E_u. In other words, the representation constructed on the basis $Q(1)$ refers to the A_{1g} irreducible representation of the group D_{4h}, the representation with the basis $Q(2)$ refers to B_{1g}, etc.[5]

[5] As you can see from Table 4.4, the group D_{4h} consists of 10 different irreducible representations. Other irreducible representations for a square AB_4 molecule can be obtained using the remaining symmetry coordinates.

Table 4.4. Characters of irreducible representations of the group D_{4h}

D_{4h}	E	$2C_4$	C_2	C_2'	$2C_2''$	I	$2S_4$	σ_h	$2\sigma_v$	$2\sigma_d$	
A_{1g}	1	1	1	1	1	1	1	1	1	1	
A_{2g}	1	1	1	−1	−1	1	1	1	−1	−1	R_z
B_{1g}	1	−1	1	1	−1	1	−1	1	1	−1	
B_{2g}	1	−1	1	−1	1	1	−1	1	−1	1	
E_g	2	0	−2	0	0	2	0	−2	0	0	(R_x, R_y)
A_{1u}	1	1	1	1	1	−1	−1	−1	−1	−1	
A_{2u}	1	1	1	−1	−1	−1	−1	−1	1	1	T_z
B_{1u}	1	−1	1	1	−1	−1	1	−1	−1	1	
B_{2u}	1	−1	1	−1	1	−1	1	−1	1	−1	
E_u	2	0	−2	0	0	−2	0	2	0	0	(T_x, T_y)

Thus, considering the actions of symmetry operations on the displacements of atoms in a molecule during vibration, we came to the conclusion that all internal vibrational coordinates (bond lengths and angles) can and should be divided into groups of equivalent coordinates, i.e. such coordinates that are transformed into each other under the action of symmetry operations. It is these coordinates, in the case of the correct alternation of their changes, that provide the main condition for any vibrational mode - the absence of a shift in the center of gravity of the molecule during vibration. Then, in each group of equivalent coordinates, we constructed the symmetry coordinates and found that the transformation of the latter under the action of symmetry operations is described especially simply by matrices of the first (for nondegenerate vibrations), second (for twofold degenerate), or third (for threefold degenerate vibrations) order. These matrices generate irreducible representations of the point symmetry group to which the molecule refers, and the characters of the transformation matrices are a characteristic of the group, not the composition of the molecule or the basis of the representation, and therefore are known in advance for each point group.

Thermal vibrations of atoms in a molecule or crystal (just those that are found as thermal ellipsoids of atoms in the description of the structure of the compound) are not chaotic, but represent the sum of separate normal vibrations, each of which obeys the symmetry conditions of the system and is based on symmetry coordinates. In this case, the transformation matrices of the normal coordinates of vibrations constitute irreducible representations of the corresponding point group of the molecule or the factor group of the crystal. This means that each vibrational mode in the spectrum corresponds to one irreducible representation of the system, and all together they form a vibrational spectrum corresponding to the complete vibrational representation Γ of the system. The displacements of atoms in the vibrational mode, in other words, the symmetry of the mode, are specified by the corresponding irreducible representation of the group. Irreducible representations are indicated by uppercase letters with subscript and superscript characters (A, B - one-dimensional representations, E - two-dimensional, and F - three-dimensional). Letter symbols indicate symmetry or asymmetry with respect to certain symmetry operations in a given group, so they change slightly when going from one point group to another.

To classify the vibrational spectrum of a compound according to symmetry (or, as they say, a group-theoretical analysis of vibrations), means to find which irreducible representations Γ_i and in what number are found in the general representation Γ. It turns out that for this it is not

necessary to compose the matrices of the complete representation $\boldsymbol{M}(R)$ each time, and then carry out their reduction, as was schematically done above. A detailed discussion of how the symmetry analysis of molecular or crystal vibrations is carried out is the subject of the next chapter.

Thus, the symmetry operations R_j of the point group $\mathfrak{I}$ are related to each other in the same way as the elements of the algebraic group are related. On the other hand, symmetry operations transform the normal coordinates Q_i of the molecule, and the transformation matrices $\boldsymbol{M}^{(i)}(R_j)$ obey the rules of the same algebraic group. The set of matrices $\boldsymbol{M}^{(i)}$ corresponding to all symmetry operations R_j of a given point group forms an irreducible representation Γ_i of this group. All irreducible representations of the group constitute a complete representation Γ of the group. The characters of the transformation matrices forming an irreducible representation do not depend on the basis of the representation or the chemical composition of the molecule. Each normal vibration is characterized by its own set of matrices $\boldsymbol{M}_i$ and its own irreducible representation (type of symmetry). Thus, in order to find out how many normal vibrations of each type of symmetry can appear in the total vibrational spectrum of a molecule or crystal, it is necessary to find out which and how many irreducible representations Γ_i of the point group $\mathfrak{I}$ are contained in the complete representation Γ of this group.

4.6. Symmetry of crystal vibrations

The procedure for determining the symmetry of crystal vibrations is somewhat different from that considered for molecular vibrations in the previous chapter. The fact is that the vibrations of crystal are formed from the Cartesian displacements of each of the atoms that make up its lattice. But the symmetry of these displacements is determined not by the crystal group, but by the site symmetry group of the given element in the lattice.

Let us consider the symmetry of ion vibrations in the crystal lattice and external vibrations of the molecules in the structure – translational and librational (restricted rotations). For molecules, these vibrations are observed in two cases: when the molecule is a fragment of the crystal lattice of an ion-molecular (molecular) crystal, or when the molecule is in the crystal cavity, i.e. is a "guest" in the "host" lattice. In the liquid phase, translations and librations are most often very wide structureless bands, while in gas there are only the rotational states of the molecules.

The displacement of ions or molecular fragments in a crystal is specified by a polar vector. The x, y, and z components of the polar vector are transformed by symmetry operations in the same way as the corresponding

coordinate axes. Consequently, to find the type of symmetry of translational vibrations in a crystal, it is sufficient to consider the order of transformation of the coordinate axes under the action of symmetry operations of the point group of site symmetry. (See also Chap. 5). Molecular librations are described by an axial vector showing the direction of rotation according to the "screwdriver rule" (Fig. 4.9). Rotation of this rotating figure around any axis by an angle θ will change the direction of the axial vector in the same way as the polar one, and the effect of symmetry operations of the first kind on both vectors is the same.

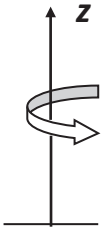

Fig. 4.9. Image of librational vibration using an axial vector

Operations of the second kind (reflection, inversion) operate in different ways. Thus, reflection in the σ_z plane does not change the direction and amplitude of the rotation shown in Fig. 4.9, and, therefore, does not change the axial vector itself (we must observe the behavior of the direction of rotation when reflected, not the arrows of the axial vector!). At the same time, the polar vector directed along z will reverse direction when reflected in the σ_z plane. Since the inversion is $I = \sigma_z C_2^z$, the action of the inversion rotation on the polar and axial vectors will also be opposite in sign. Thus, the components of the axial vector are transformed similarly to the components of the polar vector in symmetry operations of the first kind, and with the opposite sign for symmetry operations of the second kind.

Now it is easy to find the type of symmetry of translational and librational modes in a given point group. To do this, it is necessary to find the transformation matrices of the components of the polar and axial vectors and the corresponding characters and compare the latter with the known table of characters of the given point group. As an example, we will consider the external vibrations of an H_2O molecule (C_{2v} group) enclosed in a crystal cavity (Fig. 4.10), or the external vibrations of a molecular ion occupying a position in the lattice with the C_{2v} symmetry.

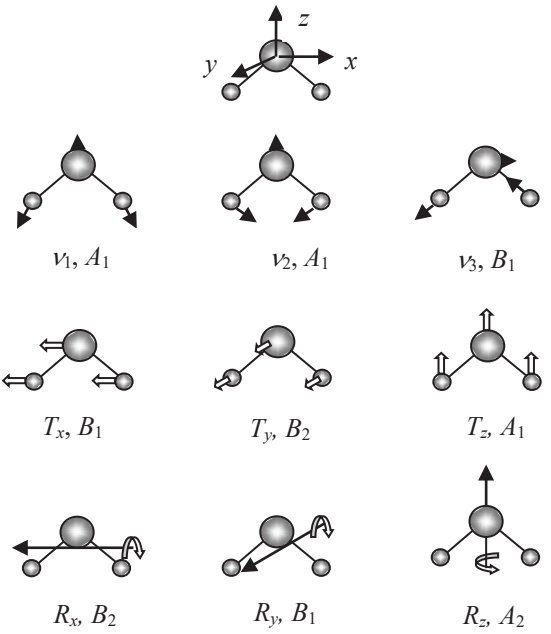

Fig. 4.10. Internal and external vibrations of H_2O

The characters of the transformation matrices under the action of the symmetry operations of the C_{2v} group on the displacements and rotations of the water molecule are given in Table 4.5.

Each of the character sequences of the transformation matrices under the action of symmetry operations matches one of the character sequences of irreducible representations contained in the table of characters of the group C_{2v} (Appendix D). The last column of Table 4.5 indicates the type of these representations.

Table 4.5. The action of symmetry operations on external vibrations of H_2O

	E	C_2^z	σ_y	σ_x	Symmetry
T_x	1	−1	1	−1	B_1
T_y	1	−1	−1	1	B_2
T_z	1	1	1	1	A_1
R_x	1	−1	−1	1	B_2
R_y	1	−1	1	−1	B_1
R_z	1	1	−1	−1	A_2

Until now, speaking about the symmetry of vibrations, we meant vibrations of molecules (or structural fragments of a crystal cell) according to their site symmetry. The vibrations of the totality of atoms and molecular fragments that make up a unit cell obey the symmetry of the cell (crystal). There is no need to consider them separately, since crystal vibrations from the point of view of their symmetry obey the same rules as molecular vibrations.

CHAPTER 5

ANALYSIS OF MOLECULAR AND CRYSTALLINE VIBRATIONS BY SYMMETRY

5.1. Analysis of molecular vibrations

As shown above, in order to calculate the number of vibrational modes and their symmetry in the total vibrational spectrum of a molecule or crystal, we must find which irreducible representations – and in what quantity – form a complete representation of a given point group. The set of irreducible representations Γ_i for any compound of the symmetry group $\mathfrak{I}$ is uniquely determined by this group itself and is known for each group. Therefore, the vibrational representations of all chemical compounds described by the same symmetry group will of course consist of the same irreducible representations. The individuality of a compound, characterized by the number of atoms and their geometrical arrangement in a molecule or unit cell of a crystal, manifests itself only in the number n_i of irreducible representations Γ_i, which appears in a complete representation. The general rule is that one-dimensional representations appear in all symmetry groups, two-dimensional in rhombohedral and higher groups, and three-dimensional only in cubic systems.

In the general case, applicable for any physical systems possessing symmetry properties, the number n_i of irreducible representations of each type (i.e., the number of vibrational modes of each type of symmetry) in the full representation is determined by the so-called magic formula (5.1)

$$n_i = \frac{1}{g}\sum_R \chi^{(i)}(R)^* \chi(R), \tag{5.1}$$

where g is the order of the group (the total number of symmetry elements, including identity), $\chi^{(i)}(R)$ the characters of the matrices of irreducible representations of the point group (factor group) $\mathfrak{I}$, and $\chi(R)$ the characters of the transformation matrices of the considered molecule or crystal. If the first two quantities, i.e. g and $\chi^{(i)}(R)$, are characteristics of

the group, then $\chi(R)$ reflects the individuality of the molecule, its topology and composition.

The characters of the irreducible representation $\chi^{(i)}(R)$ are known for each group and are given in Appendix D. The characters of the transformation matrices $\chi(R)$ can be calculated using the expression

$$\chi(R) = U_R\,(\pm 1 + 2\cos\theta_R), \tag{5.2}$$

where U_R is the number of atoms in a molecule (unit cell) that do not change their positions under the symmetry operation R, and θ_R is the rotation angle under the symmetry operation. The expression in parentheses is

$1 + 2\cos\theta$ for rotation through an angle θ,
$-1 + 2\cos\theta$ for reflection and subsequent rotation.

Expressions (5.1) and (5.2) admit a simple and easy-to-remember interpretation. Indeed, if any atom does not change its position under the action of the symmetry operation, then in the corresponding transformation matrix at the intersection of the row and column related to the position of the given atom (i.e., on the diagonal), there will be 1, and for the atom moving to another position there will be 0. Therefore, the character of the transformation matrices is simply equal to the number of atoms remaining in place during the symmetry operation (the number of ones on the diagonal). The factor $(\pm 1 + 2\cos\theta R)$ in (5.2) is the trace of the rotation matrix (see Appendix G) through an angle θ with or without reflection.

The calculation procedure is quite simple for molecules and consists of sequentially finding all the numerical parameters necessary for formula (5.1) to be applied. As an example, let us analyze the vibrations of the SiO4 tetrahedron.

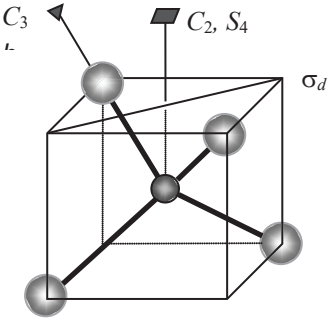

Fig. 5.1. Symmetry elements of the T_d group

Step 1. Determination of the symmetry group. This information is either known in advance, or can be easily found from the definition of a set of molecular symmetry elements (see Appendix B). For symmetry group SiO_4 – T_d see Fig. 5.1.

Step 2. Drawing up a table to determine the characters $\chi(R)$ of transformation matrices SiO_4 (Table 5.1):

Table 5.1. Determination of the characters $\chi(R)$ of the transformation matrices of the SiO4 tetrahedron

T_d	E	$8C_3$	$3C_2$	$6S_4$	$6\sigma_d$
θ_R, degrees	0	120	180	90	0
$2\cos\theta_R$	2	–1	–2	0	2
$\pm1 + 2\cos\theta_R$	3	0	–1	–1	1
U_R	5	2	1	1	3
$\chi(R)$	15	0	–1	–1	3

The operation of identity E leaves all five atoms of the molecule in their positions (in place), $U_R = 5$. Any of the eight C_3 axes of the third order leaves only two atoms in their positions, and so on. The line $\chi(R)$ is the product of the two previous lines of the table.

Step 3. Table of characters of the T_d group (Appendix D, Table 5.2). Two comments are appropriate for working with the table. First: The symbol T indicates the symmetry of the translational displacement of the entire SiO_4 tetrahedron or translational vibration of atoms in crystal lattice, and the symbol R – the symmetry of the rotational motion of the molecular fragment. Second: When counting the number of irreducible representations, each character value must be multiplied by the number of corresponding symmetry elements.

Table 5.2. Table of characters of the T_d group

T_d	E	$8C_3$	$3C_2$	$6S_4$	$6\sigma_d$	
A_1	1	1	1	1	1	
A_2	1	1	1	–1	–1	
E	2	–1	2	0	0	
F_1	3	0	–1	1	–1	$R(R_x, R_y, R_z)$
F_2	3	0	–1	–1	1	$T(T_x, T_y, T_z)$

Step 4. Counting the number of irreducible representations for the SiO_4 tetrahedron:

$$n(A_1) = \frac{1}{24}(15 - 3 - 6 + 18) = 1$$
$$n(A_2) = \frac{1}{24}(15 - 3 + 6 - 18) = 0$$
$$n(E) = \frac{1}{24}(30 - 6) = 1$$
$$n(F_1) = \frac{1}{24}(45 + 3 - 6 - 18) = 1 - R = 0$$
$$n(F_2) = \frac{1}{24}(45 + 3 + 6 + 18) = 3 - T = 2$$

We excluded one libration and one translation from the threefold degenerate vibrational modes of the F_1 and F_2 types, respectively, since the latter do not refer to internal vibrations. The final complete vibrational representation is

$$\Gamma = 1(A_1) + 1(E) + 2(F_2).$$

A_1, E, and F_2 modes are active in Raman spectra and only F_2 modes are active in IR (Appendix E).

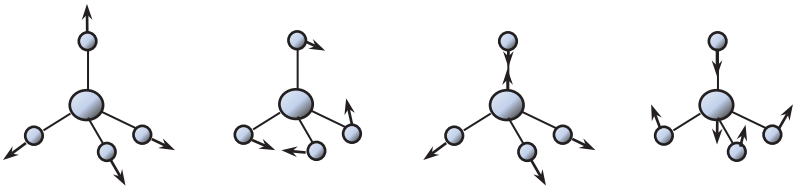

ν_1, A_1 ν_2, E ν_3, F_2 ν_4, F_2

Fig. 5.2. Vibrational modes of the SiO_4 tetrahedron

5.2. Analysis of crystal vibrations

The analysis of crystal vibrations in terms of symmetry can be done on the basis of a general method similar to that described above. This is the so-called Baghavantam–Venkatarayudu method, named after the Indian physicists who proposed it [1]. However, it turned out to be too complicated and inconvenient to use. Another approach, proposed by R. Halford and based on correlations between the positional symmetry of structural elements in the crystal lattice and the crystal symmetry [2], has proved to be much simpler and more efficient. These correlations always exist, since the positional symmetry group is a subgroup of the crystal factor group.

To analyze the vibrations of a crystal, it is necessary to know the factor group of the crystal, the coordinates of the atoms in the unit cell, and the number of formula units. In almost all cases, the analysis requires reference to International Tables for Crystallography (hereinafter ITC).

Chemical bonds in crystals can be divided into covalent, ionic, molecular and mixed ionic-covalent. For example, all silicates are the crystals with mixed ionic-covalent bonding and with isolated or interconnected SiO_4 tetrahedra. Since the force constants of Si–O bonds are usually much larger than the force constants of the cation–cation or cation–anion bonds, the vibrational modes of the corresponding structural elements are characterized by significantly different energies and can be considered as independent. For this reason, all vibrations can be divided into external (vibrations of monoatomic ions and molecular fragments as whole units) and internal (stretching and bending vibrations of a molecular fragment). Symmetry analysis is carried out separately for crystalline and intramolecular vibrations.

The general procedure of the analysis is as follows: to determine the number and symmetry of external (crystal) vibrations. First of all, the site (positional) symmetry of each structural element is determined. Then, correlations are found between the irreducible representations of the site symmetry group and the factor group of the crystal. After that, in the group of positional symmetry, those irreducible representations are noted to which translations (ions and molecular units) and librations (molecular units) refer. The displacements of atoms in crystals during the vibration process are translational displacements along x, y, and z; therefore, only those modes that refer to translations in the positional symmetry group form crystal vibrations. Motions of molecular fragments are described as displacements and restricted rotations; therefore, in the group of site symmetry of molecules, it is necessary to note irreducible representations, which include translations and librations in this group. All this information

is contained in the table of the characters of the group (see Appendix D). To determine the number and symmetry of internal vibrational modes of molecular fragments, it is necessary to draw up a diagram (or table) of correlations between the irreducible representations of the symmetry group of a free molecule, the positional symmetry group, and the factor group of the crystal.

Example 1. First of all, let us consider the simplest case – namely, we will analyze the vibrations of isostructural crystals of silicon, diamond and germanium.

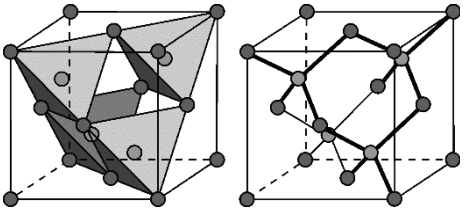

Fig. 5.3. Unit cell of silicon, diamond or germanium

Step 1. The symmetry group of the crystal is $Fd3m = O_h^7$ (227).

Step 2. A primitive crystal cell contains two silicon atoms. Each silicon atom is in the center of a tetrahedron formed by neighboring atoms (Fig. 5.3). For this reason, all the symmetry elements of the tetrahedral group pass through the silicon atom and the symmetry of the Si position in the lattice is T_d. The same follows from the information contained in the ITC for the $Fd3m = O_h^7$ (227) group.

Step 3. Correlations between the irreducible representations of the crystal group and the positional symmetry group can be obtained from the correlation listed in Table 5.3 (all the correlation tables are given in Appendix E).

Table 5.3. Correlation between irreducible representations of T_d and O_h groups.

O_h	T_d	
A_{1g}	A_1	
A_{2g}	A_2	
E_g	E	
F_{1g}	F_1	
F_{2g}	F_2	$T\,(T_x,\ T_y,\ T_z)$
A_{1u}	A_2	
A_{2u}	A_1	
E_u	E	
F_{1u}	F_2	$T\,(T_x,\ T_y,\ T_z)$
F_{2u}	F_1	

From the table of correlations (Table 5.3) it follows that the displacements T_x, T_y, and T_z of the silicon atom in the lattice of the silicon crystal form one threefold degenerate representation of F_2 in the positional symmetry group. This representation generates two threefold degenerate representations, i.e. F_{2g} and F_{1u}, in the crystal group. Hence the complete vibrational representation of the silicon crystal

$$\Gamma = 1F_{2g} + 1F_{1u}.$$

One of these representations, namely F_{1u}, describes the T_x, T_y, and T_z translations of the crystal unit cell, i.e. acoustic modes in the center of the Brillouin zone with a zero-wave vector (or, in other words, the displacement of the crystal as a whole, which is not a vibration). This follows from the table of characters for the O_h group. Therefore, for optical vibrations of silicon, we obtain

$$\Gamma = 1F_{2g} + 1F_{1u}\,(-1T) = F_{2g}.$$

It should be noted that the presence of optical vibrations in a monatomic crystal is a consequence of the fact that a primitive cell contains two silicon atoms. The Raman spectrum of crystalline silicon is shown in Fig. 5.4.

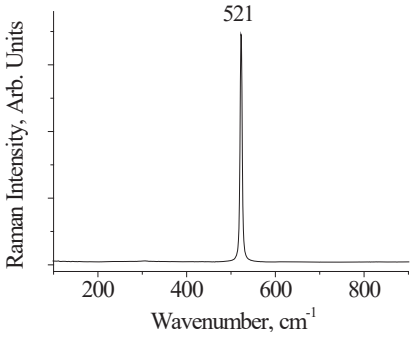

Fig. 5.4. Raman spectrum of crystalline silicon

Example 2. Garnet crystal. The unit cell of a garnet (Fig. 5.5) is very complex, and the symmetry analysis of its vibrations involves almost all the difficulties that can be encountered in the analysis of different versions of simpler ion-molecular lattices.

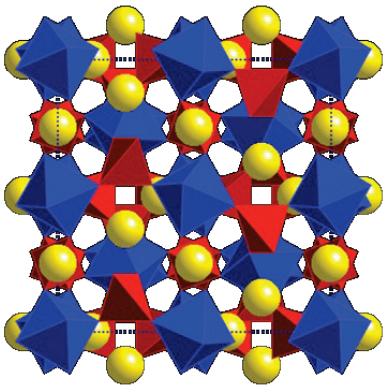

Fig. 5.5. Elementary cell of a garnet. Yellow balls – X^{2+} cations, blue octahedra of oxygen atoms contains Y^{3+} positions, red tetrahedra – SiO_4 groups.

Step 1. The general chemical formula of garnets is $X_3^{2+}Y_2^{3+}$ $(SiO_4)_3$ (X = Mg, Fe^{2+}, Mn^{2+}, Ca; Y = Al, Cr^{3+},Fe^{3+}). The factor-group of the crystal is $Ia\bar{3}d = O_h^{10}$ $(230), Z = 8$. The unit cell includes two primitives.

Step 2. The symmetry of the position of structural elements is shown in Table. 5.4. This information is usually represented in the original article on the structure of the compound, but even if only the coordinates of the atoms are indicated, the symmetry of the position of each element can easily be found from the ITC tables. For example, X^{2+} cations are located in the center of oxygen dodecahedrons. The multiplicity of their positions is 24 (three atoms in each formula unit, a total of eight formula units in a unit cell). According to ITC, there are two different 24-fold Wyckoff positions in the garnet structure, i.e. position *c* with symmetry 222 (D_2) and position *d* with symmetry $\bar{4}$ (S_4). The X^{2+}coordinates (0, 1/4, 1/8), however, only match the first one. Y^{3+} occupy octahedral positions (multiplicity 16, symmetry S_6), Si atoms are located in tetrahedral positions (multiplicity 24, symmetry S_4), and oxygen atoms occupy general positions.

Table 5.4. Coordinates and positional symmetry of structural elements in the garnet lattice

Element of structure	Coordinate	Number of positions	Wyckoff notation	Positional symmetry
X^{2+}	0, 1/4, 1/8	24	*c*	$222 = D_2$
Y^{3+}	0, 0, 0	16	*a*	$3i = C_{3i} \equiv S_6$
Si	3/8, 0, 1/4	24	*d*	$\bar{4} = S_4$
O	*x, y, z*	96	*h*	$1 = C_1$

Step 3. Determination of correlations.

As already mentioned, the positional symmetry group is a subgroup of the crystal factor group. For this reason, there is always a correlation between the irreducible representations of both symmetry groups – positional and crystal. The only difficulty is that sometimes there are several different paths leading to a possible correlation, and it is necessary to choose the only correct one. The last remark is especially important for garnet crystals due to their high symmetry and large number of symmetry operations, which make it difficult to choose the correct correlation.

The X^{2+} position is the most problematic, since there is no direct correlation between the O_h group of the crystal and the D_2 group of the positional symmetry of the cation, but only through the intermediate groups O, T_d, T_h, and D_{4h} (Fig. 5.6). Correlations drawn through each of the intermediate groups are not equivalent. There is only one criterion for choosing the "correct" intermediate group from several possible ones: all three groups - initial, intermediate and final - must have common elements of symmetry.

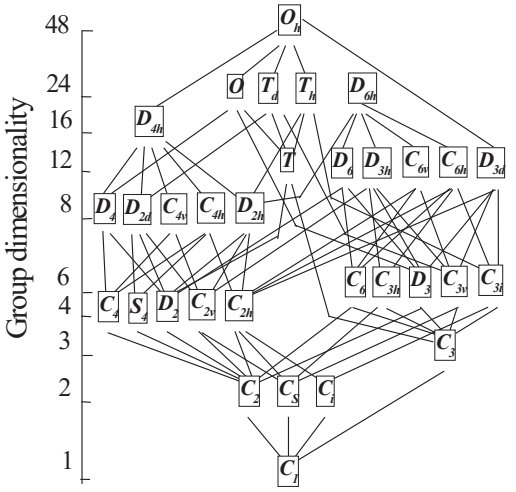

Fig. 5.6. "Tree" of correlations between different symmetry groups (from ITC)

Position X^{2+} (0, 1/4, 1/8) lies at the intersection of three rotary axes of the 2nd order: two diagonal and one C_2^z (Fig. 5.7). All three axes are symmetry elements of the X^{2+} positional symmetry group. But the groups T_d and T_h, considered as intermediate ones, do not have diagonal axes of the second order at all (for the symmetry elements of the group T_d see Appendix B) and correlations through these groups will yield to erroneous results. The remaining groups, D_{4h} and O, can both be used to find correlations, but the former is more convenient for this purpose.

This is one "bottleneck" in the choice of correlations. Another is that correlations between D_{4h} and D_2 can be carried out either through the common axes C_2' or C_2'' (see correlation tables, Appendix E). It is clear, however, that only the diagonal axis C_2'' of the group D_{4h} is common with the diagonal axis of the second order, which characterizes the position of X^{2+} in the garnet lattice (Fig. 5.7). Hence, the table of correlations between all three groups (Table 5.5-1) is as follows.

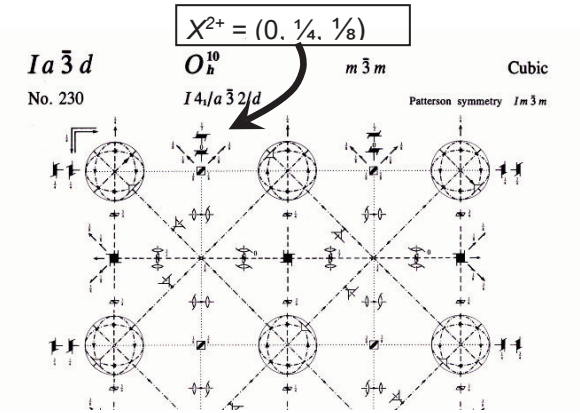

Fig. 5.7. Position of symmetry elements in a $Ia\bar{3}d = O_h^{10}$ group (fragment of a figure from ITC)

Table 5.5-1. Correlations between groups O_h and D_2 via intermediate group D_{4h}

O_h	D_{4h}	$D_2\,(C_2 \rightarrow C_2'')$
A_{1g}	A_{1g}	A
A_{2g}	B_{1g}	B_1
E_g	$A_{1g} + B_{1g}$	$A + B_1$
F_{1g}	$A_{2g} + E_g$	$B_1 + B_2 + B_3$
F_{2g}	$B_{2g} + E_g$	$A + B_2 + B_3$
A_{1u}	A_{1u}	A
A_{2u}	B_{1u}	B_1
E_u	$A_{1u} + B_{1u}$	$A + B_1$
F_{1u}	$A_{2u} + E_u$	$B_1 + B_2 + B_3$
F_{2u}	$B_{2u} + E_u$	$A + B_2 + B_3$

Now it is necessary to determine those irreducible representations in the D_2 group that characterize the translational displacements of X^{2+} cation. For this purpose, we turn to the tables of characters of the group D_2 (see Appendix D). It is easy to see that T_z translations have B_1 symmetry, T_y - B_2, and T_x - B_3 symmetry. This means that only the B_1, B_2, and B_3 irreducible representations of the positional symmetry group X^{2+} generate vibrational modes in the crystal, and we can rewrite the previous correlation table (Table 5.5-1) as follows (Table 5.5-2). In the latter table, the irreducible representations of the D_2 group generating the X^{2+} vibrations of the cation in the crystal are underlined. Each of the underlined irreducible representations of the site group gives one irreducible representation in the crystal group, i.e. each translational mode in D_2 gives one vibration in O_h, and we can add another column to the last table showing the number of vibrational modes in the crystal lattice produced by the X^{2+} cation.

Table 5.5-2

O_h	D_{4h}	$D_2\,(C_2 \rightarrow C_2'')$	
A_{1g}	A_{1g}	A	
A_{2g}	B_{1g}	$\underline{B_1}$	T_z
E_g	$A_{1g} + B_{1g}$	$A + \underline{B_1}$	T_z
F_{1g}	$A_{2g} + E_g$	$\underline{B_1 + B_2 + B_3}$	T_z, T_y, T_x
F_{2g}	$B_{2g} + E_g$	$A + \underline{B_2 + B_3}$	T_y, T_x
A_{1u}	A_{1u}	A	
A_{2u}	B_{1u}	$\underline{B_1}$	T_z
E_u	$A_{1u} + B_{1u}$	$A + \underline{B_1}$	T_z
F_{1u}	$A_{2u} + E_u$	$\underline{B_1 + B_2 + B_3}$	T_z, T_y, T_x
F_{2u}	$B2u + E_u$	$A + \underline{B_2 + B_3}$	T_y, T_x

From here we can write a representation of X^{2+} translational modes in the garnet lattice:

$$\Gamma(X^{2+}) = 1A_{2g} + 1E_g + 3F_{1g} + 2F_{2g} + 1A_{2u} + 1E_u + 3F_{1u} + 2F_{2u}.$$

Finding correlations between local groups Y^{3+} and SiO_4, on the one hand, and the factor-group of the crystal, on the other, does not cause difficulties and can be carried out by the reader independently. After that, you can write the final table for external vibrations in the garnet (Table 5.6).

Table 5.6. Correlation table of symmetry types of groups O_h, D_2, C_{3i} and S_4

O_h	X^{2+} (D_2, $C_2 \rightarrow C_2''$)		Y^{3+} (C_{3i})		SiO_4 (S_4)		N
A_{1g}	A		A_g		$\underline{A}$	R_z	1
A_{2g}	$\underline{B_1}$	T_z	A_g		$\underline{B}$	T_z	2
E_g	$A+\underline{B_1}$	T_z	$E_g(1)+E_g(2)$		$\underline{A+B}$	$T_z\ R_z$	3
F_{1g}	$\underline{B_1+B_2+B_3}$	T_x,T_y,T_z	$A_g+E_g(1)+E_g(2)$		$\underline{A+E(1)+E(2)}$	$T_x,T_y;\ R_x,R_y,R_z$	8
F_{2g}	$A+\underline{B_2+B_3}$	T_x,T_y	$A_g+E_g(1)+E_g(2)$		$\underline{B+E(1)+E(2)}$	$R_x,R_y;\ T_x,T_y,T_z$	7
A_{1u}	A		$\underline{A_u}$	T_z	$\underline{B}$	T_z	2
A_{2u}	$\underline{B_1}$	T_z	$\underline{A_u}$	T_z	$\underline{A}$	R_z	3
E_u	$A+\underline{B_1}$	T_z	$\underline{E_u(1)+E_u(2)}$	T_x,T_y	$\underline{B+A}$	$T_z;\ R_z$	5
F_{1u}	$\underline{B_1+B_2+B_3}$	T_x,T_y,T_z	$\underline{A_u+E_u(1)+E_u(2)}$	T_x,T_y,T_z	$\underline{B+E(1)+E(2)}$	$R_x,R_y;\ T_x,T_y,T_z$	11
F_{2u}	$A+\underline{B_2+B_3}$	T_x,T_y	$A_u+\underline{E_u(1)+E_u(2)}$	T_x,T_y,T_z	$\underline{A+E(1)+E(2)}$	$T_x,T_y;\ R_x,R_y,R_z$	10

Two remarks on the Table 5.6: firstly, molecular formations such as SiO_4 tetrahedrons contribute to the overall vibrational representation not only by translational displacements in the local symmetry group, but also by restricted rotations (R_x, R_y, R_z); secondly, the twofold degenerate representations of E in the positional groups C_{3i} and S_4 are complex conjugate pairs, and the components of these pairs should be regarded as distinct from each other. For this reason, they are referred to as $E(1)$ and $E(2)$ and should be considered as individual representations.

We can now write a vibrational representation for external (crystalline) vibrations in garnet:

$$\Gamma_{\text{external}} = A_{1g} + 2A_{2g} + 3E_g + 8F_{1g} + 7F_{2g} + 2A_{1u} + 3A_{2u} + 5E_u + 11F_{1u} + +10F_{2u}.$$

Step 4. Analysis of the internal (molecular) vibrations of the SiO_4 tetrahedron is also based on correlations between the symmetry of a hypothetical free molecule, positional symmetry, and crystal symmetry. In

addition to the tabular one, you can use the geometric scheme of these correlations [3], which is often found in the literature (Fig. 5.8).

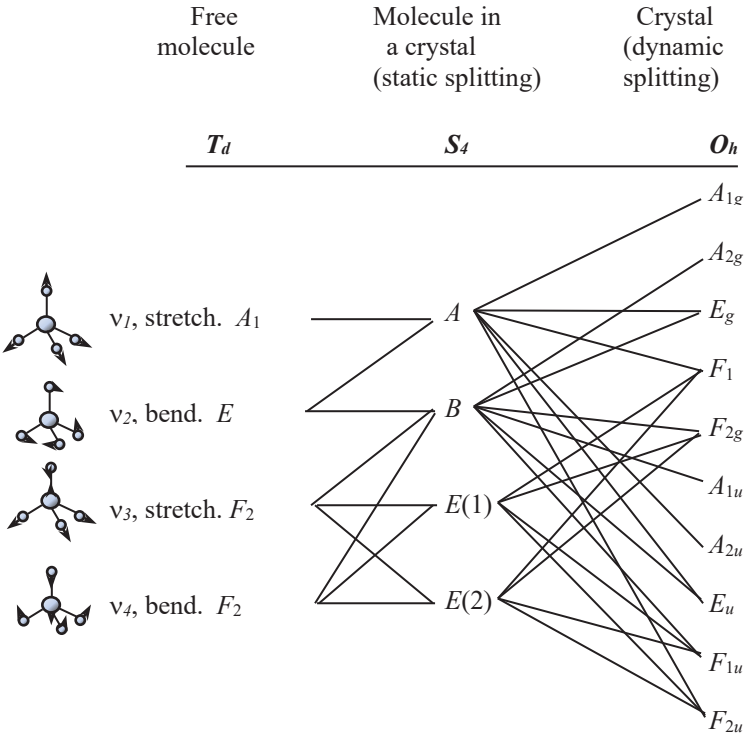

Fig. 5.8. Correlation of intramolecular vibrations of the SiO4 tetrahedron.

Correlated representations are connected by lines. This information is obtained from correlation tables (see Appendix E). Of all the possible representations for a free molecule, the scheme includes only those that are actually realized (see above the analysis of SiO_4 vibrations). From the above scheme it is easy to determine which vibrations and in what quantity arise in a garnet crystal as a result of static (transition $T_d \rightarrow S_4$) and dynamic (transition $S_4 \rightarrow O_h$) splittings of four internal vibrations of the SiO_4 tetrahedron. Thus, the A_{1g} mode of the crystal arises from one stretching A_1 and one bending E vibrations of the molecule. The A_{2g} mode comes from one bending E, one stretching F_2 and one bending F_2

vibrations of a free molecule, etc. Thus, the representation of internal SiO_4 vibrations in a garnet crystal contains:

$$\Gamma_{\text{internal}} = 2A_{1g} + 3A_{2g} + 5Eg + 6F_{1g} + 7F_{2g} + 3A_{1u} + 2A_{2u} + 5E_u + 7F_{1u} + +6F_{2u}.$$

The full vibrational representation is the sum of intramolecular and crystalline modes:

$$\Gamma = 3A_{1g} + 5A_{2g} + 8E_g + 14F_{1g} + 14F_{2g} + 5A_{1u} + 5A_{2u} + 10E_u + 17F_{1u} + +16F_{2u}.$$

A total of 97 modes of various symmetry and 237 vibrations (each *E*-mode counts as two vibrations in the total; each *F*-mode counts as three vibrations). This corresponds to the expected number of vibrations $N = 3n - 3 = 3 \cdot 80 - 3 = 237$, where $n = 80$ is the number of atoms in a primitive cell.

The data obtained are usually presented in tabular form, which is more convenient when working with spectra (Table 5.7).

Table 5.7. Analysis of vibrations of a garnet crystal $X_3^{2+}Y_2^{3+}(SiO_4)_3$ by symmetry

	X^{2+}	Y^{3+}	$T(SiO_4)$	$R(SiO_4)$	$(Si\text{-}O)_{bend}$		$(Si\text{-}O)_{stretch}$	
					E	F_2	A_1	F_2
A_{1g}, RS	–	–	–	1	1	–	1	–
A_{2g}	1	–	1	–	1	1	–	1
E_g, RS	1	–	1	1	2	1	1	1
F_{1g}	3	–	2	3	1	2	1	2
F_{2g}, RS	2	–	3	2	1	3	–	3
A_{1u}	–	1	1	–	1	1	–	1
A_{2u}	1	1	–	1	1	–	1	–
E_u	1	2	1	1	2	1	1	1
F_{1u}, IR	3	3	3	2	1	3	–	3
F_{2u}	2	3	2	3	1	2	1	2

It should be remembered that three acoustic modes of the crystal form one F_{1u} representation. It follows from the selection rules (see Appendix F) that A_{1g}, E_g and F_{2g} modes are active in Raman scattering, while F_{1u} modes are active in IR.

This completes the analysis of garnet vibrations by symmetry.

Finally, while we analyzed the vibrations by symmetry of crystals with isolated SiO_4 groups, the concept of isolated molecular fragments (in

the structural sense) is also valid for pairs and three-, four-, and six-membered rings of SiO_4 tetrahedra in silicate crystals. In other words, this approximation remains valid as long as the molecular fragments exist inside the unit cell. In crystals, where SiO_4 groups yield endless chains, planes, or three-dimensional frameworks, the approximation of molecular fragments is inapplicable. In this case, it is necessary to consider the oxygen and silicon atoms of the SiO_4 tetrahedra as individual and determine the symmetry and the number of vibrations for each of them in the same way as was done above for the X^{2+} cations in the garnet lattice. In this case, the displacements of atoms in infinite chains or planes will be determined by Cartesian coordinates, and not intramolecular, as in isolated molecular units.

5.3. Number of vibrations

The number of degrees of freedom of a molecule consisting of m atoms is $3m$. However, the displacement of a molecule as a whole along the x, y, and z axes, as well as rotation around these axes, does not refer to vibrations. Therefore, the total number of vibrations of the molecule is $N = 3m - 6$.

In linear molecules, where the rotation around the axis of infinite order does not apply to the rotation of the molecule (i.e., does not cause a change in the arrangement of atoms), the total number of vibrations is $3m - 5$.

If a crystal cell contains n atoms, then the total number of vibrations is $3n - 3$ (unlike molecules, where rotation about an axis represents an independent degree of freedom, in a crystal the cell rotation is described by translational displacements of atoms). However, due to the fact that a crystal can be atomic (ionic), mixed ionic-molecular or purely molecular, and vibrations can be divided into internal and external, counting the number of vibrations for each type becomes somewhat complicated, although their total number remains unchanged. Let the primitive crystal cell contain p individual atoms (ions) and M - molecular groups, each of which consists of m atoms. The total number of atoms in a cell is $n = p + mM$. In this case, the separation of vibrations into external and internal is as follows:

Total number of vibrations	$N = 3n - 3 = 3(p + mM) - 3;$
External vibrations:	
translations	$3(p + M) - 3;$
librations	$3M;$
Internal vibrations	$3M(m - 2).$

As already noted, each twofold degenerate mode is represented in the total number by two vibrations and each threefold degenerate mode is represented by three. The calculation of the number of vibrations is performed per one primitive crystal cell. Information about how many primitive cells are contained in a single unit cell is included in the designation of the space group. The quantitative relationship between cells is given in Appendix A.

CHAPTER 6

RAMAN TENSOR AND SELECTION RULES IN VIBRATIONAL SPECTRA

As was established in Chapter 1, the intensity of the bands in the IR absorption spectra is determined by the dipole moments of the vibrational modes, and in the Raman spectra, by the change in polarizability during the vibration. Consequently, the selection rules by symmetry in both types of vibrational spectra will be determined by the reaction of the components of the dipole moment and the polarizability tensor to the action of the symmetry operations of the point group to which the given molecule or crystal refers. Therefore, in order to establish the selection rules, it is necessary, first of all, to consider precisely these quantities from the point of view of the properties of their symmetry.

6.1. Polarizability tensor and Raman tensor

The direction of the vector of the induced dipole moment $\boldsymbol{P}$ in a crystal or molecule generally does not coincide with the direction of the external electric field $\boldsymbol{E}$ (Fig. 6.1) and the $\boldsymbol{P}$ components are linear combinations of the external field components. Therefore, for the dipole moment $\boldsymbol{P}_x$ along the x-axis we can write

$$\boldsymbol{P_x} = \alpha_{xx}\boldsymbol{E}_x + \alpha_{xy}\boldsymbol{E}_y + \alpha_{xz}\boldsymbol{E}_z, \tag{6.1}$$

where α_{xx} is the polarizability of the molecule along the x axis under the action of the field component $\boldsymbol{E}_x$, α_{xy} is the polarizability along the x axis under the action of the field component $\boldsymbol{E}_y$, etc. Similar expressions are valid for the $\boldsymbol{P}_y$ and P_z components.

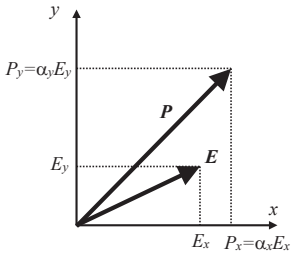

Fig. 6.1. Relationship between the external electric field ***E*** and the induced dipole moment ***P*** of a crystal or molecule

Hence, the expression for the total dipole moment ***P*** can be written in matrix form:

$$\begin{bmatrix} P_x \\ P_y \\ P_z \end{bmatrix} = \begin{bmatrix} \alpha_{xx} & \alpha_{xy} & \alpha_{xz} \\ \alpha_{yx} & \alpha_{yy} & \alpha_{yz} \\ \alpha_{zx} & \alpha_{zy} & \alpha_{zz} \end{bmatrix} \cdot \begin{bmatrix} E_x \\ E_y \\ E_z \end{bmatrix} \tag{6.2}$$

Thus, the polarizability is a tensor quantity, more precisely, a symmetric second-rank tensor, in which

$$\alpha_{xy} = \alpha_{yx},\ \alpha_{xz} = \alpha_{zx},\ \text{and}\ \alpha_{yz} = \alpha_{zy} \tag{6.3}$$

(six independent components in total). The derivative of the polarizability with respect to the normal coordinate, which determines the intensity in the RS, is also a symmetric tensor of the second rank and is called the Raman tensor or the RS tensor.

6.2. Selection rules for first order processes

The essence of the selection rules in IR and RS of the first order, i.e. with the transition of a molecule or crystal from the ground vibrational state to the first excited state, is very simple and does not differ from that in many other physical processes. The general rule is that for the interaction of two different systems (photons, phonons, magnons, electron wave functions, etc.), their symmetry must be the same. In quantum mechanics, the probability of the transition M_{if} from the initial state i to the final state f is determined by the matrix element

$$M_{if} = \int \psi_i^* M \psi_f dx \tag{6.4}$$

where M is the considered moment (dipole, magnetic, or quadrupole). The matrix element M_{if} (intensity of transition) is a constant and should not depend on the symmetry operation. Therefore, if the integral (6.4) changes sign for some symmetry operation, then this means that $M_{if} = -M_{if} = 0$ and the transition is forbidden. For first-order IR and RS processes (i.e., with the participation of only one vibration), the initial state is always totally symmetric. Therefore, in order for the integral (6.4) to be nonzero, it is necessary that the transition moment M and the wave function of the final state either do not change sign during symmetry operations, or change it simultaneously, so that their product remains constant in sign. In other words, the symmetry of the wave function of the final state and the moment of transition M should be the same.

In the act of IR absorption, one photon disappears and one vibration arises. Consequently, the moment of transition in this case is determined by the polarization vector of the incident photon, and the symmetry of the wave function of the excited vibration should exactly correspond to the symmetry of the incident photon, i.e. its polarization vector. Therefore, having determined the symmetry of the polarization vectors x, y, and z in a given point group, we will know which types of symmetry of vibrations of a molecule or crystal from the entire set of vibrational modes are active in the IR spectrum.

In the process of scattering, the moment of transition is determined by the component of the Raman tensor, which depends on the directions of the polarization vectors of the incident and scattered photons, and in order to determine the activity of one or another phonon in the spectrum, it is necessary to know the symmetry of the components of the Raman tensor. The latter are defined by two indexes; therefore it is transformed as the product of the corresponding coordinate axes. For example, α_{xx} is converted as x^2, α_{xy} as xy, etc.

As an example, consider the transformation of the components of the dipole moment μ and the polarizability tensor $\alpha_{\rho\sigma}$ of the H_2O molecule under the action of symmetry operations in the C_{2v} group (point group of the molecule).

Table 6.1. Transformation of the components of the dipole moment and the Raman tensor under the symmetry operations of the group C_{2v}

		E	C_2^z	σ_y	σ_x	
μ_x	x	1	−1	1	−1	B_1
μ_y	y	1	−1	−1	1	B_2
μ_z	z	1	1	1	1	$A1$
α_{xx}	x^2	1	1	1	1	A_1
α_{yy}	y^2	1	1	1	1	$A1$
α_{zz}	z^2	1	1	1	1	A_1
α_{xy}	xy	1	−1	−1	−1	A_2
α_{xz}	xz	1	−1	1	−1	B_1
α_{yz}	yz	1	−1	−1	1	B_2

The first column of Table 6.1 shows the transformed components, the second column – coordinate axes or their combinations, which change according to the same law, and the next four – the results of symmetry operations. So, for example, the x direction changes sign when rotated around the z axis by 180° and does not change when it is reflected in σ_y plane. The character of the transformation matrix in the first case is −1, in the second +1. The last column shows the irreducible representations, according to which the components of the dipole moment and the Raman tensor are transformed. To verify this, it is necessary to refer to the tables of the characters of the irreducible representations (see Appendix D).

It can be seen that μ_x, μ_y and μ_z of the H_2O molecule are transformed as irreducible representations of B_1, B_2 and A_1, respectively (Table 6.1); therefore, vibrational modes of these types of symmetry will be active in IR absorption. The tensor components are transformed as A_1, A_2, B_1 and B_2 (Table 6.1); therefore, all four possible vibration modes of the C_{2v} group are Raman-active.

As follows from Table 6.1, the total symmetric representation A_1 includes the diagonal components α_{xx}, α_{yy} and α_{zz} and does not include off-diagonal α_{xy}, α_{xz} and α_{yz}. It means that the Raman tensor for a given type of symmetry consists only of nonzero diagonal components, different in magnitude, since the directions x, y and z in the orthorhombic system are not equivalent to each other. Thus, the Raman tensor for A_1 vibration in the C_{2v} group is as follows:

$$T_{A_1}(C_{2v}) = \begin{pmatrix} a & 0 & 0 \\ 0 & b & 0 \\ 0 & 0 & c \end{pmatrix}$$

The component α_{xy} is transformed as an irreducible representation of A_2, α_{xz} as B_1, and α_{yz} as B_2; therefore the Raman tensors of vibrations of type A_2, B_1 and B_2 in the C_{2v} group have the form

$$T_{A_2}(C_{2v}) = \begin{pmatrix} \cdot & d & \cdot \\ d & \cdot & \cdot \\ \cdot & \cdot & \cdot \end{pmatrix}; \quad T_{B_1}(C_{2v}) = \begin{pmatrix} \cdot & \cdot & e \\ \cdot & \cdot & \cdot \\ e & \cdot & \cdot \end{pmatrix};$$

$$T_{B_2}(C_{2v}) = \begin{pmatrix} \cdot & \cdot & \cdot \\ \cdot & \cdot & f \\ \cdot & f & \cdot \end{pmatrix}$$

Thus, the set $T_{A_1}, T_{A_2}, T_{B_1}, T_{B_2}$ of Raman tensors describes the selection rules in RS in the C_{2v} group.

Each symmetry group has its own set of symmetry elements. Of course, the transformation of the dipole moments and the components of the Raman tensor in each point group will be characterized by irreducible representations that are characteristic only for this point group. These irreducible representations constitute the selection rules in IR and RS.

Above, we used intuitive rather than strict mathematical rules to define Raman tensors of various types of symmetry for the group C_{2v}. The tensors that are active in Raman scattering vibrations for all 30 crystal classes established by Loudon [1] are presented in Appendix F, and Appendix G shows the basic techniques for working with Raman tensors to improve the efficiency of polarization measurements of crystals.

What does knowledge of the Raman tensor give for a certain type of symmetry of vibrations? For nonoriented objects, i.e. powders or liquids, practically nothing. But if the spectrum of an oriented crystal is recorded, then the combination of the directions of polarization of the incident and scattered light relative to the crystallographic axes of the sample indicates which types of symmetry of vibration are active in this spectrum (see also Chapter 7). For example, if the direction of polarization vectors of both incident and scattered light coincides with the *x* (or *y* or *z*) axis of the crystal, then in this case the *xx* (*yy*, *zz*) components of the Raman tensor will be recorded in the Raman spectrum, which, as we now know, correspond to only totally symmetric modes. In other words, in this case, a spectrum of totally symmetric vibrations is recorded. To give this fact a mathematical form, we can write in the general case

$$I(\mathrm{RS}) = A\,[\boldsymbol{e}_i^{\sigma}\boldsymbol{\alpha}_{\sigma\rho}\boldsymbol{e}_s^{\rho}]^2 \quad (\rho, \sigma = x,y,z), \tag{6.5}$$

where A is a constant and $\boldsymbol{e}_i^{\sigma}$ and $\boldsymbol{e}_s^{\rho}$ are the unit vectors of polarization of the incident and scattered radiation along the σ, ρ axes of the crystal (compare this expression with (1.32, 1.33)).

Totally symmetric vibrations always exist in a molecule or crystal and are always active in Raman scattering.

For molecules and crystals with an inversion center, there is an *alternative prohibition rule*: vibrations active in the RS are prohibited in the IR, and vice versa. At the same time, vibrations, which are even with respect to the inversion operation, are active in the RS, and they are odd in the IR.

When scattering by molecules in liquid and gas occurs, the polarization factor $[\boldsymbol{e}_i^{\sigma}\alpha_{\sigma\rho}\boldsymbol{e}_s^{\rho}]^2$ in relation (6.5) must be averaged over all directions; therefore, in this case, the degree of depolarization is usually measured $\eta = I_{\perp}/I_{\parallel}$, i.e. the ratio of the Raman intensities measured at crossed and parallel polarizations of the incident and scattered light. In crystals, where the crystallographic axes can be rigidly defined with respect to the laboratory coordinate system, polarization factor allows us to find individual components of the Raman tensor and thus determine the symmetry of vibrations in the spectra, which is perhaps the most attractive advantage of Raman spectroscopy of crystals.

6.3. Selection rules for second order processes

For a strictly harmonic oscillator, whose potential energy is a quadratic function of a coordinate, only transitions with a change in the vibrational quantum number by unity are possible. In other words, if the system is in the ground state, transitions from the ground state to the first excited state are observed in the IR and Raman spectra. However, due to anharmonicity[6], transitions from the ground state to the second (third, etc.) excited state or transitions with a simultaneous change in the quantum number for two (or several) vibrations become possible. The lines in the spectra at the frequency $2\omega_i$ are called overtones, and at the frequency $(\omega_i \pm \omega_j)$ are called composite tones. In this case, the composite tone $(\omega_i + \omega_j)$ is called summarized, and $(\omega_i - \omega_j)$ is called difference. The probability of second-order processes in Raman scattering is small; therefore, the lines of

[6] This refers to the anharmonicity of both types: mechanical, due to the deviation of potential energy from the quadratic law, and electro-optical, when the dipole moment and polarizability cease to be a linear function of vibrational coordinates.

overtones and composite tones are either very weak or not detected at all. The reason for their appearance in the spectrum will be discussed in detail in Chapter 9.

In the processes of absorption and scattering of the second order, the moment of transition M in the integral (6.4) remains the same as in the processes of the first order. Therefore, the selection rule for second-order processes is the same as for first-order processes, namely: the symmetry of the excitation is determined by the symmetry of the moment M. (It is valid for any two-particle processes such as, for example, scattering with the simultaneous participation of a phonon and a magnon). The only difference is how the symmetry of the excitation is determined. In second-order processes, the symmetry of the overtone or composite tone is determined by the direct product of the types of symmetry of each participating vibration. For example, the symmetry of summarized tone $(\omega_i + \omega_j)$ is

$$\Gamma(\omega_i + \omega_j) = \Gamma(\omega_i) \times \Gamma(\omega_j). \tag{6.6}$$

The direct product $\Gamma(\omega_i) \times \Gamma(\omega_j)$ of the irreducible representations $\Gamma(\omega_i)$ and $\Gamma(\omega_j)$ is very easy to find. The characters of the representation of the direct product $\Gamma(\omega_i) \times \Gamma(\omega_j)$ are equal to the product of the characters $\Gamma(\omega_i)$ and $\Gamma(\omega_j)$. Hence, having determined the characters of the direct product, it is easy to find to which representation (or the sum of several representations) of the group they correspond.

Example 1. Let us find the symmetry of the composite tone $\nu_3 + R_z$ of the H_2O molecule (i.e., the asymmetric stretching vibration and the librational mode R_z). The symmetry of the ν_3 mode is B_1 and the mode R_z – A_2 (see Fig. 4.10). Let us write down from the table of characters of the group C_{2v} (see Appendix D) the characters of the representation B_1 and A_2 (Table 6.2, second and third rows, respectively).

Table 6.2. The product of characters of the representations A_2 and B_1 in the group C_{2v}

	E	C_2^z	σ_y	σ_x
B_1 (ν_3)	1	–1	1	–1
A_2 (R_z)	1	1	–1	–1
$B_1 \times A_2$	1	–1	–1	1

The last row of Table 6.2 is the result of multiplying the two previous rows by each other. These are the characters of the direct product $B_1 \times A_2$. We turn again to the character table of the group C_{2v} and find that the characters of the direct product coincide with the character string of the representation B_2.

Thus, the direct product of B_1 and A_2 is transformed according to the irreducible representation of B_2:

$$B_1 \times A_2 = B_2.$$

Example 2. Let us find the symmetry of the overtone of the F_{2g} type vibration of group O_h (this group includes a garnet crystal). Let us turn to the table of characters of the irreducible representations of the group O_h (Table 6.3; See also Appendix D).

Table 6.3. Characters of the irreducible representations of the O_h group and the direct product $F_{2g}\times F_{2g}$

O_h	E	$8C_3$	$3C_2$	$6C_4$	$6C_2'$	I	$8S_6$	$3\sigma_h$	$6S_4$	$6\sigma_d$
A_{1g}	1	1	1	1	1	1	1	1	1	1
A_{2g}	1	1	1	−1	−1	1	1	1	−1	−1
E_g	2	−1	2	0	0	2	−1	2	0	0
F_{1g}	3	0	−1	1	−1	3	0	−1	1	−1
F_{2g}	3	0	−1	−1	1	3	0	−1	−1	1
A_{1u}	1	1	1	1	1	−1	−1	−1	−1	−1
A_{2u}	1	1	1	−1	−1	−1	−1	−1	1	1
E_u	2	−1	2	0	0	−2	1	−2	0	0
F_{1u}	3	0	−1	1	−1	−3	0	1	−1	1
F_{2u}	3	0	−1	−1	1	−3	0	1	1	−1
$F_{2g}\times F_{2g}$	9	0	1	1	1	9	0	1	1	1

The last line of Table 6.3 shows the characters of the representation $F_{2g} \times F_{2g}$. This representation is reducible, and its reduction consists of finding in those irreducible representations of the group O_h, the sum of the characters which will form the character row of the representation $F_{2g} \times F_{2g}$. It can be seen that the resulting collection is formed by the sum of the characters of the irreducible representations A_{1g}, E_g, F_{1g} and F_{2g}. Hence,

$$F_{2g}\times F_{2g} = A_{1g} + E_g + F_{1g} + F_{2g}.$$

Taking into account the fact that none of the components of the dipole moment or the Raman tensor in the O_h group transforms according to the F_{1g} representation, and the three remaining representations are active only in Raman scattering, we find that a vibrational mode with a frequency $2\nu_i(F_{2g})$ can be observed in the Raman spectra corresponding to A_{1g}-, E_g- or F_{2g}-types of symmetry.

A following characteristic of the direct product should be noted: the direct product then contains a totally symmetric representation when its factors belong to the same type of symmetry. From this property of the direct product the selection rules in IR and RS for the first-order processes considered above are followed. The point is that the ground state in which the system is stated before the act of absorption or scattering is always totally symmetric. The act of absorption can be characterized as a process involving two "particles" - a photon and a phonon (the symmetry of a photon is characterized by a dipole moment). The scattering act is described by the participation of two photons, the symmetry of which is characterized by a component of the scattering tensor, and a phonon. In both cases, the direct product of the symmetry of the dipole moment and the phonon, and the components of the RS tensor and the phonon, must contain a totally symmetric representation. Therefore, both factors must have the same symmetry type.

The selection rules for the wave vector in a crystal are less rigorous for second-order processes than for processes involving a single phonon. The point is that the condition of proximity to zero of the wave vector of the scattered phonon (Sec. 3.4 in Ch. 3) should now be satisfied for the sum of the wave vectors of two phonons; therefore, phonons from any point of the Brillouin zone can participate in scattering, as long as their wave vectors are multidirectional, and their vector sum is close to zero. The density of phonon states, however, is maximal at the center and at the edges of the Brillouin zone, making second-order scattering processes most probable precisely at these points.

CHAPTER 7

THE TECHNIQUE OF RAMAN SPECTROSCOPY

7.1. Block diagram of Raman spectrometer

The physical process yielding to the appearance of inelastic Raman scattering was considered in Ch. 1. Here we will discuss the experimental methods and features of Raman spectra obtaining. A typical Raman spectrometer includes an excitation source, an input device, a dispersing device, and a detector (Figure 7.1).

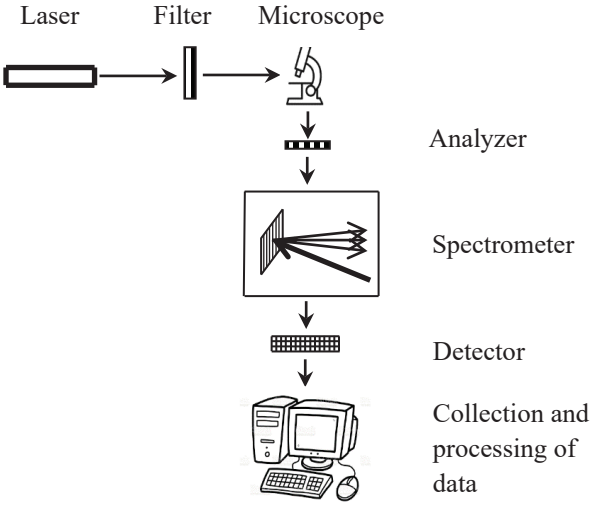

Fig. 7.1. Raman spectrometer block diagram

As a source of monochromatic radiation, gas lasers with generation in the visible region of the spectrum are usually used, i.e. Ar +, Kr +, He-Cd, and He-Ne lasers, since gas lasers differ from solid-state lasers in high stability of the radiation frequency, and the width of the laser lines of these

devices operating in a single-mode mode is very small (10^{-2} – 10^{-3} cm^{-1}), much less than the width of vibrational lines in the spectrum (1 – 10 cm^{-1}). The angular divergence of the beam is also negligible, which makes it technically simple to collimate and focus. Nevertheless, in recent years, solid-state lasers based on AYG crystal with a laser line at 1064 nm and with subsequent frequency doubling to 532 nm have been increasingly used. These devices are not demanding to operate and are inexpensive.

The preliminary monochromator (or interference filter) is used to clean the generation line from accompanying emission lines, which are present in the spectrum of the laser radiation. The intensity of the emission lines is much lower than the intensity of the laser line, but much higher than the intensity of the bands in the Raman spectrum.

Currently, as an input device, a microscope is usually used, which focuses laser radiation on the sample surface and simultaneously serves to collect scattered radiation. This geometric scheme of spectrum registration is called *back-scattering*.

A film polaroid or a Glan prism installed in front of the entrance slit of the spectrometer is used to analyze the polarization of the scattered radiation.

7.2. Types of spectral device for Raman spectroscopy

One of the main features of Raman scattering is its weak intensity (i.e., the probability of the scattering process), which is on the order of 10^{-6} - 10^{-12} of the intensity of the exciting radiation. Another important feature of the method (from an experimental point of view) is the spectral proximity of the scattered light to the excitation line. Indeed, in many cases, the Raman spectrum starts from 5 cm^{-1} (glasses, semiconductor superlattices, and molecular crystals), which in terms of wavelengths in the visible region means a breaking from the exciting line by about 1 Å. These characteristics determine very stringent requirements for spectral equipment.

For registration of Raman spectra, classical scanning spectrometers, modern spectrographs (Raman microscopes) and Fourier spectrometers are used.

A traditional scanning spectrometer, as a rule, consists of a double monochromator, in which the spectrum is swept over a narrow exit slit and detected by a photomultiplier (Fig. 7.2). The advantages of such a spectrometer include a low noise level (i.e. a high degree of suppression of background radiation due to double monochromatization), a very high spectral resolution (usually better than 0.1 cm^{-1}), the ability to detect low

Raman frequencies (starting from about 2-10 cm^{-1}) and correct reproduction of the shape of the scattering line (in the case of a correct design solution). However, the rather long time required to register one spectrum (usually tens of minutes) makes this type of device not very convenient for use.

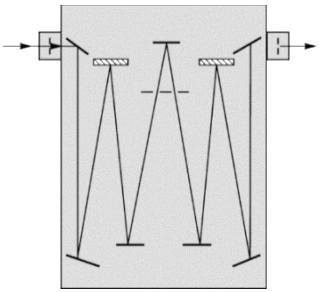

Fig. 7.2. Optical design of double scanning monochromator

The next type of spectral device for Raman spectroscopy is the two-stage spectrometer-spectrograph, which has been widely used for the past 40 years (Fig. 7.3). The first stage of the device is a double monochromator

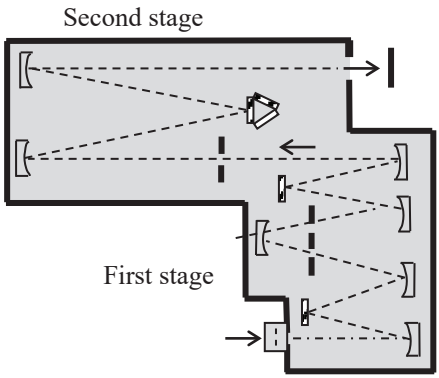

Fig. 7.3. Triple Raman spectrometer-spectrograph.

with dispersion subtraction. In it, the light that has passed through the entrance slit of the device is decomposed into a spectrum, from which laser (Rayleigh) radiation is cut off with the help of the middle slit. The diffraction grating of the second monochromator is set so that its dispersion is "directed" in the opposite direction, and the spectrum created

in the first monochromator is folded back into a beam of white light in the second monochromator. The third monochromator, which is the second stage of the device, usually operates in the spectrograph mode, i.e. all the light, which is decomposed into a spectrum, falls on a two-coordinate detector, a CCD-matrix (abbreviation for “coupled charge device”).

Modern CCD-matrices have a very high sensitivity, and the characteristics of each pixel of the matrix are close to the characteristics of a photomultiplier operating in photon counting mode. The ability to "accumulate" the spectrum, reading and adding to the previous result and each time improving the signal-to-noise ratio, makes the time of the entire spectrum collection very short – from a few seconds to several minutes. However, the spectral resolution of the device is limited, as usual, by the focal length of the second-stage spectrograph and, which is a new one, by the geometric pixel size. Moreover, since the charge accumulated by one pixel in the process of spectrum registration can partially “spread” to two neighboring ones, the real spectral resolution is limited by a width of 2–3 pixels and is usually no better than 1–5 cm^{-1}. For this reason, the shape of narrow spectral lines cannot be reproduced correctly. The low-frequency part of the spectrum can be recorded starting from 50–60 cm^{-1}.

In recent years, devices have appeared (they are usually called Raman microscopes) which differ from the previous ones by replacing the first stage with so-called notch-filters or edge-filters, which serve to cut off the laser line (Fig. 7.4). Due to the simplified optical design and significant progress in the manufacture of notch filters with high optical parameters, these devices have proven to be the most popular in applied Raman spectroscopy. Let's consider their characteristics in more detail.

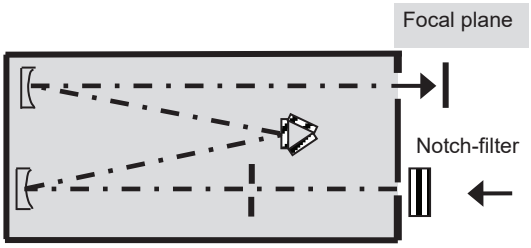

Fig. 7.4. Raman microscope with notch filter

1. *Transmission.* The transmission of a spectrometer is inversely proportional to the number of optical elements in it, mainly mirrors and gratings. Each mirror results in a loss of about 10% of the light flow, and each grating results in a loss of 40-50% of the light. The spectrograph with

a notch filter includes only one grating and two mirrors – much less than in other types of instruments (Figs. 7.2-7.3). For this reason, Raman microscopes are significantly superior in transmission to other spectrometers. This means that at the same power of exciting radiation, the intensity of the spectrum obtained with a Raman microscope will be much higher. However, the power of the incident radiation is usually the critical value: in the Raman experiment, the incident radiation is focused on the sample surface into a spot about 1 micron in diameter; therefore, the lower its power, the lower the local heating of the sample will be. For colored and readily decomposing chemical compounds, this circumstance is perhaps the most critical from the point of view of the possibility of obtaining their spectrum. Therefore, devices with high transmission, such as the LabRAM HR Raman microscope, Horiba, and Jobin Ivon, significantly expand the scope of Raman spectroscopy. In addition, the use of laser radiation sources of lower power gives a significant gain in their cost, which also plays an important role.

2. *Resolution.* The resolution of an optical device is determined by its linear dispersion $S = (\delta\varphi/\delta\lambda)\cdot F$, where $(\delta\varphi/\delta\lambda)$ is the angular dispersion, and F is the focal length. Angular dispersion depends on the dispersing element (diffraction grating) and is usually varied by using gratings from a standard set (600–2400 lines/mm) for all types of Raman spectrographs. The focal length of the instrument is constant and is determined by the distance from the grating to the exit slit of the spectrometer or the focal plane of the spectrograph. As already mentioned, in the case of two-coordinate detectors (CCD-matrices), the spectral resolution is also limited by the pixel size. Typically, spectrometers/spectrographs are designed in such a way that the entrance slit of the device is projected onto its focal plane with a certain magnification factor close to unity. Moreover, if the projection width of the entrance slit turns out to be less than the width of the detector pixel, the reading device still perceives this signal as from a whole pixel. In addition, the charge that appears on one pixel when it absorbs light quanta spreads to neighboring pixels. As a result, the real spectral resolution of the detector matrix (i.e., the minimum half-width of the recorded line) turns out to be equal to the wavelength interval corresponding to approximately two pixels (Fig. 7.5).

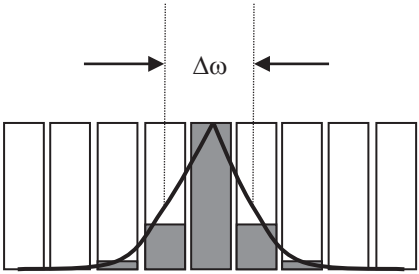

Fig. 7.5. When only one central pixel is illuminated, the half-width of the recorded line is perceived to be approximately two pixels due to the spreading of the charge (the amount of charge is proportional to the filled area)

Thus, to obtain a high spectral resolution, it is necessary to give preference to spectrometers with a large focal length (instrument base) and detectors with a minimum physical pixel size (with a standard CCD matrix width of 1 inch, the latter condition is equivalent to the requirement of the maximum number of pixels per line). An important parameter of a spectral device is the presence of replaceable diffraction gratings in it, which make it possible to switch (with a loss of spectral pass band) to recording a spectrum with a high resolution.

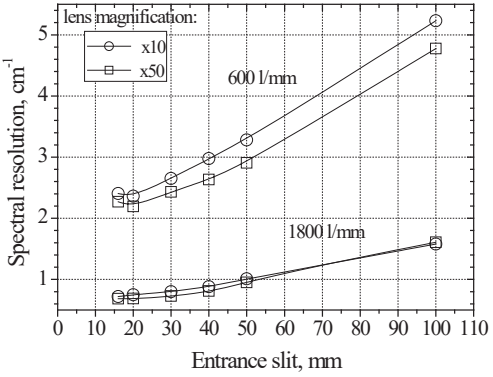

Fig. 7.6. Half-width of emission lines of Ne gas in an electric discharge (emission from a low-pressure Ne lamp) for various diffraction gratings and input objectives of different magnifications (LabRAM HR spectrometer, Horiba, Jobin Yvon, spectrometer magnification 0.9, and CCD matrix with 2048 pixels per row).

The experimental determination of the resolution of the device is carried out by registering an optical spectrum consisting of narrow lines, the width of which can be neglected. For this purpose, as well as for

wavelength calibration of the spectrometer, the emission spectrum of a low-pressure neon lamp is best suited. To reliably determine the spectral resolution, the spectrum is collected at different widths of the entrance slit, and then the dependence of the half-width of the spectral lines on the parameters of the entrance slit is plotted (Fig. 7.6). Fig. 7.6 shows that the resolution of the device reaches its limiting value when the width of the entrance slit is about 30 microns.

3. *Confocality and image transmission to the entrance slit.* These design features apply to all types of spectrometers and are useful to know to better control the spectrum acquisition process.

The confocality of the spectrometer sets the spatial resolution of the spectrum over the depth of the sample, i.e. selects an area on the surface or in the depth of the sample from which the spectrum is collected. The essence of this technique is illustrated in Fig. 7.7.

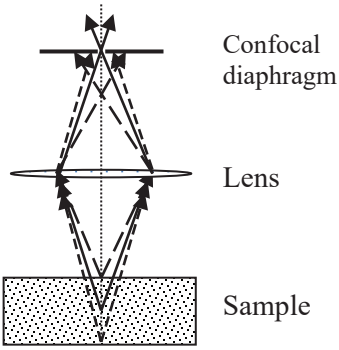

Fig. 7.7. Diagram of the confocal diaphragm

By adjusting the aperture of the confocal diaphragm and the distance from the objective to the sample, you can select the area of interest for recording the spectrum. This is especially important when working with "samples in the medium", for example, with crystals in a high-pressure anvil cell or with inclusions in a mineral.

Image transmission to the entrance slit is an important parameter from the point of view of obtaining a spectrum with the least loss in intensity. The experimenter is always interested in setting the entrance slit as narrow as possible to obtain a high spectral resolution, but in this case large losses of the light flux can occur if the width of the slit turns out to be much less than the diameter of the image of the exciting radiation spot transmitted to the slit.

First of all, it is necessary to find out what the optimal width of the entrance slit should be. This depends on the pixel size of the detector and the magnification factor of the spectrograph (i.e., with what magnification the entrance slit is projected in the focal plane of the instrument), since it is pointless to set the slit narrower than the width of one pixel (taking into account the magnification of the spectrometer). In addition, taking into account the effect of charge spreading, it can be assumed that the slit width, which is approximately equivalent to the width of two detector pixels, is close to optimal. For a LabRAM HR Raman spectrometer, the magnification is 0.9, and the pixel width for currently existing CCD standards can be 26 μm (1024 pixels per line) or 13 μm (2048 pixels per line). Figure 7.6 shows the dependence of the spectral resolution of the spectrometer on the width of the entrance slit for a CCD matrix with 2048 pixels per row. It can be seen that, at a slit width of 20–30 μm, the resolution becomes practically limiting in full agreement with the above estimate. It is also worth recalling that with an excessively narrow entrance slit (10–20 radiation wavelengths), diffraction effects at the edges of the slit become significant and should be taken into account (i.e., the slit itself begins to work as a diffraction grating).

Now it is easy to clarify the question of transferring the image to the entrance slit. If d_0 is the diameter of the spot of focused laser radiation on the sample, m is the magnification factor of the lens of the microscope that collects the scattered radiation, and k is the magnification of the optical path of the spectrometer from the objective to the entrance slit, then the diameter d of the image on the slit is

$$d = mkd_0. \tag{7.1}$$

The values of d_0 and m are related to each other and the product $m \cdot d_0$ remains approximately constant for lenses of different magnification. Therefore, the critical parameter is the gain k of the lens-slit path. For the LabRAM HR spectrometer $k = 0.28$. With a 100x "Olympus" type lens, d_0 is about 1 μm. Hence $d = 28$ μm. Thus, the size of the image of the spot of light at the entrance slit is consistent with its optimal width.

4. Contour of a spectral line. The contour of an ordinary line in the vibrational spectrum is Lorentzian [except for some special cases, such as the strong interaction of the vibration with the electron continuum (Fano interaction), or polariton effects in the IR spectrum, broad bands of hydrogen bond vibrations, etc.] and is given by the expression:

$$L(\omega) = \frac{\Gamma}{2\pi} \frac{1}{(\omega-\omega_0)^2+\frac{\Gamma^2}{4}}, \tag{7.2}$$

where Γ is the half-width (full width at half-height) and ω_0 is the position of the center of gravity of the line. The real contour of the line recorded by the instrument is the convolution of the instrumental function $a(\omega)$ of the spectrometer and the Lorentz contour, i.e. integral

$$g(\omega') = \int_{-\infty}^{\infty} a(\omega' - \omega) L(\omega) d\omega \tag{7.3}$$

(the problem of the line contour in a real device is considered in detail in [1]). In modern devices, the distortion (aberration) of optical elements, i.e. diffraction gratings and mirrors, are small and can be neglected; therefore, the instrumental function of the device mainly includes the instrumental functions of the input and output slits. The instrumental function of the entrance slit consists of the diffraction of light at the edges of the slit and a component due to its finite width. The diffraction component a_{diff} is proportional to $D/\lambda F$, where D is the effective aperture of the device (almost equal to the size of the diffraction grating), F is the focal length of the device, and λ is the wavelength of light. The D/F ratio is around 0.1. Hence the $a_{\text{diff}} \approx 0.2$ μm. Consequently, when the width of the entrance slit s_{in} is greater than 15–20 μ, the diffraction effects at the edges of the slit can also be neglected, and the instrumental function of the entrance slit turns out to be due to its geometric shape, i.e. rectangular strip. The geometric image of the entrance slit is transferred to the focal plane of the device, where the detector is installed, with a certain coefficient k_{dev}, which increases or decreases the size of the entrance slit. In other words, the flow of monochromatic light filling the entrance slit of the device will appear on the detector matrix as a rectangular strip with the width $s_{\text{in}}k_{dev}$. Unlike a scanning spectrometer with a variable width of an exit slit, in a Raman microscope the role of an exit slit is played by a pixel with its fixed physical size, and the instrumental function of such an "exit slit" is the one shown in Fig. 7.5. Without performing here the cumbersome calculations of integral (7.3) (which are still only a certain approximation of the instrumental function of a real device), we can say that if the width of the vibrational line is greater than the spectral resolution of the device (item two of this section), the line contour will be close to natural, that is Lorentzian. This condition is usually satisfied for vibrational spectra obtained at room temperature (and above), since in this case the lines are already significantly broadened and their half-width is a few inverse centimeters. At low temperatures, for example the temperature of liquid

helium, the half-width of the vibrational mode can reach values of 0.1–0.5 cm^{-1}, i.e. below the limit of spectral resolution of the currently widespread Raman microscopes. In this case, of course, the instrumental functions of the entrance slit and the detector become important, and the line contour will be best described by the Voight function, which is a convolution of the Lorentz and Gaussian distributions:

$$V(\omega) = \int_{-\infty}^{\infty} G(\omega')L(\omega - \omega')d\omega', \tag{7.4}$$

where

$$G(\omega) = \frac{1}{\sigma\sqrt{2\pi}} e^{-\frac{(\omega-\omega_0)^2}{2\sigma^2}} \tag{7.5}$$

is the Gaussian distribution, in which the quantity σ is related to the half-width Γ by the ratio

$$\sigma = \frac{\Gamma}{2\sqrt{2ln2}}. \tag{7.6}$$

In practice, however, the most commonly used is a slightly modified Voight function called a pseudo Voight function.

7.3. Polarization measurements

As already mentioned in Ch. 6, the possibility of polarization measurements of oriented crystals is perhaps the most attractive feature of Raman spectroscopy in relation to IR spectroscopy. Polarized spectra contain experimental information on the type of symmetry of vibrational modes, and for low-symmetry crystals – also on the crystallographic direction of individual bonds in the cell. The optical scheme for recording Raman spectra is shown in Fig. 7.8.

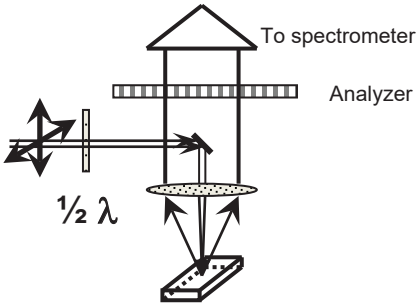

Fig. 7.8. Optical scheme for recording the Raman spectrum.

In this case, it is assumed that the sample is oriented, i.e. the directions of its edges in the figure correspond to certain crystallographic axes. Laser radiation is usually polarized, and the direction of polarization can be changed using phase plates. The polarization of the scattered light is set by a polaroid (or Glan prism). In Figs. 7.1 and 7.8 these elements are designated as the "Analyzer". Since each type of symmetry of vibrational modes is characterized by its own (individual) Raman tensor, different combinations of the direction of polarization vectors of the incident and scattered light relative to the crystallographic axes of the oriented single-crystal sample determine the type of symmetry of the recorded spectrum. For example, the Raman tensor of totally symmetric vibrations for all crystals with symmetry above monoclinic has only diagonal nonzero components; therefore, totally symmetric modes can be recorded only in the spectra of the *aa*- (or *bb*-, *cc*-) configuration, i.e. when the polarization vectors of the incident and scattered light are parallel to the *a* (or *b*, or *c*) axis of the crystal. The Raman tensors of all types of vibrations for the D_{2h} group have the form

$$D_{2h}: \quad \underset{A_g}{\begin{pmatrix} a & 0 & 0 \\ 0 & b & 0 \\ 0 & 0 & c \end{pmatrix}} \quad \underset{B_{1g}}{\begin{pmatrix} \cdot & d & \cdot \\ d & \cdot & \cdot \\ \cdot & \cdot & \cdot \end{pmatrix}} \quad \underset{B_{2g}}{\begin{pmatrix} \cdot & \cdot & e \\ \cdot & \cdot & \cdot \\ e & \cdot & \cdot \end{pmatrix}} \quad \underset{B_{3g}}{\begin{pmatrix} \cdot & \cdot & \cdot \\ \cdot & \cdot & f \\ \cdot & f & \cdot \end{pmatrix}}. \tag{7.7}$$

To measure the spectrum of B_{1g} modes, it is necessary to set the polarization of the incident light parallel to the *a* axis of the crystal, and the scattered one – *b* (or vice versa), i.e. measure the *ab*- (i.e. *xy*-) component of the scattering tensor, etc. This procedure is necessary for determining the symmetry of vibrational modes and is very useful in assigning bands in the experimental spectrum.

7.4. "Leakage" of polarization

When measuring the polarized spectrum, the bands, which are forbidden in a given configuration, are often observed as weak lines (for example, weak lines of totally symmetric modes are observed in cross polarizations, and vice versa). This is due to the polarization "leakage". The reason for its appearance is that the scattered light is collected not only for the "correct" Raman tensor, but also for the one that is rotated through an angle θ (Fig. 7.9).

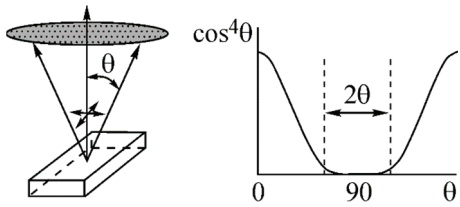

Fig. 7.9. The origin and quantity of polarization "leakage"

When the coordinate system rotates, the elements of the Raman tensor change as $\cos^2$ (see Appendix G). The intensity of scattered light is proportional to the square of the element of Raman tensor. Thus, when the crystal (coordinate system) rotates, the Raman intensity changes as $\cos^4$, and to determine the polarization "leakage" L, it is necessary to calculate the integral

$$L = \int_{90-\theta}^{90+\theta} cos^4\theta \cdot d\theta. \quad (7.8)$$

For the numerical aperture $A = \sin\theta = 0.6$ of the input lens, $\theta = 37°$, the polarization "leakage" $L = 0.033$ (3.3%).

7.5. Fourier-raman spectroscopy

The use of Fourier spectrometers for recording Raman spectra have become real in recent years, although the frequency of their use does not compete with the frequency of the use of dispersive devices. But if the principle of the operation of a dispersive spectrometer is usually not discussed, then the physical (and mathematical!) reason for the appearance of the spectrum in a Fourier spectrometer needs to be explained, and here we will briefly discuss this problem without going into the technical features of this type of device.

The function of the spectral part of the Fourier spectrometer is performed by an interferometer, which can have a different design, but most often an interferometer made according to the Michelson scheme is used (Fig. 7.10).

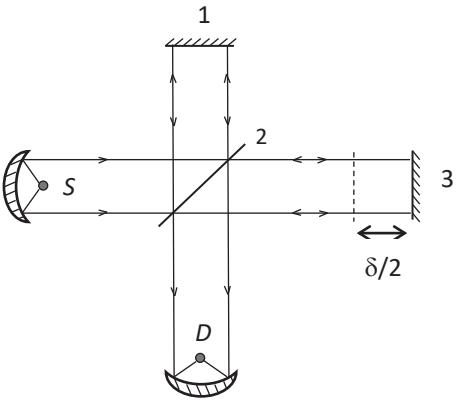

Fig. 7.10. Diagram of a Michelson interferometer.

The light from the source *S* is split by the beam splitting plate 2 into two identical flows in the direction of the mirrors 1 and 3. The light reflected from the mirrors gets the detector *D* at the end of the path. Let us imagine that the light emitted by the source is a monochromatic wave. In this case, due to the division of light into two streams, the detector will fix radiation, the intensity of which depends on the path difference δ of the two monochromatic waves: from zero, when both waves reach the detector in antiphase, to the maximum value, if the path difference turns out to be zero.

The path difference δ can be adjusted if one of the mirrors, for example, mirror 3, is made movable. In this case, i.e. when the mirror 3 is displaced, the light intensity on the detector will change sinusoidally, i.e. the detector will record the signal shown in Fig. 7.11, a.

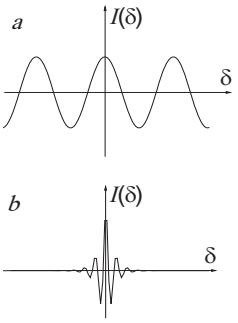

Fig. 7.11. Interferograms of monochromatic radiation (a) and white light (b)

The sinusoid shown in Fig. 7.11,a can, like any other function, be expanded in a Fourier series, but the expansion will be represented by only one term, namely sin (ωt), in which the only harmonic ω is the frequency of our monochromatic wave. In other words, the resulting spectrum will consist of only one line at the frequency ω. Now let's complicate the experiment a little by imagining that the source emits light consisting of two monochromatic waves with frequencies ω_1 and ω_2. In this case, when mirror 3 is displaced, the detector will record the result of the interference of the two waves, i.e. a picture depicting the result of the addition (beating) of two waves ω_1 and ω_2. Now the Fourier series of the function I (δ) will consist of two harmonics, ω_1 and ω_2. It is not difficult to extend this thought experiment to light consisting of any number of monochromatic waves. For example, if the source emits white light, i.e. the sum of an infinite number of monochromatic waves, then, theoretically, at the output (i.e., after expanding the signal in a Fourier series), we should also obtain a structureless curve consisting of many non-resolved lines. However, in this case, the real interferogram will turn out to be as shown in Fig. 7.11, b. After mathematical processing, this interferogram transforms into a single peak with a maximum in the center, since at zero path difference, the radiation for all wavelengths is added. Now that we know how the interferometer works, in order to obtain a Raman spectrum, it is necessary to replace the source S with a sample on which the exciting radiation is incident. To record the IR absorption spectrum, it is necessary to replace the source S with a source of white light in the IR region, and place the sample in the channel between the beam splitter and the detector.

The most complex technical part of Fourier spectrometers, both Raman and IR, is a movable mirror, which, on the one hand, must have a sufficient displacement length (the greater this length, the less the influence of the edges of the spectrum and the higher its quality), while on the other hand this displacement must be controlled with high precision, on the order of fractions of the incident light wavelength. This problem is usually solved using an auxiliary interferometer, which, when the mirror 3 is displaced, counts the number of interference maxima from the generation line of the additional built-in laser and thus controls the mirror displacement.

The most important difference for Raman spectroscopy between a Fourier spectrometer and a dispersive spectrometer is that, in the former, for the excitation of the spectrum, as a rule, a solid-state laser with generation in the near-IR region at a wavelength of 1.06 μm is used. This greatly reduces the likelihood of luminescence occurring during spectrum registration and significantly expands the list of compounds suitable for

spectrum acquisition. On the other hand, the farther the excitation line is from the energy of allowed electronic transitions in the crystal, the weaker the Raman spectrum. This disadvantage is usually compensated for by an increase in the power of the exciting line. In addition, work in the near-IR region is associated with the need to visualize the incident radiation beam, which, like the design features of the sample placement, makes it difficult to work with small crystals, polarization measurements, and low-temperature measurements. Taking into account all these features, it should be said that the Fourier spectrometer in Raman spectroscopy is expedient to be used for recording the spectra of compounds with a high level of luminescence (biological objects, many natural minerals), as well as the spectra of easily decomposing highly colored compounds.

CHAPTER 8

FREQUENCY, INTENSITY, POLARIZATION AND THE BANDWIDTH OF THE BANDS IN THE VIBRATIONAL SPECTRA

Any spectral line, including a vibrational one, is characterized by four parameters: peak position, intensity, width (half-width) and polarization. Despite the fact that each of these parameters is very important, and together they completely characterize the spectral band, their detailed analysis still presents a complex spectral problem.

8.1. Vibrational frequency

The vibrational frequency is the main characteristic of the vibrational mode, since, taking into account the mass of vibrating atoms, it determines the force constant of the bonds, which is directly related to the type of bond and its order. Let us consider sequentially several different aspects that determine the behavior of vibrational frequencies.

1. *Characteristicity.* When analyzing the vibrational spectra of various compounds, it was noticed that the vibration frequencies of some bonds or functional groups vary very little from compound to compound. Such frequencies were called characteristic or group frequencies. The characteristicity of vibrations is the property that makes vibrational spectroscopy the most important method for analyzing the composition of compounds.

The reasons for the characteristicity of vibrations are understandable and underlie the fundamental concepts of both the nature of chemical bonds and the mechanism of vibrations. The vibrations of a molecular fragment or just any bond will be the more characteristic, the less influence the force constants of this fragment from neighboring atoms or ligands are exposed to. For example, in the series of carbon-carbon bonds, i.e. C≡C, C=C, C–C, the vibration of the triple bond is really characteristic (2100-2300 cm^{-1}), since the only additional (fourth) bond of each carbon atom with the nearest atom is not able to significantly change the force

constant of the triple C≡C bonds, regardless of whether this atom is a donor of electron density, or its acceptor. Double C=C still refers to some extent to the characteristic, but the frequency of its stretching vibrations falls in most cases in the region of 1600-1800 cm^{-1}, reaching 2100 cm^{-1} in some linear molecules. The vibration of a single C–C bond is not at all characteristic, and it falls in the region of 600-1500 cm^{-1}, since in this case three additional bonds to each carbon atom can change the force constant C–C within wide limits, depending on the nature of the ligand atoms. In addition, the frequency of C–C vibrations falls into the region where their kinematic interaction with other vibrational modes is quite probable.

The stretching vibrations of $(SiO_4)^{4-}$, $(PO_4)^{3-}$, and $(SO_4)^{2-}$ anions in salts and crystals of minerals are characteristic, since they are largely "closed" from the environment and the covalent bond inside the anion is much stronger than the bond with the surrounding lattice cations.

Examples of characteristic vibrations are given in Appendix H.

However, in addition to inductive effects acting on the force constant, there is also a kinematic relationship between vibrations, i.e. interaction of vibrations that reduces their characteristicity (see item 4 for details). The interaction of modes is determined by their symmetry (only modes of the same symmetry can interact) and the distance between the modes on the frequency scale. It is commonly accepted that the kinematic interaction between two modes is inversely proportional to the square of the difference between their frequencies, $\Delta\omega^2$. Therefore, the higher the frequency of the vibration, the more it is detuned from other vibrations, and the more likely the characteristicity of this vibration. In other words, vibrations of light atoms with large force constants of the bonds are most often characteristic.

A quantitative measure of characteristicity is usually the share of participation of the considered bond in a given normal vibration. If this share is 50% or more, then the vibration can be considered characteristic. The degree of participation of a bond in normal vibration can be estimated using quantum chemical calculations, as well as an experiment in which the vibration frequencies of an ordinary compound and its isotopically substituted analog are compared.

The concept of vibrational characteristicity is extremely useful in assigning vibrational modes in the spectrum. It plays a particularly important role in vibrational spectroscopy of organic compounds, where the set of elements that make up the compound is not as diverse as in inorganic chemistry. As an example, Appendix H shows the frequencies of characteristic vibrations in the most common inorganic and organic compounds. It can be seen that in organic compounds, the vibrations of the

basic bonds CC, CN, CO, CH, and NH are often characteristic in frequency (and, often, in intensity).

Inorganic compounds with their heavy atoms and weak force constants, as a rule, do not possess sufficient characteristicity of vibrations, and the assignment of lines in the spectra of inorganic compounds often does not differ with the certainty that can be achieved when working with the spectra of organic compounds. However, the vibration frequencies of molecular fragments in the crystal, anionic and cationic, in most cases, rather weakly depend on the composition of the crystal matrix and are characteristic (Appendix I).

2. *Crystalline effects.* In crystals, in addition to the usual factors controlling the vibrational frequencies (i.e., the force constants and atomic masses), frequency changes can be observed due to static (crystal) and dynamic (Davydov's) splitting. We have already considered both of these phenomena when discussing the symmetry of vibrations. The first is the result of a decrease in the symmetry of a fragment in the crystal lattice, and the second is the interaction of vibrational modes that are identical in frequency and symmetry (in principle!). The order of magnitude of both types of splitting is shown in Figs. 8.1 and 8.2, which show the vibration frequencies of SiO_4 tetrahedra in the olivine structure. We see that crystal splitting can be an order of magnitude larger than dynamic.

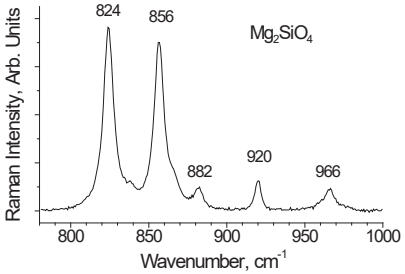

Fig. 8.1. Raman spectrum of forsterite, Mg_2SiO_4, in the range of stretching vibrations of the SiO_4 tetrahedron

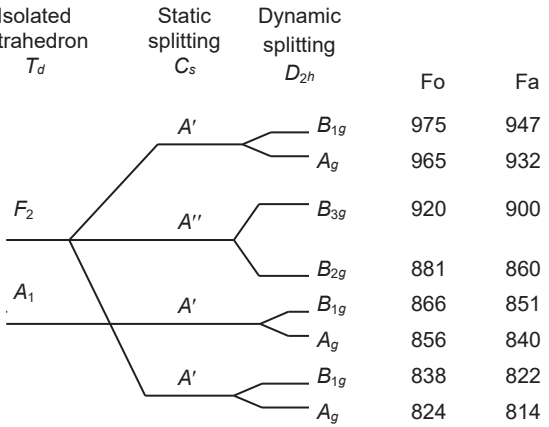

Fig. 8.2. Static and dynamic splitting of stretching vibrations SiO4 tetrahedron in olivine crystals [1]. Fo - forsterite, Mg_2SiO_4, Fa - fayalite, Fe_2SiO_4, Mo - monticelite, Mn_2SiO_4

3. *Mode behavior.* In solid solutions, the response of vibration frequencies to a change in composition can be different. It is customary to distinguish between one- and two-mode behaviors of vibration frequencies. In the first case, the vibration frequencies smoothly change their values in the interval, the boundaries of which are set by the vibrational spectra of the terminal terms of a series of solid solutions. In the second, the frequencies practically do not change with a change in the composition relative to those observed for the terminal members, but their intensities change. An example of a two-mode frequency behavior is the spectra of Si-Ge [2] or GaAs-InAS solid solutions. What does the frequency behavior depend on? The answer is quite simple: it depends on whether or not the frequency ranges in which the dispersion curves lie for the vibrations of atoms of each type in their sublattice overlap. If the frequency regions overlap, then one-mode behavior will be observed, if not, it will be two-mode behavior.

In complex oxides, however, which are the majority of silicate minerals, the unit cell usually contains several types of atoms and molecular groups. Their translational vibrations are close in frequency, and strongly mix with each other, which leads to single-mode behavior in almost all cases.

4. *Interaction of vibrations.* As mentioned above, modes of the same symmetry interact with each other, and this interaction increases with the approach of vibration frequencies. The most famous case of frequency interaction in vibrational spectroscopy relates to the vibration spectrum of the carbon dioxide molecule, CO_2. The molecule is linear, the wavenumber of its bending vibration ν_2 is 667 cm^{-1}, and the wavenumber of the symmetric stretching mode ν_1 should have been 1340 cm^{-1}, according to calculations, but instead of this, two modes, 1285 and 1388 cm^{-1}, are recorded in the spectrum, almost equally away from the expected value. It turned out that the wavenumber of the overtone of the bending mode, $2\nu_2$, almost exactly coincides with the assumed frequency ν_1, and that there is a strong interaction between them, the result of which is that, instead of two different modes, ν_1 and $2\nu_2$, two components of the same vibration are obtained, but one of the components has a larger contribution bending component, and the other - stretching. In this case, the wavenumbers of each of the components are equidistant from their assumed values in the absence of interaction. The physical reason for the interaction is that both modes, ν_2 and the overtone $2\nu_2$, are totally symmetric, and in each of them there is not only a change in the angle between the CO bonds, but also a slight change in the length of the C–O bond. It is the latter that makes the overtone interact with the symmetric stretching mode ν_1. This phenomenon was considered and theoretically substantiated for the first time by E. Fermi in 1931 and received the name the Fermi resonance.

The theoretical description of the interaction is well known. Let there be two interacting harmonic oscillators ω_1 and ω_2 with an interaction constant β^2, while the quantities ω_1 and ω_2 characterize the vibrations of "pure" (non-interacting) systems. The equations of motion for both oscillators when they interact will be written as

$$\ddot{q}_1 + \omega_1^2 q_1 + \beta^2 q_2 = 0$$

$$\ddot{q}_2 + \omega_2^2 q_2 + \beta^2 q_1 = 0. \qquad (8.1)$$

At interaction, the system will be characterized by a different frequency Ω, therefore, we are looking for a solution in the form of harmonic vibrations

$$q_1 = q_1^0 \sin(\Omega t), \qquad q_2 = q_2^0 \sin(\Omega t), \qquad (8.2)$$

where q_1^0, q_2^0 – new vibration amplitudes. Substituting (8.2) into (8.1) we obtain:

$$(\omega_1^2 - \Omega^2)q_1^0 + \beta^2 q_2^0 = 0$$

$$\beta^2 q_1^0 + (\omega_2^2 - \Omega^2)q_2^0 = 0. \tag{8.3}$$

In order for the system of equations (8.3) to have a solution with respect to Ω, it is necessary that the determinant composed of its coefficients is equal to zero:

$$\begin{vmatrix} \omega_1^2 - \Omega^2 & \beta^2 \\ \beta^2 & \omega_2^2 - \Omega^2 \end{vmatrix} = 0. \tag{8.4}$$

From here

$$\Omega_{\pm}^2 = \frac{1}{2}[(\omega_1^2 + \omega_2^2) \pm \sqrt{(\omega_1^2 - \omega_2^2)^2 + 4\beta^4}]. \tag{8.5}$$

For $\Omega = \Omega_+$

$$\frac{q_1^0}{q_2^0} = \frac{\omega_1^2 - \omega_2^2 + R}{2\beta^2} = \frac{2\beta^2}{\omega_2^2 - \omega_1^2 + R}, \tag{8.6}$$

and for $\Omega = \Omega_-$

$$\frac{q_1^0}{q_2^0} = \frac{\omega_2^2 - \omega_1^2 - R}{2\beta^2} = \frac{2\beta^2}{\omega_1^2 - \omega_2^2 - R} \tag{8.7}$$

where $R = \sqrt{(\omega_1^2 - \omega_2^2)^2 + 4\beta^4}$.

The result contained in expression (8.5) shows that the stronger the interaction between the oscillators, the more the initial frequencies ω_1 and ω_2 move away from each other during vibrations in phase (Ω_+) and out-of-phase (Ω_-).

The interaction of vibrational frequencies is a special case of the interaction of two close energy states: for example, electronic levels, which is widely known in quantum mechanics.

8.2. Bands intensity in the Raman spectra

The intensity of Raman lines is rarely analyzed in experimental studies. This is due to the fact that the scattering intensity is determined by the derivative of the bond polarizability in the normal coordinate, i.e. the derived quantity, which is not directly measured, but can be calculated using modern quantum-chemical programs. However, the calculation of the vibrational spectrum of crystals (and the intensities of vibrational modes) is still not widespread. In addition, the numerical calculation reflects the properties of the model embedded in it, and its results depend on how close this model is to the properties of a real crystal.

Meanwhile, the line intensity contains information not only of a general nature, i.e. about the dipole moments or the polarizability of the bonds that make up the crystal, but also about the symmetry of the wave functions of the states that form these bonds. The latter are especially important, since they allow a qualitative assessment of the degree of participation of various valence states of cations and anions in the formation of a chemical bond between them.

It is not surprising that it is often difficult for an experimenter to understand why the intensity of some lines in the Raman spectrum is high, while others, on the contrary, are extremely low. There are, however, general patterns that have been identified empirically and may be useful in working with spectra. For example, if the vibrational mode of any structural fragment active in the Raman spectrum of a crystal is generated by a mode from the positional symmetry group of this fragment, which is also active in Raman scattering, then it will be intense in the spectrum, in contrast to the mode that was generated from the inactive vibration of the group positional symmetry. The lines of totally symmetric vibrations in Raman spectra usually have a smaller half-width and, therefore, a higher peak intensity compared to degenerate modes.

However, these are separate observations. To understand the correlations spectrum – structure and spectrum – chemical bond, approaches are needed that make it possible to evaluate the behavior of intensities in vibrational spectra at the microscopic level. To illustrate this thesis, we present below an example of estimating the intensity of Raman lines of characteristic vibrations, based on an analysis of the symmetry of vibrations and the positional symmetry of the valence states of cations. Taking into account the fact that the change in the polarizability of bonds during vibration occurs mainly due to the higher occupied molecular orbitals, the symmetry of which should correlate with the symmetry of the valence states of atoms, it is natural to assume that the vibrational mode

will be intense in the spectrum if its symmetry coincides with the symmetry of the valence atomic states. The latter assumption is not a special case, but rather a general rule in spectroscopy for interacting systems, from which follows, for example, the order of interaction of vibrational modes with each other, selection rules, etc.

Let us consider the proposed method for estimating the intensities in the Raman spectra using the example of zircon crystals [3], the polarized Raman spectra of which are shown in Fig. 8.3.

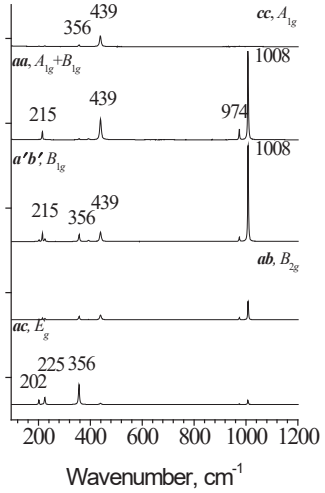

Fig. 8.3. Polarized Raman spectra of a zircon crystal $ZrSiO_4$. The notation *a′b′* means a 45° rotation of the crystal around the *c* axis

The spectra are characterized by a number of features, but we are only interested in those of them that are related to the intensity of stretching vibrations of the SiO_4 tetrahedron. According to the classification of zircon vibrations (Table 8.1), the Raman spectrum should contain one ν_1 (A_{1g}) mode and two ν_3 (B_{1g} and E_g) modes of internal stretching vibrations of SiO_4. All three vibrations are found in the spectrum (Figure 8.3). The line of totally symmetric vibration A_{1g} is observed at a frequency of 974 cm^{-1}, but its intensity in the *aa* spectrum is much higher than in *cc*. The intensity of the B_{1g} vibration at 1008 cm^{-1} is about 10 times higher that of the A_{1g} line, and this is the most intense line in the Raman spectrum. Finally, the intensity of the E_g mode (923 cm^{-1}) is so low that the corresponding band is hardly detected in the spectrum. This behavior of the intensity of the stretching vibration bands of the SiO_4

tetrahedron is difficult to explain, proceeding only from the positional symmetry of the latter.

Table 8.1. Symmetry analysis of Zircon ZrSiO4 vibrations ($I4_1/amd = D_{4h}^{19}, Z = 4$)

$ZrSiO_4$	Zr	$T(SiO_4)$	$R(SiO_4)$	SiO_4 (bend.) ν_2	SiO_4 (bend.) ν_4	SiO_4 (stretch.) ν_1	SiO_4 (stretch.) ν_3
A_{1g}				1		1	
A_{2g}			1(c)				
B_{1g}	1(c)	1(c)			1		1
B_{2g}				1			
E_g	1(ab)	1(a,)	1(a,b)		1		1
A_{1u}				1			
A_{2u}		1(c)		1		1	
B_{1u}			1(c)				
B_{2u}				1		1	
E_u		1(a,b)	1(a,b)		1		1

Let us assume that the intensity of stretching vibrations of SiO_4 depends not only on the polarizabilities of the Si–O bonds, but also on the electronic states of the Zr atom. The valence electrons of zirconium are shared with the surrounding oxygen atoms; therefore, the internal vibrations of SiO_4 groups also modulate the electron density of Zr^{4+}–O bonds. To analyze these bonds, it is necessary to take into account the symmetry of not only the valence states of Zr, but also the orbitals of those eight oxygen atoms that surround zirconium.

In order to simplify the analysis procedure, we will try to describe the Zr–O interaction by considering only the symmetry of the valence electrons of zirconium. The electronic state of Zr – $4d^2 5s^2$ and all four valence electrons take part in the bond. The site symmetry of Zr is lowered from O_h for a regular dodecahedron to D_{2d} in the crystal lattice. The valence orbitals of zircon are transformed into the D_{2d} point group of site symmetry and the D_{4h} factor group of the crystal according to the irreducible representations indicated in Table 8.2.

Table 8.2. Symmetry of the valence states of the Zr atom in the positional symmetry group and the factor group of the crystal

State	s	d_{xy}	d_{xz}	d_{yz}	d_{x2-y2}	$d_{z}2$
Site group D_{2d}	A_1	B_2	E	E	B_1	A_1
Factor group D_{4h}	A_{1g}	B_{2g}	E_g	E_g	B_{1g}	A_{1g}

In a perfect dodecahedron, the oxygen atoms surrounding the zircon are located at the vertices of a cube. In the $ZrSiO_4$ crystal, there are two crystallographically independent sets of Zr–O bonds (Fig. 8.4), one of which is formed by four short bonds, and the other – four long ones. The length of the short Zr–O bonds is 2.13 Å, and the length of the long bonds is 2.27 Å. Short bonds produce an almost planar coordination of Zr atoms in the *ab*-plane of the crystal. Bonds from another set are located in the *ac*-plane and are perpendicular to the first (Fig. 8.4). A consequence of this distortion of the dodecahedron is a more complete participation of the $d_{x^2-y^2}$ (B_{1g}) and *s* (A_{1g}) orbitals of the metal in the Zr – O interaction (Fig. 8.5).

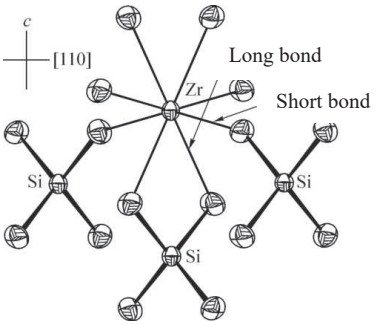

Fig. 8.4. The nearest environment of the Zr atom in the zircon $ZrSiO_4$ lattice

Since the *d* orbitals are more delocalized, their contribution to the change in polarizability and Raman intensity should also be more significant. This circumstance can precisely explain the high intensity of the 1008 cm^{-1} SiO_4 mode of stretching vibrations in the B_{1g} spectrum (see Fig. 8.5), which has the same symmetry as the $d_{x^2-y^2}$ orbital of the metal. In addition, the described distortion of the dodecahedron also explains why the intensity of the totally symmetric A_{1g} valence mode with a frequency of 974 cm^{-1} is much higher in the *aa* spectrum than in the *cc* spectrum.

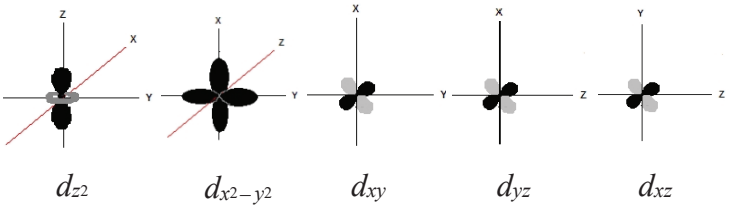

Fig. 8.5. Schematic representation of *d*-orbitals.

A complete interpretation of the vibrational spectrum of zircon is given in Ref. [3].

As already mentioned, the scattering intensity can increase manifold (i.e., hundreds and thousands of times) under conditions of resonance, i.e. when approaching the frequency of the excitation line to the energy of the allowed electronic transition in the compound. An example of a practically accurate resonance is the scattering of gaseous iodine, I_2, when excited by the TEM_{001} mode of 514.5 nm line of Ar^+ ion laser. The spectrum is shown in Fig. 8.6. The spectrum exhibits a very intense line of the scattering at $\omega = 210$ cm^{-1} and the overtones 2ω, 3ω, 4ω, etc., which show practically the same intensity. For comparison, the figure shows also the spectrum of I_2, but when excited by another line of an argon laser, 488 nm, under identical conditions of registration. As can be seen, in the second case, the scattering intensity turns out to be lower than the detection level.

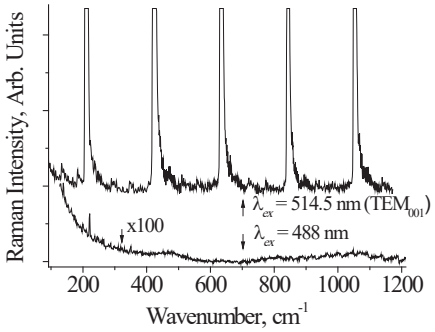

Fig. 8.6. Raman spectrum of gaseous I_2 upon excitation with various argon laser lines. Both spectra were obtained under exactly the same registration conditions.

The temperature dependence of the Raman line intensity is determined by the Boltzmann population [Ex. (1.31) in Chapter 1] of the corresponding vibrational states and is proportional to $A\cdot(n + 1)$ (A is a constant) for Stokes scattering and $A\cdot n$ for anti-Stokes scattering [see (1.32) and (1.33) in Chapter 1]. In the temperature range 0-300 K (most often used in temperature measurements), the population of vibrational states with a frequency above ~ 600 cm-1 is close to zero and the intensity of Stokes scattering on these vibrations is practically independent of temperature (if there are no chemical reasons for this). The intensity of the low-frequency modes changes significantly due to the Boltzmann factor. Fig. 8.7 shows an example of the change in the integrated intensity of the 52 cm^{-1} mode in paracetamol crystals as a function of temperature.

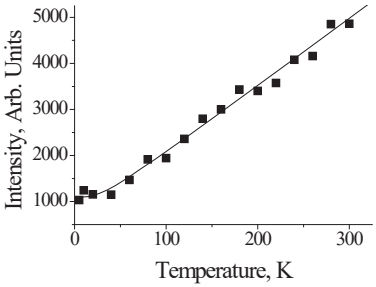

Fig. 8.7. Integral intensity of the 52 cm^{-1} mode in the paracetamol crystal as a function of temperature. The solid curve is the Boltzmann population of the state, plotted from expression (1.31).

8.3. Polarization of bands in the Raman spectra

Polarization, or, in other words, activity, is understood as the dependence of the band intensity in the spectrum on the directions of the polarization vectors of the incident and scattered light. Despite the fact that in all cases the band polarization is directly related to the scattering tensor, the goal and results of polarization measurements for low- and high-symmetry compounds are different. If in a low-symmetry molecular crystal the polarization of some intense bands is determined by vibrations predominantly of one of the corresponding chemical bonds of the molecule, then in a highly symmetric crystal, it is determined by joint vibrations of a group of equivalent coordinates. The division of objects into low- and high-symmetry is not strict, and so, for definiteness, we will consider here crystals belonging to the tetragonal and higher symmetry systems to be highly symmetric, while molecular crystals in which molecules do not have symmetry elements at all, except for identity (for example, amino acids), and the crystal formed from them, can have second-order rotational axes and/or reflection planes.

In highly symmetric crystals, the band polarization is determined by the symmetry of a given mode, which, in turn, is described by the corresponding Raman tensor. This property of vibrations makes it possible to experimentally determine the type of symmetry of each mode in the spectrum; it was discussed in detail in item 7.3 of the previous chapter. However, in low-symmetry crystals, for example, monoclinic crystals, all vibrations are non-degenerate, and characterized by two types of symmetry (i.e., *A* and *B*, see Appendix D), the eigenvector of which are insignificantly different from each other. Therefore, knowledge of the types of symmetry of bands in the spectrum of a monoclinic crystal is not important and does not allow one to significantly simplify and make reliable its interpretation. This is especially important for low-symmetry

molecular crystals, the spectra of which, as a rule, consist of many tens of bands. However, such systems exhibit another remarkable property of vibrations, which makes the measurement of polarized Raman spectra extremely useful.

As an example, we present here measurements of the polarized spectra of garnet crystals (crystals with the highest possible symmetry) and L-serine crystals, which are low-symmetry.

Highly symmetric crystals. As we saw in Chapter 5, the vibrational spectrum of garnet crystals consists of 237 vibrations, of which 97 different vibrational modes are formed (twofold degenerate modes include two vibrations, threefold degenerate ones - three vibrations). The question may arise: is it realistic to assign bands in a spectrum consisting of 97 vibrational modes? Let us try to briefly consider this problem [4].

Analysis of vibrations by symmetry shows (Chapter 5) that the spectrum of vibrations active in IR consists of 17 intramolecular and crystalline modes of only one symmetry F_{1u},

$$\Gamma(\text{IR}) = 17F_{1u},$$

while the spectrum of Raman-active vibrations includes

$$\Gamma(\text{Raman}) = 3A_{1g} + 8E_g + 14F_{2g}$$

The fact that the IR spectrum consists only of vibrations of the same symmetry makes polarization measurements of these spectra unnecessary and extremely complicates the task of their interpretation. It is known that modes with the same symmetry can mix with each other. Therefore, it is rather difficult to assign the observed bands in the IR spectrum without invoking additional information, for example, a detailed quantum-chemical calculation.

The situation with the Raman spectra of garnets is completely different. The spectrum of totally symmetric vibrations contains only three modes – librational, bending and stretching vibrations of SiO_4 tetrahedron – the frequencies of which should differ from each other to an extent sufficient for their confident assignment without invoking quantum chemical calculations. The information obtained on the frequencies of totally symmetric vibrations will greatly facilitate the assignment of vibrational modes of other types of symmetry.

Thus, it is necessary to measure the polarized spectra of the garnet crystal and establish vibrations of A_{1g}, E_g and F_{2g} types in them. In Appendix G it will be shown that if the laboratory axes in which the

directions of the polarization vectors of the incident and scattered radiation are determined coincide with the crystallographic axes of crystal of O_h symmetry (i.e., with the C_4 axes), then the Raman tensor can be written as

$$\begin{vmatrix} A_{1g}+4E_g & F_{2g} & F_{2g} \\ F_{2g} & A_{1g}+4E_g & F_{2g} \\ F_{2g} & F_{2g} & A_{1g}+4E_g \end{vmatrix}.$$

This tensor makes it possible to measure F_{2g} vibrations and the $A_{1g}+4E_g$ combination, which may be insufficient for a reliable interpretation of vibrational modes in the spectrum. However, if we rotate the crystal around the z axis by 45° (in this case, the x and y laboratory axes turn out to be directed between the C_4 axes of the crystal), then the Raman tensor will change the form:

$$\begin{vmatrix} A_{1g}+E_g+F_{2g} & 3E_g & F_{2g} \\ 3E_g & A_{1g}+E_g+F_{2g} & F_{2g} \\ F_{2g} & F_{2g} & A_{1g}+4E_g \end{vmatrix}.$$

In the last "rotated" tensor, in spite of the fact that the diagonal components became even more complicated, it became possible to measure only the E_g vibration in the xy-spectrum. Therefore, by comparing the polarized spectra of a crystal “normally” oriented and rotated by 45 ° about the z axis, we obtain the possibility of selective determination of vibrations of all types of symmetry in the O_h group. It is this situation that is depicted in Fig. 8.8, where the polarized spectra of an oriented cubic single crystal of garnet are given. The upper spectrum refers to the case when the crystallographic axes of the sample are parallel to the laboratory axes, and the polarizations of the incident and scattered light are parallel to the x (or y, or z) axis of the crystal. The second spectrum was obtained at cross polarizations of the incident and scattered light and for a sample rotated by 45 ° relative to the laboratory axes. The orientation of the sample relative to the light polarization vectors (i.e., laboratory axes) is shown in Fig. 8.8.

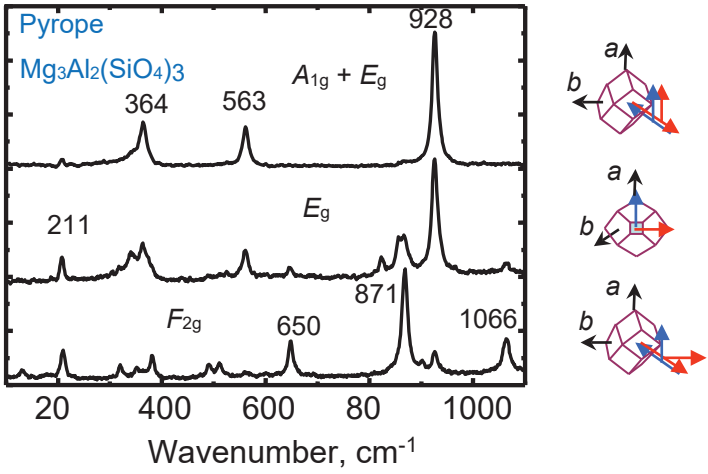

Fig. 8.8. Polarized Raman spectra of oriented pyrope single crystals. The crystal orientation and scattering geometry are shown on the right. The direction of light propagation is shown by long arrows, and the direction of polarization with respect to the crystal axes – is shown by short arrows. Incident radiation is indicated in blue, scattered radiation - in red.

We see that the spectrum of totally symmetric A_{1g} vibrations of garnet consists of three intense modes, which fully agrees with the results of the analysis of vibrations by symmetry. In this case, the high-frequency mode 928 cm^{-1} should be assigned to stretching vibrations of SiO_4, the intermediate one (563 cm^{-1}) - to bending vibrations, and the low-frequency mode (364 cm^{-1}) - to librations of SiO_4 (see Table 5.7).

Librational, bending, and stretching SiO_4 vibrations of other types of symmetry should have frequencies close to the frequencies of analogous totally symmetric modes. Thus, we have determined the ranges of vibrational frequencies for rotational and internal vibrations of SiO_4 in pyrope (and other garnets).

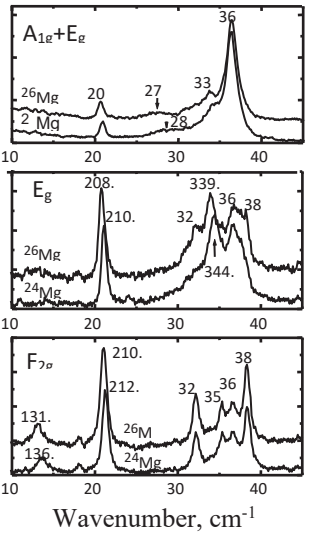

Fig. 8.9. Spectra of isotope-substituted pyrope crystals

To find the frequency ranges of translational vibrations of X^{2+} and SiO_4, let us turn to the spectra of isotopically substituted compounds, i.e. to the spectra of pyrope crystals, in one of which all natural magnesium ions are replaced by the isotope ^{24}Mg, and in the other ^{26}Mg (Fig. 8.9). It can be seen that the bands at 136 and 210 cm^{-1} show the largest frequency shift with isotope substitution. Both of these modes are related to mixed translational vibrations of Mg and SiO_4.

Low-symmetry crystals. In low-symmetry crystals in the absence of axes of symmetry of the third and higher orders, the molecules in neighboring cells are arranged in such a way that if any of the bonds of the molecule turns out to be directed along the crystallographic axis, then this direction is retained throughout the crystal. Since the component of the polarizability of the bond in the longitudinal direction is much higher than the values of the polarizability in the transverse directions, the vibration of this bond will be intense only in the spectrum in which the direction of the polarization vectors of the incident and scattered light coincides with the direction of the bond. In other words, the polarized spectra of low-symmetry molecular crystals maintain a constant relationship between the intensity of any mode and the orientation of the corresponding chemical

bond in the crystal. As an example, consider the spectra of a serine crystal [5].

Serine, $(NH_3)^+–CH(CH_2OH)–(COO)^-$, is one of the most important amino acids in proteins. The serine molecule is shown in Fig. 8.10, and a fragment of the crystal structure along the a–direction in Fig. 8.11.

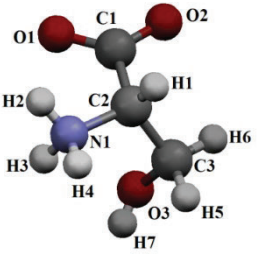

Fig. 8.10. Serine molecule in the form of a zwitterion

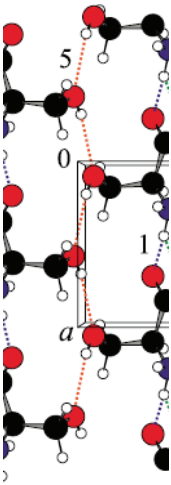

Fig. 8.11. Fragment of the structure of *L*-serine along the ***a*** direction of the crystal

The polarized Raman spectra of serine crystals at low (3 K) and room (295 K) temperatures are shown in Figs. 8.12, *a* and *b*. The 3468 cm^{-1} line (Fig. 8.12, *a*) refers to the stretching vibrations of the O-H intermolecular hydrogen O-H···O bond. The direction of the O-H bond coincides with the direction of the crystallographic axis ***a*** (Fig. 8.11), so the line is intense in the *aa* spectrum and has almost zero intensity in the *bb* and *cc* spectra. If the crystal had not been oriented in advance, then the ***a*** direction in it could be reliably established from the maximum intensity of the 3468 cm^{-1} line. At room temperature (Fig. 8.12, *b*), the line turns into a wide structureless band, which is often observed for vibrations of the hydrogen-bonded fragment of the molecule.

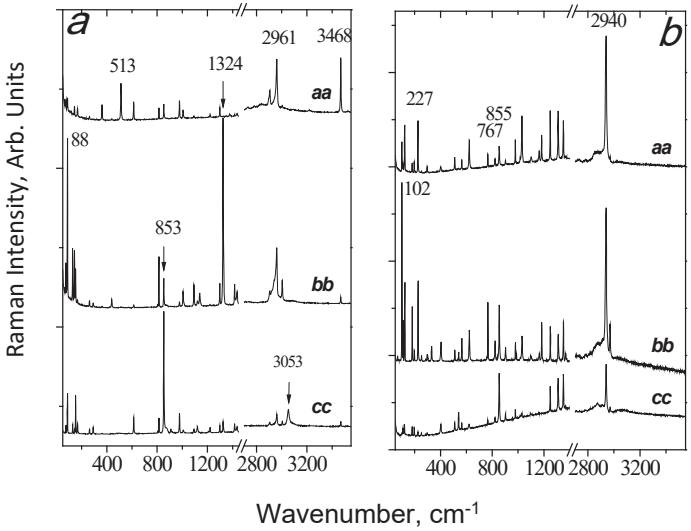

Fig. 8.12. Polarized Raman spectra of serine crystals at 3 K (*a*) and 295 K (*b*). In the designation of the polarization of the spectrum, the first symbol refers to the direction of the polarization vector of the incident light, the second – to the scattered light.

In addition to the 3468 cm^{-1} band, other lines are observed in the spectra, which are recorded in the polarized spectra in only one crystallographic direction.

The 1324 cm^{-1} mode is intense in the *bb* spectrum at low temperatures and refers to the vibration of the C3–O3 bond. The 853 cm^{-1} mode is intense in the *cc* spectrum and refers to the vibration of the C2–C3 bond. It can also be noted that the polarization of the 1324 cm^{-1} line changes slightly at room temperature, while the polarization of the 853 cm^{-1} line remains unchanged. This means that the molecular fragment, including C3H5H6 and O3H7 atoms, slightly rotates around the C2–C3 bond with increasing sample temperature.

Thus, if polarization measurements of the spectra of high-symmetry crystals make it possible to establish the type of symmetry of vibrational modes, then the same measurements of low-symmetry molecular crystals turn out to be extremely useful both for assigning lines in the spectrum and for studying the issues of the orientational mobility of molecules in the crystal lattice.

Angular dependence. If the direction of the chemical bond does not coincide with the direction of any crystallographic axis, as discussed above, then the intensity of the band of the corresponding vibration in the polarized spectra should be proportional to $\cos^4\alpha$, where α is the angle of inclination of the bond to the chosen axis of the crystal (see Section 7.4 "Polarization leakage" in Chapter 7). However, this situation is only hypothetical. In a real crystal, even of low symmetry, there are always second-order rotational axes and/or reflection planes, due to which the angle of inclination α of the bond to the crystal axis in one cell changes by $-\alpha$ in the neighboring cell. In this case, to correctly determine the bond orientation, it is necessary to measure the angular dependence of the intensity, i.e. changes in the band intensity when the crystal is rotated in the selected crystallographic plane relative to the polarization of the incident and scattered light. Using the angular dependence of the intensity, one can establish, for example, the orientation of guest molecules in the cavities of the host crystal lattice or the orientation of single chemical bonds in a unit cell. In addition, in some cases, the angular dependence makes it possible to obtain information about the properties of vibrations that are not available in other ways.

The mathematical description of the angular dependence of the scattering intensity is very simple. The scattering tensor of totally symmetric vibrations is

$$\begin{pmatrix} l & \cdot & \cdot \\ \cdot & p & \cdot \\ \cdot & \cdot & q \end{pmatrix} \tag{8.8}$$

where l, p and q are the derivatives of the polarizability of the molecule along the principal molecular axes x, y, and z, respectively. When turning molecule around, for example, the z-axis by an angle θ of the zz component of the Raman tensor remains unchanged, while the other two change as

$$xx \rightarrow l\cdot\cos^2\theta + p\cdot\sin^2\theta, \tag{8.9}$$

$$yy \rightarrow p\cdot\cos^2\theta + l\cdot\sin^2\theta. \tag{8.10}$$

The measured intensity in the spectrum is proportional to the squared component of the scattering tensor, and the intensity xx- scattering will be equal to

$$\boldsymbol{I}_{xx}(\theta) = (l\cdot\cos^2\theta + p\cdot\sin^2\theta)^2 = l^2\cdot\cos^4\theta + p^2\cdot\sin^4\theta. \qquad (8.11)$$

(The vectors l and p are orthogonal, so the cross term $2lq\cdot\sin^2\theta\cdot\cos^2\theta$ vanishes.) In chemical bonds, two transverse components of polarizability (p and q in tensor 8.8) are much smaller than the longitudinal one, and they can be considered zero; therefore, the scattering intensity changes upon rotation like $\cos^4\theta$. If a single bond in a crystal, for example, O–H bond, is inclined to the crystallographic axis by an angle $\pm\,\alpha$ (the "±" sign arises under the conditions of the symmetry of the unit cell), then $I(\theta)$ is determined by the sum

$$I(\theta) = D\cdot[\cos^4(\theta+\alpha) + \cos^4(\theta-\alpha)], \qquad (8.12)$$

where D is a constant and the angle α can be determined from the measurement angular dependence of the intensity.

Measurement of the angular dependence of the intensity is especially important for O–H bonds (hydrogen-bonded or not), since the position of the hydrogen atom in X-ray structural studies is established only approximately. Using the example of O–H···O vibrations of the hydrogen bond of H_2O molecules in the cavities of the mineral bikitaite, $Li_2[Al_2Si_4O_{12}]\cdot 2H_2O$, we will show what information can be extracted from the analysis of the angular dependence of the intensity [6].

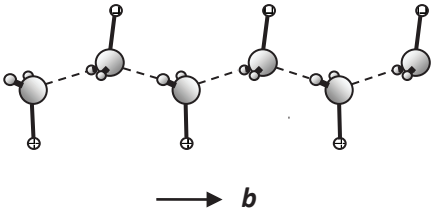

Fig. 8.13. A chain of H_2O molecules in a channel of a bikitaite crystal

Water molecules in the channel cavity of bikitaite are hydrogen bonded into an endless chain, forming the so-called one-dimensional ice (Fig. 8.13). According to the structural data of various authors, the line connecting two oxygen atoms in the O-H···O bond is inclined to the b axis at an angle of 38.4° or 34.5°. Fig. 8.14 shows the angular dependences of the intensity of the stretching band of O–H vibrations at 3400 cm^{-1} and the bending mode at 1640 cm^{-1} in the crystal plane a^*b, in which the hydrogen-bonded O–H are located. The angular dependence of the intensity of bending vibrations is described by expression (8.12) with α = 37° ± 2, which is in very good agreement with both structural data at

∠OH···O ~ 180°, while the angular dependence of the valence band indicates the value α = 0°. This disagreement can be understood by considering the properties of vibrations in an infinite H_2O chain. During bending vibrations, the bond length in O-H···O changes very weakly; therefore, the interaction between vibrations in neighboring bonds is negligible. This means that the vibrations are localized within one bond and the angular dependence of the intensity is determined by the direction in the crystal of individual O–H bonds. O-H···O stretching vibrations in bikitaite are not localized due to the hydrogen bond between individual bonds, i.e. are completely analogous to phonon vibrations in a crystal, and the direction of the derivative of the polarizability is determined by the direction of the H_2O chain as a whole, rather than its individual bond.

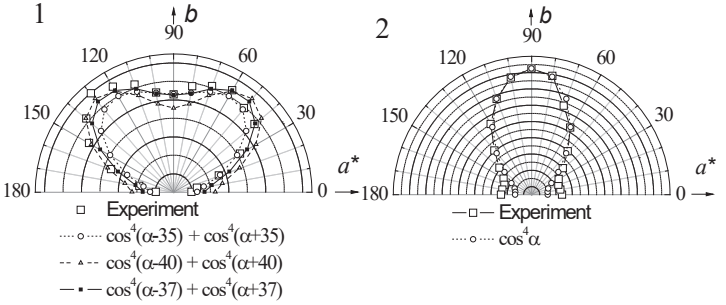

Fig. 8.14. Angular dependence of the intensity of bending (1) and stretching (2) H_2O vibrations in bikitaite.

Thus, measurements of the angular dependence of the intensity, in addition to its main purpose, i.e. revealing the direction of the bond in the crystal from the Raman spectra, can in some cases solve another problem, namely, the determination of the degree of localization of the intramolecular vibration in the crystal.

Finally, there is another interesting example of the application of polarized spectra. We are talking about the analysis of polycrystalline films and the determination of the orientation of the molecules in them.

If in crystals the type of vibrations and their intensity can be determined by the scattering tensor (see also Chapter 6), then in completely misoriented systems (gases, liquids) the distinctive features of individual modes related to their type of symmetry disappear due to the averaging of

the Raman tensor over all directions. In this case, vibrations can be divided into polarized and depolarized.

Polycrystalline oriented films represent an intermediate case between single crystals and completely misoriented objects. In them, the microcrystals making up the film are oriented relative to the substrate (i.e., the base plane of each microcrystal is parallel to the substrate), but misoriented in the plane of the film with respect to each other. Consequently, the polarized spectra of such systems will simultaneously contain both the properties of oriented and misoriented objects, and to obtain information about the structure of microcrystals, it is necessary to use Raman tensors averaged around one of the directions. In Ref. [7], such a general approach for the analysis of polarized spectra of intra- and intermolecular vibrations of compounds was developed and applied to determine the orientation of copper phthalocyanine (CuPc) molecules in thin films. The measurement results made it possible to draw quite definite conclusions about the belonging of the compound to one or another polymorphic structure.

8.4. Spectral bandwidth

The fundamental reason for the broadening of the spectral line in molecules and perfect crystals as a result of the anharmonicity of the potential of interatomic and intermolecular interactions will be discussed in detail in Chapter 9. Here we only note the following: as mentioned above, the bandwidth is determined by the lifetime of the excited vibration; in crystals, the vibrational state is an excitation propagating in the crystal lattice, i.e. a phonon; and since the collision of a phonon with some lattice irregularity yields to a change in its energy or wave vector, the lifetime in this case is determined by the phonon free path. Phonon scattering can occur either on lattice defects or on distortions of the periodic lattice potential caused by other phonons. In the first case, the bandwidth will be determined by the concentration of lattice defects. Usually, noticeable broadening of vibrations is observed at high defect concentrations. The best-known examples are solid solutions and amorphous compounds. In the former, the concentration of phonon scattering centers depends on the composition and usually takes on a maximum value at a 1:1 composition of the components of the solid solution. In amorphous compounds (glasses), long-range order is absent and the phonon mean free path is limited by several lattice periods (often by the radius of the first coordination sphere). In this case, the width of vibrational modes can reach values of 100-200 cm^{-1}. The phonon bandwidth caused by scattering by crystal lattice defects is independent of temperature.

CHAPTER 9

AMPLITUDE AND ANHARMONICITY OF VIBRATIONS

Physical quantities called the amplitude and anharmonicity of vibrations are closely related to each other. Indeed, the theory of vibrations adopted in vibrational spectroscopy is based on the harmonic approximation, in which the displacements of atoms during vibration are considered small enough to neglect the effects of anharmonicity. However, there are no purely harmonic processes, and the degree of anharmonicity just depends on the amplitude of the vibrations. For this reason, we will cover both of these concepts in one chapter.

9.1. Amplitude of vibrations

Let's rewrite the expression (2.23) from Chapter 2 for the amplitude of oscillations:

$$q_{max}(n) = \sqrt{\frac{2\hbar(n+\frac{1}{2})}{\mu\omega}}\,. \tag{9.1}$$

Root mean square deviation

$$\delta q(n) = \sqrt{\frac{\hbar(n+\frac{1}{2})}{\mu\omega}} = \frac{q_{max}(n)}{\sqrt{2}}\,. \tag{9.2}$$

If the reduced mass is taken in atomic mass units, and the vibration frequency is in inverse centimeters, then the standard deviation, expressed in angstroms, is:

$$\delta q(n) = 5.8 \cdot \sqrt{\frac{n+\frac{1}{2}}{\mu\omega}}\ (\text{Å}). \tag{9.3}$$

Let us estimate the numerical value of the vibration amplitudes of diatomic molecules, from light H_2 to heavy I_2 (Table 9.1).

Table 9.1. Vibration amplitudes of zero and first excited states of some molecules

	ω, cm^{-1}	μ, amu	d, Å	$\delta q(0)$, Å	$\delta q(0)/d$, %	$\delta q(1)$, Å	$\delta q(1)/d$, %
H_2	4160	0.5	0.74	0.09	12.1	0.156	21
O_2	1555	8	1.208	0.037	3.1	0.064	5.3
Cl_2	556	17.7	1.988	0.041	2.1	0.072	3.6
I_2	180	63	2.666	0.038	1.4	0.067	2.5

The table shows that the order of magnitude of the vibration amplitudes is a few percent of the bond length, but for light hydrogen it is quite significant. It would seem that the vibrations of heavy atoms (oxygen, chlorine, and iodine) can be considered almost harmonious, but hydrogen atoms are not. However, this statement is not indisputable and needs verification. The bond length is defined as the distance between the centers of atoms, while the potential curve of interaction between atoms is determined through the interaction of their shells. All internal electron shells of heavy elements do not participate in the interaction, but at the same time they significantly increase the distance between the centers. For this reason, the vibrations of all atoms, heavy and light, can hardly be considered negligible, and anharmonic effects must be taken into account in all cases. It is indisputable, however, that the absolute value of the anharmonicity of vibrations of light atoms with their high relative change in bond lengths during vibrations should be higher. Experimental confirmation of this assumption will be presented in clause 9.3 of this chapter.

9.2. Anharmonicity of vibrations

As mentioned above, the harmonic potential, in which the potential energy is proportional to q^2 (q is the vibrational coordinate), is only an approximation. Real interaction is always anharmonic. Despite the wide variety of interatomic and intermolecular interactions (covalent, ionic, van der Waals, etc.), the potential curves describing each of them have common features for all, namely: as atoms (molecules) approach each other, the repulsive forces grow faster, and when the bond is stretched, the

restoring forces change more slowly than in the quadratic potential. This feature of the interaction potential is the basis for the emergence of the most widespread and significant anharmonicity.

Calculating the interaction potential is a difficult task in quantum mechanics. The complexity is determined by the fact that molecular vibrations consist of displacements of both the nuclei and the electronic component. It is not possible to take into account both types of displacements simultaneously in a general form. Therefore, proceed as follows. It is believed that the electronic system of a molecule is practically inertialess and has time to track the displacements of nuclei during vibration (adiabatic Born-Oppenheimer approximation). Then the interaction energy can be calculated for various fixed distances r between the nuclei and thus the shape of the interaction potential in the molecule is determined (Fig. 9.1). It is usually written as

$$U(r) = \frac{Z_1 Z_2 e^2}{4\pi\varepsilon_0 r} + V(r), \tag{9.4}$$

where Z_1, Z_2 and e are the charges of the nuclei and the electron, respectively. The first term on the right-hand side describes the repulsion at short distances, and the second - the interaction close to van der Waals, when the bond is stretched.

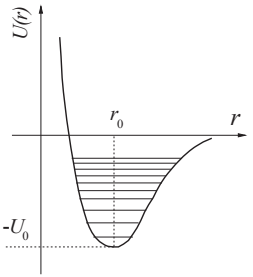

Fig. 9.1. Real potential of interatomic interaction

We will consider the vibrations to be small and expand the interaction energy $U(q)$ in a series in terms of the small parameter $q = (r\text{-}r_0)$:

$$U(q) = U(0) + \left(\frac{dU}{dq}\right)_0 q + \frac{1}{2}\left(\frac{d^2U}{dq^2}\right)_0 q^2 + \frac{1}{6}\left(\frac{d^3U}{dq^3}\right)_0 q^3 + \\ + \frac{1}{24}\left(\frac{d^4U}{dq^4}\right)_0 q^4 + \cdots \tag{9.5}$$

The subscript "0" means differentiation at $q = 0$. The interaction energy is determined up to a constant, so we set $U(0) = 0$. In addition, since $q = 0$ refers to the equilibrium point, the first derivative is also equal to 0. Expression (9.5) can be rewritten as

$$U(q) = aq^2 + bq^3 + cq^4, \tag{9.6}$$

where a, b and c are constants, and a is always positive. The first term on the right-hand side refers to the harmonic law, while the other two naturally reveal a deviation of the potential from the harmonic one. Moreover, the presence of a cubic term makes the potential asymmetric, and a term in the fourth power – steeper or flatter, depending on the sign of c in (9.6) (Fig.9.2). In the real potential of interaction, the repulsive forces are greater than the restoring forces, so the third derivative must be negative.

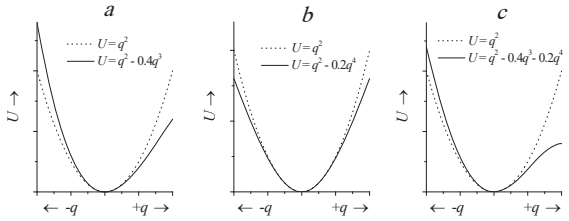

Fig. 9.2. The form of the interaction potential with allowance for the anharmonic terms of the third (a), fourth (b) and both (c) orders. The dashed line is a purely harmonic potential.

The anharmonicity of the interaction potential manifests itself in vibrational spectroscopy by several very strong effects. Let's take a quick look at them.

9.3. Dependence of vibrational frequencies on temperature. Anharmonic contributions[7]

The strongest consequence of cubic anharmonicity is the thermal expansion of solids. Indeed, due to the predominance of repulsive forces over restoring forces, any movement of atoms (molecules) in the crystal lattice reveals an increase in the distance between them, a change in the

* Set out in accordance with Ref [1].

lattice parameters, and a change in the vibration frequencies of all modes (phonon renormalization). With an increase in the thermal population of vibrational states, the average atomic displacement <*x*> changes accordingto [2] at large *T* as

$$\langle x \rangle = \frac{3b}{4a^2} k_B T, \tag{9.7}$$

with *a* and *b* constants from expression (9.6). It is proportional to temperature, which is the reason for the thermal expansion of the crystal lattice.

In vibrational spectra, anharmonicity manifests itself, first of all, in the temperature dependence of the mode vibrational frequency. As a rule, the frequencies of crystal vibrations decrease with increasing temperature due to both cubic anharmonicity and fourth-degree anharmonicity.

There are only three types of atomic vibrations that cause the effect of renormalization of the frequency of a given phonon. These are 1) zero point motions; 2) "thermal baths", i.e. equilibrium vibrations of the lattice; and 3) the phonon under consideration itself, where the vibrations of atoms of which increase the interatomic distances and suppress the frequency of "themselves".

The renormalization value $\Delta_{anh}(T) = \omega(T) - \Omega$, where Ω is the frequency of the hypothetical “bare” (harmonic) phonon, is thus formed from three contributions:

$$\Delta_{anh}(T) = \Delta_0 + \Delta_{th}(T) + \Delta_{ph} . \tag{9.8}$$

Here, Δ_0, $\Delta_{th}(T)$, and Δ_{ph} stand for anharmonic contributions from zero point motions, equilibrium lattice vibrations, and the phonon itself, respectively. At $T = 0$ K, the "thermal bath" disappears and

$$\Delta_{anh}(0) = \Delta_0 + \Delta_{ph} . \tag{9.9}$$

Fig. 9.3 shows a typical dependence of the vibrational frequency of any mode on temperature.

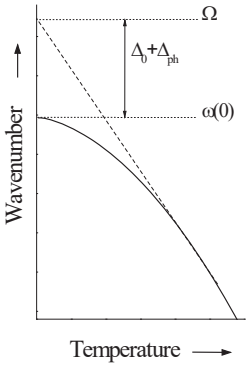

Fig. 9.3. Typical temperature dependence of the phonon vibrational frequency (solid curve). The dashed line shows the extrapolation of the high-temperature rectilinear section of the dependence to $T = 0$ K to obtain the value of the harmonic phonon frequency.

At $T = 0$ K (conventionally) the frequency of the observed phonon is lower than the frequency of the "bare" phonon due to the anharmonic contributions (negative, by definition) of zero-point motions and of the phonon itself. As the temperature rises, various vibrations of the crystal are excited, and the mode frequency decreases due to the anharmonic contribution of the "thermal bath". Thus, the observed experimental dependence is the result of the action of the "thermal bath", and its anharmonic contribution can be determined exactly for any temperature as

$$\Delta_{th}(T) = \omega(T) - \omega(0). \tag{9.10}$$

The problem, however, is as follows. The "thermal bath", one for the entire crystal, is directly responsible for such a macrocrystalline parameter as thermal expansion (and its coefficients). The vibrational spectrum of a polyatomic crystal usually contains several different vibrations (or even tens), and each mode is characterized by its own eigen vector and dependence $\omega(T)$. On the other hand, among all the vibrations of the crystal that make up the "thermal bath", there are always those in which the displacements of the atoms have a very weak effect on the eigen vector of the mode under consideration. In other words, the function $\omega(T)$ is controlled not by all vibrations of the "thermal bath", but only by those of them whose eigen vector causes modulation of the bond length, which is relevant for the mode. Determination of these specific for a given mode vibrations is the main purpose of this chapter.

At present, the temperature dependence of the vibrational frequency is described by expression (9.11) proposed by Balkansky et al. [3]:

$$\omega(T) = \omega_0 + C\left(1 + \frac{2}{e^{x/2}-1}\right) + D\left(1 + \frac{3}{e^{x/3}-1} + \frac{3}{\left(e^{x/3}-1\right)^2}\right), \qquad (9.11)$$

where $x = \hbar\omega/kT$, C and D are constants. The authors of [3] consider the scattering process as the absorption of a photon $\hbar\omega_I$, emission of a photon $\hbar\omega_S$, and the appearance of an optical phonon Ω, which then decays due to anharmonicity into two phonons, three phonons, etc. It is for this reason that the description (9.11) of the anharmonic change in frequency with temperature practically coincides with the description of the dependence of the half-width of the mode $\Gamma(T)$, proposed earlier by Clemens [4] (see expression (9.20) below). But if the simulation of $\Gamma(T)$ by the phonon decay process is quite justified (the width of the spectral line is determined by the lifetime of the excited state), then the transfer of this scheme to the dependence $\omega(T)$ raises questions. The decay rate of a phonon ω into, for example, two other $\omega/2$ is proportional to the population of the vibrations $\omega/2$, and therefore the expression (9.11) can be considered to describe the anharmonic frequency shift if we assume that such a shift is determined only by the populations of phonons $\omega/2$ and $\omega/3$. However, phonons with a fixed frequency $\omega/2$ and $\omega/3$ can with a high probability fall on the dispersion branches of acoustic vibrations and correspond to acoustic phonons with a wave vector far from the highly symmetric points of the Brillouin zone. Such phonons are characterized by a low density of states, and their eigen vectors may have little or no relation to the eigen vectors of the phonon under consideration ω. In other words, the general and most important effect of anharmonicity on the state of the crystal, which is expressed in a change in the lattice parameters with temperature and, as a consequence, the force constants of all bonds, is, in fact, replaced in (9.11) by the population of only two phonons $\omega/2$ (or three phonons $\omega/3$), the characteristics of which are not established. Formally, expression (9.11) can be used to describe the experimental dependence $\omega(T)$ due to the presence of adjustable parameters in it, but it has very little relation to the real process of changing the vibration frequency in a solid.

Usually, when calculating the anharmonic corrections to the energy levels of the oscillator, the cubic term and the fourth-order term from (9.6) are considered as perturbations to the harmonic potential (see, for example, [5]). It turns out that the correction to the energy caused by the cubic term is zero in the first order of the perturbation theory and is calculated in the second order. The term of the fourth degree has a nonzero value of the correction already in the first order of the perturbation theory. For this reason, both corrections turn out to be comparable (or almost comparable) in magnitude and the anharmonic shift of the energy of

vibrational states $\Delta\varepsilon_n$, characterized by the vibrational quantum number n, is proportional to $(n + n^2)$ for both cubic and fourth-order anharmonicity:

$$\Delta\varepsilon_n^{(\text{cubic})} = a_3(30n^2 + 30n + 11), \tag{9.12}$$

$$\Delta\varepsilon_n^{(\text{quartic})} = a_4(6n^2 + 6n + 6). \tag{9.13}$$

Hence, the energies of the states of the anharmonic oscillator are determined as follows:

$$\varepsilon_n = \hbar\omega_0(n + 1/2) + G(n^2 + n) + G_0 \tag{9.14}$$

where a_3, a_4, G and G_0 are constants. However, we are not interested in the energy levels of the anharmonic oscillator, but in its oscillation frequency, which we define in the same way as for the harmonic one:

$$\hbar\omega = \varepsilon_{n+1} - \varepsilon_n = \hbar\omega_0 + 2G(n + 1). \tag{9.15}$$

Thus, we have obtained an obvious result, which is expressed in the fact that the shift of the vibration frequency with temperature depends, first of all, on the population of the state n of the phonon itself. At a finite temperature, several states with close values of n are usually partially excited, and it is necessary to use instead of n its average value $<n(\omega,T)>$, determined by the Planck formula:

$$\langle n\rangle = \frac{1}{e^x - 1}. \tag{9.16}$$

Hence, in the first approximation, the dependence $\omega(T)$ can be represented as

$$\omega(T) = \omega(0) + A<n>, \tag{9.17}$$

where A is a constant that includes both the coefficients of various types of anharmonicity from expressions (9.12) – (9.14) and various numerical factors.

As we will see below, expression (9.17) will in some cases be sufficient to describe the temperature dependence of the vibrational mode. However, in the general case, it is also necessary to take into account the crystalline modes i, the frequencies of which are lower than the frequency of the phonon ω under consideration, though their thermal excitation can

also affect the ω(*T*) dependence. Thus, in (9.17) it is necessary to add one more term and the final expression for describing the dependence ω(*T*) should look like this:

$$\omega(T) = \omega(0) + A\langle n\rangle + B_i\langle n_i\rangle, \tag{9.18}$$

where $\langle n_i\rangle$ is the phonon population ω_i ($\omega_i < \omega$).

We will consider the use of expression (9.18) to describe the dependence ω(*T*) and the justification for the choice of additional modes ω_i using various examples relating to inorganic and molecular crystals.

9.3.1. Inorganic crystals

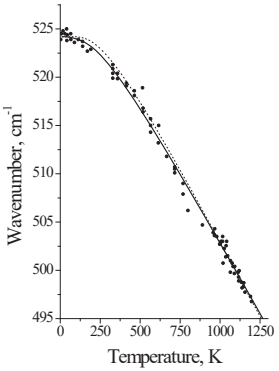

Fig. 9.4. Dependence of the vibration frequency ω of crystalline silicon on temperature [3]. The dotted curve is drawn according to expression (9.17), the solid - according to expression (9.18), taking into account the thermal population of the additional mode 120 cm^{-1}

Fig. 9.4 shows the experimental values of the vibrational frequency of a silicon crystal (mode F_{2g} in the center of the Brillouin zone) in a wide temperature range obtained in Ref. [3]. The description of the experimental temperature dependence by the excitation of just one phonon ω = 524 cm^{-1} (dotted curve in Fig. 9.4) already gives a very good result at high temperatures*. However, at low temperatures (from 0 K to ~ 500 K), a slight excess of the fitting curve over the experimental one is observed. Consequently, in this interval, it is necessary to take into account the

* High temperatures, as follows from the theory of Balkansky et al. [3], should be characterized by the manifestation of fourth-order anharmonicity. However, it can be seen from (9.12) and (9.13) that the magnitude of the shift of the energy of vibrational states is proportional to ($n + n^2$) for both cubic and fourth-order anharmonicity, and the determination of the individual contribution of each type is an almost impossible task.

excitation of vibrational modes $\omega_i < \omega$, which correct the anharmonic shift of the vibration ω. The difference between the curve obtained by expression (9.17) and the experimental $\omega(T)$ is such that modes ω_i with frequencies in the range of 100–150 cm^{-1} should be used as additional ones. This follows from the fact that the maximum deviation of the fitting curve from the experimental dependence is observed at a temperature $T^* \sim$ 200 K (Fig. 9.4), which, taking into account the relation $\hbar\omega_i \sim kT^*$, corresponds to thermal excitation of phonons with $\omega_i \sim$140 cm^{-1}. However, the choice of the numerical value of the phonon ω_i and its characteristics can be made with greater certainty. Fig. 9.5 shows the well-known dispersion branches of various phonons in silicon.

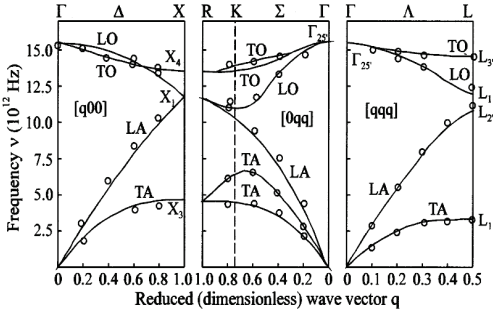

Fig. 9.5. Dispersion of phonons in silicon

It becomes clear why exactly these frequencies are decisive for the low-temperature part of $\omega(T)$. Indeed, transverse acoustic phonons *TA* at high-symmetry points *L* (110 cm^{-1}), *X* and *R* (150 cm^{-1}) of the Brillouin zone, on the one hand, have a high density of states, and, on the other hand, can effectively modulate the Si-Si bond length (see Chapter 3).

The characteristics of longitudinal acoustic *LA* phonons are already much worse from the point of view of their density of states, and the vibration frequencies at high-symmetry points are about 400 cm^{-1} (Fig. 9.5). Thus, the choice of just *TA* phonons at points L, *R*, and *X* as additional modes influencing the change in frequency ω with temperature acquires a quite reasonable interpretation. At high temperatures, the dependence $\omega(T)$ is determined by the phonon population ω with allowance for only the average value $\langle n \rangle$. The fitting curve in Fig. 9.4 (solid) was drawn according to relation (9.18) at the values ω_i = 120 cm^{-1} and $\omega(0)$ = 524 cm^{-1}. The coefficients *A* and B_i are 19.0 and 0.7 cm^{-1}, respectively. The ratio of *A* and B_i shows that the main contribution to the

value of the anharmonic frequency shift ω is made by the temperature excitation of the backgrounds ω themselves as vibrations that have a maximum effect on the length of the Si-Si bond.

Let us consider another textbook example of the manifestation of anharmonicity in inorganic crystals - the temperature dependence of the frequency of the Raman-active mode in diamond. Structurally and chemically (from the point of view of the type of atom-atomic interaction), diamond is very close to silicon, but the frequency ω in diamond is much higher, and the temperature range for measuring the frequency is much wider. Fig. 9.6 shows the results of measurements of the function ω(*T*) in diamond, obtained in [6,7].

In diamond, as in silicon, taking into account the excitation of only one phonon ω = 1333 cm^{-1} (dotted curve in the figure) is insufficient to describe the low-temperature part of the experimental ω(*T*) and it is necessary to select additional modes ω_i. In diamond crystals, there are several dispersion branches suitable for their use in expression (9.18). These are *TA* phonons at point *L* (540 cm^{-1}) and *X* (780 cm^{-1}), and *LA* phonons at L (1050 cm^{-1}) (Fig. 3.6 in Chapter 3). However, taking into account only *TA*(*L*) phonons with a frequency of 540 cm^{-1} as ω_i yields a completely satisfactory description of the experimental function ω(*T*). In Fig. 9.6 the solid curve is drawn according to expression (9.18) with the parameters: ω = 1333 cm^{-1}, ω_i = 540 cm^{-1}. The coefficients *A* and B_i are equal to 63 and 7 cm^{-1}, respectively. As in the previous case, the excitation of the additional mode is involved in only a small fraction of the ω (T) dependence.

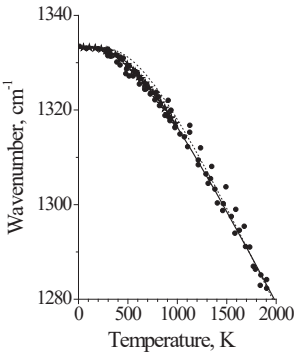

Fig. 9.6. Dependence of vibration frequency ω in diamond; asterisks – [6], dots - [7]. Solid lines are drawn according to the expression (9.17) (dotted curve) and (9.18) (solid curve)

Thus, the temperature dependence of the vibration frequency of monoatomic inorganic crystals of silicon and diamond is quite adequately

described by a simple and physically justified process of temperature excitation of vibrational states that modulate the vibrational coordinate which is relevant for the phonon under consideration. These include, first of all, the phonon ω under consideration itself, as well as one or several additional states ω_i, which, as a rule, are related to acoustic phonons at one of the highly symmetric points of the Brillouin zone. The latter should be characterized by a high density of states and a vibrational coordinate close to the actual phonon coordinate ω.

9.3.2. Molecular Crystals

Molecular crystals differ from most inorganic crystals by the presence of several different types of bonds, i.e. weak intermolecular van der Waals, weak intermolecular hydrogen, and strong intramolecular covalent bonds. For this reason, intermolecular crystalline modes have practically no effect on intramolecular vibrations and vice versa. The frequencies of intramolecular vibrations are usually high, lying in the region of 500 – 3000 cm^{-1}, and the melting point of most molecular crystals falls in the region of 300-400 K. This means that when measuring the vibrational spectrum in the temperature range 5 K – 300 K, the equilibrium population of intramolecular excited vibrational states practically does not change and remains equal to zero. Therefore, the change in the vibration frequency of the intramolecular mode with temperature is very often caused not by its anharmonicity, but by chemical reasons associated with changes in the temperature of hydrogen bonds and the inductive propagation of this change to intramolecular bonds. For this reason, the sign of the change in the frequency of the intramolecular mode can be either negative or positive.

Crystalline intermolecular modes have, as a rule, very low vibrational frequencies and fit well into the temperature range available for measurement. Often these modes exhibit very interesting behavior. As an example, consider the spectrum of the α-S_8 crystal. Crown-like S_8 molecules (Fig. 9.7) are formed by covalent S-S bonds, and the interaction between S_8 molecules in the crystal is purely van der Waals, which determines the low frequency of intermolecular vibrations.

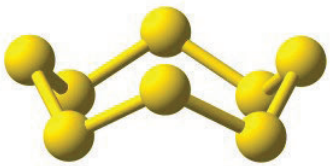

Fig. 9.7. The structure of the S_8 molecule in the α-S_8 crystal

Fig. 9.8 shows the spectrum of α-S_8 crystal modes at 5 K, and Fig. 9.9 – temperature dependence of one of the mixed crystalline modes 86 cm^{-1}, including translations and librations of S_8 molecules.

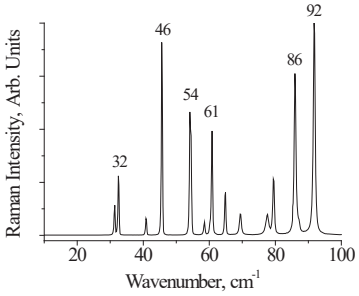

Fig. 9.8. Spectrum of crystalline vibrations of α-S_8 at 5 K

The presented curve of the $\omega(T)$ dependence is interesting in that it is described by the equilibrium population of only one vibration, i.e. of the phonon ω itself, without involving additional modes ω_i, despite the fact that, in addition to the assumed acoustic modes, a sufficient number of low-lying optical vibrations is observed in the spectrum. The absence of the need to attract additional vibrational states is possibly due to the shape of the dispersion curves of acoustic vibrations and the low density of those states that effectively modulate the coordinates that are relevant for ω. And although the presented reason is purely hypothetical and needs to be substantiated, for the model of anharmonicity of the vibrational mode proposed by Balkansky et al. [3], the shape of the acoustic branch does not matter, and in any case, the interaction with two phonons $\omega/2$ should have provided another, more rapid decay of the frequency of a given vibration with temperature. Therefore, the discovered experimental fact is important for us in that it confirms the validity of the assumption adopted for the description of the dependence $\omega(T)$ (i.e., expressions (9.17) and (9.18)), based on the concept of the population of vibrations and, first of all, the considered vibration.

In Fig. 9.9, the dashed line shows the extrapolation of the slope of the $\omega(T)$ dependence to zero temperature. This extrapolation gives the value of the vibration frequency of the "bare" phonon Ω, i.e., cleared of all three anharmonic contributions (see expression 9.8). The difference between the values of Ω and the frequency of the $\omega(0)$ mode in the spectrum at 0 K is equal to the sum $\Delta_{ph} + \Delta_0$.

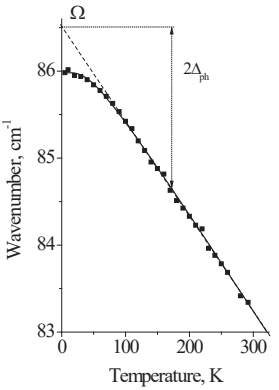

Fig. 9.9. Temperature dependence of the intermolecular vibration frequency in the α-S_8 crystal. The solid curve is drawn according to expression (9.17) at ω = 86 cm^{-1}, A = 1.4 cm^{-1}.

Finally, let us consider the temperature dependence of the mode of translational vibrations of water molecules in the structure of ice I_h, ordinary H_2O, and deuterated D_2O. This case is important in that it makes it possible to determine the degree of anharmonicity of the O-H···O hydrogen bond in the crystal. The spectra of both structures in the region of translational vibrations of water molecules at 5 K are shown in Fig. 9.10, while Fig. 9.11 shows the dependence ω (T) for ice D_2O.

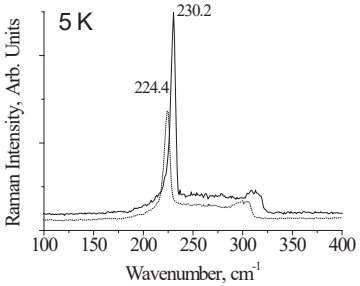

Fig. 9.10. Spectrum of ice H_2O (solid curve) and D_2O (dotted curve) at 5 K in the region of translational crystalline vibrations

To describe the dependence ω(T) in D_2O, shown in Fig. 9.11, in addition to taking into account the population of the 225 cm^{-1} mode itself, it is necessary to use the population of the additional ω_i mode, as has already been encountered in silicon and diamond crystals. In the D_2O (and H_2O) crystal, the mode ω_i = 120 cm^{-1}, which is related to acoustic vibrations of the ice lattice, serves as an additional mode.

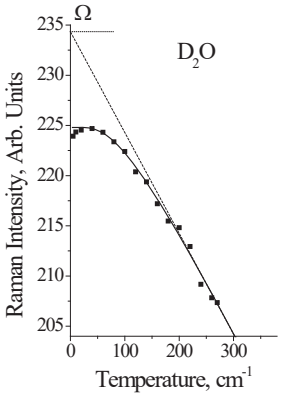

Fig. 9.11. Dependence of the frequency of translational vibrations of D_2O molecules in the structure of ice D_2O (I_h). The solid curve is drawn according to expression (9.18) at ω = 224.8 cm^{-1}, ω_i = 120 cm^{-1}, A = 20.0 cm^{-1}, and B_i = 8 cm^{-1}

The anharmonicity coefficient A = 20 cm^{-1} for the hydrogen bond in ice crystals is much higher than this value for the van der Waals bond in α-S_8 crystals, where A = 1.4 cm^{-1}.

The procedure for estimating the values of the anharmonic contributions of zero-point motions Δ_0 and the phonon itself Δ_{ph} in complex cases, when the temperature change in frequency is determined by the population of two or more different vibrations, is already less definite in comparison with the simple example shown in Fig. 9.9 for the α-S_8 crystal. However, it is not difficult to determine the frequency of the "bare" phonon and the sum of the anharmonic contributions Δ_0 and Δ_{ph}. Fig. 9.12 shows the values of $\Delta_0 + \Delta_{ph}$ for vibrations of bonds of various types – van der Waals (α-S_8), hydrogen OH···O (ice, benzoic acid), and covalent [α-Sn, Ge, Si, C (diamond)].

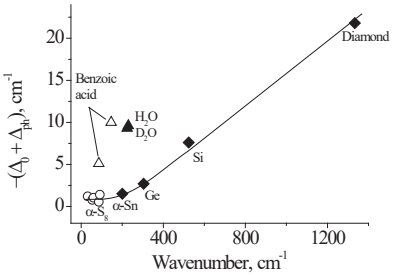

Fig. 9.12. The sum $\Delta_0 + \Delta_{ph}$ of anharmonic contributions to vibrations of different types of bonds.

The absolute value of anharmonicity increases markedly on going from α-Sn_8 to diamond. However, the value of the vibrational frequency of crystals in a given sequence also increases to the same extent.

Therefore, the relative anharmonic change in the vibrational frequency remains practically constant for all compounds.

9.4. Anharmonic interaction of normal vibrations

In Chapter 2, it was shown that any normal vibration of a molecule is constructed from the vibrations of all bonds at the same time, but some – to a greater extent (possibly much more), others to a lesser extent. Consequently, due to cubic anharmonicity, the excitation of any vibrational mode will cause a change in the eigen vectors in the molecule, and this will inevitably affect both the frequency of this mode itself and the frequency of any other mode. In a crystal, the excitation of, for example, a longitudinal phonon, will provoke not only a change in the interatomic distances along the chain of atoms, but also in the transverse direction (stretching the crystal along one crystallographic direction leads, as a rule, to compression along the other, perpendicular direction, and vice versa). In other words, there is an anharmonic relationship between different vibrational modes in molecules and crystals.

In addition, the anharmonic potential of the interatomic interaction shown in Fig. 9.1, can be represented as a sum of several harmonics, but with different coefficients of rigidity (force constants) $f = \frac{d^2U}{dx^2}$. Consequently, a vibrational state with a certain energy and a fraction of anharmonicity can theoretically be described by the sum of several different harmonic states. This phenomenon is the reason for the violation of the selection rules in the vibrational spectrum, and the appearance of overtones and combined tones in it.

The anharmonic coupling between vibrations also determines a finite width of the spectral band (a harmonic oscillator would appear in the spectrum as an infinitely narrow line) and broadening of the mode with increasing temperature. Indeed, the band width ΔE is determined by the lifetime of the excited state. In turn, the lifetime depends on how quickly the energy of the excited state dissipates in the medium as a result of the decay of a given vibration into other vibrations of lower energy or the emission of a quantum of light*. The decay rate is precisely determined by

* The value of the oscillator damping, determined by the radiation, is of the order of 10^{-3} s^{-1} ($\Delta\tau \sim 10^3$ s), which, according to expression (8.6), corresponds to the band half-widths of $\sim 10^{-15}$ cm^{-1}. In other words, the losses of vibrational energy to radiation are negligible and do not determine the actually observed half-widths of vibrational bands.

the anharmonic relationship between all modes participating in the decay process and the population of those vibrational states into which a given phonon decays. (Vibrations obey Bose-Einstein statistics, in which the probability of a boson occurring is proportional to the number of bosons in a system with the same energy). In this case, the first factor will set the band width at each fixed temperature, and the second - the dependence of the width on temperature. Clemens [4] and Balkansky [3] obtained a very simple and convenient expression for describing the temperature dependence of the linewidth under the assumption that the excited vibration ω decays into two others ω_1 and ω_2 of lower energies so that

$$\omega = \omega_1 + \omega_2 \ . \tag{9.19}$$

In this case [3]:

$$\Gamma(T) = G\left(1 + \frac{2}{e^{x/2}-1}\right) + H\left(1 + \frac{3}{e^{x/3}-1} + \frac{3}{\left(e^{x/3}-1\right)^2}\right), \tag{9.20}$$

where $x = \hbar\omega/kT$, G, H – constants. Here, the first term on the right-hand side refers to the decay of a phonon into two others with the same energy ω/2 (cubic anharmonicity with the participation of three particles), and the second – to the decay into three phonons ω/3 (fourth-degree anharmonicity with the participation of four particles). However, it should be borne in mind that the proposed scheme for the decay of a phonon into two others is only an assumption that is quite obvious only for optical phonons in crystals, where there is always a pair of acoustic vibrations of the same or different frequencies that satisfy the requirements of (9.19). In molecules or molecular crystals, the process of dissipation of the energy of an excited intramolecular vibration has, possibly, a more complex structure, in which it is necessary to take into account the equilibrium population of all vibrational states.

Along with mechanical anharmonicity, i.e. deviation of the potential energy from the quadratic law, there is also electro-optical anharmonicity. The latter is determined by the nonlinear dependence of the dipole moment and polarizability on vibrational coordinates. As a result of optical anharmonicity in expansion (1.6, Chapter 1), second-order terms of the type $\left(\frac{\partial^2 \alpha_{\rho\sigma}}{\partial \xi_k^2}\right)_0 \xi_k^2$ and $\left(\frac{\partial^2 \alpha_{\rho\sigma}}{\partial \xi_k \partial \xi_l}\right)_0 \xi_k \xi_l$ turn out to be noticeable (nonzero). Both types of anharmonicity cause violation of the selection rules and the appearance of higher-order vibrational modes in the spectrum.

The intensity of vibrational modes in Raman spectra is usually weaker by several orders of magnitude than in IR absorption spectra. For this reason, overtones and combined tones are very often observed in IR spectra and much less often in Raman spectra. The appearance of second-order bands in the Raman spectrum means a very strong anharmonicity of the corresponding vibrational modes. In crystals of complex oxides, to which most of the minerals belong, the so-called “rattling” modes have a strong anharmonicity. These modes arise when an atom (ion) occupies a too "free" position in the lattice. An example of such an ion is Mg^{2+} in a garnet (pyrope) lattice (Fig. 9.13).

The magnesium ion occupies an octahedral position in the lattice and has, accordingly, six contacts with oxygen ions, four of which are normal, with the remaining two (in the *trans*-position) too long. For this reason, the vibration frequency of Mg^{2+} along "normal" bonds is about 300 cm^{-1}, and along long ones - 133 cm^{-1}. It is intuitively clear that the energy potential corresponding to "long" contacts should be significantly lower than the quadratic potential near equilibrium and approach the quadratic

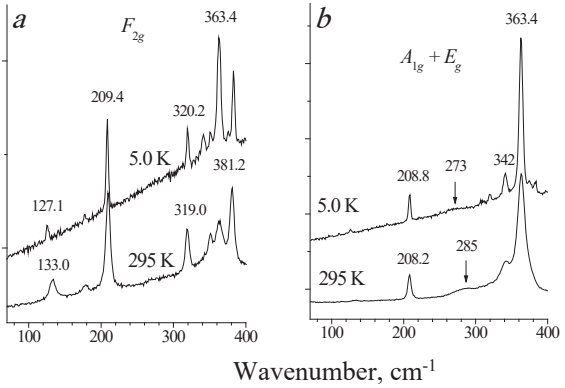

Fig. 9.13. Polarized spectra of pyrope crystals ($Mg_3Al_2Si_3O_{12}$) at 5 and 295 K. The triple degenerate mode of 133 cm^{-1} in the spectrum of F_{2g} vibrations (a) refers to translational vibrations of the Mg^{2+} ion along the long Mg–O bond in the crystal lattice, and the broad band at 285 cm^{-1} in the spectrum $A_{1g} + E_g$ (*b*) - to the overtone of this vibration [8]

potential or even become steeper at maximum ion deviations (at turning points), i.e. demonstrate strong anharmonicity. Therefore, in the Raman spectrum of pyrope (Fig. 9.13), along with the 133 cm^{-1} line, there is a broad band at ~ 285 cm^{-1}, which is related to the Mg^{2+} vibration with a

doubled frequency [10]. The overtone frequency turns out to be even slightly higher than the doubled frequency of the fundamental tone, since the state with the quantum number $n = 2$ falls on the region of the "steep" potential. Another example of strong anharmonicity is given in Chapter 13.

CHAPTER 10

NONLINEAR EFFECTS IN RAMAN SCATTERING

The process of inelastic light scattering described in Chapter 1 is called spontaneous Raman scattering. In it, we assumed that the external electromagnetic field E is small and the induced polarization of the system P depends linearly on the external field $P = \alpha(q)E$, where the polarizability $\alpha(q)$ does not depend on the field E, but depends on the vibrational coordinate [see expression (1.3) in Ch. 1]. But the polarizability of a system is determined by the reaction of its electron shell to an external field. Obviously, this reaction cannot remain constant for any value of the external field, just as the force constant of the bond does not remain constant at large deviations from equilibrium. For this reason, a series expansion can be used to describe the induced polarization with increasing incident radiation intensity:

$$P = \alpha E + \frac{1}{2}\beta E^2 + \frac{1}{6}\gamma E^3 + \cdots. \qquad (10.1)$$

In systems with an inversion center, when the direction of the external field changes, the direction of the vector P should also change, due to which the coefficient β is identically equal to zero. The presence of nonlinear terms in expression (10.1) for the polarization of the system reveals a number of complex physical phenomena in Raman scattering, which we will consider briefly in order to only give an idea of the essence of the processes occurring. There is no need for a detailed description of nonlinear processes, since they are all complex experimentally, require non-standard (and expensive) techniques, and are not used in conventional applied spectroscopy.

The numerical value of the polarizability coefficients very quickly decreases in the series α, β, γ (by about 10^{10} times in each subsequent term), therefore, the appearance of nonlinear effects usually begins at sufficiently high powers of the incident radiation, when the field E exceeds 10^9 V/m.

10.1. Stimulated Raman scattering (SR)

For definiteness, we will consider the process of scattering in a gas medium consisting of tetrahedral molecules of the XY_4 type. The induced polarization of a molecule reveals its interaction with an external electromagnetic field and the energy of this interaction W is determined by the expression:

$$W = -PE = -\alpha(q)E^2. \tag{10.2}$$

Therefore, if $\partial\alpha/\partial q \neq 0$ (and this is true in most cases when atoms are displaced in a molecule), a force arises in the field of the incident wave,

$$F = -\frac{\partial W}{\partial q} = \frac{\partial \alpha}{\partial q}E^2, \tag{10.3}$$

which acts on the vibration of the molecule. The scalar product PE in (10.2) is maximum for collinear vectors; therefore, the resulting force F is maximum for displacements of atoms in the molecule that do not change the direction of the vector P with respect to the direction of the field in the incident wave. In an unexcited state, the molecule performs zero-point motions. From the chaotic motions of atoms representing zero-point motions, those displacements at which the induced polarization P remains parallel to the direction of the external field begin to increase under the action of the force F. In the case of strong fields, this force becomes sufficient to initiate a normal vibration in a molecule. Of the four normal vibrations of the XY_4 molecule, only the fully symmetric vibration ν_1 (see Appendix I) best satisfies the condition of the maximum force F. Thus, if the incident electromagnetic wave has sufficient intensity, vibrations ν_1 initiated by the external field begin to appear in the system and an inverse population of these vibrations is created. But, by creating an inverse population, the incident wave loses energy and is transformed into a wave with energy $\hbar\omega_L - \hbar\omega$, where ω_L is the frequency of the incident wave, and ω is the vibrational frequency of the molecule. This last wave is realized in the form of scattered radiation. However, in contrast to spontaneous scattering, in which each scattering center has an indefinite phase of vibration, as a result of which the scattering is incoherent and equally

probable in all directions*, in this case the scattered radiation of one excited center stimulates the scattering of another excited center (see the remark on the nature of Stokes scattering in Chapter 1). Thus, the state of the photon scattered by the second center is set by the state of the photon scattered by the first center. This means that the radiation from any center of scattering is in phase with the already existing scattered light, which creates the necessary condition for the appearance of coherently scattered light. In other words, the degree of coherence in stimulated scattering of light is many times higher than the degree of coherence of spontaneously scattered light. The result of this process is the interference of radiation from all scattering centers and the appearance of a high-intensity scattered light beam in the direction of the incident wave, while the incident wave itself is attenuated.

The amplitude of the vibrations arising under the action of the incident wave is proportional to E^2 (10.3). Consequently, the induced polarization of the molecule (through which the dielectric susceptibility of the entire medium is also expressed, see Ch. 1) can be written on the basis of (10.1) as

$$P = P_{\text{linear}} + P_{\text{non-linear}} = \alpha E + \gamma E^3, \tag{10.4}$$

where γ is the cubic nonlinear polarizability. The last expression is the rationale for classifying the SRS process as nonlinear effects. The SRS process itself begins when the intensity of the incident wave reaches a certain threshold value and then exponentially gains strength as it propagates through the medium [1, 2].

10.2. Hyper Raman scattering (HR)

In expression (10.1), the second term is proportional to $E^2 = E_0^2\cos^2(\omega_L t) = E_0^2[\cos(2\omega_L t) + 1]/2$. For nonzero hyperpolarizability β (in noncentrosymmetric crystals), expression (10.1) yields the appearance of two effects: second harmonic generation (due to the 2ω argument) and hyper-Raman scattering. The second harmonic generation process does not contain the vibrational spectrum of the crystal, and we do not dwell on it. Let us consider the question of hyper-Raman scattering in more detail.

* Scattering by a totally symmetric vibration occurs in a plane perpendicular to the direction of polarization of the incident light, and is represented in the form of a toroid (according to the law $\cos^2\theta$).

If monochromatic radiation of sufficiently high intensity falls on the sample, then absorption of two photons in one act can take place; in this case, scattering with a frequency of $2\omega_L \pm \omega_{ik}$ is observed (Fig. 10.1). This process is called hyper-Raman scattering. The probability of simultaneous absorption of two photons is small; therefore, the intensity of hyper-RS is also weak, but often amplifies due to resonance (i.e., when the energy $2\omega_L$ approaches the allowed electronic transition).

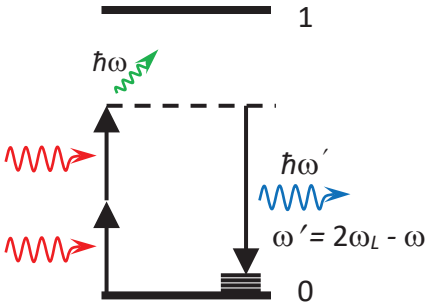

Fig. 10.1. Scheme of the occurrence of hyper-Raman scattering

The scattering intensity is proportional to the square of the incident radiation intensity and, therefore, this process is nonlinear. However, the greatest interest in HR is caused by the fact that this process is three-wave (two incident photons and one scattered one), as a result of which the HR tensor β is a tensor of the third rank, since it is determined by three indices – *i*, *j*, and *k* – related to direction of the polarization vectors of photons in Cartesian coordinates. If the spontaneous Raman tensor α contains 9 components, of which 6 are independent, then the tensor β consists of 27 components, of which 10 (maximum) are independent. In this case, some "silent" (i.e., unobservable in spontaneous Raman scattering) modes can be observed in HR. Finally, since the HR spectrum is observed in the region of doubled frequencies $2\omega_L$, i.e. far from the frequency of the excitation line ω_L, then low-frequency vibrational modes located in spontaneous Raman scattering too close to the Rayleigh scattering line can be easily detected.

10.3. Coherent anti-stokes Raman scattering (CARS)

In a medium where two coherent light beams ω_{01} and ω_{02} propagate, with $\omega_{01} > \omega_{02}$, four-wave mixing processes can be observed (in contrast to the three-wave mixing described in the previous paragraph).

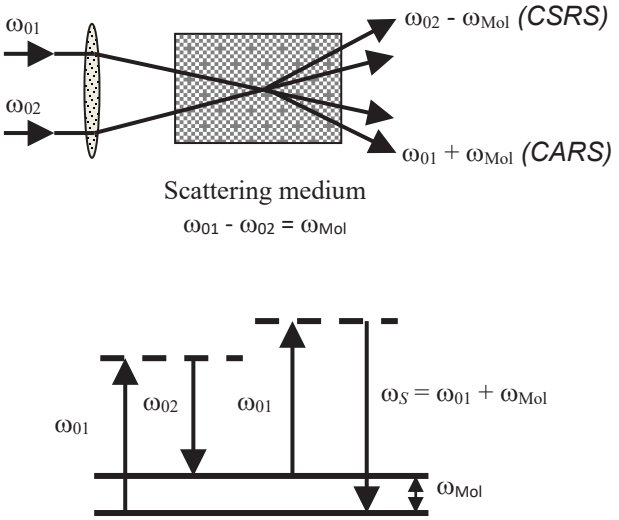

Fig. 10.2. CARS scheme

For this, it is necessary that the last term in expression (10.1) containing γ be nonzero. In this case, along with the generation of the third harmonic, two very interesting processes become possible: coherent anti-Stokes scattering (CARS) and coherent Stokes (CSRS) Raman scattering. If the frequency ω_{01} is kept constant, and ω_{02} varies, then at $\omega_{01} - \omega_{02} = \omega_{Mol}$, where ω_{Mol} is one of the vibration frequencies of a molecule or crystal observed in spontaneous Raman scattering, the intensity of the scattered light increases sharply.

The CARS process is depicted in Fig. 10.2. At the first stage, photon $\hbar\omega_{01}$ excites an electron to a virtual state. Then the quantum of light $\hbar\omega_{02}$ stimulates the transition of the electron to the vibrational level E_k. At the third stage, the $\hbar\omega_{01}$ quantum again excites the electron to a virtual state,

after which the electron returns to its initial state with the emission of a light quantum with energy $\hbar\omega_s = \hbar\omega_{01} + E_k$. Obviously, changing ω_{02} so that the entire region of vibrational states is covered, one can obtain the CARS spectrum. It is also obvious that the vibrational states themselves do not take part in the process, i.e. do not appear or disappear at the end of the CARS act. This process is called parametric and requires phase synchronization. It is shown in Fig. 10.3, where

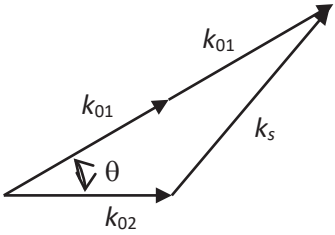

Fig. 10.3. Geometry of CARS

the wave vectors of the incident light k_{01} and k_{02} are fixed in direction; therefore, the direction of the wave vector of the scattered radiation k_s is also fixed. For this reason, CARS generates a low-divergence, sharply directed, and scattered radiation beam. Selection rules for CARS are the same as for spontaneous RS, therefore all modes active in RS are also active in CARS. The scattered light intensity in CARS is proportional to the square of the number of scattering molecules and the square of the incident radiation power ω_{01} and ω_{02}, i.e. the CARS process is substantially non-linear.

10.4. Surface enhanced Raman scattering (SERS)

When small metal particles, most often gold or silver, are enveloped in molecules, the intensity of Raman scattering can increase by a factor of 10^{10} - 10^{14}, so that it becomes possible to record the spectrum of a single molecule. The reasons for this gigantic effect are not completely clear (at least at the time of writing), but usually two versions are considered, electromagnetic and polarization.

In the first of them, the incident electromagnetic wave E falls into resonance with the plasma oscillations of the electron gas of a metal particle, exciting dipole oscillations in it, which, by emitting, amplify the incident wave (surface plasmons are often considered). The magnitude of this effect is proportional to E^2. The resulting amplified field causes

Raman scattering on the vibrations of the molecule on the particle surface, while the scattered radiation is also in frequency resonance with the plasma oscillations of the metal particle and is amplified by the same mechanism as for the incident wave. The magnitude of the latter effect is also proportional to E^2. The total gain is proportional to E^4. The higher the frequency of the vibrational mode, the farther the scattered radiation is detuned from the incident radiation, and the weaker the amplification effect, since both frequencies cannot simultaneously be in exact resonance with the plasma oscillations. The plasma frequency of Au and Ag particles lies in the blue region, but the molecules adsorbed on the surface shift it to the green-yellow region, "pulling" the frequency of the most commonly used Ar^+ ion laser generation lines. If the metal particles are too small in size and consist, for example, of several atoms, then the electron gas is not formed in them and the SERS effect is not observed. If the particles are too large, then the effect also weakens, since in large particles the dipole radiation of the electron gas is small. In addition, SERS strongly depends on the shape of the metal particles and their relative position on the substrate surface.

The SERS polarization mechanism considers the chemical bond of an adsorbed molecule with a metal surface, which is carried out mainly through the lone electron pair of the molecule. In this case, charge transfer between the molecule and the metal is assumed. The chemical theory is not able, however, to independently explain the gigantic SERS value and is usually considered in tandem with the electromagnetic one.

10.5. Resonance Raman scattering (RR)

If the energy of the incident radiation approaches the energy of the electronic transition (see Figs. 1.1-1.3), then the probability of electron excitation increases sharply, and the probability of phonon scattering also sharply increases [see expression (1.33) and subsequent in Ch. 1]. In this case, the so-called resonant Raman scattering, or "hot" luminescence, is observed. Resonant scattering is especially interesting because not all vibrational modes of the spectrum are involved in this process, but only those that are "relevant" for a given electronic transition (i.e., modes modulating the energy distance between allowed electronic states and, thus, modulating the intensity of electronic absorption). Resonant modes become more intense in the spectrum by hundreds and thousands of times. This helps to better understand both vibrational and electronic spectra. An interesting example of resonant scattering by “actual” modes is the spectra of (acetylacetonate)-dicarbonyl iridium (I), $Ir(acac)(CO)_2$. Fig. 10.4 shows

the packing of $Ir(acac)(CO)_2$ molecules in a crystal, and Fig. 10.5 - its spectra at the laser excitation lines, 633 nm and 488 nm.

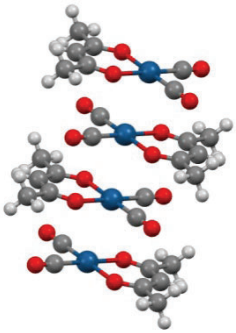

Fig. 10.4. Packing of $Ir(acac)(CO)_2$ molecules in a crystal. Iridium ions are located along the ***a*** crystal axis.

$Ir(acac)(CO)_2$ crystals are strongly colored, and their absorption spectra are characterized by the presence of an absorption band in the visible region. The molecules in the lattice do not form hydrogen bonds. In addition, the iridium atoms are separated from each other at a rather large distance, 3.166 Å, and their relative position is characterized with a short contact, but not a chemical bond. The Raman spectra (Fig. 10.5) contain more in-depth information.

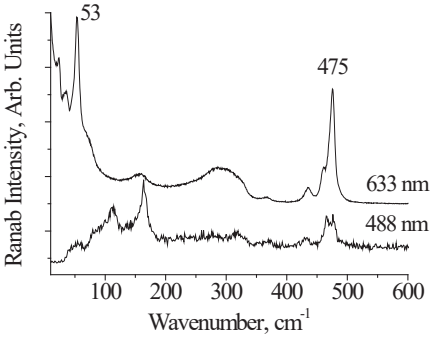

Fig. 10.5. $Ir(acac)(CO)_2$ spectra excited by laser lines at 633 and 488 nm.

When excited by the 633 nm line, which falls into the absorption band of the crystal, the 53 cm^{-1} mode turns out to be the most intense in the spectrum, while when excited by the 488 nm line, it is practically

absent. This mode belongs to Ir-Ir vibrations, and its appearance in the resonance spectrum indicates that the exciting laser line is in resonance with molecular orbitals occurring due to the interaction of neighboring iridium ions. In other words, a direct Ir-Ir chemical bond occurs in the crystal. The intensity of another mode, 475 cm^{-1}, increases (but to a lesser extent) upon excitation of the spectrum in the red region. This mode is assigned to Ir-O vibrations. The displacement of iridium ions in the latter mode also modulates the energy distance between the Ir–Ir molecular orbitals.

Resonance scattering is often used for spectroscopy of large biological molecules, in which the number of vibrational modes is very large and difficulties arise in their assignment (often the lines in the spectrum of large molecules overlap, causing broad structureless bands). If such a molecule contains fragments that have an electronic transition in the visible region, for example, a metal-ligand bond in hemoglobin, then by adjusting the laser radiation to the transition energy, one can sharply increase the vibration intensity of bonds directly adjacent to this fragment and, thus, highlight them in the general spectrum. In addition, since the intensity of the vibrational mode at resonance can increase up to 10^6 times, it is possible to obtain a resonance spectrum of a compound present in very small amounts. So, if spontaneous Raman scattering usually requires at least 10^{-2} Moles of a substance, then in resonance scattering this value can be reduced to 10^{-8} Moles. An example of the resonance scattering spectrum of I_2 molecules is given in Chapter 8 in Fig. 8.8.

CHAPTER 11

HYDROGEN BONDING

An interaction between atomic and molecular systems can be divided into three main types: Coulomb, van der Waals, and chemical. Chemical interactions are usually divided into several types to make them more definite: covalent, ionic, donor-acceptor, hydrogen, etc. However, each of them is based on the well-known interaction of atomic or molecular orbitals. The different degree of overlap of the orbitals and the distribution of electron density on them (the occupancy of the orbitals) reveals the specified structuring of the chemical interaction.

The Coulomb and van der Waals interactions are isotropic, and the chemical one is directional. This is their main difference. The consequence of directionality is the variety of structures that arise during chemical interaction. The hydrogen bond energy is about an order of magnitude higher than the van der Waals energy, but is the weakest among all types of chemical bonds.

In recent years, the hydrogen bond has been much less discussed in the literature. Modern quantum-chemical programs are excellent at calculating molecules and crystal fragments, including those that involve a hydrogen bond. The result of the calculation is usually a description of the molecular orbitals and the vibrational spectrum of the compound. This is very important information. However, researchers are often interested in issues related to trends, functional dependencies, and the main factors influencing certain characteristics of compounds to make it possible to predict their properties from their composition and structure. This fully applies to the assessment of the characteristics of hydrogen bonds. In this chapter, an attempt is made to discuss issues related to the general principles of hydrogen bond formation. Knowledge of these principles makes our work conscious and allows for meaningful experimentation.

The hydrogen bond, being, in fact, a conventional chemical bond, is significantly inferior to the latter in strength (energy), but even more significantly surpasses it in a variety of properties. The length of a hydrogen bond of the same type can vary over a broad area, and its spectroscopic parameters in vibrational spectra vary so much that the

reliable assignment of the bands in the spectrum to hydrogen bond vibrations is still a difficult problem.

Over the past 50-70 years, numerous attempts have been made to describe hydrogen bonds, mainly in terms of their structural parameters and manifestations in vibrational (IR and Raman) spectra. A large number of monographs and reviews on hydrogen bonds in various systems have appeared [1-10]. However, the authors' desire to give an exhaustive description of the structural parameters and spectra of all compounds that form the full range of hydrogen bond properties led to excessive detail in the description of experimental data, complicating a clear presentation of the subject of the research. The complexity of the definition (or classification) of the hydrogen bond lies in the fact that it can involve various groups of atoms of the periodic table (oxygen, nitrogen, carbon, halogens, and metals), and in some cases, individual molecular orbitals. And in each case, the properties of the bond become deeply individual. In addition, the simplest (and most common) hydrogen bond consists of three atoms: donor, acceptor, and hydrogen. And if the structural position of the donor and acceptor is determined with acceptable accuracy, then the position of the hydrogen atom on the bond is often not established at all, but is set by the experimenter. However, it is the latter parameter that determines the spectral properties of the hydrogen bond. It is therefore clear that for many years, right up to recent years, hydrogen bonding constituted a difficult (almost incomprehensible) problem.

The purpose of this chapter is not a detailed description of each of the huge number of hydrogen bond manifestations, but an exposition, close to phenomenological, of the conditions and features of the occurrence of hydrogen bonds in a wide range of their energies.

It is assumed that the reader has a basic understanding of the hydrogen bond. Therefore, many of its non-fundamental details are not considered here: single- and multicenter bonds, bond angle, etc. Moreover, in order to focus the reader's attention on the main physical and chemical aspects of the hydrogen bond, and not on all possible manifestations of it, further in the text we will consider mainly the OH···O bond as the most widespread and studied.

11.1. Definition, brief history, main stages of development

According to the IUPAC, 2011 recommendation "*The hydrogen bond is an attractive interaction between a hydrogen atom from a molecule or a molecular fragment X–H in which X is more electronegative than H, and*

an atom or a group of atoms in the same or a different molecule, in which there is evidence of bond formation" [11].

This strict definition is already fraught with the above-mentioned tendency to excessive detail and is perceived upon first reading with some difficulty. For this reason, readers are offered here another, possibly imperfect, but simpler and more compact definition: *The hydrogen bond is a weak chemical bond between the X–H group of one molecule and the electronegative Y atom of another* (*or the same*).

Usually a hydrogen bond is written as X–H···Y, where the dots represent the hydrogen bond itself. In this notation, X–H is a terminal fragment of one molecule, and Y is a terminal fragment of another molecule. X is a hydrogen bond donor, and Y is an acceptor. The electronegativity of an element is not constant and depends on the specific chemical conditions (for more details, see section 2.2).

The hydrogen bond was discovered at the beginning of the last century. It is not possible to establish the exact date of its discovery, since it is not clear from the publications of those years what exactly the authors had in mind when describing chemical reactions involving the polar group X–H. For the first time, the concept of hydrogen bonding appeared in the work of Huggins [12] and almost simultaneously in Latimer and Rodebusch [13]. The term "hydrogen bond" was first used by L. Pauling in 1930 [14]. But real interest in hydrogen bonding arose only a few more years later, when Bernal and Fowler [15] suggested that a high degree of short-range order in the structure of liquid water is provided by intermolecular bonds, which were then attributed to hydrogen bonds. This work, which assumes a tetrahedral environment for each water molecule due to interactions with neighboring molecules, presently known as the "Bernal-Fowler rule", served as a powerful impetus for the study of hydrogen bonds. However, in those years, practically the only experiment providing information on the state of the hydrogen bond in a compound was IR absorption spectroscopy. But in the IR (and then in Raman) spectra, the hydrogen bond is well recorded only for weak bonds and very unreliably - for moderate and strong ones. For this reason, until about the 1990s, there was only a quantitative accumulation of information on the hydrogen bond, which allowed J. Pimentel and O. McKellan to declare in their famous monograph [2]: "Currently, the H-bond theory is the subject of considerable controversy, its qualitative predictive power is limited, and it can hardly make quantitative predictions. Apparently, it can be argued that the significance of the H-bond in the general theory of chemical bonding is not yet understood in all details."

The next stage in the study of the theory of hydrogen bonding was the work of Morokuma [16], the appearance of which in 1971 was due to the development of reliable computer methods for calculating molecular states. In the proposed approach, presently known as Morokuma decomposition, the chemical bond between atoms is broken down into separate components (electron repulsion, charge transfer, polarization, and dispersion forces), from which the total interaction is calculated as a function of the distance between atoms. Morokuma's work did not become the last word in the development of the theory of hydrogen bonding, but dispelled (and this is its value) numerous attempts to attribute some unusual properties to the hydrogen bond. Morokuma showed that the interactions that form a hydrogen bond make it virtually indistinguishable from any other chemical bond, with the only exception that all these interactions in a hydrogen bond are relatively weak.

After the appearance of Morokuma's work, it was long believed that hydrogen bonding occured due to the lone pair of electrons of the acceptor, which spread to the filled X–H orbital of the donor. However, first Benoit and Marx [17] in 2005, and then Wang et al. [18] in 2014, using a high-level quantum-chemical calculation (work [18] was also reinforced by the experiment data), showed that an important role in the formation of hydrogen bonds is played by the quantum uncertainty of the position of the proton. In fact, these last two works have finally established the nature of the hydrogen bond, after which various interpretations in its definition should disappear. It is the ideas in [17 and 18] about the role of quantum uncertainty in the coordinates of atoms participating in the formation of hydrogen bonds that underlie the interpretation of its nature and that are adopted here.

11.2. General description

In a conventional chemical bond, the distance between interacting atoms can vary within small limits, while the interaction potential changes monotonically and predictably. In a hydrogen bond, a change in the donor-acceptor distance $d_{X\cdots Y}$ causes a dramatic change in the potential function of the proton on the bond. This is the basis of the complex manifestation of hydrogen bonds in vibrational spectra, which for many years made it difficult to understand its nature.

Therefore, to solve the main issues related to hydrogen bonding, it is necessary to consider how the potential function of the proton on the bond, the strength of the hydrogen bond, the O–H vibration frequency, and other characteristics change depending on $d_{O\cdots O}$.

A huge amount of experimental material has been accumulated in the literature characterizing weak and moderate hydrogen bonds. There are much fewer works dealing with strong and extremely strong bonds, and the Raman spectral studies of compounds with such bonds presented in this work were performed for the first time. This is due to the fact that, as a rule, the fixing of strong hydrogen bonds in vibrational spectra requires measurements at low temperatures. Such measurements, while not presenting fundamental difficulties, require, however, expensive equipment and are time-consuming and therefore not widespread. But first, let's briefly consider the general properties of hydrogen bonds.

11.2.1 Potential energy of a proton on a hydrogen bond

In a weak O–H···O hydrogen bond, the proton practically does not interact with the oxygen-acceptor, but is fully localized at the oxygen-donor, forming a strong ordinary covalent bond with the latter.

Therefore, the potential function of the proton along the hydrogen bond at large values of $d_{O\cdots O} > 2.7$ Å can be represented as a curve with two minima, one deep near the donor, and the other shallow near the acceptor (Fig. 11.1). Both vibrational states, the zeroth and the first excited (denoted in Fig. 11.1 as "0" and "1"), are located in a deep minimum.

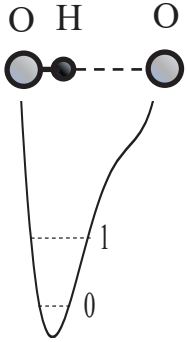

Figure 11.1. Proton potential function for a weak hydrogen bond, $d_{O\cdots O} \geq 2.7$ Å

A decrease in the $d_{O\cdots O}$ distance enforces the interaction of a proton with an acceptor. In this case, the energy minimum for a proton near the acceptor deepens, and for the intermediate H-bond ($d_{O\cdots O} \sim 2.6$ Å) the potential curve for a proton looks like in Fig. 11.2.

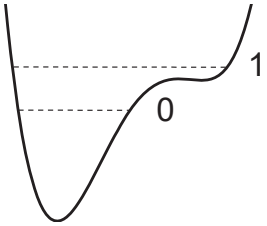

Figure 11.2. Proton potential function for a moderate hydrogen bond, $d_{O\cdots O} \sim 2.6$ Å.

The main difference between the moderate hydrogen bond and the weak (and, as we will see below, from the strong and extremely strong) is that now the proton potential is not harmonic, and the known solutions of the vibrational problem for the harmonic potential can't be attributed to the case. In the potential of the moderate hydrogen bond, the excited vibrational state can be located above the barrier separating the minima near the donor and acceptor, i.e. in a wide potential well formed by both minima, and the zeroth vibrational state is in a narrow minimum near the donor atom. In this case, the ratio of the energy of the stationary states, the zeroth and the first excited, can differ appreciably from that of the traditional solution for a harmonic oscillator.

With a further decrease in $d_{O\cdots O}$ and the transformation of the H-bond from moderate to strong, the interaction of the proton with the acceptor becomes so strong that it is compared with its interaction with the donor, while the energy minima for the proton near the donor and acceptor become identical, leaving a barrier with a height of U_0 between them ("deep tunneling regime", Fig. 11.3). This situation formally means that the electronegativity of the donor and the acceptor is equal, but in reality, most often, we are talking about the complete identity of the donor and acceptor molecules. The condition of identity is necessary for the formation of a strong hydrogen bond, but not sufficient. The second condition is the high electronegativity of the donor and acceptor.

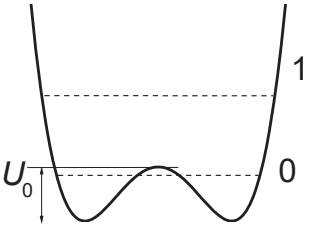

Figure 11.3. Proton potential function for a strong hydrogen bond ("deep tunneling regime"), $d_{O\cdots O} \sim 2.5$ Å.

If U_0 turns out to be less than the energy of zero-point vibrations of the proton in the bond (more on this below), then the zero vibrational state, as well as the excited state, gets a wide minimum, and double-well potential of the proton becomes single-well.

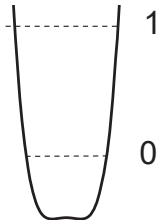

Figure 11.4. Proton potential function for an extremely strong hydrogen bond ("ultrashort, centered HB"), $d_{O\cdots O} < 2.3$ Å.

Finally, as the donor and acceptor approach further, an extremely strong hydrogen bond is formed ("ultrashort, centered HB", Fig. 11.4), in which there is practically no barrier between the minima, and the shape of the potential curve of the proton becomes close to harmonic. The latter case is a linear symmetric hydrogen bond O···H···O. However, the preparation of compounds with a linear symmetric bond is not an easy task from the point of view of chemistry.

11.2.2. The bond energy as function of its length. Uncertainty of the proton coordinates, uncertainty of the O···O distance

Benoit and Marx [17] and then Wang et al. [18], using the procedure for calculating the Feynman path integrals for the O–H···O system, determined the positions of the proton on the H-bond for the case of weak, moderate, strong, and extremely strong hydrogen bonds. The main result of these works is that the bonded proton is considered not as a mathematical point, but as the proton density distribution, which is the result of the quantum uncertainty of the proton coordinates – an indisputable fact, but not explicitly taken into account in earlier theoretical works (Fig. 11.5).

Due to quantum uncertainty, the proton density distribution function, having a finite width comparable to the potential space for a proton at a bond, begins to spread with decreasing $d_{O\cdots O}$ from a minimum at a donor atom to a minimum at an acceptor atom. In other words, part of the proton density turns out to be near the acceptor oxygen and interacts with it according to the same scheme as with the donor oxygen (Fig. 11.6).

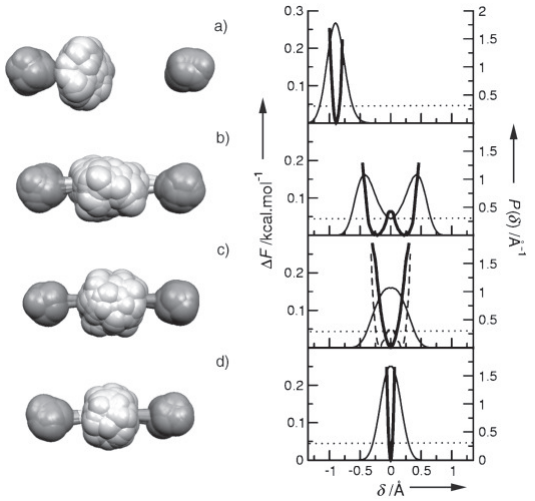

Figure 11.5 Calculation [17] of the distribution function of proton density (left) and potential energy of a proton (right) depending on the length of the O–H···O bond: a) weak bond, $d_{O\cdots O}$ = 2.85 Å, b) strong bond, $d_{O\cdots O}$ = 2.43 Å, c) strong bond, $d_{O\cdots O}$ = 2.29 Å, d) extremely strong bond, $d_{O\cdots O}$ = 2.17 Å. δ = R_{OaH}–R_{ObH}. (See also Fig. 1 in [17]). The horizontal dotted line indicates the thermal energy level kT at 25 K. (The figure is reproduced with permission from ref. [17], copyright (2005) European Chemical Societies Publishing).

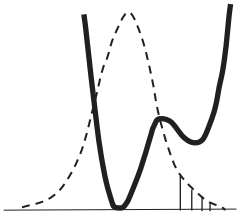

Figure 11.6. The assumed proton density distribution (dotted curve) at $d_{O\cdots O}$ < 2.6 Å. The region of the proton density spread into the adjacent well is shaded.

It is this effect that causes, on the one hand, the strengthening of hydrogen bonds, and on the other, a decrease in the frequency of the νO-H vibration (for more details on the mechanism of formation of the proton vibration frequency, see the next paragraph 11.2.3). The closer the donor and acceptor are to each other, the greater part of the proton density is in the potential well of the acceptor, the stronger the interaction of the proton with the acceptor and the tougher the hydrogen bond. At large values of $d_{O\cdots O}$, the proton density distribution function does not reach the adjacent

minimum (case (a) in Fig. 11.5). However, a weak hydrogen bond occurs in this case as well. What's the matter here? The point is that the quantum uncertainty of the coordinate is a property of not only the proton, but also the donor and acceptor. The uncertainty of the coordinates of each of them is approximately half that of the proton, but in total, all three uncertainties make possible the formation of a hydrogen bond even at a large $d_{O\cdots O}$ in the range of 2.7 - 3.0 Å.

The fact that the quantum uncertainty of the coordinates of oxygen atoms is about half that of protons can be shown as follows.

The root-mean-square deviations (standard deviation) of the coordinate q and the momentum p of the particle in a quantum harmonic oscillator are written as:

$$\delta q(n) = \sqrt{\frac{\hbar\left(n+\frac{1}{2}\right)}{m\omega}} \tag{11.1}$$

$$\delta p(n) = \sqrt{\hbar m\omega\left(n+\frac{1}{2}\right)}, \tag{11.2}$$

where ω is the frequency of the oscillator, n is the vibrational quantum number, and m is the mass of the particle. Hence, for zero-point vibrations of the particle ($n = 0$), we get:

$$\delta q(0) \cdot \delta p(0) = \frac{\hbar}{2}. \tag{11.3}$$

In other words, the quantities $\delta q(0)$ and $\delta p(0)$ are equal to the quantum uncertainties of the coordinate Δx and the momentum Δp, which are related by the Geisenberg uncertainty relation:

$$\Delta x \cdot \Delta p = \hbar/2. \tag{11.4}$$

The value of the standard deviation of the coordinate can be rewritten as

$$\delta q(0) = \sqrt{\frac{\hbar}{2m\omega}} = \sqrt{\frac{\hbar}{2m\sqrt{\frac{k}{m}}}} \sim m^{-1/4}. \tag{11.5}$$

An oxygen atom is 16 times heavier than a hydrogen atom, hence the standard deviation $\delta q(0)$ and the quantum uncertainty of its coordinate Δx are two times less than that of a proton.

The particle momentum and the quantum uncertainty of the particle momentum in the oscillator are proportional to its energy $p = \sqrt{2mE}$. Hence, the uncertainty of the proton's coordinate is inversely proportional to its binding energy (see uncertainty relation) and thus depends on the rigidity of the hydrogen bond. The energies of the vibrational states of the proton, the zeroth and first excited, are maximal for the weak and extremely strong bonds (Figs. 11.1 and 11.4, respectively), and minimal for the moderate and strong bonds corresponding to the initial phase of the transition from the double-well potential to the single-well potential (Figs. 11.2 and 11.3). From the uncertainty relation, it follows that the maximum uncertainty of the proton coordinate should fall on the case presented in Figs. 11.2 and 11.3, and the minimum - in Figs. 11.1 and 11.4. It is the pattern that manifests itself in the calculations of Benoit and Marx [17] (Fig. 11.5).

Thus, the energy of the hydrogen bond depends on the degree of propagation of the proton density to the neighboring (acceptor) minimum and is determined by the donor-acceptor distance. But neither the depth of the minimum at the acceptor, nor $d_{O\cdots O}$ are independent parameters, but are derived from another quantity - the electronegativity of the acceptor, i.e., the ability of the acceptor to take on the electron density and, thus, interact with the hydrogen atom. The latter value is determined by the degree to which the atomic orbitals of the oxygen acceptor are filled when molecular orbitals are formed in the "acceptor" molecule. If the oxygen-acceptor orbitals are completely saturated (theoretically), then the oxygen loses the ability to interact with the hydrogen atom of another molecule and the hydrogen bond is not formed. And the strongest O–H···O hydrogen bond occurs when the oxygen-acceptor bond with "its" molecule is close to an ordinary bond, and the oxygen needs an additional electron density to saturate its orbitals. In this case, the saturation of the oxygen-donor and oxygen-acceptor are the same and the resulting hydrogen bond becomes symmetrical. Thus, the entire spectrum of the strength (energy) of the O-H···O hydrogen bond is determined by the electronegativity of the oxygen acceptor, which determines the corresponding length of the $d_{O\cdots O}$ bond.

11.2.3 The proton vibrational frequency as function of a length of the hydrogen bond

With the formation of a hydrogen bond, even a weak one, the resulting additional minimum near the acceptor deforms the potential curve for the proton near the donor so that the minimum becomes asymmetric and wider. A formal consequence of the broadening of the

potential well is a decrease in the frequency of the proton vibration, since the latter value is proportional to the force constant k, determined by the slope of the potential well: $k \sim d^2U/dx^2$. However, the dependence of the proton vibrational frequency on the distance $d_{O\cdots O}$ is complex, and it is necessary to consider it in more detail.

From the text of the previous paragraph, it follows that the penetration of the proton density into the neighboring potential well near the acceptor enforces the hydrogen bond H···O and weakens the O–H bond, since both are carried out by the valence electron of the same hydrogen atom. For a long time, determining the dependence of the frequency ν_{O-H} on the distance $d_{O\cdots O}$ was a priority goal in the study of hydrogen bonding. There is no need for it now, since, as already mentioned above, the vibrational frequency ν_{O-H} of any hydrogen bond can be calculated with a high accuracy. As general remarks on the dependence of ν_{O-H} on $d_{O\cdots O}$, the following can be given. The change in νO-H with the strengthening of the hydrogen bond can be monotonic only as long as both vibrational states, the zeroth and the first excited, are placed in the same potential minimum near the donor, which is valid in the range of bond strength from weak to moderate. However, at $d_{O\cdots O} \sim 2.6$ Å, the moment comes when the excited state is "pushed out" from a narrow minimum into the region of a wide potential well formed by the combination of two potential minima (Fig. 11.2). At this point, the energy of the excited state drops sharply due to an increase in the size of the oscillator and the corresponding lengthening of the de Broglie wavelength of the proton.

In fact, the wave functions describing the vibrational states of the harmonic oscillator are found in the solution of the Schrodinger equation and for the zeroth and first excited states are written as

$$\psi_0(q) = \frac{1}{N_n} e^{-\frac{\beta^2 q^2}{2}}, \tag{11.6}$$

$$\psi_1(q) = \frac{2\beta q}{N_n} e^{-\frac{\beta^2 q^2}{2}}, \tag{11.7}$$

where N_n is the normalizing factor, and q is the coordinate, $\beta = \frac{1}{q_{max(0)}}$.

Figure 11.7 Wave functions of the harmonic oscillator. Vertical dashed lines indicate the turning points of the classical oscillator.

According to de Broglie, a quantum particle is also a wave, the length of which in the case of rectilinear movement of the particle is determined by its momentum *p*:

$$\lambda = \frac{h}{p}. \tag{11.8}$$

The wave functions shown in Fig. 2.7 are de Broglie waves. The zeroth state is represented by a half-wave, and the first excited is represented by one full period of the wave length of λ determined by the size of the oscillator (the wave must "fit" in the oscillator, and that is the substance of the boundary conditions). From here

$$p = \frac{h}{\lambda} = \sqrt{2mE}, \tag{11.9}$$

$$E = \frac{h^2}{2m\lambda^2} \sim \frac{1}{\lambda^2}, \tag{11.10}$$

where *E* is the energy of the vibrational state. (It should be noted that a comparative estimation of the energy of the vibrational state by the de Broglie wavelength is possible only within a lone stationary state, for example, only for the zeroth state, or only for the first excited state). In addition, as already noted above, the shape of the potential curve of the oscillator, shown in Fig. 11.2, is far from harmonic, and this circumstance will radically change the solution both for the energy of the stationary states and for the ratio between the energies of the zeroth and first excited states.

When the excited state is pushed out from a narrow minimum to a broad one (Fig. 11.2), the de Broglie wavelength of the excited proton increases by 1.5-2 times, and the energy of the excited state decreases by 2-4 times compared to what it would be in the absence of a wavelength

jump (Fig. 11.8). At the same time, the zeroth state remains in a narrow minimum and the size of its potential space and energy remain virtually unchanged. (An indirect confirmation of this assumption can be found in the calculations of Wang et. al. [18]).

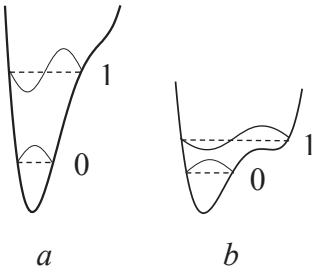

Figure 11.8. Schematic representation of the ground and excited vibrational states for a weak (*a*) and moderate (*b*) bonds.

In other words, of the two states, $E(0)$ and $E(1)$, only the second one is greatly reduced due to the unusual shape of the potential curve. As a result, the vibrational frequency $\nu_{O-H} = E(1) - E(0)$ also strongly decreases, and ν_{O-H} as a function of $d_{O\cdots O}$ should fall sharply in the region of $d_{O\cdots O} \sim 2.6$ Å (Fig. 11.9). This is the most dramatic moment in the evolution of hydrogen bonding.

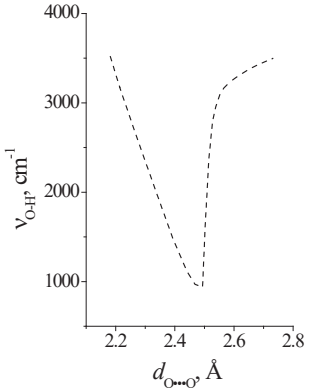

Figure 11.9 Assumed dependence of O–H vibrational frequency as a function of distance $d_{O\cdots O}$ for O-H···O hydrogen bonding.

The sharp decreasing of the ν_{O-H} is possible only by the fact that the potential shown in Fig. 11.2 is not harmonic, does not include the known solutions for the eigenvalues of energy in a quantum harmonic oscillator,

and the relationship between the energy of stationary states, according to which the energy of the zeroth state in a harmonic oscillator is $\hbar\omega/2$, and the energy of the first excited state is $3\hbar\omega/2$, is violated. However, the idea of the wave function in the form of a de Broglie wave "inscribed" in the size of the oscillator remains in this case as well.

The next stage on the dependence of the vibrational frequency OH occurs at a distance of $d_{O\cdots O} \sim 2.5$ Å (Fig. 11.3). At this distance, the barrier between the potential minima becomes less than the energy of zero-point motions, and now the zeroth state is pushed out into a wide minimum of united potential. The potential for a proton takes the traditional single-well form, the ratio of the energies of the zeroth and excited states also becomes close to the usual one, and the difference between them is set to $\hbar\omega$. Starting from this point, the width of the potential well narrows as the $d_{O\cdots O}$ decreases, and the ν_{OH} dependence should again display a monotonous change, but this time in the direction of higher frequencies (Fig. 11.9).

It is possible to estimate what the distance $d_{O\cdots O}$ should be, so that the wavenumber of a proton vibration in a single-well potential again takes the value about 3600 cm^{-1}, as in the case of a very weak hydrogen bond. The vibrational frequency of a proton of a weak O–H···O bond is determined by the O-H force constant, while the vibration of a strong symmetric O···H···O is determined by two identical O···H force constants. Therefore, in order that ν_{O-H} in both types of potential be equal, each of the force constants O···H of the symmetric bond must be twice as small as one force constant O–H of the weak bond. But if the force constant of O–H turns out to be half, then the frequency will decrease to ~ 2500 cm^{-1}. The last value corresponds to the length of the O–H ~ 1.1 Å. Hence, the proton vibration in the single-well potential of the extremely strong O···H···O bond with a frequency of ~3600 cm^{-1} will take place at $d_{O\cdots O} \sim$ 2.2 Å.

To experimentally confirm the dependence of the proton vibration frequency on the $d_{O\cdots O}$ distance, presumably determined by the curve in Fig. 11.9, it is necessary to gradually reduce the $d_{O\cdots O}$ distance in the same compound. It is possible with the application of external pressure. Such an experiment was carried out when measuring the vibrational spectrum of ice under outer pressure [19, 20]. It was shown that at a pressure of about 60 Gpa, the spectrum of ice changes radically: the mode of stretching vibrations of H_2O at ~1500 cm^{-1} (according to [19]) or ~2700 cm^{-1} (according to [20]) disappears, and instead a new mode about 800 cm^{-1} appears. The latter rises to ~ 1500 cm^{-1} with a further increase in pressure.

In addition, the Raman intensity of the O–H vibrations drops to zero, while the IR intensity, on the contrary, increases with a very strong broadening of the absorption band. It can be seen that the changes in the Raman spectra observed in [19, 20] at outer pressure are quite consistent with the scenario described above. (It should be noted, however, that the authors themselves interpreted this as a phase transition ice VII – ice X). Therefore, in view of the results [19, 20], the wavenumber ~800 cm^{-1} should be taken as the lower limit of the proton vibration frequency on the O–H···O bond, and this minimum value should be attributed to a moderate hydrogen bond, and not to a strong or extremely strong one, as assumed earlier [21]! Thus, the arrangement of the vibrational states of a proton in the potential of an moderate hydrogen bond, when the zeroth state remains in a narrow minimum at donor oxygen, and the first excited state falls into a wide minimum (Fig. 11.2), causes the fundamental change in the Raman spectra: a sharp and significant decrease in the frequency of O–H and a weakening in the scattering intensity to zero.

The experiment with ice [19, 20] perfectly illustrates the behavior of the O–H···O hydrogen bond as a function of the $d_{O\cdots O}$ length, but the O–H···O bond itself in liquid and crystalline water is not a conventional O–H···O bond. The fact is that the oxygen atom of the same H_2O molecule is both a donor and an acceptor of the hydrogen bond simultaneously, whereas in all other compounds, the oxygen-donor and oxygen-acceptor are physically different atoms. What does this change in the state of the O–H···O bond? First of all, the rate at which the bond strength changes with a change in the $d_{O\cdots O}$ distance. In an isolated H_2O molecule, the electron shell of the oxygen atom is saturated due to two ordinary O–H covalent bonds, and its electronegativity is close to zero. For this reason, the O–H···O hydrogen bond formed in liquid and crystalline water is very weak with a proton vibrational frequency of around 3200-3400 cm^{-1}. (Due to the weak hydrogen bond, the melting point of ice is very low and we have life on Earth as it is). When the $d_{O\cdots O}$ length is shortened, for example, under external pressure, and the hydrogen bond is strengthened, the hydrogen atoms begin to share their electron density with neighboring oxygen atoms, as a result of which their bond with “their” oxygen weakens, and the saturation of the electron shell of this oxygen from “their” protons decreases, provoking an increase in its electronegativity. Hence, the electronegativity of the oxygen atom is variable and increases with decreasing $d_{O\cdots O}$. In other words, the donor and acceptor properties of the H_2O molecule in liquid water or in a crystal increase strictly at the same rate with a decrease in $d_{O\cdots O}$. This trend is not limited by anything and, it would seem, by increasing the external pressure, one can achieve an

extremely strong hydrogen bond in crystalline H_2O with a proton frequency of 3000-3600 cm^{-1}. However, this is not the case. The H_2O molecule in both the liquid and the crystal is surrounded by four other molecules and forms two donor and two acceptor bonds. But four hydrogen bonds can only be equivalent to two ordinary covalent bonds of an oxygen atom, one ordinary bond of oxygen as a donor, and one bond of the same oxygen atom as an acceptor. In other words, the energy of an ordinary covalent bond is divided in liquid or crystalline water between two protons, limiting the maximum possible frequency of their vibrations at low $d_{O\cdots O}$ to a value of 2000-2500 cm^{-1}.

To estimate the height of the barrier U_0, for which a transition from moderate to strong bonds can occur, it is necessary to establish an energy criterion for the transition. Comparison of U_0 with the value of thermal energy kT, which is usually used when comparing energy states, is not applicable in this case, since, in the case of vibrations, it is valid only for temperatures at which vibrational states with a large quantum number n are excited (otherwise, "ultraviolet catastrophe"!). The frequency of the proton vibrations on the hydrogen bond is high, so the excitation of vibrations with a large quantum number is possible only at high temperatures and is not realized in compounds with hydrogen bonds. Therefore, the criterion for the transition from a double-well potential to a single-well potential is the ratio of the barrier height U_0 and the energy of zero-point vibrations of the proton. The latter value at low temperatures turns out to be much higher than the energy kT. Fig. 2.3 shows a situation in which the energy of zero-point vibrations begins to exceed the value of the barrier U_0. It is this case that signifies the initial phase of the transition of the double-well potential of the proton to the single-well potential, or, in other words, the transition from a moderate bond to a strong one. The use of kT as a transition criterion can yield a significant underestimation of the distance $d_{O\cdots O}$ at which this transition occurs.

It should also be noted that the relationship between the strength of the hydrogen bond, the width of the potential minimum of the proton, the de Broglie wavelength, and the energy of the vibrational states can be used to estimate the vibrational frequencies of a proton on a hydrogen bond of any rigidity. In other words, the main effect of hydrogen bonding, i.e. the dependence of the proton vibrational frequency on the $d_{O\cdots O}$ distance, is a consequence of the change in the width of the potential minimum of the proton and the corresponding change in the de Broglie wavelength.

11.2.4 Half-width of the O–H···O vibrational bands

When the O–H···O hydrogen bond changes from a weak to moderate one, the bandwidth of the O–H vibration increases very much, and its peak intensity often weakens so that the band becomes barely noticeable in the spectrum. Among several reasons for the band broadening considered in the literature, there is one that is reliably confirmed experimentally.

The bandwidth of the vibrational band is inversely proportional to the lifetime of the excited vibrational state and for hydrogen O–H···O the bond is determined by the interaction of the high-frequency O–H vibration with other modes, including low-frequency crystalline modes. Crystal vibrations yielding a modulation of the O···O distance are translational optical vibrations of hydrogen-bonded molecules relative to each other. The latter are the vibrations of the hydrogen bond itself. Their frequency for medium-sized molecules (for example, organic molecules with a mass of 50-100 at. units) lies in the region of ~100 cm^{-1}, i.e. well below the $\nu_{O–H}$ frequency. This means that the frequency of the $\nu_{O–H}$ stretching vibration can follow the change in the $d_{O\cdots O}$ distance, which results from the excitation of intermolecular vibrations. In other words, two modes, the high-frequency valence $\nu_{O–H}$ and the low-frequency phonon mode of lattice vibrations, interact with each other, and this interaction is proportional to the interaction parameter $\chi = \Delta\nu / \Delta d$, i.e. the slope of the $\nu_{O\text{-}H}$ dependence on the $d_{O\cdots O}$ distance.

As an example, Fig. 11.10 shows the diagram of the hydrogen bonds of the H_2O molecule and the OH-groups in the cavity of the hemimorphite mineral, $Zn_4Si_2O_7(OH)_2{\cdot}H_2O$, and Fig. 11.11a – the spectra of stretching vibrations of H_2O molecules and OH-groups in the cavities of hemimorphite at 4 K and 300 K, demonstrating the change in the width of the vibrational modes with temperature. In this case, the temperature controls the population of low-frequency crystalline modes. In fact, the frequencies of crystal phonons are usually in the range of 50-300 cm^{-1}. The Boltzmann population of such phonons varies from 0 to 1 in the temperature range 4-300 K.

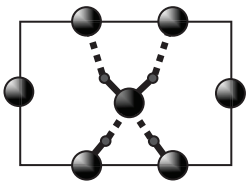

Figure 11.10 The system of hydrogen bonds of the H_2O molecule (in the center) and the OH groups in the cavity of the hemimorphite mineral.

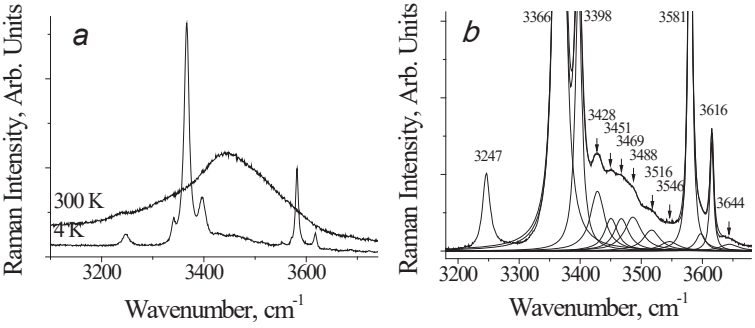

Figure 11.11 *a* - Spectra of the stretching vibrations of H_2O molecules and OH groups in the hemimorphite cavity at 4 K and 300 K. The H_2O molecule in the cavity forms a hydrogen bond with the OH groups of the crystal as a donor (lines ~ 3400 cm^{-1} at 4 K) and as an acceptor (~ 3600 cm^{-1}); *b* – Spectrum (4 K) of the combined modes of the stretching vibrations of H_2O molecules in the cavity of hemimorphite with translational modes of H_2O itself and of the lattice of the host crystal [22].

The higher the population of phonon states, the greater the probability of interaction of high-frequency O–H vibrations with crystal modes, the shorter the lifetime of the excited state and the larger the mode bandwidth. This explains both the strong increase in the bandwidth with temperature and this bandwidth itself. The fact that the active interaction of the O–H stretching vibration with the lattice phonons actually takes place can be seen from Fig. 11.11*b*, where the region of the combined modes in the Raman spectrum of hemimorphite is shown in close-up, i.e. scattering by combinations of ν_{O-H} with lattice phonons (in this case, with translational vibrations of the H_2O molecules themselves and the lattice of the host crystal).

11.2.5 Intensity of O–H···O vibrational bands

It is well known that when the wavenumber of ν_{O-H} of the O–H···O hydrogen bond becomes less than 2700 cm^{-1}, the intensity of the band in the Raman spectra decreases to almost zero, and the band itself becomes extremely inexpressive, consisting of several maxima with intensity at the spectrum noise level (see, for example, [23]). Finally, in many compounds with the moderate bond, the O–H band is not observed at all.

We have already discussed above that for the moderate hydrogen bond the situation can arise, as shown in Fig. 2.2, in which the excited vibrational state is pushed out into the wide united minimum and the zeroth state remains in the narrow minimum. In this case, the proton appears in different positions in the ground state and in the excited state: the unexcited proton is located in a narrow minimum next to the one of the oxygen atoms while the excited proton is located in the center of the bond. Therefore, the excitation of vibrations requires the proton to be displaced along the bond. However, in the Raman spectroscopy, the incident electromagnetic radiation interacts with the electron shell of the atoms rather than with their nuclei, since the frequency of the incident radiation ($\sim 2 \cdot 10^4$ cm^{-1}) is an order of magnitude higher than the frequency of nuclear displacement ($\sim 2 \cdot 10^3$ cm^{-1}). (In IR absorption spectroscopy, the frequency of the incident electromagnetic radiation must be equal to the frequency of the fundamental mechanical vibrations of the molecule to excite the vibrational quantum. In Raman spectroscopy, the frequency of incident radiation is high, much higher than the frequencies of mechanical vibrations of atoms; therefore, the field of an incident electromagnetic wave causes a displacement not of atoms, but only of their electron shells. This results in the appearance of Hertzian dipoles and Rayleigh, i.e. frequency upshifted, scattering. However, the reaction of the electron density to an external field depends on the polarizability of chemical bonds, which is modulated by mechanical vibrations. The latter are slow compared to the frequency of the incident radiation. It is the modulation of the polarizability of the system during the vibrations that causes the appearance of Raman scattering at the vibrational frequency of a molecule or crystal. Thus, the difference between IR absorption and Raman scattering is that the incident radiation interacts with vibrating atoms in the first case and with their electronic subsystem in the second). As a result, the processes accompanied by atomic displacements are not revealed in the Raman spectra but can be active in IR absorption spectra. In other words, the damping of the scattering intensity on O–H vibrations for the moderate bonds is a result of the shape of the potential curve (Fig. 11.2), at which the proton, passing from the zeroth vibrational state to the first excited state, is forced to change its position on the bond. This circumstance greatly complicates the study of the properties of the moderate hydrogen bond and, possibly, served as a source of errors in the past, when some bands in Raman spectrum were assigned to O–H vibrations of the moderate hydrogen bond without sufficient experimental justification. As we will see below (sections 11.3 and 11.4), the intensity of the scattering is restored as soon as the energy of both states, the zeroth

and the first excited, becomes higher the barrier between potential wells and the coordinate of the proton ceases to depend on its vibrational state again.

11.2.6 How does single-well potential occur?

The reasons and conditions for the formation of a single-well potential and their characteristics are quite simple, but we will briefly discuss them, since in section 11.3, the width of the potential well and the height of the barrier will become the most needed parameters when interpreting experimental results.

There are three factors that determine the $d_{O\cdots O}$ distance, the barrier height U_0, and, as a consequence, the hydrogen bond strength.

1. Identity of a donor and an acceptor, which in practice simply means the formation of a hydrogen bond by two identical molecules. If the molecules are different, then the interaction of the proton with the donor will always be stronger than with the acceptor, and the O–H length is shorter than H···O. It prevents the formation of the minimum $d_{O\cdots O}$ and strong hydrogen bond. When the molecules are completely identical, the concepts "donor" and "acceptor" lose their meaning.
2. Electronegativity of oxygen-donor and oxygen-acceptor. It was already mentioned above that electronegativity determines how strongly an oxygen atom interacts with a proton, i.e. how close a proton can come to an oxygen atom, both as a donor and an acceptor.
3. Thermal vibrations. Thermal vibrations increase the distance between atoms due to anharmonic processes. In a molecular crystal, the vibrational spectrum starts from 20-40 cm^{-1}. Consequently, the excitation of equilibrium thermal vibrations starts from 40-60 K. In other words, the minimum possible hydrogen bond length can be established only at $T \leq 40$-60 K.

In the harmonic approximation, the particle energy is proportional to the square of the deviation of the particle coordinate from the equilibrium position, $U(x) = kx^2$, where k is the force constant. If the minimums in the double-well potential are deep enough, then each of them can be considered as harmonic. Then, for a double-well symmetric potential, in which the middle of the length between the donor and the acceptor is chosen as the origin, and the distance from the origin to each of the

minima is denoted as ±Δ, the potential function of the proton is written as follows

$$U(x) = \{[k(x+\Delta)^2]\cdot[k(x-\Delta)^2]\}^{1/2} = \pm k(x+\Delta)(x-\Delta). \qquad (11.11)$$

Hence, at $x = 0$, the height of the barrier U_0 (choosing a positive value) is

$$U_0 = k\Delta^2. \qquad (11.12)$$

The force constant depends on the electronegativity of the oxygen atoms and does not change for a given compound (the exception is the H_2O molecule, see above). Distance Δ depends on the external pressure and the temperature of the crystal, which determines the population of thermal vibrations. In other words, with an increase in external pressure or a decrease in temperature, the barrier height U_0 decreases; therefore, it is easy to obtain the situation shown in Fig. 11.3, at which both vibrational states are within the wide united minimum and the scattering becomes active.

11.3 Experimental study of strong hydrogen bonds

Chemical compounds with a strong and extremely strong O-H···O hydrogen bond, in the spectra of which the transition to a single-well potential is confidently detected, are quite rare. In addition, the transition itself, as a rule, is stretched in temperature, and begins at T <150 K (the reasons for this will become clear from the subsequent text). In other words, a detection of the transition to a single-well potential requires Raman measurements in the temperature range 5 K - 300 K, which is not a widespread practice. In this work, Raman spectra of benzoic acid crystals, where the early stage of the transition to a single-well potential is observed, glycine phosphate crystals with the stable state of the single-well potential (Fig. 11.3), and dimethylphormamid $[(DMF)_2H]_2$ with the extremely strong hydrogen bond (Fig. 11.4) were obtained. Consider the spectra of these compounds in the sequence presented.

11.3.1 The features of the vibrational spectrum of benzoic acid

Despite the fact that benzoic acid belongs to tautomeric compounds (more about them in Chapter 11.4), at low temperatures the benzoic acid dimers in the crystal are distorted due to crystalline effects so that one

O–H···O bond becomes shorter than the other (Fig. 11.12), and it is these short bonds that show in the spectra the signs of the transition to a single-well potential.

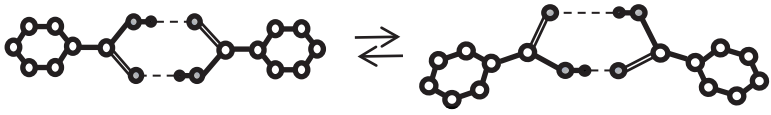

Figure 11.12. Dimers of benzoic acid in a crystal at room and low temperatures.

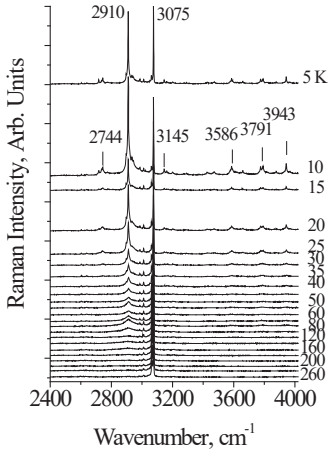

Figure 11.13. Raman spectra of crystals of benzoic acid in the high-frequency region at different temperatures [24].

Fig. 11.13 shows the Raman spectra of crystals of benzoic acid in the high-frequency region of O–H and C–H stretching vibrations. At low temperatures ($T \leq 60$ K), a series of narrow and weak in intensity lines appear in the spectra – a phenomenon that is not observed in other H-bonded compounds. In addition, also at temperatures below 60 K, a narrow line appears in the spectrum at 2910 cm^{-1}, the intensity of which becomes very high (higher than the intensity of the C–H stretchings) at a temperature of 10-15 K. With a further decrease in temperature from 10 to 5 K, the intensity of both the series of weak lines and the 2910 cm^{-1} line begins to decay.

The distance in wavenumbers between weak narrow lines is not constant and does not form any regular series; therefore the entire series cannot be interpreted as resonant repetitions of a combination of O-H

vibrations and any mode (or group of modes). However, upon closer examination, it can be found that the lines in the emerging low-temperature series are located at approximately the same intervals as the modes of crystalline and intramolecular vibrations in the range of 50-1700 cm^{-1}.

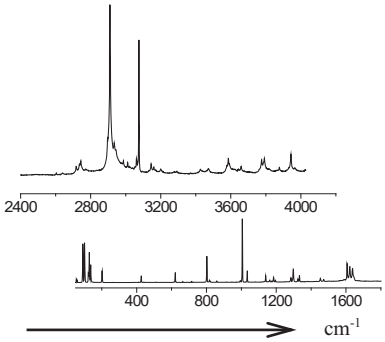

Figure 11.14. A comparison of the high-wavenumber (2400–4000 cm^{-1}, top) and intramolecular (50–1700 cm^{-1}, bottom) vibrations at T = 10 K

Fig. 11.14 shows the spectra of intramolecular (bottom) and high-frequency (top) vibrations at 10 K. One can see that weak narrow lines in the high-frequency spectrum (2400-4000 cm^{-1}) are located and separated from each other in the same order as the modes of the intramolecular vibrations (50-1700 cm^{-1}). In other words, the spectrum of weak modes in the high-frequency region is indeed a second-order spectrum, consisting of the combined tones of the hydrogen-bonded stretching vibration O–H and intramolecular vibrations. The O–H stretching itself is not recorded, but its frequency should fall within the range of 2600-2650 cm^{-1}.

Due to the distortion of the dimer, the lengths of two O–H···O hydrogen bonds become different when the crystal temperature decreases. In this case, the predicted O–H stretching mode at ~2600 cm^{-1} is evidently related to the shortest O-H···O hydrogen bond, and 2910 cm^{-1} – to the longer one. The emergence of the second-order spectrum means that those intramolecular vibrations that modulate $d_{O\cdots O}$ distance become capable to a very strong interaction with the O–H valence mode of the short hydrogen bond, much stronger than, for example, the well-known interaction of lattice phonons modulating the O···O distance in a crystal with common (weak and moderate) O–H···O hydrogen bonds. Earlier (see Chapter 11.2, paragraph 11.2.3 and Fig. 11.9) it was noted that at the moment when the excited vibrational state is pushed out to the wide minimum of the unified

potential, the wavenumber of the proton vibration should sharply decrease due to an increase in the size of the oscillator. At this, even a negligible modulation of the O···O distance can cause a significant change in the ν_{O-H} frequency. It is the phenomenon that causes the very strong interaction of the corresponding intramolecular modes with the O–H stretching vibration, the interaction that provokes the emergence of a second-order spectrum. In benzoic acid crystals at low temperatures, the length of the short O–H···O bond does not yet reach critical values and the excited vibrational state is not yet pushed into the wide minimum, but those intramolecular vibrations, which modulate the length of the short O–H···O bond, produce the conditions for this length to fall into the zone of a rapid drop in the proton vibration frequency and, as a consequence, a strong interaction between intramolecular and O–H vibrations of the short hydrogen bond. This phenomenon is able to produce soliton states in crystals (Davydov's solitons). No change in the peak position of the second order bands and the mode at 2910 cm^{-1} was observed at different temperatures. This probably means that the arising new state of the short hydrogen bond is not stable, but exists only as a result of the vibrational interaction.

Thus, the transition of the potential from double-well to single-well in benzoic acid crystals is not complete, and is characterised by its initial stage, which arises only when the intramolecular modes modulate the bond length. This is quite understandable, taking into account that the $d_{O\cdots O}$ distance in benzoic acid dimers is rather long, ~ 2.6 Å, and for a complete transition to the single-well potential a bond length less than 2.5 Å is required.

As will be shown in the next section, the vibrational frequency of a proton in the steady-state single-well potential of a strong hydrogen bond is very low, ~ 930 cm^{-1}, while the ν_{O-H} frequency in benzoic acid immediately before the transition to the single-well potential is much higher - around 2600 cm^{-1}. This means that a discontinuity in the dependence of ν_{O-H} on the $d_{O\cdots O}$ distance should occur, as was suggested above (see Fig. 11.9).

11.3.2 Strong hydrogen bonds. Glycine Phosphate

Glycinium phosphite crystal, $C_2H_8NO_5P$, contains in its structure two short O–H···O hydrogen bonds with lengths of 2.49 Å and 2.53 Å [25-28]. The oxygen atoms in each of these bonds are identical and the proton potential is described at room temperature as a symmetrical double-well potential. Fig. 11.15 shows the fragment of the crystal structure.

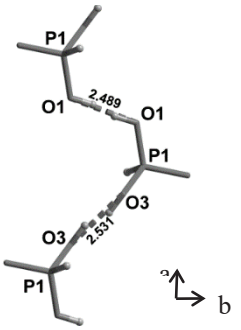

Figure 11.15. Fragment of the crystal structure of glycine phosphate

IR spectrum of glycinium phosphite at ambient temperature is shown in Fig. 11.16. Figs. 11.17 *a* and Fig. 11.17 *b* show the Raman spectra of glycinium phosphite in the range 900-1000 cm^{-1} at various temperatures (a) and at differen polarization of incident and scattered light relative to the crystallographic axes (b).

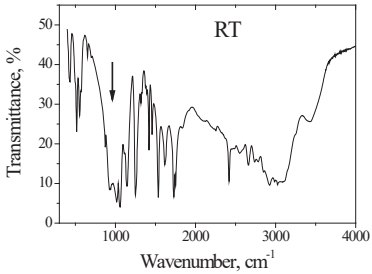

Figure 11.16. IR-spectrum of glycinium phosphite at room temperature. The arrow shows the expected position of the hydrogen bond absorption band. The Raman band in this region appears only at low temperatures (see Fig. 11.17, *a*).

A strong hydrogen bonding in glycinium phosphite arises between P–O bonds of the PO_3H_2 anions (Fig. 11.15). These bonds have different lengths, 1.513 and 1.529 Å at room temperature, and their vibrations appear in the Raman spectrum (Fig. 11.17 *a*,*b*) as two lines, one of which, the low-frequency mode at 964 cm^{-1}, is assigned to stretching vibration of O–P–O fragment with the maximum contribution from the long P–O bond, and the other, high-frequency mode at 971 cm^{-1}, is assigned to the O–P–O vibration with the predominant contribution from the short P–O bond. (Here and below, the vibrational wavenumbers refer to a temperature of 5 K). An assignment of the Raman bands related to the stretching vibrations of the main chemical bonds in the crystal was made on the basis of a quantum chemical calculation presented in [29].

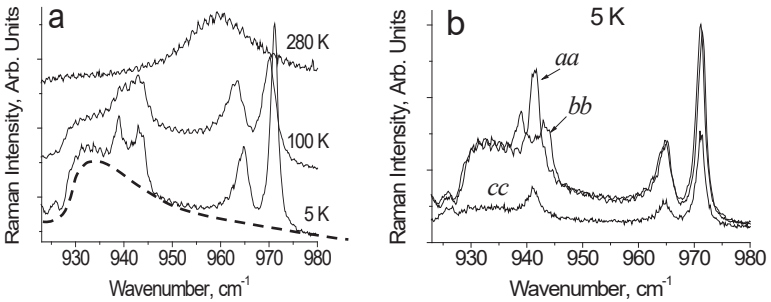

Figure 11.17 *a*,*b.* Raman spectra of glycinium phosphite in the range of the hydrogen bond vibrations at different temperatures (*a*) and orientation of the polarization vector of the incident and scattered light relative to the crystallographic directions (*b*)

With temperature decreasing, the relative integral intensity of the 964 and 971 cm^{-1} modes decrease and two other modes at lower frequency, 939 and 943 cm^{-1}, arise (Fig. 11.17 *a*). In addition, a broad structureless band in the region of 930-980 cm^{-1}, shown by the dashed line, also appears in the spectrum. The shape of the latter is completely unusual: the maximum intensity of the band falls on its low-frequency edge, i.e. at ~ 930 cm^{-1}, and the minimum is at high-frequency (i.e., approximately at 980 cm^{-1}).

Fig. 11.17 *b* shows the polarized spectra of the crystal at 5 K, obtained for different crystallographic directions. It can be seen that a broad band appears only in the *ab*-plane of the crystal, in which both O-H···O hydrogen bonds lie. The relative integral intensity of the broad band as a function of temperature is shown in Fig. 11.18.

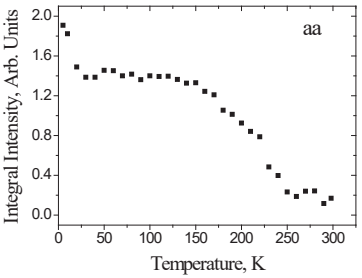

Figure 11.18. Relative integral intensity of the 930-980 cm^{-1} band as a function of crystal temperature

Short O-H···O bonds in the crystal form infinite chains along the *a* axis, however, the bonds themselves in the chains alternate in length and direction (Fig. 11.15). Since the oxygen atoms in each bond are pairwise completely identical to each other, the protons in each pair must be able to occupy positions with equal probability both at one oxygen atom and another. The identity of the oxygen atoms creates chemical conditions for the formation of a strong hydrogen bond; while the potential function of the protons at room temperature is symmetric double-well. At the same time, both oxygen atoms belonging to the same PO_3H_2 group cannot simultaneously act as acceptors, since this creates a deficiency in the valence of phosphorus atoms in this group. Thus, at a low temperature, a conflict situation should arise, in which the protons, on the one hand, should be ordered along the entire length of the O–H···O bond chain (i.e., over the entire crystal), and, on the other hand, should be distributed equiprobably near both oxygen atoms in each pair. This contradiction disappears when the protons on each of the O-H···O bonds occupy the position in the midpoint of the bond. The last condition means the formation of a single-well potential.

The theoretical calculation fulfilled in [17] and the consideration presented in the previous sections of this work show that the $d_{O\cdots O}$ distance around of 2.5 Å or less provides the formation of a single-well potential. The $d_{O\cdots O}$ distance of 2.43 Å was called in [17] a threshold for the transformation of the pronon potential to a single-well and the thermal energy kT at low temperatures served as the criterion. However, as already mentioned, the only correct criterion is the energy of zero-point motions $\hbar\omega/2$, which, for a reasonable value of ω, is much higher than kT. Consequently, the threshold value of the $d_{O\cdots O}$ distance is also higher than that assumed in [17], and the $d_{O\cdots O}$ in glycinium phosphite fully ensures the formation of a single-well potential.

The interpretation of the above experimental results is as follows. At room temperature, both hydrogen bonds are symmetric double-well due to the high value of the barrier height U_0. However, due to phonon-assisted jumping, the protons on the hydrogen bond are statistically distributed between both positions on the bond. The conflict between the statistical distribution of the protons and the valence ability of phosphorus atoms reveals at T > 50 K a sharp increase in the half-widths of most bands in the spectrum, and their peak positions show significant dispersion.

With temperature decreasing and freezing of the vibrations, the $d_{O\cdots O}$ distance and the height of the barrier decrease. The appearance of two additional (to the bands at 964 and 971 cm^{-1}) O–P–O stretching modes at 939 and 943 cm^{-1} (Fig. 11.17 *a,b*) at low temperature occurs due to the

strengthening of the hydrogen bonds, i.e. to the displacement of the protons towards the center of the bond. Simultaneously with the appearance of two last modes, a broad band at 930-980 cm^{-1} arises in the spectrum (dashed curve in Fig. 11.17 *a*).

The band is recorded only in the *ab*-plane of the crystal and in addition demonstrates an unusual contour, which strongly differs from the Lorentzian or Gaussian contours (Fig. 11.17 *a,b*). Both of these arguments allow us to attribute the band to the vibrations of protons of the strong hydrogen bond.

Fig. 11.19 shows a qualitative interpretation of an unusual contour of the proton band.

It has already been mentioned above that the $d_{O\cdots O}$ distance is not fixed and is determined by the Gaussian distribution due to the quantum uncertainty of the oxygen atom coordinates (see Section 11.2.2).

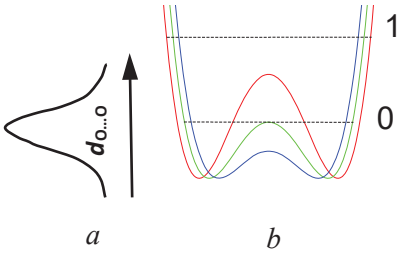

Figure 11.19 *a,b.* The occurrence of an unusual contour of the proton vibrational band: (*a*) - distribution of $d_{O\cdots O}$ distances, arising from the quantum uncertainty of the coordinate of oxygen atoms; (*b*) - energy of zeroth motions relative to the barrier U_0 for short (lower curve), medium (middle curve) and long (upper curve) $d_{O\cdots O}$ distances.

One can assume that the most probable $d_{O\cdots O}$ distance in glycinium phosphite corresponds at low temperatures to the potential curve where the ground vibrational state of the proton coincides with the top of the barrier (Fig. 11.19, *b*, green curve). Then the ground state for larger $d_{O\cdots O}$ appears lower than the potential barrier (Fig. 11.19, *b*, red curve) and falls within the region where the scattering on proton vibrations is forbidden. For shorter $d_{O\cdots O}$ (Fig. 11.19, *b*, blue curve), both the ground and the excited states appear within the same wide potential minimum, and the scattering becomes Raman-active again. This particular circumstance is responsible for the unusual shape of the scattering band in glycinium phosphite (Fig. 11.19, *a,b*). The low-wavenumber edge of the broad band, where the

Raman intensity is maximal, should be assigned to the proton vibrations on the O-H···O hydrogen bond with $d_{O\cdots O}$, at which the zero-point energy achieves the top of the barrier and both the ground and the first excited states get the wide minimum. Thus, the glycinium phosphite crystal is a perfect example of how the evolution of the hydrogen bonding transfers to a new stage at which both the ground and the first excited vibrational states appear within the same wide minimum of the single-well potential.

The proton vibrations in the single-well potential of a strong O-H···O hydrogen bond were observed for the first time in Raman spectra (as far as we know). The structural parameters of the bonds [25-28] required for the transition from a symmetric double-well to a single-well potential are close to those predicted theoretically [17]. The energy of the zero-point motions $\hbar\omega/2$ of a proton, which is estimated as ~ 1000 cm^{-1} from a vibration frequency of ~ 2000 cm^{-1} for moderate hydrogen bonds, significantly exceeds the theoretical value of the barrier between wells at short hydrogen bonds [17], which allows us to talk about the proton vibrations in a single-well potential. The unusual contour of the proton vibrational band can further serve as the most important criterion for the experimental confirmation of the potential conversion to a form in which the barrier between adjacent minima is preserved, but the energy of zero point motions of the proton exceeds its height. With a further decrease in the O···O distance of the hydrogen bond, the potential barrier decreases, the bond becomes extremely strong and the potential well gets the traditional form of a harmonic potential (Fig. 2.4), in which the contour of the vibrational band also turns out to be an ordinary Gaussian.

11.3.3. Extremely strong hydrogen bond in $[(DMF)_2H]_2$

The $[(DMF)_2H]_2[W_6Cl_{14}]$ is one of the rare compounds in chemistry in which a very short O···H···O hydrogen bond is realized. Fig. 11.20 shows a fragment of the structure in which oxygen atoms of DMF (N,N-Dimethylformamide) molecules can occupy two different positions with the creation of the O···H···O hydrogen bonds, the lengths of which are 2.36 Å (0.7 O1/O2 occupancy) and 2.46 Å (0.3 O1/O2 occupancy) [30]. (Numerical values are given for a temperature of 140 K).

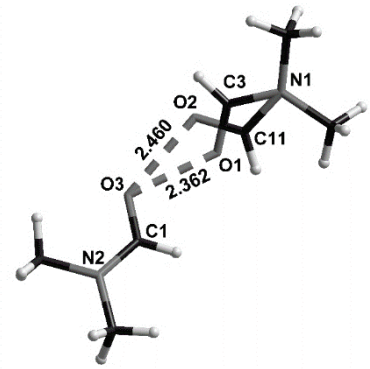

Figure 11.20. The structure of $[(DMF)_2H$

The C–O bond lengths are 1.272 Å (at O···O = 2.37 Å) and 1.266 Å (at O···O = 2.474 Å). Both of the latter quantities indicate that the C–O bonds are close to ordinary bonds and, therefore, the shell of the oxygen atoms is not saturated, and their electronegativity is high. This data, together with the complete identity of oxygen atoms, creates favorable conditions for a generation of an extremely strong symmetric O···H···O hydrogen bond.

Since the $d_{O\cdots O}$ distances in $(DMF)_2H$ are significantly shorter than that in glycine phosphate, the proton potential in $(DMF)_2H$ should be the same as shown in Fig. 11.4, and the expected frequency of the proton vibrations is much higher as compared with glycine phosphate.

Fig. 11.21, *a* shows the Raman spectra of the compound in the region of proton vibrations on hydrogen bonds in the temperature range 5 K - 300 K. As the temperature decreases, two broad bands, 1370 and 1450 cm^{-1}, arise in the spectra. At these, the low-frequency band appears at T ≤110 K, and the high-frequency band – at T ≤ 60 K. In addition, the intensity of the 1422 cm^{-1} narrow band, which is weak at room temperature, begins to increase together with the intensity of both broad bands. The wavenumber of the 1422 cm^{-1} mode is close to the vibrational frequency of the ordinary C–O bond (~ 1300 cm^{-1}) and much lower than the wavenumber of the double C = O bond (~ 1800 cm^{-1}).

This is quite consistent with the structural data and with the assumption that the oxygen atoms involved in the emergence of the hydrogen bonds are electronegative. The intensity of the C–O vibrational

mode is the result of a resonant response to the appearance of the hydrogen bonds in the Raman spectrum.

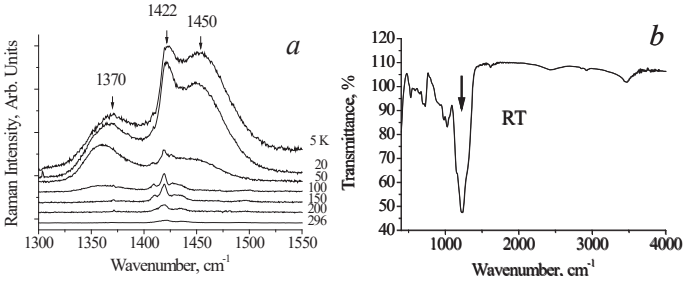

Figure 11.21. (*a*) Raman spectra of $[(DMF)_2H]_2[W_6Cl_{14}]$ in the region of proton vibrations at various temperatures. (*b*) IR-spectrum of $[(DMF)_2H]_2[W_6Cl_{14}]$ at room temperature [30]. The arrow shows the expected position of the hydrogen bond absorption band. The correspondng Raman bands in this region arise only at low temperatures (*a*).

The broad bands at 1370 and 1450 cm^{-1} correspond to proton vibrations on the strong hydrogen bond. Even though this bond is characterized by a double-well potential, the barrier U_0 between the minima of the latter is low due to short $d_{O\cdots O}$ distances (Fig. 11.3). The proton vibrational frequency for such potential is directly proportional to the rigidity of the hydrogen bonding. Therefore, the modes at 1370 cm^{-1} and at 1450 cm^{-1} should be assigned to the vibrations of the longer and the shorter of these two hydrogen bonds, respectively. The temperature dependence of the intensity of these two modes is the most interesting manifestation of their features and requires a detailed discussion.

First of all, both bands appear at low temperatures. Formally, this behavior is no different from that observed in the glycine phosphate crystal. However, as we saw above, the barrier U_0 between the minima is proportional to the force constant of the hydrogen bond (the slope of the potential curve), and the square of half the distance between the minima (see expression (11.12)). In the $(DMF)_2H$ dimer, the steepness of the minima is so great that even with a small lengthening of the O···O distance due to thermal vibrations of the crystal, the barrier height U_0 changes sufficiently strongly to become higher than the energy of the zero point motions of the proton at room temperature, i.e. in a position in which Raman scattering by proton vibrations is forbidden. With a decrease in temperature and freezing of crystalline vibrations, the hydrogen bond

length becomes shorter, and the barrier becomes lower, and both vibrational states turn out to be in a wide minimum, becoming Raman-active. In other words, strong hydrogen bonding remains strong at higher temperatures, but the steepness of the potential curve and thermal vibrations make the barrier height U_0 too high at room temperature in relation to the energy of zero-point motions.

For the same reason, the band at 1450 cm^{-1} is revealed in the spectrum at lower temperatures than the band at 1370 cm^{-1}. This mode corresponds to the vibrations of the strongest of the two hydrogen bonds; therefore, it appears in the Raman spectrum only when all crystal vibrations, including most low-frequency modes (≤ 40 cm^{-1}), are frozen so that the barrier is diminished until an acceptable value.

The proposed interpretation is well illustrated by the sequence in which the bands of proton vibrations on the bonds of different rigidities appear with decreasing temperature (Fig. 3.10) and agrees with the assumption that the appearance or the disappearance of proton vibrational bands in the Raman spectra of moderate and strong bonds is controlled by the positions of the energies of the ground and the first excited vibrational states relative to the barrier between the minima.

The transition of the ground proton state at a low temperature from the narrow minimum next to the donor to the wide minimum of the unified potential (as it takes place in glycinium phosphite and in $(DMF)_2H$ has another unexpected effect. It is well known that measuring the O···O distance by two different methods of X-ray diffraction and neutron diffraction reveals somewhat different values. This is caused by the fact that X-rays are scattered on electronic shells of the atoms while neutrons are scattered on atomic nuclei.

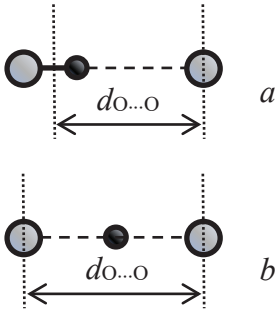

Figure 11.22. X-ray measurement of $d_{O\cdots O}$ distance at localization of a proton near the donor (*a*) and in the midpoint of the donor-acceptor bond (*b*). The true distance between the centers of oxygen atoms in the figure is the same.

In the case of hydrogen bonding, the electron shell of the donor oxygen is partially shifted towards the proton due to chemical interaction

with the latter. For this reason, the position of the donor atom measured in X-ray diffraction is also shifted towards the proton and to the oxygen acceptor, while the obtained $d_{O\cdots O}$ distance is slightly underestimated, which plays no significant role in most cases. However, as mentioned above, in the case of strong and maximally strong hydrogen bonds, the proton is localized next to the donor at high temperatures and between the donor and the acceptor at low temperatures. Therefore, the position of the oxygen donor determined by X-ray diffraction will be shifted from its true state at high temperatures and will not be shifted at low temperatures (Fig. 11.22). At the same time, the $d_{O\cdots O}$ value will be seemingly increasing as the temperature decreases, while its real value can be only decreasing, and it was really observed in glycinium phosphite and in $(DMF)_2H$ at low temperature. This effect can be the reason for misinterpretation of data obtained from structural studies using X-ray diffraction.

11.4. Tautomeric hydrogen bonds

11.4.1 What is the proton tautomerism?

Proton tautomerism occurs in the systems with intermolecular hydrogen bonding X–H···Y where the donor and the acceptor are indistinguishable and the proton can jump between them. The simplest compound containing a tautomeric bond (referred to hereafter as the τ-bond) is the formic acid dimer (Fig. 11.23). Left (*L*) and right (*R*) tautomers of this dimer are identical and constitute a six-membered τ-ring formed by two O-H···O hydrogen bonds and two carboxyl groups.

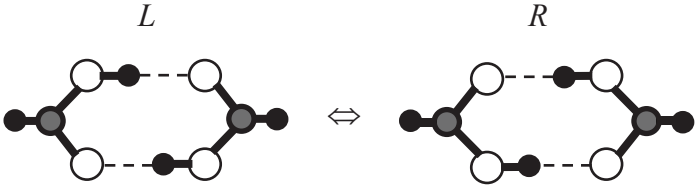

Figure 11.23. *L* and *R* tautomers in dimer of formic acid

When plotted along the direction of hydrogen τ-bonds, the proton potential function is a curve with two identical wells (Fig. 11.24 *a*). In the case of a symmetric double-well potential, the protons must have the opportunity of a coordinated transition between the wells, which occurs as a result of protons hopping over the potential barrier or tunneling through

the barrier. However, the symmetric double-well potential is realized only for isolated molecular formations in the gas phase. In solids, the coordinated motion of charge-carrying protons to the neighboring potential well affects the interaction between a given τ-ring and the τ-rings of the neighboring molecules where this transition is not yet completed. In other words, the energies of *L*- and *R*-tautomers in the crystal lattice differ by the value *A* (Fig. 11.24 *b*). Therefore, the tunneling must be accompanied by the absorption of the phonon ω_A ($\hbar\omega_A = A$), and the temperature dependence of the tunneling rate is determined by the average value of the vibrational quantum number of phonons ω_A and is anti-Stokes in nature.

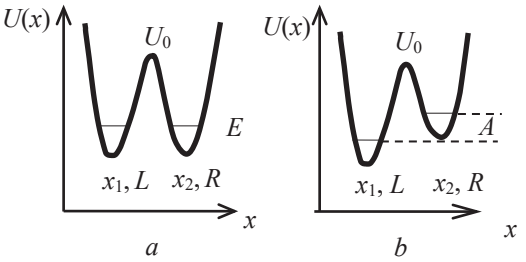

Figure 11.24 *a*, *b*. Potential energy of the proton on the τ-bond of an isolated dimer (trimer, etc.) in the gas phase (*a*), the same energy of a real dimer in the crystal (*b*). *E* is the particle energy in the potential well, U_0 is the barrier height, and (x_1, x_2) are the coordinates of potential energy minima. *A* is the difference between the energies of *L*- and *R*-tautomers in the crystal lattice.

The structures of compounds allowing proton tautomerism are diverse and include crystals with infinite chains, dimers, trimers, and tetramers [31]. Moreover, both the same type atoms (O-H···O, N-H···N) and different type atoms (O-H···N, N-H···O) can be donors and acceptors in tautomeric hydrogen bonds (Fig. 11.25). Oxygen atoms in carboxylic acids, the τ-bonds of which will be considered here, are not highly electronegative. For this reason, the corresponding hydrogen O-H···O bonds are borderline between moderate and strong. And the nature of the symmetric double-well potential in τ-bonds differs from that considered above for the usual (not tautomeric!) O-H···O hydrogen bond.

If a τ-bond is realized by atoms of different types, the potential curve of the proton on each bond is asymmetric, as in Fig. 11.24 *b*, but the total energy of both tautomers is described by a symmetric curve, as in Fig. 11.24 *a*.

Proton transfer along τ-bonds has been broadly studied by the techniques of pulsed NMR spectroscopy and inelastic neutron scattering INS [32–42]. A theory of coordinated motion of hydrogen atoms along the hydrogen bonds of carboxylic acid dimers was developed by Skinner and Trommsdorff [36].

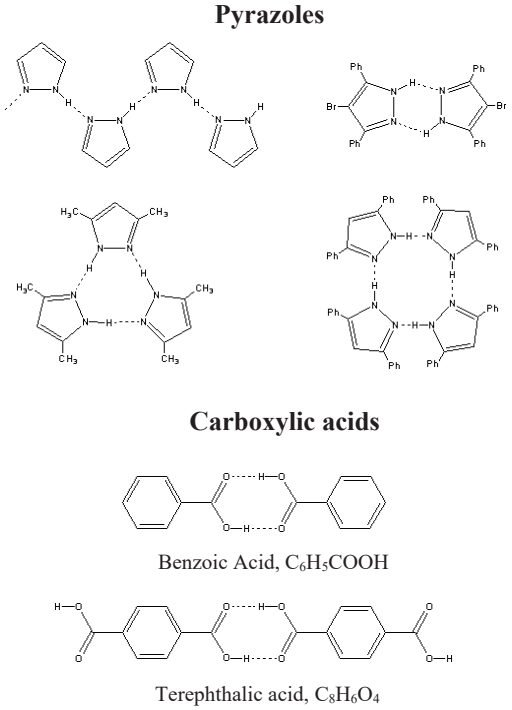

Figure 11.25. An example of compounds with τ-bond

The present work is an attempt to obtain the data on the behavior of protons on the O-H···O τ-bond using simple and easily available Raman spectroscopy. For this purpose, Raman spectra of compounds with symmetric (the chains of terephthalic acid, $C_8H_6O_4$, TPA, Fig. 11.26 *a*), quasi-symmetric (benzoic acid dimers, C_6H_5COOH, BZ, Fig. 11.26 *b*) and asymmetric (ibuprofen dimers, $C_{13}H_{18}O_2$, IB, Fig. 11.26 *c*) τ-bonds were considered in a temperature range of 5 K - 300 K.

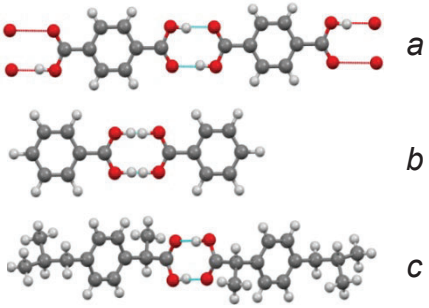

Figure 11.26. (a) Chains of TPA molecules with symmetric τ-bonds, (b) BZ dimers with quasi-symmetric τ-bonds, and (c) IB dimers with asymmetric τ-bonds. A slight deviation from symmetry in the benzoic acid dimer arises due to the crystalline effect, in which one of the four oxygen atoms of the τ-bond has a shorter contact with the environment than the other three. The asymmetry of dimer IB is due to two different carbon substituents adjacent to the α-carbon of the hydroxyl group.

Behavior of protons on the τ-bond is quite complicated and is characterized by several independent processes.

1. At large distances $d_{O\cdots O}$ (> 2.6 Å), a coordinated proton transfer along the τ-bond is mainly due to proton hopping over the potential barrier U_0 with the participation of phonons $\hbar\omega_U \sim U_0$ (phonon-assisted hopping). The barrier height U_0 in various compounds with O-H···O τ-bonds is as high as 500 – 1000 cm^{-1} [37]; therefore, this process is more effective at high temperatures. Back and forth transitions between *L*- and *R*-tautomers as a result of hopping do not change the length and the strength of hydrogen bonding, but they switch the positions of C–O and C=O bonds in the carboxyl groups. Therefore, the main effect of proton hopping is manifested exactly in the behavior of vibration frequencies of these two bonds.
2. At low temperatures, owing to the freezing of vibrations, the $d_{O\cdots O}$ distance becomes shortest, and the barrier height becomes smallest for a given compound. In compounds with a strong hydrogen bond ($d_{O\cdots O}$ < 2.6 Å), this makes probable the coordinated transfer of both protons along the τ-bond as a result of tunneling through the barrier. The tunneling, as well as proton hopping, does not change a force constant of τ-bond but

switches the C–O and C=O bonds between themselves. The latter effect is accompanied by the changes in the lengths of C–O and C=O bonds with the tunneling rate, which is usually ~10^9 s^{-1} [37], and the amplitude approximately an order of magnitude higher than that of equilibrium (thermal) vibrations of these bonds. Therefore, proton tunneling and proton hopping are associated with forced vibrations of C–O and C=O bonds of the carboxyl group with the result that the frequencies of their normal vibrations are subject to the anharmonic shift [43]. Thus, the temperature dependence of the C–O or C=O stretching vibrations is an indicator of both protons tunneling through the barrier and proton hopping over the barrier U_0. The tunneling is significantly slowed down as a result of deuteration, since the probability of tunneling is proportional to exp $(-B\sqrt{m})$, where m is the mass of the tunneling particle and B – constant.

3. The proton distribution function in a potential well is delocalized because of the quantum uncertainty principle and spreads partly to a neighboring (empty) potential well (Fig. 11.27). This process has been already discussed in detail above. The smaller the $d_{O\cdots O}$ distance and the crystal temperature, the more efficient the spread of proton coordinate. When the hydrogen is replaced by deuterium, the quantum uncertainty of the deuteron on the bond decreases insignificantly, by a factor of $2^{1/4} = 1.19$ (see Chapter 11.2), as was confirmed by the calculations of Wang et al. [18].

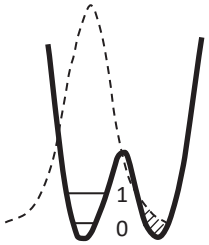

Figure 11.27. The assumed distribution of the proton density (dashed curve) at $d_{O\cdots O} < 2.6$ Å. The shaded area shows the region where the proton density penetrates into the neighboring well.

It should be noted that, in contrast to hopping and tunneling, where a coordinated transition of protons to a neighboring well occurs in a random τ-cycle of the crystal lattice and regardless of the environment, the spread of the proton density to a neighboring potential minimum as a result of the quantum uncertainty of the proton coordinate occurs in all τ-cycles of the lattice simultaneously and to the same extent and therefore does not reveal

a change in the energy state of protons due to their interaction with neighboring cycles. In other words, the scheme shown in Figure 11.24 *b* is not valid in the case of proton density delocalization.

Thus, when analyzing the experimental data, we will proceed from the following assumptions.

1. Coordinated proton tunneling on the τ-bond occurs mainly at low temperatures, and proton hopping occurs mainly at high temperatures;
2. Tunneling changes the energy of their interaction with the environment and requires the participation of phonons ω_A (Fig. 11.24 *b*);
3. Spread of proton (deuteron) distribution function to the neighboring well increases the hydrogen τ-bond (Fig. 11.24 *a*);
4. Proton tunneling and proton hopping do not change the force constant of the τ-bond but modulate the length of C–O and C=O bonds of the τ-ring;
5. Deuteration of the τ-bond virtually does not affect the degree of proton sharing and significantly slows down the tunneling.

From this, the modes of translational vibrations of the τ-bond, ω_τ, and the vibration of the C–O and C=O bonds of the τ-ring are most important and informative for the analysis of hopping and tunneling. The experimental assignment of spectral bands to the translational vibrations was done for all compounds using temperature dependence of corresponding frequencies and quantum-chemical calculations. In the case of terephthalic acid and ibuprofen, the assignment was additionally confirmed by the deuteration on the τ-bond [43, 44]. The structural parameters of O-H···O τ-bonds and experimental and calculated frequencies $\omega_{O\cdots O}$ are listed in Table 11.1.

Table 11.1. The length of the hydrogen bond and the frequency of translational vibrations ωτ in the studied compounds

Composition	$d_{O\cdots O}$, Å	ω_τ, cm^{-1}	
		Calculation [43,44]	Experiment, 5 K
TPA(H)	2.62 [45]	114	106
TPA(D)		113	105
BZ	2.63 [46]	–	86
IB(H)	2.66 [47]	108	104
IB(D)		–	103

11.4.2 Quantum delocalization of protons

Fig. 11.28 shows the temperature dependences of the peak position of the translational modes for three different compounds.

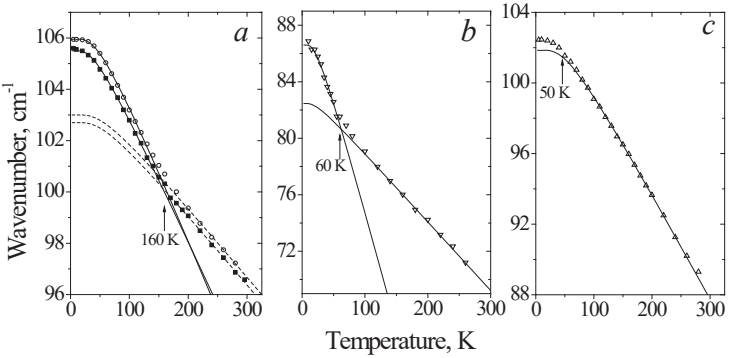

Figure 11.28. ω_τ as function of temperature in (a) symmetric TPA(H) (filled circles) and TPA(D) (filled squares), (b) quasi-symmetric BZ, and (c) asymmetric IB tautomeric bonds. Solid curves are plotted from the anharmonic shifts of the phonon ω determined by its thermal population [48]. The arrow marks the position of the breakpoint of $\omega_\tau(T)$.

The temperature dependence $\omega_\tau(T)$ of the symmetric τ-bond in TPA (Fig. 11.28, *a*) has a characteristic breakpoint whose position on the temperature scale correlates with the beginning of the freezing of translational vibrations, i.e. the temperature where the average value of the quantum number n of the mode at 106 cm^{-1} becomes smaller than unity. The breakpoint in the temperature dependence $\omega_\tau(T)$ is also observed in the crystals with a symmetric N-H···N τ-bond [23]. In the quasi-symmetric τ-bond in BZ (Fig. 11.28, *b*), there is also a breakpoint in the $\omega_\tau(T)$ dependence, but it corresponds to a lower temperature than the beginning of phonon freezing at 87 cm^{-1}. Finally, a breakpoint in the $\omega_\tau(T)$ dependence in the asymmetric case of IB (Fig. 11.28, *c*) is negligible and is observed at $T < 50$ K.

Based on $\omega_\tau(T)$ dependence of the symmetric τ-bond in TPA (Fig. 11.28, *a*), one can propose that the transition of the vibrational state of the translational mode from the excited state ($n = 1$) to the zeroth state ($n = 0$) diminishes the x_1–x_2 distance between potential energy minima of τ-bonds until the proton wave function starts to spread to the neighboring well to increase the hydrogen bonding. As can be seen in Fig. 11.28, the slope

changing of the $\omega_\tau(T)$ in TPA(D) is registered at virtually the same temperature as in TPA(H). This experiment convincingly confirms the above assumption that the low-temperature change in the frequency of the translational vibration is due to the delocalization of the proton (deuteron) wave function into the neighboring well rather than its physical transfer, since in the latter case the probability of tunneling decreases significantly with increasing mass of the tunneling particle (for more details see [49]).

Fig. 11.28 shows that the higher symmetry of τ-bond the higher temperature of the breakpoint. It means that the degree of proton sharing is maximal for the equal proton energy states in the neighbor potential wells, that is in the case presented in Fig. 11.24, a. In principle, the breakpoint of $\omega_\tau(T)$ should be observed in any X-H···Y hydrogen bonds with sufficiently small X···Y distance but, however, this distance itself also depends on symmetry of the given bond, i.e. to what extent the donor and acceptor are similar each other by their electronegativity.

11.4.3 Proton hopping in ibuprofen

IB is an example of the asymmetric τ-bond (Fig. 11.26 *c*). In this case, left- and right-tautomers are initially unequal in terms of energy states and are characterized by the energy difference ΔE. For this reason, the $\omega_\tau(T)$ dependence shows very small proton sharing (Fig. 11.28 *c*) and the proton tunneling should be negligible. Since the proton tunneling and the proton hopping equally affects the structure and energy of compounds, the registration of hopping in the IB spectra is greatly facilitated in the absence of tunneling.

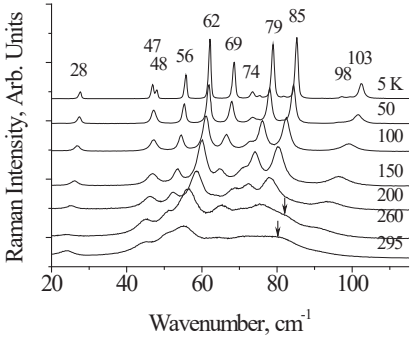

Figure 11.29. Low-frequency spectra of ibuprofen crystals at different temperatures [43]. The arrow marks the position of a new high-temperature mode at ~90 cm^{-1} arising at T ≥ 150 K.

At low temperatures, the translational vibration of the IB τ-bond is represented by a single mode at ~103 cm^{-1} corresponding to the *L*-tautomer; an additional band appears above 150 K at 93 cm^{-1} (Fig. 11.29, shown by an arrow), which corresponds to translational vibrations of the *R*-tautomer.

Fig. 11.30 *a*, *b* shows temperature dependence of the integral intensity of these two translational modes in the original and in deuterated ibuprofen. The temperature dependences of these two intensities (the modes at ~ 100 cm^{-1} and at ~ 90 cm^{-1}) show a pronounced activation character, i.e. demonstrate two τ-bond states separated by the energy Δ*E*. Solid lines in Fig. 11.30 are plotted according to the expressions which take into account the population of states for Δ*E* values equal to 80 and 70 MeV in original and deuterated crystals, respectively (Fig. 11.30) [43].

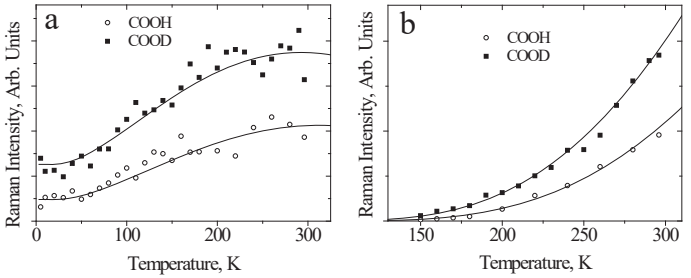

Figure 11.30 *a,b.* Temperature dependence of the integral intensity of ~100 cm^{-1} mode (a) and ~90 cm^{-1} mode (b) in normal IB (H) and deuterated IB (D) crystals. The ΔE value is 80 meV for IB (H) and 70 meV for IB (D). More details in [43].

However, the true value of this experiment lies in the fact that it makes it possible to reliably establish the effect of the proton transfer on the spectral characteristics of the crystal.

Fig. 11.31 *b* shows the peak position of the stretching C=O vibration of the carboxyl group in the ibuprofen dimer as a function of temperature. When the temperature rises from 5 K, the frequency of the C=O stretchings of the *L*-tautomer (at low temperatures, only the *L*-tautomer exists) has to, on the one hand, decrease as a result of ordinary anharmonic processes, and, on the other, increase, since, due to the same anharmonic processes, the involvement of the terminal C=O group in the hydrogen OH···O = C bond weakens, which is always accompanied by an increase in frequency. Figure 11.31 *b* shows that the second process acts somewhat more efficiently and $\omega_{C=O}$ slightly increases in the temperature

range 5 K–150 K. But at T≥150 K, the frequency $\omega_{C=O}$ suddenly begins to decrease exponentially, and the exponent of this process and the activation process of the *R*-tautomer is the same, i.e. ~80 MeV (Fig. 11.31 *b*). In other words, the change in $\omega_{C=O}$ is strictly correlated with the appearance of the *R*-tautomer, both in terms of temperature and rate of change.

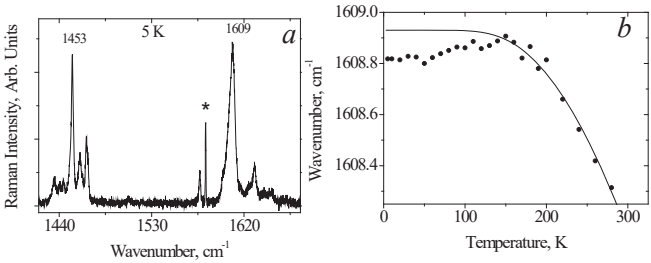

Figure 11.31. (*a*) The spectrum of ibuprofen (COOH) at 5 K in the range of C=O vibrations. The asterisk marks the position of line of Ne lamp, which was registered at each temperature for correction of the spectra; (*b*) Temperature dependence of the position of the 1609 cm^{-1} band peak of the C=O stretching vibration. The solid curve is plotted under the condition that a change in the mode frequency is caused by an activation process with ΔE=80 meV.

The reason for the unusual behavior of the $\omega_{C=O}$ mode is as follows. The transition from *L*- to *R*-tautomer and vice versa causes the C–O and C=O bonds of the carboxyl group to change places. In this case, an ordinary C–O bond, becoming a double, is significantly (by about 0.1 Å) shortened, and a double C=O bond is lengthened by the same amount. This process occurs with the frequency of proton hopping on the τ-bond, which in benzoic acid crystals is in the range 10^8-10^{11} s^{-1} in the temperature range 5 K - 300 K (see, for example, [39-42]). Thus, the bond lengths of the carboxyl group experience forced vibrations with frequency of hopping and a very large amplitude, several times higher than the amplitude of normal vibrations. (Strictly speaking, it is not vibrations, but changes of length with a great frequency). Forced vibrations of the carboxyl group give rise to the same anharmonic phenomena as normal vibrations, as a result of which the C=O bond lengthens, and the frequency of normal vibrations begins to decrease with the appearance of proton jumping, which is observed in Fig. 11.31 *b*. Thus, the dependence $\omega_{C=O}$ (*T*) can be used as a very sensitive tool for characterizing proton hopping at high temperatures and proton tunneling at low temperatures in systems with τ-bond. To our knowledge, no forced vibrations of chemical bonds

with any frequencies have been observed before. Consequently, this phenomenon can be attributed to a new type of forced vibrations.

The dependence shown in Fig. 4.9 *b*, also confirms the earlier conclusion that there is no tunneling at low temperatures (i.e., in the range 5 K - 150 K) in IB.

11.4.4 Proton tunneling

The described experiment with the frequency of C=O vibrations has no particular importance for ibuprofen, since the process of proton hopping is clearly demonstrated by the dependence of the intensity of ω_τ translational modes in the crystal (Fig. 11.30 *a*,*b*). However, it is a very sensitive tool to characterize both proton hopping and proton tunneling to the neighboring well in other compounds such as TPA chains with symmetric τ-bonds.

As was mentioned above, the coordinated transfer of the protons to the neighboring potential minimum should be accompanied by the absorption of the phonon ω_A ($\hbar\omega_A = A$, Fig.11.24 *b*), and the function of the tunneling rate vs temperature dependence is determined by the average value of the vibrational quantum number of phonons ω_A and has an anti-Stokes character.

Fig. 11.32 shows the $\omega_{C=O}(T)$ dependences in TPA (H) and TPA (D). In this case, the anharmonic shift of the frequencies of C=O vibrations is proportional to the tunneling rate and is associated with the energy change by the value of A at low temperatures and proton jumps over the barrier U_0 at high temperatures. The solid curves show the dependence of the 1611 cm^{-1} mode of the C=O stretchings at low temperatures and are drawn according to the expression $\omega(T) = \omega(0) - C\langle n\rangle$, where $\langle n\rangle$ is the average quantum number of phonon ω_A, and C is a proportionality constant (see [48]).

As can be estimated from Fig. 11.32, the value of A is approximately equal to 12 meV in TPA(H) and to 9 meV in TPA(D). The constant C is 2.2 cm^{-1} in TPA(H) and 0.75 cm^{-1} in TPA(D). The latter fact suggests that the probability of proton tunneling is significantly higher than that of deuteron, which is in agreement with theoretical concepts. A slight linear increase of the $\omega_{C=O}$ at T > 100 K in both compounds (dashed straight lines in Fig.11.32) is the result of weakening of the hydrogen τ-bond at elevated temperatures and gradual termination of tunneling. It testifies that the hopping rate is low in TPA(H) and even lower in TPA(D). Possibly, no jumps take place in the latter case at all. It should be noted that the above numerical parameters of the barrier A and the fact that no jumps with high

rates occur at elevated temperatures disagree with previous data [37], where A and the barrier U_0 were reported to be 16.25 MeV (130 cm^{-1}) and 75 MeV (600 cm^{-1}), respectively.

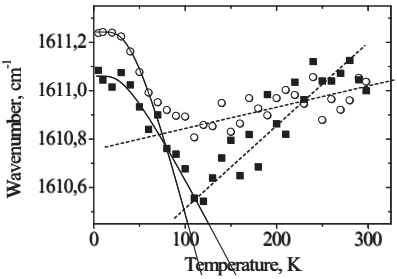

Figure 11.32. Temperature dependence of the C=O vibrational wavenumber of TPA(H) (circles) and TPA(D) (squares) carboxylic groups. Solid curves show temperature dependences of the thermal population of phonons ω_A (see the text); the dependences above 100 K are imaged by dashed lines, which are drawn approximately.

The Raman spectra of the compounds with tautomeric O-H···O hydrogen bonding in the temperature range 5 K – 300 K perfectly illustrate the behavior of protons on the τ-bonds. The spectra allow one to separate by temperature different mechanisms of proton density distribution, and the study of hopping and tunneling processes becomes possible with the help of a simple and available Raman spectroscopy technique. The results presented in this work largely coincide with those reported previously [32–42]. However, we believe that the description of proton behavior in τ-bonds obtained here using Raman spectroscopy complements the knowledge obtained from the works based on nuclear magnetic resonance (NMA) and inelastic neutron scattering (INS) methods. Undoubtedly, the two latter methods provide highly reliable data, but they are able to fix only the final phase of the tunneling process associated with proton transfer between the wells. In addition, at very low temperatures, only the more stable tautomer is noticeably populated, the protons are arranged in an ordered way, and the the tunneling rate is low. In this case, the NMR T_1 relaxation time is too large to be registered. The INS signal also becomes very weak. Therefore, none of these techniques can be used appropriately to study the dynamics at very low temperatures [36].

Also, the change in the energy of the process (in this case, the vibration frequency), which can be fixed in the Raman experiment, is of

the order of tenths of an inverse centimeter (hundredths of millielectronvolts), which seems to be beyond the capabilities of NMA and INS.

11.5. Brief characteristic of N–H···O and C–H···Y hydrogen bonds

11.5.1 N–H···O hydrogen bond

Despite the enormous importance of N–H···O hydrogen bonding in biological systems, their properties have not yet been fully established.

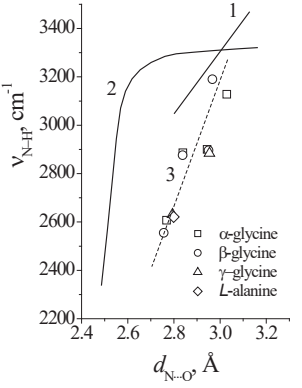

Figure 11.33. ν_{N-H} stretching vibrations in the N–H···O hydrogen bond as a function of N···O distance. 1 – N–H···O in compounds of various types [50], 2 – N–H···O bonds in conjugated systems [51], 3 – N–H···O in amino acid crystals

The dependence of the ν_{N-H} wavenumber on the N···O distance, known until recently [50], turned out to be significantly weaker than the analogous dependence for the O–H···O bond, and is shown in Fig. 11.33 by straight line 1. This dependence is characterized by the slope $\chi = \Delta\nu/\Delta d_{N\cdots O} = 1400$ cm^{-1}/Å, i.e. even slightly less than for the weak O–H···O bond. The range of both $d_{N\cdots O}$ and ν_{N-H} variation is also relatively narrow.

The above dependence is fulfilled for most chemical compounds of various types with N–H···O bond. It is possible, however, to synthesize the compounds in which the N–H···O bond becomes very strong [51]. In a chain of conjugated bonds with an embedded N-H···O hydrogen bond, for example,

–C=C–N–H···O=C–C= ↔ =C–C=N···H–O–C=C–,

ordinary C–C and double C=C cease to exist as different bonds, and some intermediate one-and-a-half bond is established between the carbon atoms (this situation is also often realized for N–H···O embedded in the aromatic ring). This phenomenon in chemistry is called bond resonance. In this case, the hydrogen atom in N–H···O should also occupy some intermediate position between the N–H···O and N···H–O states, i.e. to be equidistant from both atoms, nitrogen and oxygen, which is a condition for the occuring of a strong bond. Fig. 11.33 curve 2 shows the found ν_{N-H} wavenumber vs N···O distance in the hydrogen bond N–H···O for conjugated systems [51]. This dependence is already similar to that for the O–H···O bond.

Dependence 2 (Fig. 11.33) indeed shows a sharp decrease in the ν_{N-H} frequency at $d_{N\cdots O} < 2.6$ Å, which is associated with an increase in hydrogen bonding. However, at $2.6 < d_{N\cdots O} < 3.0$ Å, the frequency of N–H stretchings in chains of conjugated bonds is not lower but even higher than the ν_{N-H} obtained in [50], which does not fit into the concept of hydrogen bond strengthening proposed by the authors of [51]. Finally, in the crystals of amino acids, N–H···O hydrogen bonds reveal another, different from 1 and 2, dependence of ν_{N-H} on the N···O distance (dashed line 3, Fig. 11.33). In the latter case, for $d_{N\cdots O}$ in the range of 2.8 - 3.0 Å, the ν_{N-H} is significantly lower than in the previous two cases. Thus, the N–H···O hydrogen bond in compounds of various types demonstrates a significantly different functional dependence of the N–H vibrational frequency on the N···O distance. This makes it completely different from that of O–H···O bonds.

There are two reasons for the fundamental difference between O–H···O and N–H···O hydrogen bonds. One of them, the main one, is that the nitrogen atom, in contrast to the oxygen atom, can have different oxidation states in chemical compounds. Indeed, the vibrational frequency of hydrogen-bonded N–H should substantially depend on the charge state of the nitrogen atom, and each of these states will have its own specific dependence of the ν_{N-H} on the N···O distance. Another reason, less obvious, relates directly to the mechanism of the hydrogen bond formation. Donor oxygen atoms in O–H···O use predominantly *p*-atomic orbitals to make O–H bonds, while donor nitrogen atoms in N–H···O use mainly hybridized sp^n-atomic orbitals to bond with a hydrogen atom. In the latter case, the degree of participation of the *s*- or *p*-components will depend on the charge of the acceptor atom (i.e., in both cases, the acceptor oxygen) [52]. This is the Bent's rule [53], according to which, in the X–H···Y hydrogen bond, the hybridized orbitals of the X atom have predominantly

s-character in the case when they are directed to the electropositive substituent (i.e., Y), and predominantly *p*- character – in the case of an electronegative substituent. The character of the hybridized orbitals on the X–H···Y bond determines the ratio of the radii of the X and hydrogen atoms and, consequently, the length of the X–H bond. Thus, with the *s*-character of hybridized X orbitals, the X–H bond length decreases, and the ν_{X-H} vibrational frequency increases. For *p*-character, the opposite is true.

Thus, the ν_{N-H} frequency is not a good descriptor for the strength of the N–H···O hydrogen bond. This is the main difference between the N–H···O and O–H···O bonds. As mentioned above, the donor oxygen atom in O–H···O mainly uses only *p*-atomic orbitals for bonding with the hydrogen atom in any type of compound. For this reason, there may be just one dependence of ν_{O-H} on $d_{O\cdots O}$ in O–H···O hydrogen bonds, which manifests itself in a wide range of bond lengths and vibrational frequencies (Fig. 11.9).

11.5.2. Weak C-H···Y bonds. "Blue" shift

Hydrogen C-H···Y bonds are very weak, with an energy of interaction comparable to the energy of van der Waals bonds, but the spectroscopic manifestation of these bonds has been reliably established. In the literature, however, there is no information on the experimental dependence of the ν_{C-H} stretching vibrations on the C···Y distance similar to those that exist for O–H···O and N–H···O bonds. The reason for this is not so much the smallness of the effect, but rather the unusual properties of the C-H···Y hydrogen bond. The fact is that along with the usual shift of the ν_{C-H} to the low-frequency region during the occuring of the C–H···Y hydrogen bond (“red” shift), sometimes ν_{C-H} is shifted to the high-frequency region (“blue” shift). This phenomenon remained unclear for a long time, and only in the last decade has a quantum-chemical model appeared which satisfactorily explains the nature of the "blue" shift.

The reason for the unusual behavior of the C–H···Y bond was the carbon atom, which, unlike other donor atoms, actually uses the hybridized atomic sp^3 orbitals in the formation of valence interactions with neighbors. In this case, the Bent rule, which was discussed in the previous section, comes into force. And, taking into account the weakness of the C–H···Y bond in general, the effect of the Bent rule can shift the ν_{C-H} frequency to both high-frequency and low-frequency regions.

11.6. Conclusion

As shown above, an extremely strong hydrogen bond can occur under two conditions: 1) complete identity of the donor and acceptor atoms and 2) high electronegativity of both the donor and acceptor. From this point of view, the hydrogen O–H···O bond seems to be almost ideal for the realization of a strong bond. Another common bond in chemistry, N–H···N, yields to O–H···O in the second condition – the electronegativity of nitrogen atoms. On the other hand, the strongest hydrogen bond that exists in nature is the symmetric F···H···F, the energy of which is explained precisely by the very high electronegativity of fluorine atoms. But the F···H···F bond is more of a curiosity in chemistry in terms of its prevalence than the subject of serious research.

The electronegativity of oxygen-acceptor is the parameter that sets the rigidity of a hydrogen bond in a wide range, from weak to extremely strong. It is the low or zero electronegativity of oxygen atoms that can explain the fact that in many framework silicates or aluminosilicates, a water molecule included in the crystal cavity practically does not interact with the neighboring oxygen atoms. In framework crystals, oxygen atoms forming a cavity in the lattice are, as a rule, bridging between two silicon atoms. The valence orbitals of such oxygen atoms are saturated, and they do not show a tendency to interact with the hydrogen atoms of the H_2O molecule included in the cavity.

Finally, the O–H···O hydrogen bond very often acts as the base of another extremely interesting and important phenomenon in chemistry – tautomerism. Tautomeric O–H···O hydrogen bonds allow us to investigate complex processes of proton dynamics on a hydrogen bond - tunneling and jumping, significantly expanding our knowledge of the behavior of quantum particles such as the proton.

CHAPTER 12

VIBRATIONS OF THE H_2O MOLECULE IN THE CAVITIES OF BERYL AND OTHER MINERALS

This chapter will mainly consider the application of Raman spectroscopy to study the states of single molecules isolated in cavities of mineral crystals.

Many minerals have small cavities in their structure, often forming channels in the crystal. In such cavities "foreign" atoms or small molecules such as H_2O, CO_2, N_2, CH_4, etc. can be included. Thus, these crystals are part of a wide and extremely interesting chemical class of inclusion compounds. Most interest in research inclusion compounds represents the guest-host interaction, the orientation of the guest molecule in the cavity, and the behavior of the included molecules under various external conditions, i.e. pressure and temperature.

Beryl, $Be_2Al_3Si_6O_{18}{\cdot}xH2O$, of space group P6/mcc, is a framework structure consisting of hexagonal six-membered tetrahedral rings (Fig. 12.1), which are crosslinked in the (0001) plane by tetrahedra and octahedra to form a three-dimensional framework. The cavities are formed by oxygen atoms of the beryl lattice (open circles in Fig. 12.1). The six-membered rings are stacked over one another to produce infinite channels running parallel to (0001). The rings form bottlenecks with a diameter of about 2.8 Å, in which large alkali cations, such as K, Na (dark circles in Fig. 12.1), can be incorporated. In cavities (diameter about 5.1 Å) between the bottlenecks, various molecules (H_2O and CO_2) and neutral atoms (Ar) can be incorporated.

Over the past 70 years, numerous studies have been made to investigate the nature of molecular H_2O in beryl. It was shown that two different types of H_2O can be held in the channel cavities, namely Type I and Type II (Fig. 12.1).

The spectral properties of both types of water molecules differ significantly, which makes it possible to study them separately.

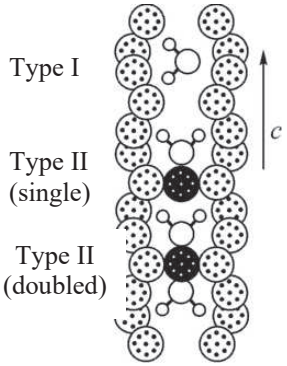

Fig. 12.1. Positions of water Type I and II in beryl channel. White doted circles are oxygen atoms; black doted circles are alkali ions. The *c* axis of the crystal coincides with the axis of the channels and is the rotary axis C_6.

12.1. H_2O, Type I

The raman spectrum of beryl in the frequency range of H_2O vibrations, type I (the absence of alkali cations in the crystal), is shown in Fig. 12.2. The spectrum contains only one band with a peak position at 3607 cm^{-1}, and is related to the totally symmetric stretching mode ν_1 (see Fig. 4.10). Asymmetric stretching vibration ν_3 is not observed at room temperature. This fact alone indicates that the interaction of the H_2O molecule with the environment is very weak.

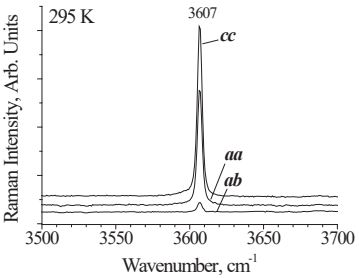

Fig. 12.2. Polarized Raman spectra of H_2O molecules, type I in beryl cavities at room temperature.

The orientation of the type I water molecule in the cavity can be easily determined based on the dependencies given in Figs. 12.3 and 12.4. Fig. 12.3 shows the angular dependences of the intensity ν_1 in the *ab* plane (perpendicular to the channel axis) and in the *ac* plane (including the channel axis).

It follows from the figure that the molecule does not have a preferred orientation in the *ab* plane, but is oriented in a certain way in the *ac* plane. Since the polarizability of a bond is determined by its longitudinal

component and the angle between the O–H bonds in H_2O is greater than 90°, the maximum intensity ν_1 in the direction of the *C*-axis of the crystal (Fig.12.3) indicates such a preferred orientation of the molecule in the cavity, at which its vector H···H is directed along the axis of the channels.

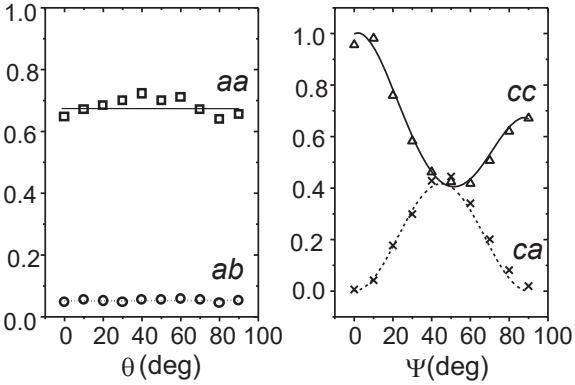

Fig. 12.3. Angular dependence of the intensity of the stretching vibrations ν_1 at 3607 cm^{-1} in the beryl cavity. In each of the figures, the zero value of the rotation angle means the direction of the polarization vector of the incident and scattered light parallel to the axis *a* (figure on the left) or *c* (figure on the right). An increase in the angle means rotation of the crystal by a given amount in the *ab* (left) and *ac* (right) planes with the direction of the polarization vectors unchanged.

However, the IR absorption spectra provide unambiguous information about the H_2O orientation in the beryl cavity (Fig. 12.4). In them, the line 3700 cm^{-1}, related to vibration ν_3 and indicating the direction of the dipole moment in the vibration, i.e. direction of the vector H···H of the molecule, is intense in the spectrum in which the polarization vector of the incident wave is parallel to the *c* axis of the crystal, and has zero intensity for polarization perpendicular to the axis channels. Thus, the H_2O molecule, type I is oriented in the beryl cavity as shown in Fig. 12.1 in relation to the channel axis and has a free orientation in the plane perpendicular to the channel direction.

As the crystal temperature decreases, the Raman spectra change significantly (Fig. 12.5) and exhibit several remarkable features.

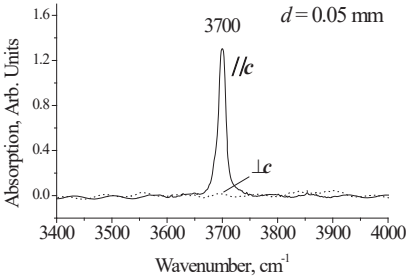

Fig. 12.4. IR absorption spectra of H_2O in beryl. The incident wave is polarized along (solid curve) and perpendicular (dotted curve) to the *c* axis of the crystal.

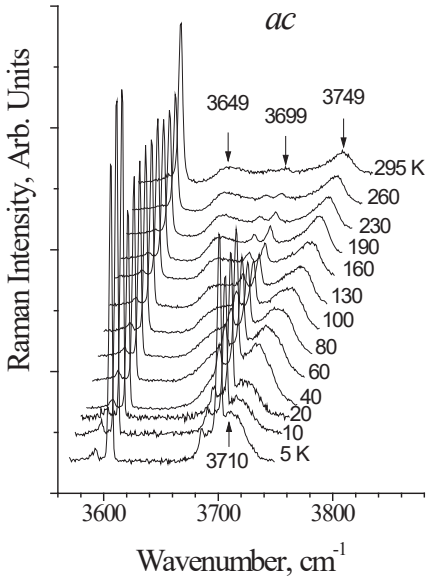

Fig. 12.5. Spectra of H_2O in beryl at different temperatures. Each subsequent spectrum is shifted relative to the previous one by 5 cm^{-1} for better visualization.

First of all, the intensity of the ν_3 mode (3704 cm^{-1} at 5 K), which is almost zero at room temperature, becomes noticeable at 5 K. This means that changes in the polarizabilities of the O–H bonds of the water molecule in the ν_3 vibration no longer cancel each other out, as this takes place in a completely free molecule. In other words, the molecule becomes asymmetric due to the interaction of one of its hydrogen atoms with the environment.

The most sensitive parameter of the interaction of a molecule with the environment is the frequency of the stretching vibration itself, ν_1 or ν_3.

Fig. 12.6 shows how the intensity of the ν_3 mode and the frequency of the ν_1 mode change with temperature. Both dependencies reveal saturation at ~ 50 K. The change in the frequency ν_1 is so small (~ 2 cm^{-1}) that it is, possibly, only a reaction of the cavity size to the temperature change, but does not indicate the formation of a hydrogen bond between the H_2O molecule and the cavity. The intensity of the ν_3 mode at low temperatures, although nonzero, is also rather weak. Perhaps this is due to the displacement of H_2O from the center of the cavity, which will cause to the appearance of an asymmetric crystal field on the molecule.

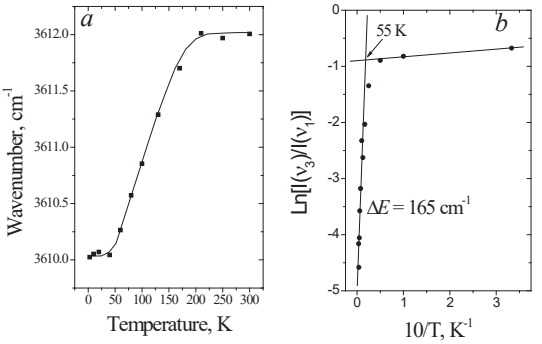

Fig. 12.6. Dependence of the vibrational frequency ν_1 (*a*) and the intensity ratio ν_3/ν_1 (*b*) on temperature

Of greatest interest in the spectra is the behavior of a broad band with a maximum at 3712 cm^{-1} and manifested in the spectrum as a shoulder of the ν_3 mode. This band is shifted to a high-frequency region with increasing temperature and at the same time it appears in a low-frequency side mirroring of ν_3 mode. Obviously, these bands represent the summarized (Stokes) and difference (anti-Stokes with respect to low-frequency vibration, which "perishes" during scattering) combined tones of the ν_3 mode and vibrations ω with a very low frequency. Since the combined tones appear in the *ac* spectrum simultaneously with the ν_3 mode of the B_1 symmetry, the symmetry of the so far unknown mode ω must be A_1 in order for their direct product to remain the B_1 symmetry.

Fig. 12.7 shows the deconvolution of a low-temperature spectrum into components, from which it follows that the Stokes part the spectrum consists of a set of combined lines $\nu_3 + \omega_n$, where $\nu_3 = 3703.7$ cm^{-1} and $\omega_1 = 6.3$ cm^{-1}. However, the position of the maxima of the decomposition components does not remain constant, as might be expected for a harmonic oscillator, but increases as the vibrational states with large n are populated, reaching ~ 50 cm^{-1} at room temperature (Fig. 12.5).

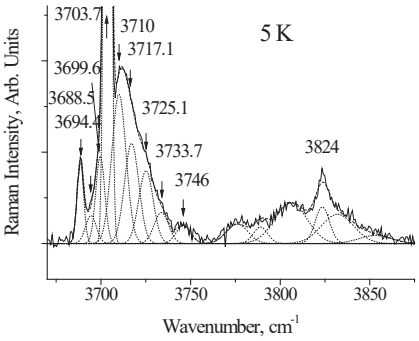

Fig. 12.7. Deconvolution of low-temperature Raman-spectrum into individual components.

The observed "inverse anharmonicity" (i.e., an increase in the frequency of the vibrational transition with increasing temperature, and not its decrease, as it happens for ordinary vibrational modes) can take place only in two cases. In the first of them, the H_2O molecule should be so free in the crystal cavity that the potential function of its interaction with the environment can be described by the state of a “particle in in the box”. In this case, the emerging discrete states are determined by the expression [1]

$$E_n = \frac{\pi^2 \hbar^2 n^2}{2ma^2} \tag{12.1}$$

where m is the mass of the particle, a is the width of the potential well, i.e. the difference between the size of the cavity and the molecule, and the ground state corresponds to $n = 1$. From (12.1) it follows that the energy of the transition between neighboring vibrational states will increase as n^2, that is, increase rapidly when the excited states are populated.

In the second case, the observed combined tones should be attributed to the rotational states of H_2O in the cavity, since the energy of the latter is determined by expression (2.56) from Chapter 2 and is proportional to J^2 +

J, where *J* is the rotational quantum number. In other words, the energy of rotational transitions between neighboring excited states increases even faster than for translational modes of a particle in a box. It should be noted that the rotational states of the free H_2O molecule in the gas phase are well known and noticeably exceed the values of the frequencies observed here. Therefore, in this case, we can only talk about hindered rotations of the molecule in the cavity.

For the correct assignment of the combined modes observed in Figs. 12.5 and 12.7, it is necessary to a) determine which of the assumed types of motion have A_1 symmetry, and b) estimate the energy of states with an increasing quantum number for various types of motion.

Determining the symmetry of states is not a simple task, since the result depends on how the cavity affects the movement of H_2O molecules. If a molecule is completely free and does not interact with the environment, then the symmetry of its translational and rotational displacements is determined by the irreducible representations of the symmetry group of the molecule itself, i.e. C_{2v}. This analysis has been done before, in Chapter 4 (see Table 4.5 and Figure 4.10). It can be seen that, in this case, the T_z translations (i.e., displacements along the C_2 axis of the molecule) belong to totally symmetric vibrations. However, if the crystal cavity restricts (slows down) the movement of molecules, then the symmetry of the displacements is determined by the symmetry group of the cavity C_{6h}. As can be seen from the table of characters of the C_{6h} group (Appendix D), rotations R_z of the H_2O molecule are totally symmetric, where the subscript *z* refers to the crystal coordinate system and means rotation around the C_6 axis of the cavity. For the final assignment of combined modes, let us calculate the energy of states for translational vibrations of a molecule in the box and for its hindered rotations (Table 12.1).

It can be seen that the hindered rotations of the H_2O molecule around the C_6 axis in the crystal cavity correspond to the experiment to a greater extent than the H_2O translations. However, the fact that the experimental increase in the transition energy with an increase in the quantum number is ahead of even the strongest theoretical dependence makes it appropriate to consider the nature of hindered rotations in more detail.

Table 12.1. Energies of transitions $n \rightarrow n+1$ (cm^{-1}) between neighboring states for different types of motion

Changing the quantum number n or J	Harmonic oscillator	«A particle in the box»	Hindered rotations	This work
0→1	ω=6.3 $см^{-1}$	ω=6.3 $см^{-1}$	ω=6.3 $см^{-1}$	ω=6.3 $см^{-1}$
1→2	ω	10.5	12.6	13.4
2→3	ω	14.7	18.9	21.4
3→4	ω	18.9	25.2	30
4→5	ω	23.1	31.5	42.3

The hexagonal cross section of the cavity (i.e., the presence of the C_6 axis) makes the potential of interaction of the H_2O molecule with the environment as shown in Fig. 12.8. Since the molecule rotates, its potential energy is higher than the height of the barriers, and in Fig. 12.8 it is shown with a dashed line. When a molecule is between barriers, its energy is equal to E_1, and its momentum is $p_1 = \sqrt{2mE_1}$. When above the barrier, the energy – E_2, and the momentum – $p_2 = \sqrt{2mE_2}$. Therefore, passing over the barriers, the molecule loses speed and its rotation slows down (see Ref. [2] for details). This is hindered rotation. For us, however, it is important that with increasing temperature the size of the cavity increases, and the height of the barriers decreases. This effect will cause an increase in the frequency of hindered rotation, which is observed in Fig. 12.5.

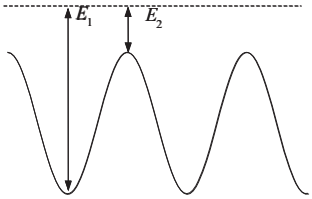

Fig. 12.8. Occurrence of hindered rotations of the H_2O molecule in the beryl cavity.

The decomposition shown in Fig. 12.7 contains not only Stokes, but also anti-Stokes components. The appearance of anti-Stokes modes at 5 K is undoubtedly due to the extremely low frequency of hindered rotation of the water molecule. It allows us, taking into account relation (1.27), to estimate the true temperature of the crystal at the place where the spectrum is

measured. The latter can differ from the crystal temperature indicated by a thermal sensor due to local heating of the sample by a focused laser beam. The temperature calculated from the ratio for the Stokes / Antistokes intensities (1.27) is 7–10 K instead of 5 K as indicated by the sensor. Thus, heating a transparent crystal by laser radiation (λ = 488 nm, radiation power ~ 1 mW at the crystal surface, spot diameter ~ 1 μm) is 2 - 5 deg.

Fig. 12.9 shows the polarized spectra of H_2O, type I in beryl at 5 K.

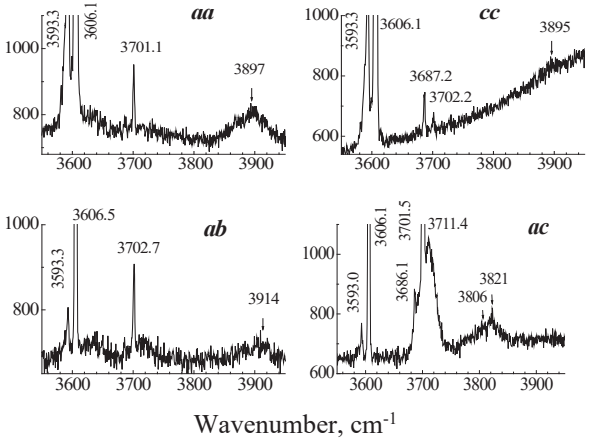

Fig. 12.9. Polarized spectra of Type I H_2O vibrations in beryl cavities at 5 K.

They have wide and weak bands spaced about 200 cm^{-1} from ν_1 or ν_3, which must be attributed to combined modes of the ν_1 and ν_3 and external H_2O vibrations, i.e. translations or librations. It is known that the frequency of translational displacements of H_2O molecules in ice crystals, where all the molecules are united by a network of hydrogen bonds, is 230 cm^{-1} (see Figure 9.10 in Chapter 9). Since there is no interaction of H_2O with the walls in the beryl cavity, the frequency of the translational modes should be significantly lower than 200 cm^{-1}, and the observed broad bands cannot be attributed to combinations with the participation of H_2O translations. Consequently, the observed modes must be attributed to the summarized tones of stretching vibrations ν_1 or ν_3 and librational vibrations of H_2O, which arise in those cavities of the crystal in which, for some reason, hindered rotations of molecules are not realized. Table 12.2

lists the conditions for the registration of combined tones in the Raman spectra of beryl crystals.

As you can see from Table 12.2, two different vibrations with frequencies of 193 and 212 cm^{-1} take part in the combined modes. To determine their symmetry and make the correct assignment, it is necessary to establish the symmetry of the combined vibrations. But now, in contrast to the case described above, we must consider the symmetry of both types of vibrations in the C_{3v} group of the H_2O molecules themselves, since all vibrations are carried out in fixed positions of the molecule, for which the cavity symmetry has no effect. This is easy to do, taking into account the orientation of H_2O, type I in the cavity, and the relationship between the axes of the crystal and the molecule (Table 12.2).

Table 12.2. Wavenumber of components (cm^{-1}) and symmetry of the combined modes of the second order Raman spectra of H_2O molecules

Wavenumber of combination mode	Geometry of scattering	Components wavenumber	Symmetry of the molecular mode
3895	(*aa*, *cc*)	ν_3 (3702) + 193	A_1
3914	(*ab*)	ν_3 (3702) + 212	A_2
3821	(*ac*)	ν_1 (3606) + 215	A_2 or B_1

Knowing the symmetry of the combined mode and one of its components (ν_1 or ν_3), it is easy to find the symmetry of the second component according to the rules of the direct product for second-order spectra:

$aa,\ cc \rightarrow A_1 = B_1\ (\nu_3) \times B_1 \rightarrow B_1\ (T_x,\ R_y)$

$ab \rightarrow B_2 = B_1\ (\nu_3) \times A_2 \rightarrow A_2\ (R_z)$

$ac \rightarrow (A_2,\ B_1) = A_1(\nu_1) \times (A_2,\ B_1) \rightarrow A_2\ (R_z),\ B_1\ (T_x,\ R_y)$

Hence it follows that one of the components of the recorded combined vibrations should be assigned to the librations R_z (212 cm^{-1}), and the other – to R_y (193 cm^{-1}). Here, the designations for the directions of the restricted rotation refer to the coordinate axes of an isolated molecule (see Fig. 4.1). The difference in the libration frequencies of the H_2O molecule around the z and y molecular axes corresponds to the difference in its moments of inertia I_z and I_y.

12.2. H_2O, Type II

The question of the behavior of H_2O molecules, type II in the beryl cavity at different temperatures was practically not considered in literature. Fig. 12.10 shows polarized spectra natural crystals of beryl containing H_2O molecules of both types, I and II. The bands at 3599 and 3664 cm^{-1} refer to the ν_1 and ν_3 modes of H_2O molecules, type II, respectively. The fact that the antisymmetric ν_3 mode is intense in the *ac* spectrum and is not observed in *ab*, unambiguously indicates the orientation of the molecule in the cavity, as shown in Fig. 12.1: vibration ν_3 is intense in the plane, and parallel to the plane of the molecule.

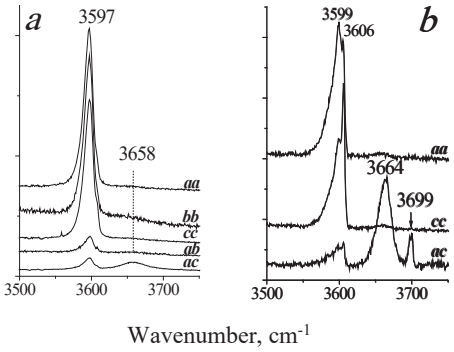

Fig. 12.10. Polarized Raman spectra of beryl crystals containing H_2O molecules of both types, I and II. *a* – 295 K, *b* – 3 K

In the spectra shown in Fig. 12.11, a rather strange feature is revealed: the bandwidth is 3599 cm^{-1} (ν_1 H_2O, type II) increases with decreasing temperature. Of course, this is not line broadening per se (with decreasing temperature, only vibrational modes can narrow). This means that some additional components within the ν_1 band appear at low temperatures. Indeed, the deconvolution of the spectra (Fig. 12.12) shows that the mode ν_1 consists of four components (3568, 3581, 3591, and 3599 cm^{-1}) at 3 K and only two (3568 and 3598 cm^{-1}) at room temperature.

The registration of two components of the ν_1 mode at 295 K is not surprising, since the vibration frequency depends on how much water molecules, one or two, are associated with an alkaline cation (see Fig. 12.1). In other words, one of the components, 3588 cm^{-1}, relates to a single water molecule, and the other, 3598 cm^{-1}, relates to a pair. The nature of

the additional low-temperature states, however, is quite different. To interpret the observable spectrum, it is necessary to assume that the H_2O molecule is free and rotates around the molecular axis C_2 (which coincides in this the case with the C_6 axis of the crystal channels, see Fig. 12.1).

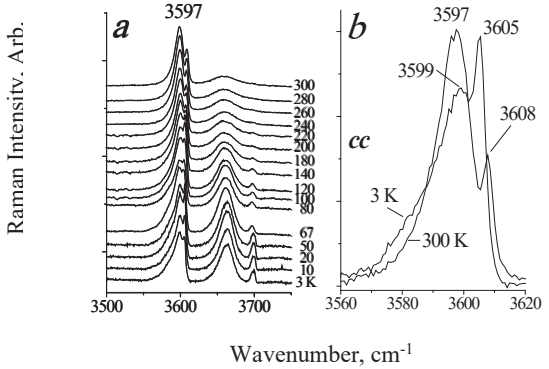

Fig. 12.11. H_2O spectra. *a* – at different temperatures, *b* – *cc* spectra at 300 K and 3 K

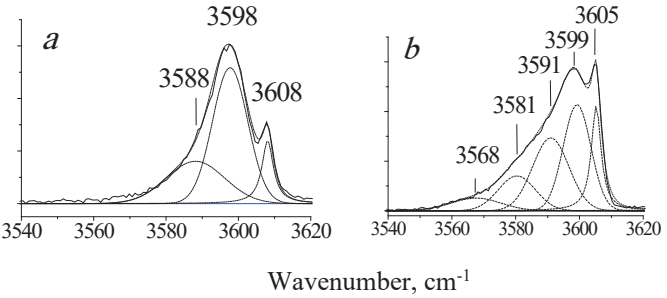

Fig. 12.12. Deconvolution of 300 K- (*a*) and 3 K-spectra (*b*) into Gaussian components

It is well known that the H_2O molecule is characterized by two different states of the nuclear spin, *ortho*- (the spins of hydrogen atoms are parallel, total spin $I = 1$) and *para*- (spins antiparallel, $I = 0$) (Fig.12.13). The moment of rotation J around the molecular axis C_2 can take odd values $J = 1, 3, 5, ...$ for *ortho*-H_2O and even $J = 0, 2, 4, ...$ for *para*-isomers. The statistical nuclear weight $(2I + 1)$ makes the ratio of *ortho*-

para isomers equal to 3:1 at room temperature, which is actually observed in the gas phase [3]. The *para* ↔ *ortho* transition is forbidden, at least in the absence of collisions or chemical interactions. Free rotation of type II H_2O molecules around the C_2 molecular axis in beryl cavities must obey the selection rules for nuclear isomers.

With a decrease in temperature, *para*-H_2O pass into the zero rotational state ($J = 0$), and the *ortho*-isomers are forced to remain in one of the excited rotational states at any temperature. In this case, *para*-H_2O molecules occupy a fixed state in the cavity, in which their interaction with the environment slightly changes, which causes a change (decrease) in the vibration frequency ν_1 of the molecule at rest. For this reason, the vibration frequencies of *ortho*- and *para*-H_2O molecules should be different at T <30 K, i.e. the temperature corresponding to the difference in the energies of the lowest *ortho*- and *para*-rotational states of H_2O [3]. Furthermore, the appearance of two additional components in the low-temperature spectrum is a consequence of the spectral separation of *ortho*- and *para*-isomers of single and paired H_2O molecules. Thus, type II H_2O molecules in beryl cavities are isolated, fixed, strictly oriented, and freely rotate around the C_2 molecular axis, and their total nuclear spin has a value of 0 or 1.

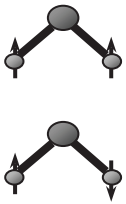

ortho-
$\boldsymbol{I} = 1$
$\boldsymbol{J} = 1,3,5$

para-
$\boldsymbol{I} = 0$
$\boldsymbol{J} = 0,2,4\ldots$

Fig. 12.13. *Ortho*- and *para*-isomers of H_2O molecules.

12.3. H_2O in cavity of other minerals

Single (isolated) H_2O molecules in crystal cavities turned out to be a very convenient object for studying the properties of the O–H···O hydrogen bond. The fact is that water molecules in crystals fill almost the entire range of possible states in terms of the number of hydrogen bonds: from H_2O not associated with the environment to H_2O with one, two, three, and four hydrogen bonds per molecule, which are the same or different in force constant. This makes it possible to differentiate the properties of hydrogen bonds and create a kind of “database” of the

properties of hydrogen bonds of H_2O and the water molecule itself under various conditions. In addition, the H_2O molecules in the cavities of crystals are ordered and oriented, which creates favorable conditions for the use of an effective apparatus of polarization Raman spectroscopy of oriented crystals to study their vibrational spectra. Finally, vibrational spectra of single molecules in crystals can be easily obtained in a wide range of temperatures (from 3 K to crystal dehydration temperatures, i.e., 300-800 °C) and external pressures.

The main spectral characteristics of hydrogen-bonded O–H stretching vibrations, i.e. their frequency, half-width, intensity and polarization, have been discussed in detail in Chapter 11. Here we will briefly discuss only those features that are inherent only in the hydrogen bonds of H_2O molecules in the cavities of mineral crystals.

Symmetry group of the H_2O molecule – C_{2v}. In a free molecule in the gas phase, the O–H bond length is 0.9572 Å, and the angle between bonds is 104.52 °. All three vibrational modes, i.e. symmetric stretching ν_1 (A_1), symmetric bending ν_2 (A_1) and asymmetric stretching ν_3 (B_1), are active in Raman and IR. The wavenumber of internal vibrations of free H_2O molecules are well known both from experimental measurements and numerical calculations: 3656.65 (ν_1), 1594.59 (ν_2), and 3755.79 cm^{-1} (ν_3).

In the cavities of crystals, the wavenumbers of stretching vibration are shifted to the low-frequency region by a small amount, ~ 50 cm^{-1}, already only due to the crystal environment. Perhaps this effect is due to the appearance of a small van der Waals interaction with the host crystal lattice. A further decrease in the frequency of H_2O vibrations occurs due to hydrogen bonding (see Chapter 11).

Very often, the two hydrogen bonds that the H_2O molecule creates in the crystal cavity as a donor are different in terms of the force constant. In this case, the concept of a symmetric and asymmetric mode loses its meaning, and the vibrations of each of the two O–H bonds become largely individual.

The intensity of symmetric and asymmetric stretching vibrations also strongly depends on hydrogen bonds with the environment. In a strictly symmetric H_2O molecule, the intensity of asymmetric mode ν_3 in Raman spectra is practically zero (Fig. 12.14). This is due to the fact that, in the asymmetric mode, changes in the polarizabilities of the O–H bonds occur in opposite phases and compensate each other, while in the symmetric mode they add up. However, as the O-H bonds in the molecule become different, their vibrations become close in intensity. In addition, this intensity is practically independent of the rigidity of the hydrogen bond as long as the bonds themselves remain in the weak range.

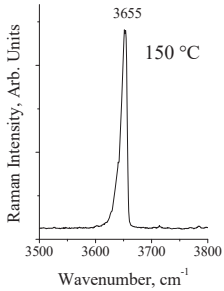

Fig. 12.14. Unpolarized Raman spectrum of H_2O in the gas phase in the region of stretching vibrations

Fig. 12.15 shows the polarized Raman spectra of O–H bond vibrations in the scolecite lattice, Ca_8 $[Al_{16}Si_{24}O_{80}]\cdot 24H_2O$, where each cavity contains three water molecules of different degrees of hydrogen bonding with oxygen ions of the host crystal. It can be seen that all lines related to O-H vibrations have approximately the same intensity, i.e. there is no noticeable change in the intensity of the bands with a change in the strength of the H-bond.

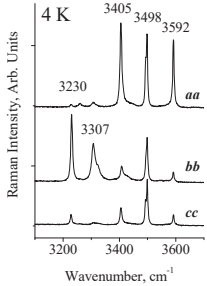

Fig. 12.15. Polarized Raman spectra of H_2O in scolecite at 4 K [4]

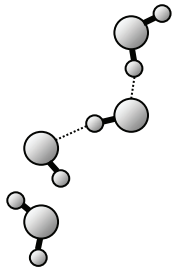

Fig. 12.16. Organization of hydrogen bonds of hydroxyl groups and H_2O molecules in a lawsonite cell, $CaAl_2(Si_2O_7)(OH)_2\cdot H_2O$.

In lawsonite (Fig.12.16), there are O–H bonds belonging to both a water molecule and hydroxyl groups, and the spread in vibration frequencies (H-bond strength) is very large - from 2780 to 3620 cm^{-1} at 4 K (Fig.12.17). But here, too, a monotonic dependence of the intensity of the bands on the frequency is not observed, which follows from the polarized spectra of lawsonite (not shown here). Thus, the intensity of O–H vibrations of the O–H···O hydrogen bond in Raman spectra is practically independent of the bond strength in the region of weak and moderate hydrogen bonds. But this does not apply to strong H-bonds (see Chapter 11).

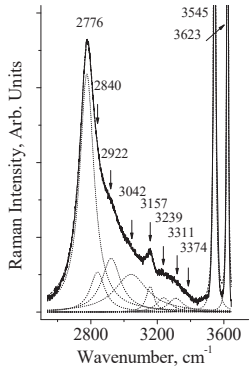

Fig. 12.17. Raman spectrum of lawsonite in the region of O – H stretching vibrations at 4 K. Weak bands on the high-frequency wing of the line at 2776 cm^{-1} refer to composite vibrations of hydrogen-bonded O – H and translational modes [5].

CHAPTER 13

SPECTROSCOPY OF MOLECULAR CRYSTALS

13.1. General remarks

Weak chemical interaction between molecules leads to the formation of molecular crystals. And although crystals of some simple substances (hydrogen, halogens, nitrogen, and oxygen), organometallic compounds, crystals of polymers and proteins are also referred to as molecular crystals, we will discuss here the most common molecular crystals formed by small organic molecules.

Intermolecular interaction in molecular crystals is determined by the weak van der Waals interaction and about an order of magnitude stronger hydrogen bonding (but still weak in relation to other, traditional types of bonds). The relationship between the one and the other can be very different. For example, amino acids have developed hydrogen bonds and are capable of forming bulky networks of hydrogen bonds, and the van der Waals interaction can be neglected. Compounds with an acetamide group, for example, paracetamol, form hydrogen bonds in only one plane, and interplanar interactions are van der Waals interactions. In crystals of benzoic acid, two neighboring molecules are linked by a strong (relatively) hydrogen bond, forming dimers, and the interaction between the dimers is van der Waals.

The most interesting feature of molecular crystals is the strong dependence of their structure on temperature and pressure. The organic molecules that make up the crystal, as a rule, are low-symmetry, the network of their bonds with neighboring molecules reflects the structure of the molecule, and the bonds themselves are weak and easily subject to stretching or compression under external influence. This causes the fact that with a change in temperature or external pressure, various intermolecular bonds in the crystal change to different degrees, as a result of which the molecules in the unit cell are forced to correct the relative orientation, tracking the change in all interactions with the environment. In other words, molecules in a cell are orientationally mobile. This mobility includes both small rotations of molecules in the cell as a whole, and

rotations of individual fragments of a molecule relative to each other, a change in the conformation of molecules, a change in the direction of hydrogen bonds (i.e., switching a bond from one acceptor to another), the emergence of multicenter hydrogen bonds, and others. Consequently, by changing the lattice parameters of a crystal, one can trace how the intermolecular interactions are organized in it. It is the mobility of molecules – orientational, conformational, in the switching of hydrogen bonds and the formation of new ones, and finally, in structural phase transitions – that is the subject of study of molecular crystals.

Another compelling reason for the need to study the dynamics of molecular crystals is as follows. Recently, approaches to the study of biological objects have been persistently developed. These compounds are so complex that the use of traditional physical methods in their usual form often encounters serious difficulties. And if NMR-, EPR-, and Mössbauer spectroscopy deal with individual nuclei (atoms) in molecules and their use can be quite effective, then all $3n$-6 normal vibrations will inevitably appear in the vibrational spectrum (excluding the case of resonance on vibrations of one selected fragment in molecule), which, of course, causes the overlap of vibrational modes and the registration of broad structureless bands in the spectrum.

At the first stage, however, one can start by investigating small components, the "building blocks" from which complex biological objects are built. Some of these components are amino acids and compounds with an acetamide group, many of which are drugs. Studies of molecular crystals formed by these compounds are extremely useful both in themselves and in terms of their properties as a component of biological molecules.

The effects observed in the vibrational spectra of molecular crystals, depending on the external influence, are so diverse that it is currently impossible to make a general description of them. Therefore, this chapter will discuss, on the one hand, the methodology and set of experimental techniques used in the study of molecular crystals, and on the other hand, we will try to show, using several specific examples, what a researcher may encounter when working with molecular crystals.

The lattice parameters can be varied using temperature or pressure. Undoubtedly, the application of external pressure is the most direct and immediate way of changing the lattice parameters. However, since the experiment is carried out at room temperature, many lines in the spectrum are already significantly broadened, and in the low-frequency region of crystal vibrations they are broadened so much that they overlap with each other and form wide bands that do not allow the correct decomposition

procedure into components. This deprives the experimenter of the opportunity to trace the wavenumber of the most interesting vibrations, namely, translational intermolecular modes, which directly reflect changes in the hydrogen bond network. A change in temperature in the range 4 K – 300 K (at higher temperatures, many molecular crystals begin to break down) also makes it possible to vary the lattice parameters, but in a smaller range than in the experiment with pressure (the lattice parameters change in the temperature range 4 K – 300 K to approximately the same degree as when the external pressure changes from 0 to 1 ÷ 2 GPa). However, with decreasing temperature, the lines narrow significantly, which, firstly, often reveals new spectral features that are inaccessible at room temperature, and, secondly, it allows one to describe the behavior of the spectral parameters of vibrational modes (frequency, half-width, and integral intensity) by well-known analytical expressions that facilitate detection and interpretation of ongoing structural changes. In what follows, we will use temperature as a tool for influencing the crystal lattice parameters.

13.2. Methodological features

Powder or crystal?

Polarization measurements of oriented crystals are needed when it is necessary to assign vibrational modes in the spectrum to the known directions of interatomic bonds in the crystal structure or to register individual spectral lines in a group of overlapping vibrational modes. In other cases, the spectra of powders are quite competitive with the spectra of crystals, but at the same time they require three times less time for registration. The difficulty in recording the spectra of both powders and crystals at different temperatures is establishing reliable thermal contact with the cryostat coolant line so that the recorded temperature of the coolant line corresponds to the sample temperature. This issue will be discussed below.

Crystal orientation

Of course, a reliable determination of the direction of the crystallographic axes is carried out on a single crystal X-ray diffractometer. However, this procedure is time consuming and not always justified. The point is that to record the temperature dependences of polarized spectra, it is necessary to have several samples (this is dictated by the measurement conditions, see below). Samples of crystals, as a rule, are small in size (up to tenths of a millimeter), and their mechanical strength is extremely low.

In other words, the prepared sample may break, be lost, or become unusable for measurements for some reason. Therefore, a reasonable alternative is to select several samples for measurement and orientate them using their Raman spectra.

Monoclinic crystals usually have the form of either elongated polyhedrons (needles) or plates, i.e. have a selected direction coinciding with one of the crystallographic axes. Let's conditionally call this selected direction the *z*-axis. The other two axes, conventionally *x* and *y*, are located in the cross section perpendicular to *z*, and to find them, it is necessary to compare the spectra polarized along the directions perpendicular to the sample faces as shown in Fig. 13.1.

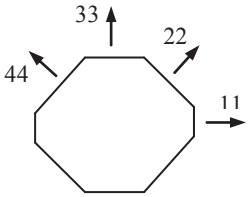

Fig. 13.1. Registration of polarized spectra in the crystal plane perpendicular to the selected z-axis to determine the orientation of the sample

For this, it is not necessary to obtain high-quality spectra in the entire range; it is sufficient to have, for example, the spectra of the low-frequency region of crystal vibrations. If a pair of spectra polarized along mutually perpendicular directions (in the figure, for example, directions 11 and 33) differ from each other in the position and intensities of the main lines, then these directions coincide with the crystallographic axes. The tabular values of the Raman tensor for a given symmetry group are determined for fixed directions of the crystallographic axes of this group. Therefore, the Raman tensor for any of the vibrational modes of the spectra under consideration takes the same value when rotated by + 45° and - 45° around *z* (the components of the rotated tensors may have different signs, but the line intensity in the polarized spectrum is proportional to the square of the Raman tensor component). Consequently, the spectra of the other pair, polarized along the directions rotated by ~ 45° relative to the first, (i.e., spectra 22 and 44), should be essentially the same. Thus, we get three selected directions coinciding with the crystal axes, and we can carry out polarization measurements. The binding of the selected directions to specific crystallographic axes of a previously known crystal structure can be done later, after obtaining complete spectra in different directions, in accordance with the intensities of characteristic vibrations in the polarized spectra. The modes of stretching vibrations

N–H···O and O–H···O of hydrogen bonds are especially useful for this purpose, since they are polarized and their being in the spectrum usually does not cause difficulties. The proposed method for determining the direction of the crystal axes is not rigorous, but it turns out to be accurate enough for carrying out polarization measurements.

Temperature measurements

Modern optical helium cryostats for Raman measurements are installed in place of the object stage of the entrance microscope of the spectrometer. Temperature controls are completely computerized, and in reality, there is only one problem - the problem of achieving full thermal contact of the sample with the cryostat cold finger. The use of various special adhesives for this purpose is not an optimal solution, since there is always the possibility of strong luminescence from the adhesive. In addition, it is often necessary to install the sample on the cold finger in such a way that the contact area between the cold finger and the crystal is minimal, for example, when installing on a thin crystal face or the end plane of a needle-shaped specimen.

An almost ideal solution is to place the sample in a heat-conducting medium, for example, metallic indium, which, on the one hand, is (subject to its high chemical purity) soft and ductile enough so that a fragile and small sample can be embedded in it, and on the other hand, provides a reliable thermal contact of the sample with the cold finger. For this purpose, cavities are made in the copper substrate, which is usually mechanically contacted to the cryostat cold finger, and filled with metallic indium. Then, in indium, pits are squeezed out in such a shape that the sample placed in them takes the desired orientation. The installed sample is pressed with indium on all sides by careful movements (the crystal is very fragile!) so that only its upper edge remains open for recording the spectrum.

Polarization measurements

When measuring the polarized spectra of molecular crystals, the following aspects should be taken into account. 1. Crystals with low symmetry are birefringent, i.e. capable to rotate the plane of polarization of the incident and scattered radiation. For this reason, it is always best to choose the direction of the polarization vector parallel to the crystallographic axis. In this case, the rotation of the plane of polarization is minimized. 2. Many crystals (for example, all crystals of amino acids except glycine) are chiral (this does not apply to racemates, i.e. crystals containing both enantiomers equally). Both effects, i.e. birefringence and chirality, can

either enhance or neutralize each other. 3. In Raman microscopes in the backscattering geometry, the effective depth of the sample, from which the scattered radiation is collected, is small and is regulated by the confocal aperture. Limiting the effective scattering depth dramatically reduces the effect of rotating the plane of polarization. Otherwise, it would be difficult to explain why the lines in the spectra presented below are often strictly polarized, i.e. demonstrate high intensity in one crystallographic direction and zero in the other two.

Registration and processing of spectra

When recording spectra for a long time, it is difficult to maintain constant conditions that provide the required spectral measurement accuracy. A slight change, for example, in room temperature, will shift the frequency calibration of the spectrometer by a few inverse centimeters. In addition, the intensity of the recorded spectra depends on the parameters of the input and output radiation paths, which the experimenter cannot fully control, as a result of which the measured spectra turn out to be different in line intensities for reasons not related to the state of the sample. Therefore, before starting to process the arrays of sample spectra obtained during temperature and polarization measurements, it is necessary to correct the spectra in wavenumber and intensity.

Wavenumber correction is achieved either by repeatedly calibrating the spectrometer during measurements, which is extremely inconvenient and does not give a 100% result, or by recording an exciting laser line (or some other reference line) in each spectrum, which, after the registration of all spectra is completed, is set for each spectrum to zero value of the wavenumber in the graphical editor. The registration of the laser line, which was practically excluded in the old-style spectrometers, has become possible in modern spectrometers (for example, LabRAM HR, and Horiba) equipped with “notch” or “edge” filters. These filters suppress the exciting laser line to such an extent that its intensity in the spectrum becomes comparable to the intensity of the Raman lines.

Vibrational spectra of molecular crystals are very complex and usually consist of several tens of lines in the range from ~ 20 to 3600 cm^{-1}. In this case, only the modes of stretching vibrations of the hydrogen atom in the C–H, N–H, and O–H bonds can be assigned with sufficient certainty. All other vibrations are mixed, and it is rather difficult to determine the degree of participation of various bonds or fragments of the molecule in them on the basis of experimental data; one can only give a tentative description. Quantum-chemical calculation of vibrational spectra of molecules using modern programs gives very good results, but it should

be borne in mind that the reliability of the calculation extends mainly to intramolecular vibrations. And if there is a need to have information about the spectrum of intramolecular vibrations, then such a calculation is uncontested. However, low-frequency crystal vibrations, as well as various deformations of molecules, and torsion modes, which are directly dependent on intermolecular interactions, are no longer so reliably determined by calculation. In addition, the calculation is carried out, as a rule, for one definite structural form of both a molecule and a crystal, and does not cover possible transformations with a change in temperature. For this reason, as a first step, one can try to find those features in the behavior of the spectral characteristics of vibrations, which, on the one hand, will help to make the assignment of the mode determined, and, on the other hand, establish the structural changes occurring in the crystal. These features are manifested primarily in the temperature dependence of the spectral parameters of the mode. The frequency of each vibration should, as a rule, decrease with increasing crystal temperature, which is a consequence of the anharmonicity of the interaction potential and the associated increase in the interatomic distance (see Chapter 9). If this does not happen, then, most likely, we are dealing with such a change in the orientation of the molecule in the cell, which causes an increase in the intermolecular hydrogen bond and subsequent inductive effects in the molecule. In addition, the rate of change in the position of the maximum with temperature is directly related to the degree of anharmonicity of the corresponding bond, intra- or intermolecular. Consequently, when evaluating the degree of anharmonicity of vibrational modes in the spectrum, one can detect those that fall outside the general trend and establish the cause of the deviation. In the case of normal behavior, the line half-width increases smoothly and exponentially with the crystal temperature, since the lifetime of the excited vibrational state decreases. Violation of this process is due to a change in the decay scheme of the excited state as a result of a change in the network of bonds between molecules. Finally, the intensity of low-frequency modes (<600 cm^{-1}) increases due to an increase in temperature of the population of a given vibrational state, and the intensity of high-frequency modes should not change normally with temperature. However, it is precisely in the behavior of the intensity of vibrations that various anomalies are most often observed, the cause of which is not always possible to find out.

Of course, the discussion of the spectra is based on concepts common to all molecular crystals, according to which the frequency range 20–200 cm^{-1} includes crystalline (intermolecular), 150-600 cm^{-1} – torsion, 600–1700

cm^{-1} – intramolecular, and 2500–3600 cm^{-1} – stretching C–H, N–H, and O–H vibrations. The latter are usually hydrogen bonded.

In order to show the effectiveness of Raman spectroscopy using polarization and temperature measurements, we will give several examples of studies of the properties of molecular crystals, covering various classes of compounds.

13.3. Spectra of crystals of amino acids

Amino acids include organic compounds, the molecule of which simultaneously contains carboxyl and amine groups (Figure 13.2). Figure 13.2, a shows the amino acid molecule as it exists in the gas phase. When a crystal is formed, the hydrogen atom of the carboxyl group is transferred to the amino group of the neighboring molecule due to the greater affinity of the nitrogen atom for hydrogen. In this case, a zwitter ion (double ion) is created, positively charged from the side of the formed NH_3^+ group and negatively from the side of the COO^- residue. (The question of the magnitude of the charge can be solved using a quantum chemical calculation).

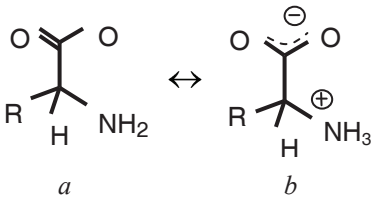

a *b*

Fig. 13.2. Amino acid in normal form (*a*) and in the form of zwitterion in crystal (*b*)

The simplest amino acid is glycine, $NH_2–CH_2–COOH$, where one hydrogen atom plays the role of the radical fragment R (Fig. 13.2).

Glycine crystallizes in three polymorphs, α, β and γ. The structure of α-glycine is shown in Fig. 13.3.

We will not discuss the entire spectrum of glycine in this section. Let us consider only a small part of it, concerning the features of the behavior of the bifurcation hydrogen N–H···O bond in the α-glycine crystal.

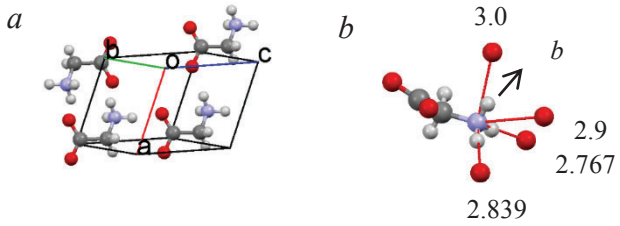

Fig. 13.3. *a* – Fragment of the α-glycine structure. *b* – A diagram of three hydrogen bonds of the NH_3 group with the acceptor oxygen atoms of neighboring molecules (the bond in the *b* crystallographic direction is bifurcational). The N···O distance (Å) is placed next to the corresponding acceptor.

The polarized spectra of low-frequency crystalline vibrations of α-glycine at 5 K are shown in Fig. 13.4. Fig. 13.5 shows the dependences of the peak position, the half-width, and the intensity of the 118 cm^{-1} mode, which is intense in the ***bb*** spectrum. All three spectral characteristics of the mode demonstrate an example of normal behavior with temperature, i.e. behavior characteristic of anharmonic vibrations (see Chapter 9).

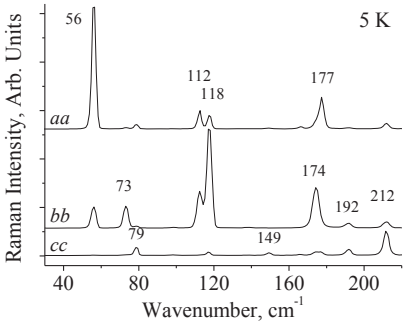

Fig. 13.4. Polarized spectra of crystalline vibrations of α-glycine at 5 K

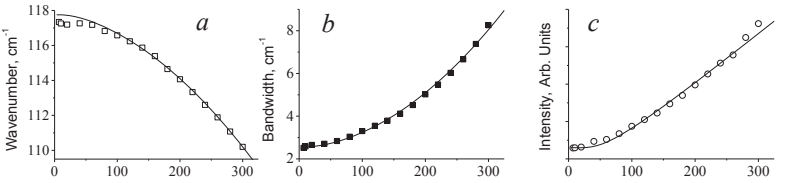

Fig. 13.5. Dependence of the peak position (a), half-width (b) and the relative intensity (c) of the 118 cm^{-1} mode on temperature of α-glycine.

Fig. 13.6 shows the dependence of the peak position of the 73 cm^{-1} mode in α-glycine as an example of the anomalous behavior of the vibrational mode on temperature.

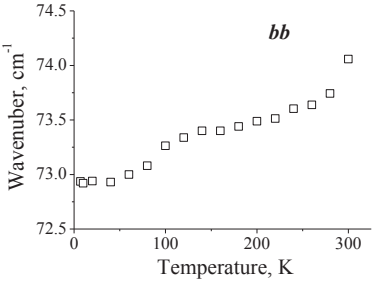

13.6. Dependence of the peak position of the translational mode 73 cm^{-1} on the temperature in α-glycine.

The unusual increase in the vibration frequency with increasing temperature is most likely related to a change in the intermolecular hydrogen bond, since the frequency range ~ 100 cm^{-1} refers to crystalline (external) vibrations. The hydrogen bond in α-glycine in the direction along the *b* axis of the crystal (i.e., in the direction of polarization of the incident and scattered light) is bifurcational (Fig.13.3, *b*), and an increase in the frequency of the mode vibration with increasing temperature can be caused either by an increase in the entire hydrogen bond (which is unlikely), or an increase in the mode of that component of the bifurcation coupling, which is characterized by a larger force constant. To find out the reason for the anomalous behavior of the mode, it is necessary to turn to what happens in the high-frequency region of the stretching N-H vibrations of a given N–H···O hydrogen bond.

The frequency range 2500-3600 cm^{-1}, the most stable and reliable from the point of view of assigning the observed lines, includes stretching vibrations of CH, CH_2 and CH_3 groups (2900-3100 cm^{-1}), hydrogen-

bonded N–H (≤3500 cm^{-1}) and O–H (≤3600 cm^{-1}). And if the vibrational frequencies of C–H usually very weakly depend on temperature, then the dependence of the vibrational frequencies of N–H and O–H is much stronger due to the change in the lengths of hydrogen bonds with a change in the temperature of the crystal. The polarization of these modes is rigidly related to the direction of the corresponding hydrogen bonds in the crystal lattice.

Fig. 13.7 shows the polarized spectra of α-glycine in the range of C–H and N–H stretching vibrations. Modes at 2975 and 3009 cm^{-1} refer to symmetric (in phase) and antisymmetric (in antiphase) stretching vibrations of the CH_2 group, respectively. Band 3127 cm^{-1} - to the vibration of one of the hydrogen-bonded N-H, 2899 cm^{-1} - to the other. The third intense and wide band, 2607 cm^{-1}, also relates to N-H hydrogen-bonded vibrations, but its position in the spectrum and some features are so atypical for a vibrational mode of this type that there are still no comments on this topic in the literature. The nature of N–H···O hydrogen bonds in amino acid crystals is discussed in detail in Chapter 11.

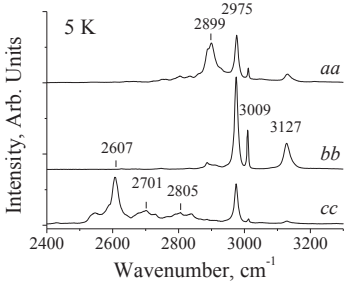

Fig. 13. 7. Polarized spectra of α-glycine in the range of C–H and N–H stretching vibrations.

Let us consider in more detail the behavior of the 3127 cm^{-1} mode, since it is related to the bifurcation hydrogen bond along the crystallographic direction *b* of the crystal (Fig. 13.3, b). This mode is complex and consists of two components, 3127 and 3135 cm^{-1} (Fig. 13.8). The dependences of the position of the maximum and the integrated intensity on the temperature of each component are shown in Fig. 13.9.

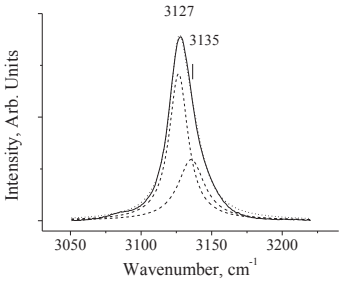

Fig. 13. 8. Deconvolution of the N–H stretching vibration mode in the N–H···O hydrogen bond along the *b*-axis of the α-glycine crystal at 5 K.

The vibrational frequencies of both components increase with increasing temperature, i.e. the hydrogen bond weakens. This unambiguously indicates that an increase in the frequency of the corresponding intermolecular translational mode 73 cm^{-1} (Fig. 13.6) is due to a change in the vibrational eigenvector. The intensity of the components changes in a mutually opposite direction. Consequently, the vibrations refer to two different states of the hydrogen bond: at a low temperature, the state with a stronger bond (mode 3127 cm^{-1}) is mainly populated, and at a high temperature, that with a weaker bond (mode 3135 cm^{-1}).

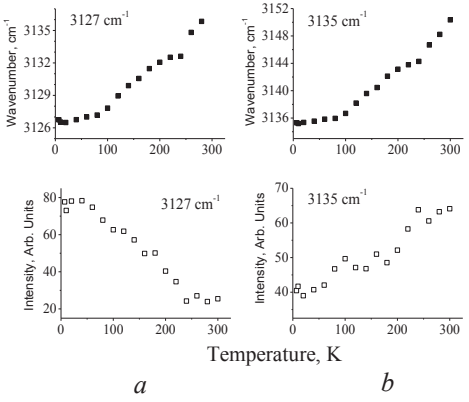

Fig. 13.9. Dependence of the peak position and the integrated intensity of the components 3127 (*a*) and 3135 cm^{-1} (*b*) of the N–H stretching mode in the N–H···O hydrogen bond along the crystallographic *b* axis of the α-glycine crystal.

These simple observations allow us to draw conclusions about the nature of the hydrogen bifurcation bond. It is often believed that in a bifurcation bond, both acceptor atoms (i.e., oxygen atoms of neighboring molecules in this case) are simultaneously bonded to one proton of the N-H group using their lone electron pairs. The experiment presented here shows that in fact a proton forms a bond either with one acceptor or with another, being able to jump from one potential well formed along the N–H···O(1) bond to another related to the N–H···O(2) bond. The integral intensities of both components are determined with low accuracy due to the proximity of their vibration frequencies and overlap in the entire temperature range; therefore, at this stage, it is not possible to determine the potential barrier between two potential wells, as well as the mechanism for changing the localization of the proton at low temperatures − over- or under-barrier (tunnel). It should only be noted that the double-well potential of the bifurcation bond should not be confused with the double-well potential of each individual hydrogen bond, in which, according to theoretical concepts, one potential well (deep) is localized near the donor atom, while the other (shallower) is near the acceptor atom.

The hydrogen bond along the *b* axis of the crystal is one of the weakest in α-glycine, and fixing the mode of translational vibrations of this bond at 73 cm^{-1} sets the lower limit of the frequencies of translational intermolecular vibrations of hydrogen bonds in α-glycine. (It will be shown below in next section that modes with frequencies of ~ 50 cm^{-1} are related to deformational intermolecular vibrations of hydrogen bonds, and this fixes the second reference point, which means that all modes with frequencies below 50 cm^{-1} are related to vibrations of van der Waals bonds).

13.4. "Anomalous" changes in the intensities of low-frequency modes in L-alanine

When discussing the low-frequency spectrum in α-glycine crystals, it was assumed that vibrational modes with frequencies below 70 cm^{-1} can refer either to bending vibrations of hydrogen bonds or to bond vibrations determined by the van der Waals interaction. Here we will try to explain what they are and how they are manifested in the spectrum of deformation crystal vibrations of hydrogen bonds. For this purpose, we present a description of the temperature dependence of the lattice vibrations of *L*-alanine crystals, demonstrating, on the one hand, the possibilities of polarization Raman spectroscopy, and, on the other hand, an attempt to

explain the phenomenon that has not had a definite interpretation in the literature for a long time [1].

In 1988, Migliori et al. [2] noticed an anomaly in the temperature dependence of the intensity of two low-frequency Raman modes, 42 and 49 cm^{-1}, in L-alanine crystals. The intensity of the 49 cm^{-1} mode in ***bb*** polarization increased too strongly with temperature, and the 42 cm^{-1} mode too weakly compared to what was expected according to Maxwell-Boltzmann statistics. However, the change in temperature in the total intensity of both modes was normal. The authors of [2] assumed the existence of dynamic localization of vibrational energy, which could create an excessive intensity of the 42 cm^{-1} mode below 150 K. Both modes exhibit a similar behavior when the external pressure changes. This problem has been discussed for a long time in the literature by various authors, and various solutions have been proposed, but a definite point of view has not been worked out.

Fig. 13.10 shows a molecule of *L*-alanine in the zwitterionic form and a fragment of the structure of the crystal lattice of L-alanine.

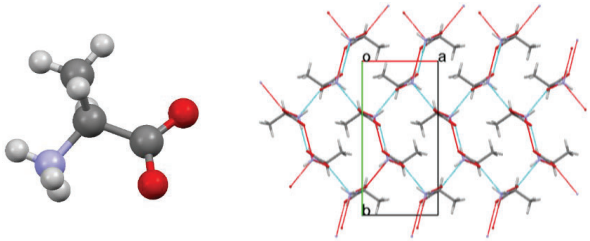

Fig. 13.10. *L*-alanine molecule in zwitterionic form and a fragment of the crystal lattice structure of L-alanine.

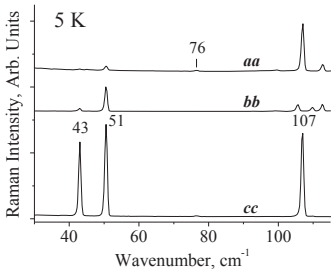

Fig. 13.11. Polarized Raman spectra of *L*-alanine crystals at 5 K in the region of lattice vibrations.

Fig. 13.11 shows the polarized spectra of *L*-alanine in the region of lattice vibrations, and in Fig. 13.12 these spectra are shown at several different temperatures. The integrated intensities of modes 42 and 49 cm^{-1} (43 and 51 cm^{-1} at 5 K, Fig. 13.11) for different polarizations and depending on temperature are shown in Fig. 13.13. To calibrate the spectra by intensity, the 856 cm^{-1} mode was used, which, on the one hand, does not relate to intermolecular vibrations, and, on the other hand, has an energy that is high enough to make the temperature dependence of the intensity negligible.

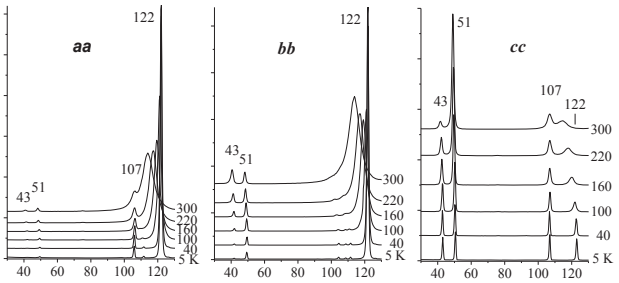

Fig. 13.12. Polarized spectra of lattice vibrations of *L*-alanine at different temperatures (polarization is indicated in the figures).

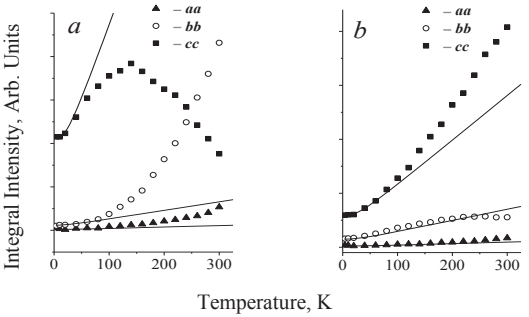

Fig. 13.13. Integral intensity of modes 42 and 49 cm^{-1} in polarized spectra depending on temperature: *a*) - 42 cm^{-1}; *b*) - 49 cm^{-1}. The solid curve for each dependence is the Maxwell-Boltzmann statistics with different initial values at low temperatures. The polarizations are indicated in the figures.

The intensity of both low-frequency modes changes with temperature in different ways, depending on the polarization of the light. The sum of

intensities for each mode (i.e., the sum of intensities in ***aa***, ***bb***, and ***cc*** polarizations) is shown in Fig. 13.14*a*, and the total intensity of both modes is shown in Fig. 13.14*b*. It can be seen that only the latter obeys the Maxwell-Boltzmann statistics (solid curve in Fig.13.14*b*).

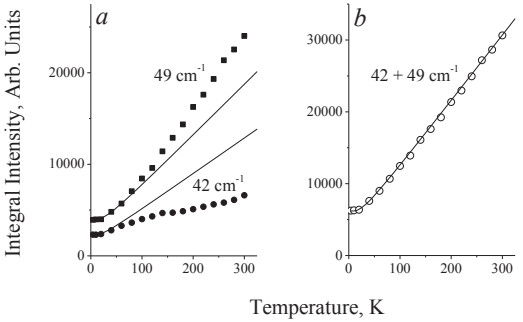

Fig. 13.14. Intensity of low-frequency modes as a function of crystal temperature: *a*) - total intensity (***aa*** + ***bb*** + ***cc***) of modes 42 cm^{-1} (solid circles) and 49 cm^{-1} (solid squares); *b*) is the sum of intensities of modes 42 and 49 cm^{-1}. Solid curves - Maxwell-Boltzmann statistics with different initial values.

Both modes show an anomalous temperature dependence of not only the intensity, but also the position of the maximum (Fig.13.15*a*). At temperatures above 150 K, the 42 cm^{-1} mode deviates from the expected dependence to low wavenumbers, and the 49 cm^{-1} mode, on the contrary, to high wavenumbers.

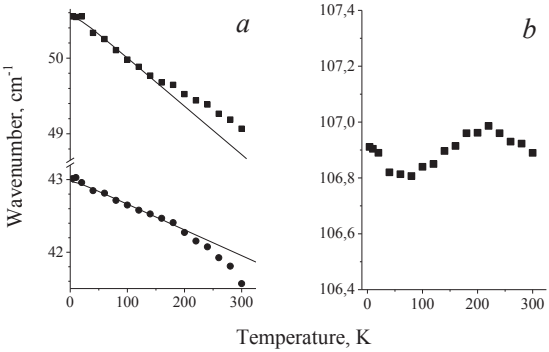

Fig. 13.15. Temperature dependence of the peak position of *a*) - modes 42 and 49 cm^{-1} and *b*) - modes 107 cm^{-1}.

To understand the anomalous behavior of low-frequency modes, it is necessary, first of all, to make their assignment. An exact description of the lattice vibrations of molecular crystals, obtained by quantum-chemical calculations, is still not available at present, but one can try to make a qualitative interpretation. The lowest vibration frequencies in molecular crystals are usually referred to as translational displacements of molecules as a whole. Taking into account the value of the force constant for a typical hydrogen N–H···O bond (~ 13 N/m) and the molecular weight of alanine (89 a.m.u), we can expect a value of ~ 100 cm^{-1} for the frequency of optical vibrations in L-alanine. The temperature dependence of the position of the maximum of the 107 cm^{-1} mode, which is intense in the ***cc*** spectrum, is shown in Fig. 13.15*b*. The presented dependence does not reveal the steady decrease in the vibration frequency expected due to the manifestation of anharmonic effects (see Chapter 9), but at the same time it agrees with the unusual behavior of the lattice parameter *c*, which demonstrates a slight decrease with increasing temperature, while the other two lattice parameters *L*- alanians, *a* and *b*, increase with temperature, which is normal. Thus, the assignment of the 107 cm^{-1} mode to the translational vibrations of *L*-alanine molecules in a chain oriented along the *c* axis of the crystal seems to be correct, which makes the assignment of the 42 and 49 cm^{-1} modes nontrivial, since the frequency of the latter is more than twice lower, and the force constant, therefore, must be four times less than the force constant of the translational modes.

Due to numerous hydrogen bonds with the environment, molecules in *L*-alanine crystals form both a three-dimensional network of hydrogen bonds and two-dimensional cycles located in mutually perpendicular crystallographic planes (i.e., *ab*, *bc* and *ac*). The crystal structure projected onto the *ab* plane is shown in Fig. 13.10. Some vibrational modes in such cycles can correspond to molecular displacements that characterize changes in angles rather than lengths of hydrogen bonds (i.e., a kind of bending vibration of hydrogen bonds). For example, these modes include the "breathing" vibration of molecules in a cycle. The frequency of the latter should be much lower than that corresponding to the translational displacements of molecules along the chain, which are related to purely stretching intermolecular vibrations of hydrogen bonds. Consequently, the 42 and 49 cm^{-1} modes can be attributed to such translational displacements of molecules, which result in "breathing" modes of molecular cycles. These latter correspond to bending vibrations of hydrogen bonds in the crystal lattice.

The key to understanding the anomalous behavior of the 42 and 49 cm^{-1} modes on temperature and pressure is the fact that the degree of

deviation of the spectral characteristics of both modes from the norm depends on the chosen crystallographic directions when recording polarized spectra (Figs. 13.12 and 13.13). This means that the orientation of the molecules in the crystal lattice relative to each other changes slightly with temperature/pressure. A change in the mutual orientation of molecules entails a change in the eigen vector of normal vibrations of the corresponding modes. The eigen vector of the vibration is directly related to its frequency. Above 150 K, the frequency of the 42 cm^{-1} mode decreases faster than expected for normal anharmonic behavior (see Chapter 9), while the frequency of the 49 cm^{-1} mode, on the contrary, is slower (Fig. 13.15*a*). Consequently, with increasing temperature, the bending component of the complex vibration increases for the first mode (i.e., the force constant and frequency decrease), while the stretching component increases for the second mode (the force constant and frequency increase with respect to the theoretically expected). The behavior of the intensity of both modes can be understood if we take into account that the intensity of stretching vibrations (i.e., vibrations in which the length of hydrogen bonds is modulated) is much higher than the intensity of bending modes (i.e., without changing the lengths of hydrogen bonds). When the bending component of the 42 cm^{-1} mode increases with temperature, the intensity of this mode should decrease, which is observed in the experiment (Fig. 13.14*a*). An increase in the stretching component of the 49 cm^{-1} mode should cause an increase in its intensity faster than that which follows from the Maxwell-Boltzmann statistics, which is also found in the experiment (Fig. 13.14*a*).

Thus, the “anomalous” effects observed with a change in temperature and pressure for the intensity and position of the maximum of two low-frequency modes in the polarized Raman spectra of *L*-alanine crystals can be interpreted within the framework of simple and clear processes and without invoking any assumptions about “phase transitions” or “dynamic localization of vibrational energy”. Constant stress in the structure, accompanied by a change in the orientation of molecules in a three-dimensional network of hydrogen bonds, can explain the observed anomalies in Raman spectra corresponding to certain crystal orientations and light polarization, as a change in the relative contributions of "stretching" and "bending" components in two lattice modes. It is noteworthy that the total intensity of both modes, summed up for all polarizations, does not show any anomalies in the temperature dependence (Fig. 13.14*b*). Since a three-dimensional network of hydrogen bonds is often formed in molecular crystals, similar anomalies in the region of low-frequency vibrations in polarized Raman spectra can be observed not only

in *L*-alanine, but also in other compounds. For example, modes with frequencies of about 50 cm^{-1} in α-glycine show similar behavior.

13.5. Delocalization of vibrations in crystals of compounds with the acetamide group

Amides are compounds with the general formula R–CO–N<. Distinguish between unsubstituted (or primary) R–CO–NH_2, monosubstituted (or secondary) R–CO–NH–R′ and disubstituted (or tertiary) R–CO–NR′R″ amides. In this work, we will mainly discuss such secondary amides in which the methyl group CH_3 is chosen as R, forming the acetamide group CH_3–CO–NH–R′. Many of these compounds are related to drugs. Crystals of compounds with an acetamide group are interesting on account of the presence in the structure of hydrogen bonded N–H···O chains (Fig. 13.16). These include acetanilide (C_8H_9NO), metacetin ($C_9H_{11}NO_2$), phenacetin ($C_{10}H_{13}NO_2$), paracetamol ($C_8H_9NO_2$), etc.

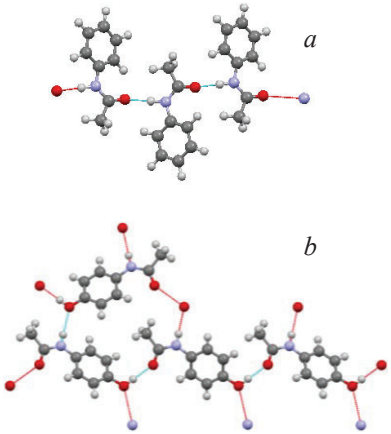

Fig. 13.16. Chains of N–H···O hydrogen bonds in the structure of acetanilide (*a*) and chains and cycles in rhombic paracetamol (*b*).

In the spectra of crystals of molecules with an acetamide group, the most interesting is the manifestation of the acetamide groups themselves for two reasons. 1. By themselves, the vibrations of the acetamide group serve as an excellent diagnostic tool for characterizing the structure of the synthesized compound. 2. The vibrational frequencies of the acetamide group directly characterize the intermolecular hydrogen bond, since this

bond in crystals is carried out precisely through the acetamide groups (Fig. 13.16). For this reason, the spectrum of vibrations of the acetamide group has been studied in detail in the literature and consists of the following modes, which have received a special designation.

1. Vibration Amide I. This is the stretching vibration C=O. Its frequency, which is usually in the range of 1700-1750 cm^{-1}, during the formation of chains of N-H···O = C hydrogen bonds in crystals decreases to 1640-1660 cm^{-1}. The stronger the hydrogen bond, the lower the frequency of the stretching C=O vibration. It confidently manifests itself in the Raman spectra.
2. Amide II-III. This mixed vibration consists of the C–N stretching and N–H (in-plane) bending. Presented by two components. The high-frequency mode ~1550 cm^{-1} contains predominantly bending N-H and is designated as Amide-II. The low-frequency component lies in the region of 1220-1350 cm^{-1}, in which stretching vibrations C-N are mostly represented, and it is designated as Amide III.
3. Another characteristic vibration of the acetamide group lies in the range of 740-800 cm^{-1}, and refers to the bending vibration N-H (out of plane). Some authors call this mode Amide-IV, others - Amide-V.

There are several more modes with a frequency below 700 cm^{-1}, related to the acetamide group, but they are less characteristic, and their assignment is more controversial.

As already mentioned, compounds with an acetamide group are very important, since some of them are part of proteins (for example, acetanilide), and others relate to drugs (for example, methacetin, phenacetin, and paracetamol). For this reason, we will briefly consider the problem associated with the vibrational spectra of these compounds. This problem was very popular in the scientific literature for a decade and a half.

In 1976, Davydov and Kislukha [3] suggested that in chains of hydrogen bonds, similar to those in crystals with an acetamide group, unusual vibrational states called solitons can arise. A few years later, the authors of [4-5] found that in the spectra of acetanilide crystals, a temperature-dependent mode, somewhat shifted in wavenumber relative to the Amide-I vibration, is observed. This mode was attributed to the occurring of a Davydov's soliton (self-trapped state), which prompted the appearance of several dozen works, mainly theoretical, devoted to the

phenomenon of self-trapping in acetanilide crystals. However, in order to be convinced of the correctness (or erroneousness) of the assignment made, it is necessary to consider in more detail both the entire spectrum of acetanilide and the spectra of other compounds with an acetamide group.

Fig. 13.17, *a* shows the temperature dependent spectra of acetanilide in the region of stretching vibrations of the hydrogen-bonded C=O group. At 5 K, the spectrum consists of three clearly distinguishable bands at 1652, 1663, and 1668 cm^{-1}. (In the literature, at low temperatures, only two lines are observed; as will be shown below, the reason for the persistence at low temperatures of the weak line at 1663 cm^{-1}, originally attributable to the Amide-I mode, is associated with the imperfection of the crystal used in this work).

At room temperature, one broad Amide-I mode at 1666 cm^{-1} and two very weak modes at 1654 and 1668 cm^{-1} dominate. Let's designate the latter as Amide I^- and Amide I^+. With a decrease in temperature, the intensity of Amide-I decreases to almost zero, while the intensities of Amide I^- and Amide I^+, on the contrary, increase (Fig. 13.17, c). In this case, the total intensity of all three modes remains unchanged.

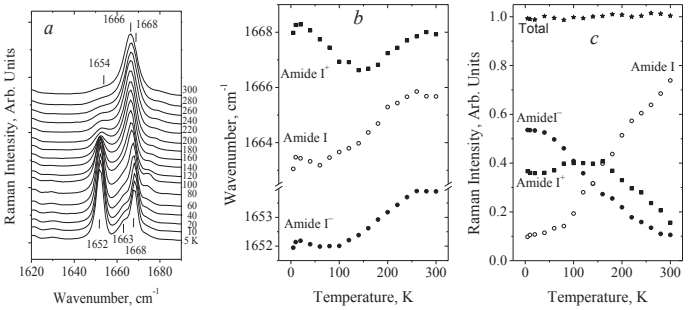

Fig. 13.17. (*a*) - spectra of acetanilide in the range of Amide-I vibrations at different temperatures; (b) temperature dependence of the peak position; and (c) integral intensity Amide-I (open circles), Amide-I^- (solid circles) and Amide-I^+ (solid squares). The asterisks show the sum of the intensities of all three modes.

In the range of Amide-II (~1550 cm^{-1}) and Amide-III (~1250 cm^{-1}) vibrations, either weak changes with temperature are observed, or are not observed at all.

Fig. 13.18 shows the change with temperature of the Amide-V mode (740 - 800 cm^{-1}) in acetanilide. It is typical for all other compounds with an acetamide group. The mode 778 cm^{-1}, weak at room temperature,

increases in frequency and intensity at cooling down, and this change is synchronized in temperature with what is observed for vibrations in the Amide-I region (Fig. 13.17).

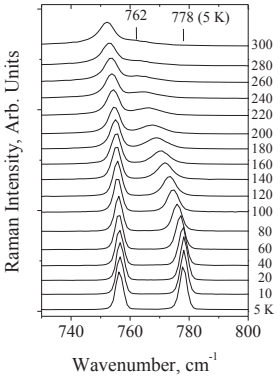

Fig. 13.18. Spectra of acetanilide in the range of Amide-V (δ_{N-H}) vibrations.

The most complex transformations of the spectrum with temperature occur in the region of stretching N–H vibrations of hydrogen N–H···O=C bonds, which are realized in crystals of acetanilide, methacetin and phenacetin (Fig. 13.19, a). At room temperature, the spectrum of N–H vibrations is represented by two broad bands at 3264 and 3296 cm^{-1} (Fig. 13.19, *a*). With decreasing temperature, two more modes gradually appear, as a result of which, at T = 5 K, four main bands are recorded with the wavenumbers indicated in Fig. 13.19, *a*. In rhombic paracetamol, the stretching vibration of O–H in the O–H···O=C hydrogen bond also consists of several broad bands, the frequencies and intensities of which change with temperature, but these bands overlap strongly, which makes it difficult to draw any definite conclusions. In monoclinic paracetamol, the O–H···O stretching mode is practically not recorded. In the spectrum of N–H vibrations of the N–H···O bond of paracetamol, rhombic and monoclinic, only one mode 3330 cm^{-1} is recorded, which varies slightly with temperature (Fig. 13.19, *b*).

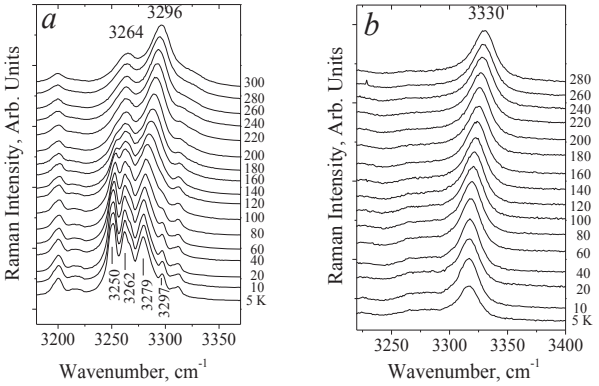

Fig. 13.19. Raman spectra of (*a*) acetanilide and (*b*) rhombic paracetamol in the region of hydrogen-bonded stretching vibrations of N–H.

The presented spectral characteristics of various crystals with an acetamide group make the version of the formation by Davydov's solitons unlikely. Indeed, the formation of two satellites, Amide I^- and Amide I^+, in all compounds with the acetamide group practically excludes the occurrence of self-trapped states. An identical temperature dependence is exhibited by modes related not only to vibrations of the C=O group, but also to vibrations of other molecular fragments, i.e. stretching N–H in N–H···O=C chains and bending (out of the plane) N–H. In addition, in paracetamol, the Amide I mode changes with temperature in the same way as in other crystals with an acetamide group, but in paracetamol there are no N–H···O=C bonds, but there are N–H···O–C and O–H···O=C bonds.

On the other hand, during low-temperature studies of the structure of compounds known from the literature, no structural (conformational) phase transitions were observed, except for the usual negligible changes in intramolecular parameters, i.e. bond lengths and angles. The spectral data also show (Figs. 13.17-13.19) that the observed changes in the Raman spectra are not due to structural phase transitions that can be fixed in X-ray structural studies. The last remark does not apply to the positions of hydrogen atoms, which are not detected reliably in X-ray diffraction.

The presence of two main bands in the low-temperature spectrum in the region of Amide-I vibrations can be interpreted as the existence of two states of the N–H···O=C (O–H···O=C) bond with different energies. Hypothetically, the occurrence of two different states can be caused by

several reasons. For example, when the methyl group $–CH_3$ is rotated around the $C–CH_3$ bond by 60°, i.e. from the staggered conformation of CH_3 with respect to the O=C bond (as shown in Fig. 13.16) to the eclipsed one, it is possible to assume the formation at low temperature of a hydrogen bond from the C–H aromatic ring to the oxygen of the carbonyl O=C group, which is additional to the already existing N-H···O=C. Finally, we can assume that there are two different proton positions with different energies on the hydrogen bond. However, any such assumptions are met with very serious objections. One of them is that of the two states with different energies at low temperatures, only that which is characterized by the lowest energy should remain. This condition is inconsistent with experiments. And second: why does the transition from a state observed at room temperature to a low-temperature one occur smoothly, and not stepwise, as for most phase transitions?

Finally, when starting to interpret the temperature dependences of the spectra of crystals with an acetamide group, it is necessary to exclude from the discussion various variants of changes in the molecular orbitals of compounds with temperature (i.e., with a decrease in the lattice parameters), which can affect the state of the hydrogen bond, since N–H···O=C and O–H···O=C behave the same way.

These remarks, as well as the structure of the considered hydrogen bonds and the behavior of the wavenumbers of Amide-I, Amide-I^-, Amide-I^+ (Fig. 13.17, *b*) and Amide-V (Fig. 13.18) on temperature, suggest the occurrence at low temperature of a specific dynamic (Davydov's) interaction of vibrations (Davydov splitting and Davydov's soliton are completely different phenomena). The specificity of the dynamic interaction in the crystals under consideration is as follows. Molecules in a crystal are linked into chains through hydrogen bonds (Figure 13.16). Formally, this means that O=C vibrations of neighboring molecules can be in phase or out-of-phase with respect to each other (we will use the term symmetric or asymmetric vibrations, although the symmetry of vibrations should be defined by the specific group symmetry of each crystal). For this reason, symmetric vibrations of the same fragment are always higher in frequency than asymmetric ones (see Fig. 3.3 from Chapter 3 and an explanation to it). This effect is more noticeable, the stronger the bonding between the fragments (O=C in this case). The hydrogen bond, however, is weak, and at elevated temperatures under conditions of high thermal populations of various vibrations, information about the vibration of one O=C fragment does not reach the neighboring fragment. This causes the fact that the distinction between symmetric and asymmetric vibrations is erased, the phase of vibrations of

each O=C group becomes random, and the vibrations themselves can be characterized as "localized", i.e. relating to only one O=C group of any of the molecules. In this case, only one localized Amide-I mode is observed in the spectrum. As the temperature decreases, the chains are geometrically ordered, and the distance between the molecules decreases due to the freezing of vibrations, especially translational donor-acceptor vibrations (more on this at the end of the section). Under these conditions, the phase of vibration of any O=C group gradually begins to form, taking into account the phase of the neighboring group. In other words, the vibrations are delocalized and acquire the features of phonons, symmetric and asymmetric, which is the essence of dynamic splitting. The higher the delocalization, the lower the temperature of the crystal, but its main property is that at any temperatures the delocalized vibrations will be characterized by two modes different in wavenumber. In a perfect crystal at a low temperature, only two modes are realized, symmetric and asymmetric. In a crystal that admits a certain degree of disorder in the chains, localized states (third mode) can be retained at any temperature, which is probably observed in the samples used in this work.

The difference between the splitting of vibrations in crystals with chains of hydrogen bonds from the well-known Davydov's splitting is that, despite the large number of O=C bonds in the unit cell (for example, there are six of them in the acetanilide cell), only those O=C that are located along one chain experience dynamic interaction. In the unit cells of each of the crystals with an acetamide group, there are only two O=C bonds along one chain. In addition, temperature-dependent delocalization of vibrations is also a distinctive feature of crystals with chains of hydrogen bonds. The classical Davydov's splitting is independent of temperature.

If in crystals of acetanilide, methacetin, and phenacetin, neighboring N–H···O=C groups are in contact with each other through the intermediate C–N unit, then in paracetamol crystals, neighboring O–H···O=C hydrogen bonds are separated by a C–N–H···O fragment (Fig. 13.16). Despite this, splitting of the O=C vibration into two components is observed in paracetamol, but the splitting magnitude is less than in other crystals. This suggests that the length of the chain section separating two O=C fragments does not play a big role if this section is formed by normal chemical bonds. The weak link of the site is the hydrogen bond. The characteristics of the bonds and the magnitudes of the splitting of the O=C vibration are given in Table 13.1. It can be seen that all characteristics are in good qualitative agreement with each other.

Finally, it is necessary to mention one more effect inherent in the chains of hydrogen bonds. Vibration Amide-V (δ_{N-H}) does not show splitting at all temperatures (Fig. 13.18). The O=C stretching vibration modulates the length of the hydrogen bond, thereby transmitting a signal along the entire chain, which yields the interaction of vibrations. In the Amide-V mode, the displacement of a proton from the plane practically does not change the length of the hydrogen bond, and this makes the interaction of Amide-V vibrations of neighboring molecules negligibly weak, and not observed experimentally. The difference in the interaction of stretching and bending vibrations in the chains of hydrogen bonds was experimentally shown using the example of chains of H_2O molecules in the cavities of crystals of the mineral bikitaite, forming "one-dimensional ice" (see Figs. 8.15 and 8.16 in the chapter 8 and the corresponding text).

If the situation with the O=C vibration is rather complicated, then the spectroscopic manifestation of vibrations in the region of stretching N–H (Fig. 13.19, *a*) is even more complicated and requires additional commentary.

First of all, the number of bands observed is unexpected, with two main bands at room temperature, and four at low temperatures. If each band is considered as a separate state of the hydrogen bond, then the corresponding set of bond lengths should be recorded in the structure of the compounds, which is not observed. For this reason, it is necessary to give a different interpretation, not related to the presence of different hydrogen bonds.

In crystals, there is only one state of the hydrogen N–H···O=C bond with the frequency of localized N–H vibration in the range of 3200-3300 cm^{-1}, but the overtone of the Amide I mode (~ 1660 cm^{-1}) also falls into this frequency range. Since both N–H and O=C are components of the same N–H···O=C bond, the ν_{N-H} and $2\nu_{O=C}$ vibrations strongly interact with each other, producing a Fermi resonance pair, which is observed in the spectra at room temperature as two broad bands at 3264 and 3296 cm^{-1} (Fig. 13.19, *a*). In this case, the interaction of vibrations means that the frequency-doubled O=C vibration causes modulation of the N–H length due to hydrogen bonding and the proximity of ν_{N-H} and $2\nu_{O=C}$ frequencies. This situation is completely analogous to that which takes place in the Raman spectra of the CO_2 molecule in the region of totally symmetric stretching vibrations - the situation that resulted in the discovery of Fermi resonance. With decreasing temperature, the N–H stretching vibration begins to delocalize (i.e., exhibit dynamic splitting) by exactly the same mechanism as the Amide-I mode (see above). In this case, each of the two emerging components of the dynamic splitting of the N–H vibration also

experiences a Fermi resonance with either the Amide-I^- or Amide-I^+ mode, as a result of which two pairs of Fermi-resonance vibrations arise (Fig. 13.19, a). Small changes in the strength (and, accordingly, in the frequency) of the hydrogen N–H···O=C bond in a series of compounds with the acetamide group cause a parallel (i.e., similar in direction and magnitude) change in the vibration frequency of both N–H and carbonyl group vibrations, as a result of which the described Fermi resonances are observed in all compounds, except for paracetamol.

In rhombic paracetamol, the stretching vibration of O–H in the O–H···O=C hydrogen bond also consists of several broad bands, the frequencies and intensities of which change with temperature, but these bands overlap strongly, which makes it difficult to draw any definite conclusions. The intensity of the O-H···O stretching mode in monoclinic paracetamol is below the detection limit.

All compounds with chains of N–H···O=C hydrogen bonds are characterized by close values of the N···O distances, and, consequently, the bond strength. What happens if the H-bond is significantly stronger or weaker than that found in acetanilide, methacetin, or phenacetin? And although the answer is clear enough, the spectra of crystals of formanilide (C_7H_7NO) and benzanilide ($C_{13}H_{11}NO$), also containing chains of hydrogen N–H···O=C bonds, were obtained. Fragments of their structures are shown in Fig. 13.20. Strictly speaking, both compounds do not relate to crystals with an acetamide group, since in the formanilide the methyl group is replaced by hydrogen, and in benzanilide by the aromatic ring. The hydrogen N–H···O=C bond is strong in formanilide and very weak in benzanilide (Table 13.1). It turned out that both modes, Amide-I^- and Amide-I^+, are present in the spectrum of formanilide at all temperatures, and in the spectrum of benzanilide there is only one, Amide-I, and also at all temperatures.

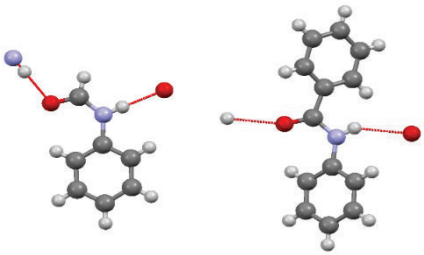

a *b*

Fig. 13.20. Chains of N–H···O = C hydrogen bonds in the structure of formanilide (a) and benzanilide (b)

Table 13.1. Lengths of hydrogen bonds, frequencies of bending Amide-V and stretching Amide-I$^-$ and Amide-I$^+$ vibrations at 5 K, as well as the difference Δ between the latter two

Compound	Type of H-bonding	D···A, Å	Amide-V, cm^{-1}	Amide-I$^-$, cm^{-1}	Amide-I$^+$, cm^{-1}	Δ, cm^{-1}
Formanilide	N-H···O=C	2.84	802	1647	1699	52
Methacetin	N-H···O=C	2.91	802	1647	1674	27
Acetanilide	N-H···O=C	2.94	778	1652	1668	16
Phenacetin	N-H···O=C	2.95	768	1648	1664	16
Benzanilide	N-H···O=C	3.15	701	1652		-
Paracetamol monoclinic	O-H···O=C	2.65	751	1637	1648	11
Paracetamol rhombic	O-H···O=C	2.72	738	1638	1650	12

The presence of dynamic splitting in formanilide over the entire temperature range and its absence in benzanilide suggests that the rigidity of the hydrogen bond is indeed the determining condition for the appearance of delocalized modes in crystals with chains of hydrogen bonds. The data given in Table 13.1 allow us to understand why the Amide-I mode in crystals of compounds with an acetamide group is localized at room temperature and delocalized at low temperatures.

Fig. 13.21*a* shows the dependence of the Amide-I splitting magnitude (i.e., the difference between Amide-I$^+$ and Amide-I$^-$ at 5 K) on the donor-acceptor distance $d_{N...O}$ in the N–H···O=C bond. It can be seen that the splitting value becomes less than 3 cm^{-1}, the value at which both modes become spectrally unresolved, at a distance $d_{N...O}$(max) ~ 2.98 Å. In acetanilide and phenacetin, the $d_{N...O}$ distance is only 0.03-0.04 Å less than the limiting $d_{N...O}$ (max). This means that an increase in the amplitude of translational lattice vibrations (for example, an N···O pair) upon their excitation in the temperature range 5 K - 300 K (see Table 9.1 in Chapter 9) is quite capable of lengthening the N···O bond in such a way, that the splitting of the Amide-I mode becomes unobservable. Thus, the phenomenon of delocalization itself, i.e. the presence of a localized mode at high temperatures and a delocalized one at low temperatures, takes place only for a rather narrow range of values of the donor-acceptor hydrogen bond distances, the range in which the crystals of compounds with an acetamide group fall.

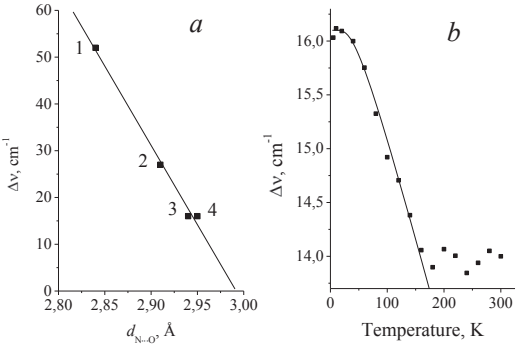

Fig. 13.21. (*a*) Dependence of the Amide-I mode splitting at 5 K on the $d_{N\cdots O}$ distance, 1 - formanilide, 2 – methacetin, 3 - acetanilide, 4 - phenacetin; (*b*) Same as a function of temperature in acetanilide.

Fig. 13.21*b* shows how the wavenumber difference $\Delta\nu = \nu$ (Amide-I^+) – ν (Amide-I^-) in acetanilide changes with temperature. The presented dependence is well described by the excitation of a phonon at ~ 85 cm^{-1} with increasing temperature, and the phonon frequency is typical for translational intermolecular vibrations of the hydrogen bond, i.e. vibrations that have the greatest effect on the temperature change in the donor-acceptor distance.

If the oscillators (i.e., C=O in this case), characterized by a force constant K and a frequency ω, are interconnected by weak springs of rigidity k, then $\Delta\omega/\omega \sim k/K$, where $\Delta\omega$ is the frequency difference between symmetric and asymmetric vibrations of oscillators. At ω = 1660 cm^{-1} and $\Delta\omega$ = 16 cm^{-1} (acetanilide, Table 13.1), $k/K \sim 0.01$. The latter relation is very realistic for the force constants O=C and N···O.

Finally, it is well known that the vibration frequency of Amide-I (and, consequently, the N–H···O=C hydrogen bond) rather strongly depends on the chemical nature of the substituent R in secondary amides. Since this work considers crystals of compounds with an acetamide group, where R = CH_3 by definition, the role of the methyl group is precisely that it sets the characteristics of the hydrogen N–H···O=C (O–H···O=C) bonds in a very narrow range. As for its possible participation in the observed spectral features from the point of view of a change in the molecular conformation (i.e., rotation of the methyl group from a staggered to an eclipsed conformation) with decreasing crystal temperature, the spectra of

formanilide provide evidence that methyl groups are not involved in the splitting of the Amide-I mode.

In conclusion, it is necessary to say the following. Molecular crystals, in which the main intermolecular interaction is a hydrogen bond, exhibit diverse and very interesting effects when the temperature of the crystal changes. All phenomena, often unusual, are based on the direction of the hydrogen bond and its lability, i.e. the ability to change the strength of interaction and direction. Raman spectroscopy is an extremely successful method for studying molecular crystals. But the effectiveness of the method is largely determined by the use of a whole complex of experimental techniques, including temperature and polarization measurements of oriented crystals, and deep processing of the results. It is the processing of the experimental results, i.e. finding the spectral parameters of all modes of the vibrational spectrum and at all temperatures that allows one to obtain experimental information that cannot be predicted in advance and, therefore, hope to be found in a quantum-chemical calculation of the vibrational spectrum. An example of this is studies of the anomalous behavior of crystal vibrations in alanine (Section 13.4) or the temperature dependence of the Amide-I mode in crystals of compounds with an acetamide group (Section 13.5). Both of these phenomena have been the subject of numerous studies in the past, but have not received a definite interpretation.

CHAPTER 14

LIGHT SCATTERING BY GLASSES AND NANOPARTICLES

14.1. Phonon spectrum in disturbed crystals – "folding" zones

The dependence of the frequency of phonon vibration on the magnitude and direction of its wave vector in the crystal is described by the dispersion curve (see Fig. 3.4). In this case, the crystal is considered ideal, and the wave vector takes values from $k = 0$ (a phonon with an infinite wavelength) to $k = \pm\pi/a$ (a phonon with the smallest possible wavelength in a crystal equal to $2a$, where a is the lattice period).

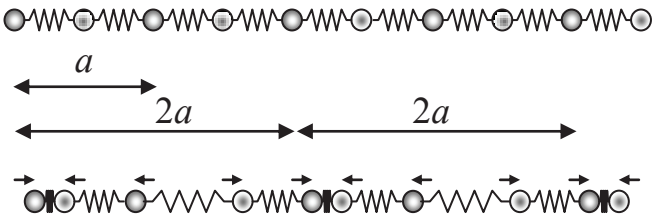

Fig. 14.1. A longitudinal optical phonon with $k = \pi/a$ for a one-dimensional chain with a period a becomes a phonon with $k = 0$ in a chain with a period $2a$.

We can imagine, however, a situation where, as a result of structural disturbances, the period of the crystal lattice is doubled. This means that the size of the first Brillouin zone will be halved. What happens to the dispersion curves in this case? A phonon with $k = \pi/a$ in an undistorted lattice is a vibration of the same amplitude but opposite in sign (phase) in two neighboring unit cells (Fig. 14.1). In a doubled cell, this vibration becomes the same in amplitude and phase with the vibration in the neighboring modified cell. In other words, a phonon with $k = \pi/a$ in an

undistorted lattice becomes a phonon with k=0 in a doubled lattice (i.e., according to the phase relations between neighboring cells, it becomes the same as the vibration in Fig. 3.3, *b*, but at the same time each cell is twice as large as in Figure 3.3, *b*). As a result, all dispersion curves are transferred to the "shortened" Brillouin zone as shown in Fig. 14.2, i.e. will be mirrored in the plane $k = \pi/2a$. We can say that in this case "the zone is folded" and instead of one optical phonon in the center of the zone we get three optical vibrations, one of which relates to the former acoustic one, but with nonzero energy.

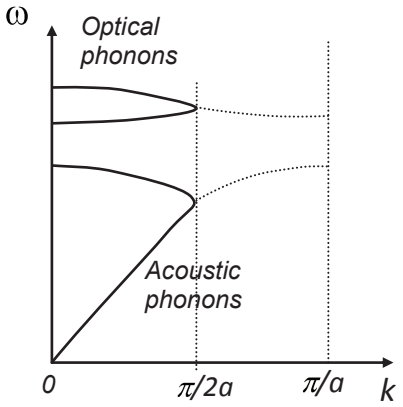

Fig. 14.2. Folding of dispersion branches as a result of doubling the unit cell of a crystal

An increase in the number of vibrations is a direct consequence of an increase in the size of the unit cell and the number of atoms in it. In cubic crystals, for example, silicon, the vibrations are degenerate at the center of the Brillouin zone and are not degenerate at its edges. In this case, the folding of the zone will cause the appearance in its center of even more phonons. With further distortion of the crystal lattice and the folding of the zones, the size of the first Brillouin zone becomes very small, and the number of vibrations in the center of such a modified zone becomes very large. Moreover, in Raman scattering, practically all vibrations of the initial dispersion curves of an ideal crystal become allowed in the wave vector; in other words, all states of the dispersion curves, optical and acoustic, become active in Raman scattering of disturbed crystals. It is said that the entire Brillouin zone is “illuminated”, meaning the states of the dispersion curves of an ideal crystal. This phenomenon is dominant when

considering the first-order light scattering mechanism in all disturbed (non-crystalline) objects, i.e. glasses, solid solutions, and nanoparticles.

14.2. Boson peak

In glasses, along with the general broadening of Raman lines, one more very interesting and important phenomenon is observed, namely, the appearance of a broad structureless maximum in light scattering in the low frequency range 5–100 cm^{-1}. At first, it was believed that the appearance of this maximum was simply related to the Bose-Einstein statistics of phonons in media, since the scattering intensity is proportional to $(n+1)$, where n is the number of existing (excited) phonons in the medium, which are, naturally, only the most low-frequency phonons at ordinary temperatures. For this reason, the observed maximum in the low-frequency scattering of glasses was called the “boson peak”. However, taking into account the statistics of phonons and measuring the scattering of glasses at low temperatures did not yield the disappearance of the boson peak.

There are currently several theoretical models to explain the nature of the boson peak in glasses. Most of them are still under development, and there is no definitive and well-established mechanism for the appearance of a boson maximum, which explains all its frequency and temperature features. However, most researchers lean towards the version that the cause of low-frequency scattering in glasses is the presence of microscopic inhomogeneities in them, such as where violation of the selection rules for the wave vector yields the "highlighting of the entire zone", as a result of which not only all states of the dispersion curves of optical vibrations, but also acoustic modes, become active in first-order Raman scattering. It is precisely the numerous “foldings” of the acoustic dispersion branch that cause the appearance of a boson peak in glasses. Thus, the presence of a boson maximum in the low-frequency Raman spectra of compounds and its intensity serve as a characteristic of the state of the compound under study and an indicator of its "non-crystallinity".

14.3. Localization of phonons in nanoparticles

Recently, much attention has been paid to the study of the properties of nanoparticles of various compounds. If we consider the formation of a crystal as an assembly of individual atoms, starting with the first, then it is intuitively clear that a formation limited, for example, to only two or three lattice periods of the future crystal, should be considered a molecule rather than a crystal. Indeed, a crystal, by definition, is characterized by the

presence of a band structure, which is formed by the interaction of a large number of atomic orbitals. The difference in the energy of neighboring levels in the crystalline zone should be much less than the value of the splitting of atomic states in the interaction of atoms - a condition that is not fulfilled for a small number of interacting atoms. On the other hand, as soon as a nanoparticle reaches a size sufficient to form a rigorous band structure with appropriate physical properties (electrical, optical, etc.), it goes over into the category of crystals. Therefore, nanoparticles are considered to be objects with sizes exceeding several lattice periods, i.e. 4-6, but less than those at which the properties of bulk crystals are formed. The upper limit for, for example, silicon, is estimated at 15-20 lattice periods. Crystalline domains with a size corresponding to the Bohr exciton radius (~5 nm for Si) are often taken for nanoparticles (see Ref. [1]).

It can also be assumed that, from the point of view of the vibrational spectrum, the nanoparticle will demonstrate the properties of a strongly damaged crystal due to lattice distortions near the surface, which, in the case of nanoparticles, has a large specific contribution. In addition, the phonon vibration excited in a nanoparticle is limited by the size of the particle, and therefore the damping at the boundary, which is usually neglected in extended crystals, should play an important role here. Finally, the last and main circumstance that distinguishes a nanoparticle from a crystal is that the nanoparticle size is much smaller than the phonon wavelength required to fulfill the wave vector selection rule (see Section 3.4 in Chapter 3) in the scattering process. In other words, the scattering of light by nanoparticles should involve phonons not from the center of the Brillouin zone with $k = 0$, as in a bulk crystal, but states with larger values of the wave vector related to the interval $0 - 2\pi/a$.

Given these circumstances, i.e. violation of the selection rules by the wave vector, leading to "lightening of the entire zone", and damping at the boundary, a model was proposed to describe the first-order scattering processes in nanoparticles with strong spatial localization (confinement) of phonons, according to which for spherical crystallites with a diameter D and phonon damping according to the law $\exp(-\alpha r^2/D^2)$, the line shape scattering is determined by the integral [2]:

$$I(\omega) \propto \int \exp\left(-\frac{q^2 D^2}{4}\right) \frac{dq}{[\omega\ q\ -\omega]^2+(\frac{\Gamma_0}{2})^2}, \qquad (14.1)$$

where Γ_0 is the natural bandwidth of the bulk crystal, and $\omega(q)$ is the phonon dispersion. Integration over the entire dispersion curve (term $[\omega(q)-\omega]^2$) yields an increase in the natural (crystal) linewidth Γ_0 by the

energy width of the dispersion dependence and a low-frequency shift of the peak position of the scattering band, and the smaller the crystal size the greater the damping.

14.4. Simulation of the scattering spectrum on silicon nanoparticles

Obtaining structural information about the state of the films of amorphous crystalline silicon is an area of large interest, since this material is widely used as active elements in solar cells.

Fig. 14.3(*a*) shows the scattering spectra of amorphous nocrystalline silicon films, in which the phase composition, i.e. the ratio of amorphous and crystalline phases, changes along the coordinate *x* of the film.

Fig. 14.3(*b*) shows the spectra for three limiting compositions of the films, i.e. a purely amorphous phase (I), amorphous-nanocrystalline (II), and predominantly nanocrystalline (III). The amorphous state is characterized by a

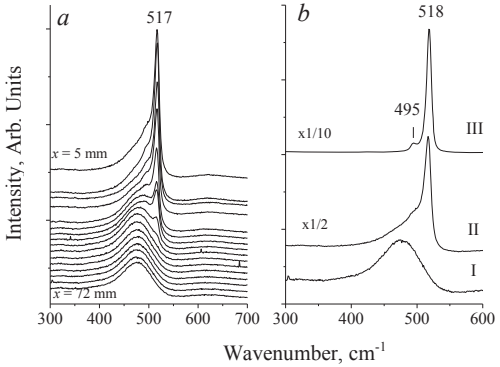

Figure 14.3. Raman spectra of amorphous-crystalline silicon films. (*a*) - spectra obtained at different points of one film depending on the distance *x* from its edge; (*b*) - characteristic spectra of films.

wide band with a maximum at ~ 475 cm^{-1}, and the position of the maximum of the scattering band of nanoparticles varies from 514 to 518 cm^{-1}, i.e. always less than the phonon frequency in a bulk crystal (520 cm^{-1}). One more feature is observed in the spectra at 495 cm^{-1}, the origin of which is not obvious. Each of the spectra shown in both figures contains all information about the phase composition of the sample, and the problem is to extract this information as complete as possible. Various

techniques are commonly used to assess the composition of a film. One can preset the composition of the sample in some simple way – for example, by having it consist of crystallites of the same size and an amorphous phase, crystallites of two different sizes, Gaussian size distribution of crystallites, etc. – and try to fit this composition to the experimental spectrum. Another simple and elegant way to assess the composition of a film is as follows [3]. The vibration frequency of the crystalline phase of silicon is 520 cm^{-1}, and the maximum of the scattering band of the amorphous phase is falls at ~ 475 cm^{-1}. Therefore, for a rough estimate of the degree of crystallinity of the sample, the ratio of the scattering intensities of the experimental spectrum at points at a frequency of 520 cm^{-1} (I_c) and 475 cm^{-1} (I_a) can be used. The I_c/I_a parameter turned out to be very convenient due to the extreme simplicity of its obtaining, although the relationship of this parameter with the real structure of the film remains rather vague. The greatest attractiveness of the I_c/I_a parameter lies in the fact that by using this procedure it is possible to process large arrays of spectral data with minimal time expenditures, which allows accumulating the results obtained and drawing conclusions about the average statistical properties of the samples under study.

So, for example, measurements of the electrophysical and spectral characteristics of films of amorphous-crystalline silicon, synthesized during the development of the technology for obtaining photovoltaic cells (solar cells), have shown that the electrical conductivity of the film changes sharply with a strictly defined composition, i.e. I_c/I_a ratio. Amorphous-crystalline films can be characterized as consisting of an amorphous phase with a weak conductivity and nanocrystalline regions with a higher conductivity embedded in it. In this case, the total conductivity of the film is mainly determined by the conductivity of the amorphous phase. With an increase in the degree of crystallinity (I_c/I_a ratio) and, accordingly, the number of nanoparticles, the average distance between nanoparticles decreases and contacts between them are realized. When the amount of contacting particles reaches a certain level, a continuous chain with high conductivity is formed in the film. This phenomenon is based on *percolation theory*.

The essence of percolation theory can be understood from the following simple example. Let there be a squared (or bulk) lattice constructed of metal wire. The conductivity of such a lattice, measured, for example, between contacts located at the corners (i.e., at the ends of its diagonal), is, of course, determined by the conductivity of the wire. Now we will randomly delete (cut) individual bonds between the lattice points. When the number of deleted bonds reaches a certain limit at which the

existing continuous path from one side of the lattice to the other is interrupted, the conductivity of the lattice drops abruptly to zero. This limit is called the percolation threshold. It turns out that the percolation threshold in bulk lattices (crystals) is approximately equal to 0.3 (i.e., about a third of all bonds between atoms in a crystal must be intact in order for a continuous path between opposite sides of the crystal to exist), and the percolation threshold for two-dimensional lattices (films) is about 0.7. It is the latter value that is critical for the observed behavior of conductivity in amorphous-crystalline silicon films.

Another approach for assessing the structure of the film, i.e. the degree of its crystallinity and the size distribution of nanocrystals was proposed in [4]. To quantitatively characterize the spectrum, we introduce the so-called trial function. For this purpose, we calculate from (14.1) the line contours for nanocrystals with a diameter of $6a_0$ (3.3 nm), $7a_0$, ..., $15a_0$ (a_0 – lattice period) and give each of them the same integrated intensity equal to 1.

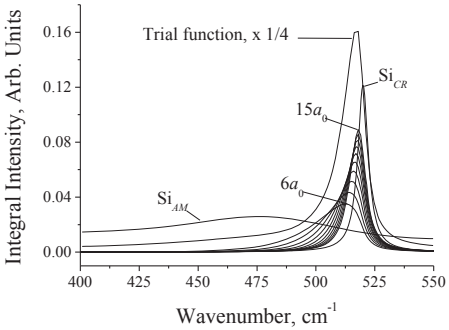

Fig. 14.4. Calculated scattering contours for particles of different diameters and the spectrum of the amorphous phase. All spectra are normalized to unit integral intensity.

The lower limit on the size corresponds to a particle with a diameter of ~ 3 nm, and the upper one - ~ 80 nm. As mentioned above, the assignment of particles with a size of less than 3 nm ($6a_0$) to crystalline formations is controversial, and for nanocrystals with a diameter of more than $15a_0$, the calculated contours in frequency at the maximum and half-width are close to each other and to the spectrum of a bulk crystal and can be replaced by the latter. The Raman band of crystalline silicon has a Lorentz profile with a frequency at 520 cm^{-1} and a half-width of 6 cm^{-1}.

The calculated contours are shown in Fig. 14.4. The same figure shows the band corresponding to scattering by the amorphous phase. This band is represented not by the calculated Gaussian or Lorentzian contour, but by the envelope curve of the experimental spectrum of the pure amorphous phase (see Fig. 14.3, a, lower spectrum) in order to take into account the scattering by acoustic phonons and second-order scattering by combined tones present in the spectrum. The basis for equivalent valuation of both amorphous and nanocrystalline components is the fact that the integral intensities (scattering cross sections) of both components are close to each other: $I_c/I_a = 0.95$ according to [5]. (The integral intensity of the crystal scattering line is, nevertheless, about 7 times higher than that of the amorphous phase, but this is due to the difference not in the scattering cross section, but in the absorption coefficient and, accordingly, the depth of penetration of the exciting light into the sample.) Adding all the contours, we get a trial function (see Fig. 14.4). Now, the degree of participation of each nanoparticle participating in the formation of the experimental spectrum of the nanocrystalline film can be estimated using the "reduction" procedure, i.e. mathematical division of the experimental spectrum into a trial function.

Reduction, according to the proposed scheme, of the spectra of films containing both amorphous and nanocrystalline components (spectrum II in Fig. 14.3, *b*) showed that the fraction of the amorphous phase in them is significant, about 90%, and the size distribution of nanoparticles is uniform, i.e. particles of different sizes are represented by approximately the same amount. However, when comparing the calculated and experimental spectra, it was found that the experimental spectrum in the region 490-500 cm^{-1} shows a feature that is not related to scattering by the amorphous or crystalline phase (Fig. 14.5).

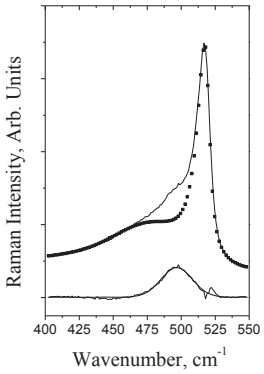

Fig. 14.5. Comparison of the reconstructed spectrum (dotted curve) with the experimental (solid curve) disregarding scattering at point *L*. The lower curve represents the difference between the experimental and calculated spectra

The difference between the two spectra, experimental and reconstructed, has the contour of a Gaussian band with a peak position at 496 cm^{-1} and a half-width of 23 cm^{-1} (Fig. 14.5, lower curve). A similar feature, but already in the form of a well-resolved spectral band, manifests itself in a sample with a high (~ 60%) content of the nanocrystalline phase (see Fig. 14.3, *b*, spectrum III). The silicon crystal relates to the cubic system, and in the center of the Brillouin zone of silicon, one threefold degenerate vibration F_{2g} is possible, including both transverse and longitudinal optical phonons (§ 5.2). As the phonon wave vector increases, i.e. when shifted along the dispersion curve to one of the symmetric points of the Brillouin zone, this vibration is split into *TO* and *LO* modes, which at point *L* (see Fig. 3.5) have values of 493 and ~ 400 cm^{-1}, respectively. Thus, the frequency of the transverse phonon *TO*(*L*) practically coincides with the position of the feature observed in the spectra of the films (495 cm^{-1} for the line in spectrum III in Fig. 14.3, *b*). First-order scattering at critical points at the boundary of the Brillouin zone is forbidden; however, in nanocrystals, due to a decrease in the phonon correlation length, the selection rules for the wave vector are violated and such scattering becomes possible. The same effect is responsible for the detection of localized phonons with $k \neq 0$, renormalized in frequency.

The proposed method, interesting and deep in content, has, however, limited application. The fact is that, as can be seen from Fig. 14.4, the contours of individual bands related to nanoparticles of a certain size have a rather large half-width, comparable to the half-width of the entire spectrum of a nanocrystalline film. As a result, the selectivity of determining the particle size distribution is rather low.

14.6. Electronic confinement in nanocrystals

In addition to the localization of phonons in nanocrystals, there is another type of confinement - electronic, which can also be used to estimate the particle size distribution. The essence of the phenomenon of electronic confinement is even simpler than that of phonon. As the particle size decreases to the nanocrystalline scale, the band gap increases. This becomes clear if we recall how the band structure of a crystal is formed. Consequently, in this case, the energy of the interband transition of nanoparticles, controlled by the luminescence spectrum, should also increase, which is actually observed [6]. Having determined experimentally the dependence of the position of the luminescence maximum on the particle size, one can then use it to proceed to the analysis of the particle size distribution, using the mathematical apparatus developed for the

phonon confinement (see above). However, the use of luminescence as a method is always associated with certain difficulties. The point is that, in addition to interband transitions, the luminescence spectrum can also contain transitions with the participation of various impurity or defect states. In this case, the intensity of both changes often in an unpredictable manner, which complicates the use of photoluminescence for the analysis of nanocrystalline films.

CHAPTER 15

FEATURES OF RAMAN SPECTRA OF CARBON DIFFERENT FORMS

Carbon occupies a special place in inorganic chemistry due to the existence of many of its allotropic forms, including such important ones as diamond and graphite, as well as formations very popular recently, such as fullerenes, nanotubes, and graphene. In the literature, there are a large number of deep and detailed reviews devoted to the vibrational spectra of various forms of carbon, and the reader can always refer to them. This chapter will only briefly discuss the most important spectral features of carbon materials. This is necessary both for understanding vibrational spectra and for using spectral characteristics for material diagnostics.

15.1. Spectra of graphite

Fig. 15.1 shows a typical Raman spectrum of a carbon film.

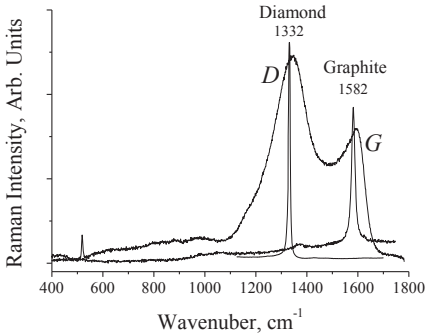

Fig. 15.1. Typical spectrum of a carbon film and spectra of crystalline graphite and diamond.

The spectrum consists of two broad bands *D* and *G* with wavenumbers at the maximum of ~1340 and ~1600 cm^{-1}, respectively. Narrow lines

represent the spectra of two well-known forms of carbon - diamond (1332 cm^{-1}) and graphite (1582 cm^{-1}). In diamond, carbon is in a tetrahedral environment, and its bonds with neighboring atoms are organized by sp^3-hybridized carbon orbitals. In graphite, carbon is embedded in a hexagonal structure organized by sp^2 orbitals. In both cases, the observed bands refer to totally symmetric stretching vibrations of the C–C bond. One could say that the spectrum of carbon in the film is very well described by these two forms. However, unexpectedly, the *D* band showed a rather complex spectral behavior. It turned out that both the intensity of the mode and its peak position depend on the energy of the exciting radiation, i.e. is of a resonant nature [1]. In the opinion of the authors of [1], the band should be attributed to scattering at one of the highly symmetric points at the boundary of the Brillouin zone, which has a double resonance character: resonance in energy associated with the distance between different dispersion branches at the boundary of the Brillouin zone, and resonance in the wave vector, since the observed transition is indirect and requires a change in the wave vector.

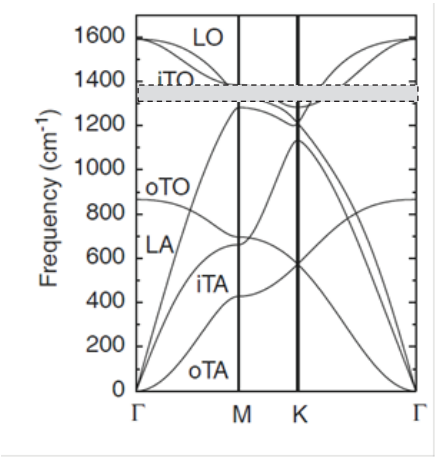

Fig. 15.2. Dispersion curves of phonons in graphite obtained in [2]. Legend of the branches: *LO* - longitudinal optical, *iTO* - transverse (in plane) optical, *oTO* - transverse (out of plane) optical, *LA* - longitudinal acoustic, *iTA* - transverse (in plane) acoustic, *oTA* - transverse (out of plane) acoustic phonons. The horizontal gray stripe in the dashed frame indicates the position of the phonon *D* on the ordinate.

Fig. 15.2 shows the dispersion curves of phonons in graphite obtained in [2]. The gray horizontal stripe in the dashed frame denotes the position

of the phonon *D* on the wavenumber scale. It is clearly seen that the most probable candidates for the generation of the *D* band in the spectrum are longitudinal *LO* and transverse (in the plane) *iTO* optical phonons at point *M* at the edge of the Brillouin zone. It is possible that both vibrations take part in the *D* mode, but what is important for us is not an exact description of the phonon, but the fact that its wave vector in the spectrum is nonzero. This circumstance determines the conditions for the appearance of a band in the spectrum.

Fig. 15.3 shows the expected scheme of electron excitation from the valence band of graphite to the conduction band in the case of the generation of a phonon with a nonzero wave vector $+k$. To complete the scattering process, the excited electron must return to the valence band, but the state in the latter, corresponding to the new wave vector of the electron, is already occupied. Therefore, the process depicted is absorption and not scattering. (In fact, this scheme is another illustration of the wave vector selection rule, see 3.5 in Chapter 3).

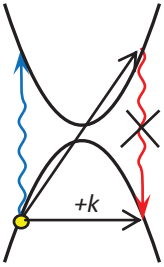

Fig. 15.3. Illustrative scheme of electron excitation in the valence band of graphite with the participation of a phonon with $k \neq 0$. The reverse transition from the conduction band to the valence band is forbidden due to the fact that the final state is occupied. The transition without changing the wave vector (along the blue arrow) and back yield either Rayleigh scattering or Raman scattering at the center of the Brillouin zone, i.e. at a frequency of ~1600 cm^{-1}, which is of no interest in this case.

For the act of scattering to take place, it is necessary to give the excited electron a reverse momentum $-k$, which transfers it to its initial state along the wave vector (Fig. 15.4). An excited electron in the conduction band can reverse the direction of the wave vector in the case of elastic scattering by a lattice defect (intrinsic, impurity, and structural). In this case, the energy of an excited electron in the conduction band does not change, and the energy of the scattered quantum of light turns out to be less than the energy of the incident radiation only by the energy of the phonon D. Thus, first-order scattering, which characterizes the D band in the spectrum, can occur only in disordered graphite, and the width and the relative intensity of the band serves as a measure of the imperfection of the lattice.

There is, however, another way of changing the wave vector of an excited electron to a value corresponding to its initial state. This requires the generation of one more phonon, equal in energy to the first, but with a

wave vector $-k$. In other words, two phonons, $+k$ and $-k$, must participate in the scattering event. But this process is second-order scattering and yields the appearance of not the D band, but $2D$ overtone. The scattering pattern in this case turns out to be the same as shown in Fig. 15.4, only the mechanism of imparting the required wave vector to the excited electron will change.

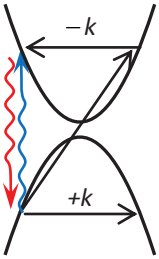

Fig. 15.4. Possible scheme for the appearance of the $2D$ band in the spectrum.

Both mechanisms presented above are realized in all carbon materials (disordered graphite, carbon nanotubes, graphene), explaining the features of their vibrational spectra: the appearance of the D band and the unusually high intensity of the $2D$ overtone. Since the path along which the electron passes to complete the scattering act is the same in both cases (Fig. 15.4), we can expect competition between these processes: the more the graphite is disordered, the higher the intensity of the D mode and the lower the $2D$ mode, and vice versa. The best confirmation is the spectrum of relatively pure graphite shown in Fig. 15.5. The D band in the spectrum is not recorded at all, but its 2D overtone is very intense.

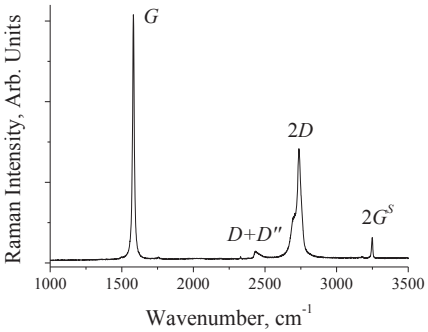

Fig. 15.5. Raman spectrum of pure graphite. The designations of the spectral lines follow Ref. [3].

15.2. Carbon nanotubes

Raman spectroscopy has proven to be a surprisingly useful and informative method for diagnosing the state of carbon nanotubes, including parameters such as single or multi-layer tubes, their diameter, chirality, purity, and others. A typical spectrum of carbon fibers consisting of nanotubes is shown in Fig. 15.6. The *D*-mode is practically absent in it, recording the high perfection of nanotubes. At the same time, the spectrum clearly shows the 2631 cm^{-1} band of the D-mode overtone (doubled in vibration frequency), confirming the validity of the assumption made above, and, in addition, low-frequency bands are recorded in the region of 100-500 cm^{-1}.

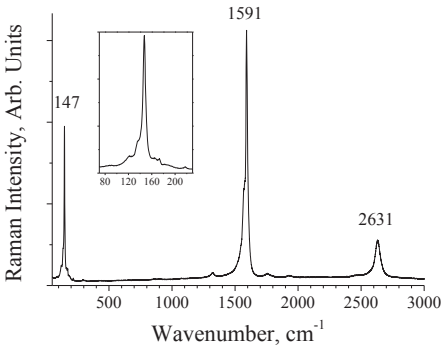

Fig. 15.6. Raman spectrum of carbon nanotube fibers.

Low-frequency bands refer to the so-called "breathing" modes (RBM, radial breathing mode), in which all carbon atoms are displaced simultaneously in the radial direction to or from the axis of the tube, causing the tube to "breathe". Since the interaction between the layers is weak, the radial displacement itself of carbon atoms practically does not reveal any noticeable change in the interatomic interaction, and this vibration should have a frequency close to zero. However, in this case, the length of the C–C bond in the plane changes insignificantly. The latter is characterized by a large force constant. Considering the simple geometrical problem of the displacement of carbon atoms to the axis of the tube (Fig.15.7), one can easily find that in such a vibration the change in the distance between carbon atoms is proportional to

$$\delta a = \frac{a}{R}\ \delta R\ , \qquad (15.1)$$

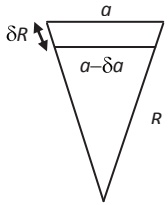

Fig. 15.7. Diagram of the change in the distance a (carbon-carbon) during the breathing vibration of a nanotube of radius R

where R is the radius of the tube, and δR is the amplitude of atomic vibrations in the breathing mode. Relation (15.1) shows that the change in the C–C bond length in vibration is a/R times less than the amplitude of radial vibrations, and the smaller, the larger the radius (or diameter) of the tube. This circumstance determines the low frequency of radial vibrations and its dependence on the geometric parameters of the tube. Fig. 15.8 shows the empirical dependence of the breathing mode frequency on the tube diameter for isolated single-walled tubes (solid curve) and tubes in a bundle (dashed curve). This relationship is extremely useful and allows you to easily determine the composition of the fiber by the diameters of the tubes that form it. For example, in the spectrum shown in Fig. 15.6, the main contribution is made by tubes with a diameter of 1.6 - 1.7 nm.

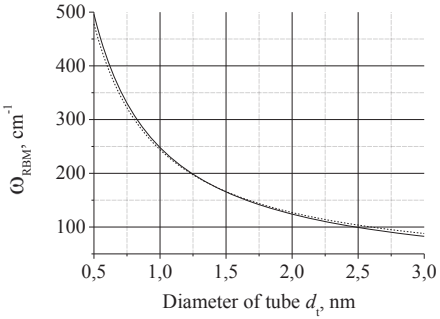

Fig. 15.8. Dependence of the breathing mode frequency on the tube diameter for isolated single-walled tubes (solid curve) and tubes in a bundle (dashed curve) [4].

As for determining the relative number of tubes of each diameter in a given fiber, in this case the situation is somewhat more complicated. The fact is that tubes of different diameters react differently to the wavelength of the exciting laser radiation; therefore, some of the tubes in the fiber will exhibit increased scattering intensity in the breathing mode due to resonance. Thus, there is no linear relationship between the intensity of the breathing mode in the spectrum, which characterizes tubes of a certain

diameter, and their number in the fiber. This nonlinearity, however, will be experimentally significant only when the difference in the diameters of the tubes that make up the fiber is noticeable. In the case shown in Fig. 15.6, the spread in the diameters of nanotubes is small, which made it possible to make a conclusion about their predominant size.

15.3. Graphene

Among the various allotropic forms of carbon, graphene is currently attracting the most attention due to its many unusual physical properties. A typical spectrum of graphene is shown in Fig. 15.9.

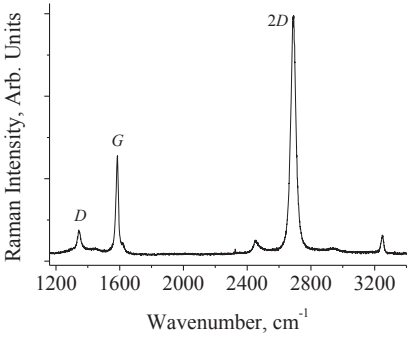

Fig. 15.9. Graphene spectrum

In theory, graphene should consist of one flat layer of carbon atoms on a suitable substrate, but sometimes, for various reasons, a film consisting of several layers of carbon is used in the study. Fig. 15.10 shows a diagnostic dependence that establishes a relationship between the vibrational frequency of the G-mode in the spectrum of the film with the number of carbon layers in it.

This dependence makes it possible to assess the state of the film under study. The reason for the appearance of this dependence is the weak van der Waals interaction between adjacent layers. However, it should be borne in mind that in the presence of deformations in the film, the G band splits into G + and G–, the intensity ratios of which can be different; therefore, it is difficult to correctly determine the value of the G mode frequency in some cases.

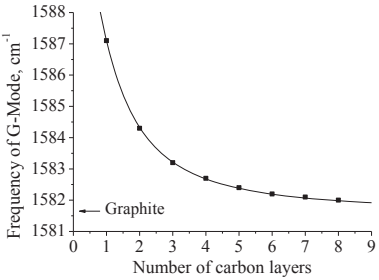

Fig. 15.10. The relationship between the vibration frequency of the G-mode and the number of carbon layers in the film [5].

One of the most interesting features of the graphene spectrum is that the intensity of the 2*D* overtone band can be very high (Figure 15.9). Sometimes this is the most intense band in the spectrum. The unusual intensity of the 2*D* overtone has long remained a mystery, and only recent work by Heller et al. [3] has introduced a sliding model to understand this strange feature.

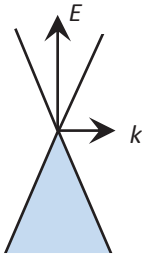

Fig. 15.11. Energy band diagram in graphene

The energy bands of graphene are schematically shown in Fig. 15.11. The dependence of the electron energy on the wave vector is linear (at small values of the latter), which reveals the formation of the so-called Dirac angle. In this case, the valence band is completely filled, and the conduction band is empty (in the absence of external electric field). If an electron in the process of scattering is excited by a quantum of light into the conduction band without changing the wave vector (arrow up in Fig. 15.12), then the wave vector of an electron in the conduction band and a hole in the valence band has the same value, and upon returning to the initial state, the wave vector of the electron also cannot change (all states with other wave vectors in the valence band are occupied)

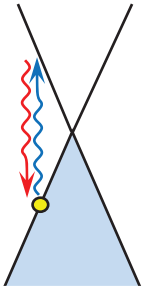

Figure 15.12. Direct and reverse transitions of an electron without changing the wave vector

Consequently, this process refers either to elastic scattering or to Raman scattering with generation (annihilation) of a phonon with $k = 0$. If, upon excitation of an electron, its wave vector changes due to participation in the scattering of a phonon with $k \neq 0$, then the position of the excited electron on the dispersion line should be as shown by the solid up arrow in Fig. 15.13, *a*.

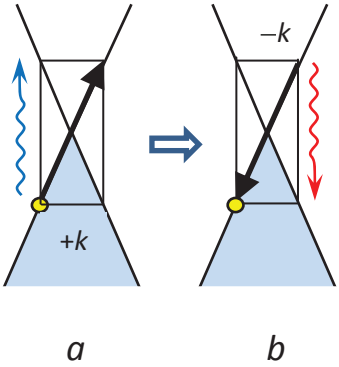

Fig. 15.13. The process of inelastic scattering in graphene with the production of two phonons, $+k$ and $-k$.

Since there are no free states in the valence band except for the hole left after the excitation of the electron, the reverse transition should be accompanied by a change in its wave vector in the opposite direction, which requires the participation (creation) of another phonon with the wave vector -*k*, equal in frequency to the first and opposite in direction (Figure 15.13, *b*).

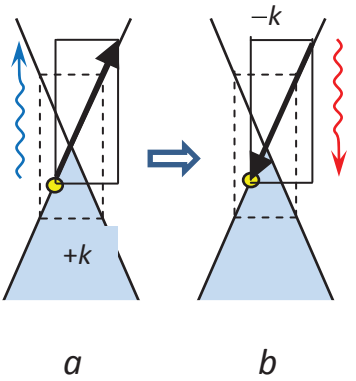

Fig. 15.14. Schematic representation of the graphene sliding model [3]

This process prioritizes scattering at the doubled phonon frequency and is similar to that shown in Fig. 15.4. However, the difference in the structure of the zones of graphite and graphene presents additional opportunities for the latter. The dependence of the state energy on the wave vector in graphene is linear ("Dirac angle"). Consequently, if we choose another initial state in the valence band, which differs from the previously considered one (Fig. 15.14), then the entire cycle of Raman scattering will proceed according to the same energy scheme as in Fig. 15.13, but in a frame shifted by a certain amount (In Fig. 15.14 both processes, initial and subsequent, are shown with dotted and solid frames, respectively).

In other words, the sliding of the frame along the straight line describing the dependence of the energy on the wave vector in graphene ensures complete identity of both terms depicted. The number of such identical terms, i.e. frame shifts along the dispersion line, is not limited. These terms represent one and the same oscillator; therefore, the scattering processes from each of the frames interfere with each other, i.e. add up. For this reason, to obtain the scattering intensity, it is necessary to first add up the changes in polarisabilities in all terms that fall into the continuous sliding region and generate a pair of scattered phonons, and then square the entire sum. In the usual procedure for calculating the intensity of scattering on independent oscillators, the sum of the squares of the intensities of each oscillator is found. It is the sliding effect that underlies the observed enhancement of the 2*D* mode intensity in graphene.

CHAPTER 16

SCATTERING BY SPIN WAVES IN CRYSTALS

Crystal magnetism is a large and complex area of solid state physics, which is usually described in separate monographs. Obviously, discussing magnetism within a short chapter is an unrealistic task and, moreover, goes far beyond the scope of this book. For this reason, this chapter is only an attempt to show in an accessible form what spin waves are and how they manifest themselves in Raman spectra. But first, let us recall the main provisions that cause the appearance of magnetism in crystals and determine its character.

The source of magnetism is an electron, which has both its own magnetic moment (spin) and the orbital angular momentum arising from the motion of the electron around the nucleus.

The magnetic moment of an atom (ion) is the sum of the spins of all electrons taking into account their directions and angular momenta and is determined by the expression

$$\boldsymbol{\mu} = \gamma\hbar\boldsymbol{J} = -g\mu_B\boldsymbol{J}, \tag{16.1}$$

where the total angular momentum $\hbar J$ is determined by the sum of the orbital $\hbar L$ and spin $\hbar S$ moments. The constant γ is called the magnetochemical (or gyromagnetic) ratio, and the value g is called the g-factor.

The magnetic moment of the filled shell of the atom is completely compensated and equal to zero. Therefore, the magnetic moment of an atom is determined, as a rule, by unfilled *d*- and *f*-shells.

The order of filling the shell (and, therefore, its magnetic moment) is determined by the Hund rules, the Pauli exclusion principle, and the Coulomb repulsion of electrons. According to Pauli's principle, two electrons can be in the same place only with opposite directions of spins. However, the localization of electrons in one place simultaneously increases both their potential energy due to the Coulomb repulsion, and kinetic energy due to the uncertainty relation $\Delta x \cdot \Delta p \sim \hbar$. The trade-off between magnetic interaction of spins, Coulomb repulsion, potential and kinetic energy determines the order of the filling of the shell. For example,

in the 3*d* shell of the Mn^{2+} ion, five *d* electrons can have identically directed spins and occupy five different states of the orbital angular momentum (m_L = 2, 1, 0, −1, −2), while their total orbital angular momentum will be zero, and the total spin = 5/2.

In a solid, the order of filling the shell of an ion can change due to the crystal field (i.e., the field of the nearest environment of a given ion). For example, the high-spin state of the Mn^{2+} ion (S = 5/2) can become the low-spin state (S = 1/2) in the crystal lattice. The question of the nature of the filling of the ion shell is solved experimentally for each compound.

At high temperatures, the magnetic moments of the ions in the crystal are directed randomly. However, as the temperature drops below the critical points (see below), the spins can be ordered. The magnetic ordering in a crystal is based on the exchange interaction between magnetic ions. The exchange interaction is understood not so much as the interaction of spins of two magnets (such forces are too weak to play a significant role), but as the interaction arising due to the overlap of atomic orbitals (and charge distributions) of neighboring ions. Moreover, all quantum-mechanical phenomena (i.e. Pauli's prohibition, the uncertainty principle, electrostatic repulsion, the relationship between kinetic and potential energy) are also decisive. It is the latter that determines the order of the arrangement of the spins of the ions in the crystal lattice.

The exchange interaction between magnetic ions can be direct (as in iron) or indirect through an intermediate nonmagnetic ion (as, for example, in MnS, where Mn^{2+} ions interact with each other due to the overlap of the initially atomic Mn orbitals on sulfur atoms during the formation of Mn-S bonds (Fig. 16.1)). In direct contact (iron), the orbitals of isolated atoms transform into narrow zones in the crystal, where a complex behavior of electrons, partially free and partially isolated on the atom, is established.

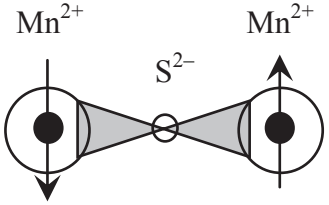

Fig. 16.1. Schematic representation of indirect exchange interaction through an intermediate atom in a MnS crystal. The directions of the spins are here established by the Pauli principle.

The exchange interaction energy U is usually written in the form

$$U = -\boldsymbol{J}\boldsymbol{S}_i \cdot \boldsymbol{S}_j \,, \tag{16.2}$$

where $\boldsymbol{S}_i$, $\boldsymbol{S}_j$ are the spins of ions i and j, and $\boldsymbol{J}$ is the exchange integral, the value of which is determined by the overlap of the orbitals. The sign of the exchange integral can be positive or negative, which, together with its value, determines the variety of magnetic phenomena in crystals.

All types of magnetism are observed in crystals: para-, dia-, ferro-, antiferromagnetism (and some others). In a ferromagnet at temperatures below the critical Curie temperature, all spins are parallel and directed in the same way, while in an antiferromagnet at temperatures below the Néel temperature, all spins are also parallel, but oppositely directed (Fig. 16.2).

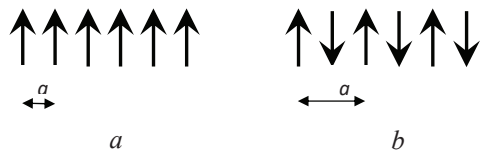

Fig. 16.2. The arrangement of spins in the chains of a ferromagnet (*a*) and antiferromagnet (*b*) below the critical points.

In a magnetic field produced by the magnetic moments of neighboring ions, each spin begins to precess (Fig. 16.3, *a*). It is these precessions, which are phase-matched along an ordered chain of spins, that form a spin wave, or magnon (Fig. 16.3, *b*). As can be seen from the figure, the spin wave is very similar to the mechanical vibration of the lattice, i.e. phonon. What is the "force constant" in a spin wave? As follows from relation (16.2), a change in the relative orientation of the spins causes a change in the interaction energy, which is the reason for the appearance of spin oscillations. Since the interaction of the spins is weak, the energy of the spin vibrations is also small: usually the frequencies of magnons are values of a few inverse centimeters.

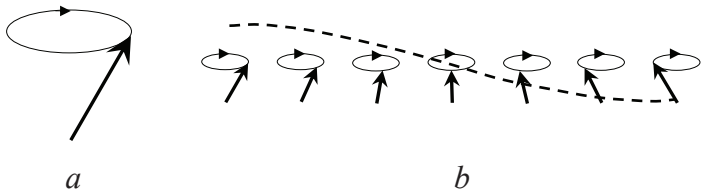

Fig. 16.3. Spin precession in the magnetic field of the crystal (*a*) and the emergences of a magnon in the chain of spins (*b*) [1].

Like phonons in a crystal, spin waves have dispersion, i.e. the dependence of their energy on the wave vector. In simple ferro- and antiferromagnetic chains (Fig. 16.2), the dispersion curves are different and are determined by the expressions [1]:

$$\hbar\omega = 4JS(1 - \cos ka) \quad \text{(ferromagnet)} \tag{16.3}$$

and

$$\hbar\omega = 4\,|J|\,S \sin ka \quad \text{(antiferromagnet)} \tag{16.4}$$

Both curves are shown in Fig. 16.4. It can be noted that both dependences resemble dispersion curves for acoustic phonons, but differ from each other, especially in the region of small values of the wave vector. (In low-symmetry crystals, where the direction of the spins does not coincide with the direction of the crystallographic axis, the magnon energy at the center of the Brillouin zone can differ from zero).

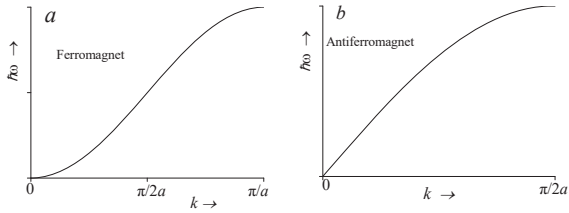

Fig. 16.4. Dispersion curves of magnons in ferro- (*a*) and antiferromagnets (*b*). The abscissa is the wave vector of the magnon in units of π/a, where *a* is the constant of the magnetic lattice (Fig.16.2).

Let us consider an example of registration of spin oscillations in the Raman spectra of the antiferromagnet MnS.

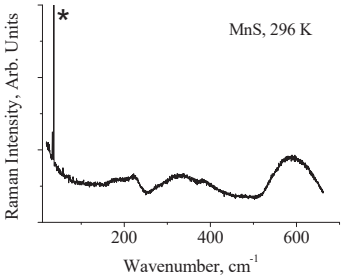

Figure 16.5. Raman spectrum of a MnS crystal at room temperature. The narrow line marked with (*) refers to the emission line of the Ar^+ laser.

MnS crystals have a cubic structure of the NaCl type. In such a structure, Raman-active modes are absent; therefore, the spectrum at room temperature consists of several broad structureless bands in the region of 200-600 cm^{-1} of extremely low intensity (Fig. 16.5). These bands are likely to be related to both the first-order forbidden scattering, which appears due to the structural imperfection of the crystal, and to the second-order scattering. However, as the crystal temperature decreases below 200 K, first a weak wing appears in the spectrum in the low-frequency region, which then, at T <120 K, develops into an intense band consisting at T = 5 K of four lines at 14, 19, 22, and 24 cm^{-1} (Fig. 16.6, 16.7).

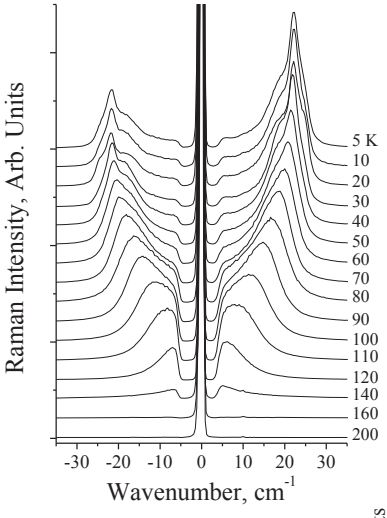

Fig. 16.6. Temperature dependence of the low-frequency Stokes and anti-Stokes parts of the MnS spectrum.

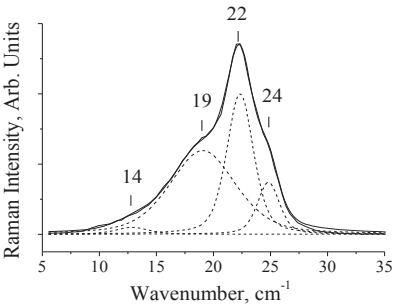

Fig. 16.7. Decomposition of the Stokes spectrum at 5 K into Voight (PsVoigt1) components.

Fig. 16.8 shows the temperature dependence of the peak position of the most intense 22 cm^{-1} mode (T = 5 K) in the range 5 K – 90 K (at higher temperatures, the determination of the peak position becomes

almost impossible). This temperature dependence is well described by the thermal population of the phonon $\Omega = 150$ cm^{-1} (solid curve in Fig. 16.8), i.e. expression

$$\omega(T) = \omega(0) - C(e^x - 1)^{-1}, \tag{16.5}$$

where $x = \hbar\Omega/kT$, and C is a constant. Note that the fitting phonon frequency $\Omega = 150$ cm^{-1} differs significantly from the frequency of the mode itself $\omega = 22$ cm^{-1}. In other words, the temperature dependence of low-frequency modes is determined not by their thermal population, but by the population of the lattice vibrations of heavy atoms, i.e. Mn.

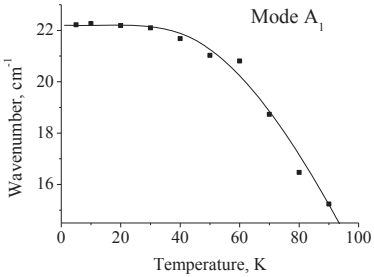

Fig. 16.8. Temperature dependence of the peak position of the 22 cm^{-1} mode. The solid curve describes the thermal population of the lattice phonon $\Omega = 150$ cm^{-1} (see text).

Registration of both the Stokes and anti-Stokes parts of the spectrum (Fig. 16.6) makes it possible to estimate the true temperature of the crystal at the point of incidence of the exciting radiation.

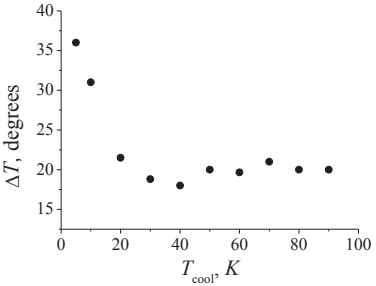

Fig. 16.9. The difference ΔT between the real temperature of the crystal and the temperature of the coolant T_{cool} (see text).

Fig. 16.9 shows the extent to which the real temperature of the crystal at the point of registration of the spectrum, calculated from the Stokes/Anti-Stokes ratio, differs from the temperature of the cryostat coolant T_{cool}. The latter is measured by a built-in sensor. Since the real temperature of the crystal upon the appearance of the first signs of the

appearance of the low-frequency spectrum is approximately 20 degrees higher than the temperature of the cryostat coolant line (Fig.16.9), the beginning of the creation of the low-frequency spectrum should be attributed to 140 K – 150 K. These data are fully consistent with the measurements of the magnetization of MnS. according to which the crystal is an antiferromagnet with the Néel temperature $T_N \cong 150$ K [2].

The formation of the low-frequency scattering band (Fig. 16.6) at the temperature at which the magnetic ordering is recorded should be attributed to the appearance of spin waves (magnons) in the crystal. Experimental evidence of this is both the coincidence of the temperature of the first signs of the appearance of a low-frequency spectrum with the Néel temperature T_N, and the dependence of the frequency of low-frequency modes on the thermal population of phonons of the MnS lattice, resulting in increase in the Mn sublattice parameter (i.e., a decrease in the value of the exchange integral).

If all spins in the chain (Fig. 16.2) precess with the same phase (i.e. $\lambda = \infty$, $k = 0$), then the interaction between any pair of spins described by expression (16.2) does not change in time, and the frequency of magnetic oscillation is zero. In other words, all the spins turn out to be parallel at any moment of time and the restoring force between the spins, which determines the force constant of the oscillations, is absent. For this reason, the dispersion curves for both ferro- and antiferromagnets start from zero at the center of the magnetic Brillouin zone (Fig. 16.4). However, in the crystal lattice, a magnetic ion can be in a crystal field that causes the spin of the ion to deflect by a certain angle with respect to the crystallographic directions and planes. In this case, the spin during precession interacts not only with other spins in the lattice, but also with the force generated by the crystal field. Therefore, in a spin wave with $\lambda = \infty$ and $k = 0$, despite the fact that the interaction between different spins still does not change with time, the additional interaction of each individual spin with the crystal field creates a restoring force (spring) that provides a nonzero frequency this oscillation, and the dispersion branches turn out to be shifted upward in wavenumber near the center of the Brillouin zone.

The Mn^{2+} ions form a sublattice in the MnS crystal, the symmetry of which in this case is also cubic, like the entire crystal (the symmetry group of the sublattice is always a subgroup of the crystal). At high temperatures ($T > T_N$), the magnetic moments of Mn^{2+} ions are completely disordered and the symmetry of the spin sublattice is also cubic O_h. In such a structure, only one three-fold degenerate vibration F_{1u}, which is forbidden in the Raman scattering, can arise. At $T < T_N$, antiferromagnetic ordering occurs in the crystals, accompanied by a slight contraction of the lattice

along the [111] direction (the main diagonal of the cube). As a result, the direction of the magnetic moments of Mn^{2+}, which is the same in one plane of the (111) type, is replaced by the opposite direction in the neighboring plane [3]. In this case, the direction of the spins itself also turns out to be not parallel to the edges of the cubic cell of the crystal, but elongated along the direction o [112] (Fig. 16.10).

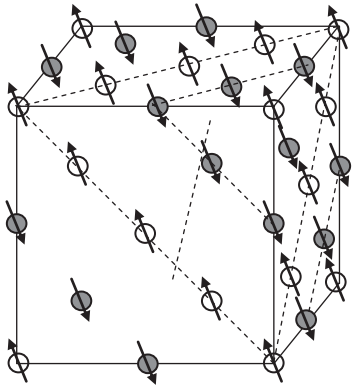

Fig. 16.10. Fragment of a face-centered cubic lattice of MnS. In the antiferromagnetic phase, the spins of the Mn^{2+} ions lie in the (111) planes of the crystal. The direction of the spin of each ion is indicated by an arrow. Sulfur atoms are not shown.

In other words, the above-described situation arises in the MnS lattice, in which the crystal field around the magnetic ion makes the frequency of the magnon with $k = 0$ nonzero. With the ordering of the spin directions, the symmetry of the spin sublattice decreases to C 2/c (and the corresponding point group C_{2h}), since when choosing the possible symmetry operations for the point group, it is also necessary to take into account the direction of the spin on each ion. In a low-symmetry spin lattice, four different types of spin oscillations are possible, A_g, B_g, A_u, and B_u, of which only even A_g and B_g are active in Raman scattering. Of the four lines observed experimentally at low temperatures (Fig. 16.7), two intense modes at 19 and 22 cm^{-1} should be attributed to allowed ones, and the remaining two weak lines at 14 and 24 cm^{-1} – to forbidden oscillations of the spin sublattice. The narrowest and most intense line at 22 cm^{-1} in the spectrum at 5 K is probably related to the A_g vibration. The calculation of the spectrum of magnetic oscillations in MnS crystals, presented in [4], gives the frequency $\omega = 19.8$ cm^{-1} at $k = 0$, which almost ideally corresponds to the frequencies observed in the experiment.

Usually, when calculating the magnon spectrum, the exchange integral $\boldsymbol{J}$ in expression (16.2) is written as the sum $\boldsymbol{J} = \boldsymbol{J}_1 + \boldsymbol{J}_2$, where $\boldsymbol{J}_1$ and $\boldsymbol{J}_2$ characterize the exchange interactions between the given spin and the spins that make up the first and second coordination spheres,

respectively. In this case, the frequency of spin vibrations in the MnS lattice at $k = 0$ can be approximately described by the expression [5]:

$$\hbar\omega_{1(2)} = S\ \sqrt{24D_{2\ 1}\ (J_1 + J_2)}\,, \tag{16.6}$$

where D_1 and D_2 are the parameters characterizing the spin anisotropy "in the plane" and "out of the plane" (Fig. 16.10). When calculating the frequency in [4], the values $J_1 = 2.433$ cm^{-1} and $J_2 = 4.343$ cm^{-1} were used. Substituting these values in (16.6), we find $D_1 = 0.484$ cm^{-1} and $D_2 = 0.361$ cm^{-1}. The value of anisotropy D (only one value) in MnS, calculated in [4], turned out to be 0.236 cm^{-1}, which is very close to the values of D_1 and D_2 found here.

In conclusion, we note one very curious property of spin oscillations that follows from the temperature dependence of their frequency. As follows from Fig. 16.8, the frequency of magnons in the region of low temperatures (T < 40 K, $kT \sim \hbar\omega$), at which their temperature generation (or freezing) occurs in the crystal, does not change within the experimental accuracy. This makes it possible to classify the spin oscillation as an almost ideal harmonic oscillator.

APPENDICES

Appendix A: Unit and primitive cells of crystals

A1. Direct space

The smallest volume, the translation of which along the basis vectors *a*, *b*, and *c*, can recreate the spatial lattice of a crystal, is called a unit cell. There are several ways to construct unit cells. The simplest is to build a parallelepiped based on the basis vectors (Fig. A1). Its disadvantage is that the unit cell obtained in this way often does not show the symmetry elements inherent in the crystal.

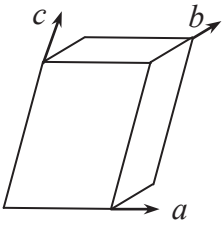

Fig. A1. The simplest way to construct a unit cell

It was found theoretically, that there are only 14 different types of unit cells that can describe the whole variety of crystal structures (Bravais lattices, Fig. A2).

Crystallographers usually choose a unit cell that reflects the crystal symmetry to one degree or another. Fig. 5.3 Chapter 5 shows the unit cell of a silicon crystal (diamond, germanium). However, this cell, which is generally accepted, is not the minimum volume required to build a crystal. The cell, the volume of which is really the smallest possible, is called a primitive cell. This latter may or may not coincide with the unit one. Fig. A3 shows a primitive silicon cell. Its volume is 4 times less than the volume of the corresponding unit cell.

In vibrational spectroscopy, it is very important to consider the distinction between unit and primitive cells, since structural information is usually provided for a unit cell, and the calculation of the number of vibrations is always done for a primitive one. Information about how many primitive cells are contained in one unit is contained in the designation of the space group. So, for all groups, the designation of which

begins with the symbol *P* (primitive), the unit cell coincides with the primitive one. In groups *A*, *B* or *C* (base-centered), one unit contains 2 primitive cells, in groups *F* (face-centered) - 4, in groups *I* (body-centered) - 2, in groups *R* (rhombohedral) - 3 or 1 (depending on the crystallographic installation).

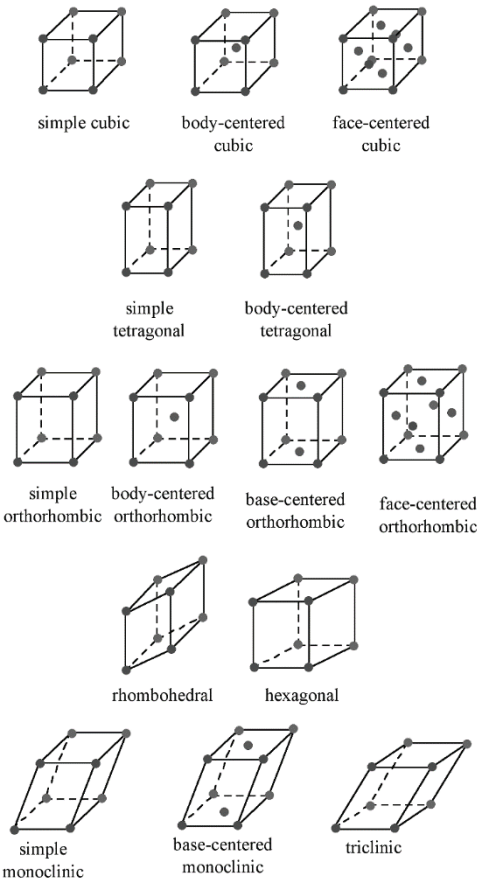

Fig. A2. 14 Bravais lattices

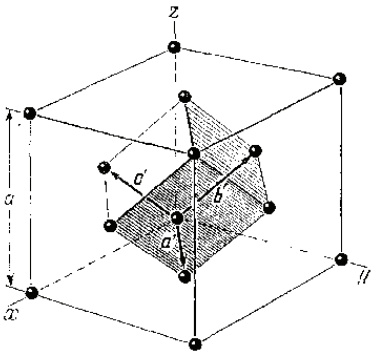

Fig. A3. A primitive rhombohedral cell built on the basis of a face-centered cubic lattice of silicon (C. Kittel, Introduction to solid state physics.)

There is, however, another way to construct a unit cell. To do this, it is necessary to fix the origin at one of the lattice sites (atoms). After that, alternately connect this lattice point with a segment with each nearest neighboring lattice points, each time dividing the segment in half and drawing a plane perpendicular to the segment through the midpoint. The resulting set of planes produces a polyhedron with only one lattice site. This polyhedron is a unit cell and is called the Wigner-Seitz cell. Despite the fact that the Wigner-Seitz cell very fully reflects the crystal symmetry, it has not become widespread in crystallography due to, possibly, a relatively complex scheme of its construction. Fig. A4 shows the Wigner-Seitz cell of a silicon crystal.

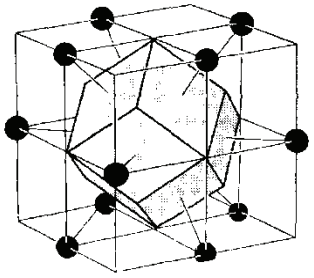

Fig. A.4. Wigner-Seitz cell for a face-centered cubic structure (silicon).

A2. Reciprocal space

The vectors $\boldsymbol{a}$, $\boldsymbol{b}$, $\boldsymbol{c}$, which make up the basis of the crystal lattice, can be associated with vectors $\boldsymbol{k}_a = 2\pi/\boldsymbol{a}$, $\boldsymbol{k}_b = 2\pi/\boldsymbol{b}$, $\boldsymbol{k}_c = 2\pi/\boldsymbol{c}$, having the dimension of reciprocal length and making up the basis of the *reciprocal lattice* of the crystal in space wave vectors. Based on the basis vectors $\boldsymbol{k}_a$, $\boldsymbol{k}_b$ and $\boldsymbol{k}_c$, a simple unit cell in reciprocal space can be constructed according to the scheme shown in Fig. A1. However, such a cell, as already mentioned, does not reflect the symmetry properties of the crystal; therefore, a unit cell in reciprocal space is usually constructed according to the same principle as the Wigner-Seitz cell in direct space. A region in k-space, built as a volume bounded by planes spaced at equal distances from the considered lattice point of the reciprocal lattice to the neighboring lattice point of this lattice, is called the *first Brillouin zone*. The first Brillouin zone (often called simply the Brillouin zone) is a unit cell in the space of wave vectors and is limited to the region $-\frac{\pi}{a} \le k \le \frac{\pi}{a}$ (in the one-dimensional case. For three-dimensional space, the inequality applies to all three directions). As we saw above, in direct space, the region constructed according to the same rules is the Wigner-Seitz cell. Since at $k = 0$ atoms do not shift from equilibrium positions in acoustic phonons, and their displacements in optical phonons do not change the symmetry of the crystal lattice (see Chapter 3), the point $k = 0$ is the only point in the Brillouin zone through which all the crystal symmetry elements pass.

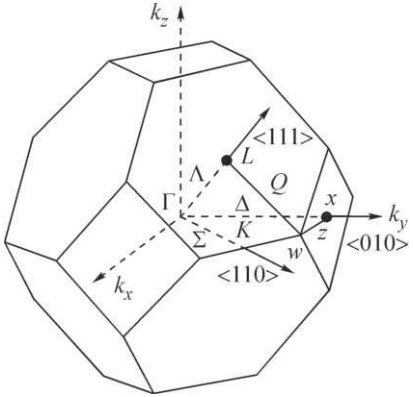

Fig. A5. Brillouin zone for a face-centered cubic lattice (e.g. silicon, zinc blende ZnS).

Consequently, its symmetry group coincides with the crystal symmetry group. This point is called the *center of the Brillouin zone* and is usually denoted by the symbol Γ. At the boundary of the Brillouin zone (cell surface), there are several points through which some of the crystal

symmetry elements pass. These are the so-called *highly symmetric points of the Brillouin zone*, despite the fact that their symmetry is below the symmetry of the center of the zone (Fig. A5). For example, the point group of the ZnS crystal is T_d, therefore, the symmetry of the Γ point of the Brillouin zone (Fig. A5) is also T_d. However, only the third-order rotary axis and the reflection plane (vertical) pass through the point L. These two operations, together with the "identity" operation, form the point group C_{3v}. Therefore, if the optical phonon of the ZnS crystal is threefold degenerate at the center of the Brillouin zone (i.e., the frequencies of the longitudinal and both transverse phonons are equal due to the physical equivalence of all three directions in the crystal), then at the point L the degeneracy is lifted and the dispersion branch is split into two - longitudinal (A_1) and transverse (E) phonons. Dispersion curves for a given crystal are usually plotted in the direction of its highly symmetric points.

As already noted, the Wigner-Seitz cells in the direct space and the Brillouin zones in the reciprocal space are constructed according to the same scheme. But at the same time, when passing from the direct space to the inverse one, the cell “turns out,” as it were: the Wigner - Seitz cell for a face-centered cubic lattice is similar to the Brillouin zone for a body-centered cubic structure, and the cell for a body-centered lattice is like a zone for a face-centered structure.

Appendix B: Symmetry of molecules and crystals

1. The symmetry of molecules (and crystals) is usually understood as the ability of a molecule as a geometric body to transform into itself under the action of symmetry operations. The value of this property and its practical utility lies in the fact that it obliges to formulate all physical laws in relation to symmetric objects in such a way that they are invariant to the application of symmetry elements.

There are five basic symmetry operations:

- identity (single operation);
- own rotation of the order of n (rotation by an angle of $2\pi/n$ around the axis of rotation);
- reflection in the plane;
- inversion at the center of symmetry (reflection at a point);
- improper rotation (rotation through an angle of $2\pi/n$ with subsequent reflection in a plane perpendicular to the axis of rotation).

The first two operations refer to operations of the 1st kind, and the next three - to operations of the second kind. Operations of the first kind rotate a symmetrical object as a whole and are physically feasible. Operations of the second kind include reflection in a plane, the image of an object during reflection is imaginary, and the operations themselves are not physically feasible.

The axes of rotation are designated by the symbol C_n. The order of the axis of rotation is determined by the number n - the higher n, the higher the order. If a molecule has several axes of rotation, the main axis is considered to be the axis of the highest order. In linear molecules, the axis of rotation passing through all atoms is the axis of infinite order C_∞. In nonlinear molecules, the most common axes are 2-, 3-, 4-, and 6-orders. Very rarely - axes of the 5th order. In crystals, there are no 5th-order axes.

If there is a twofold rotation axis C_2, then applying this operation twice brings the object back to its original state and operation C_2 is the only one. However, in the case of the C_3 axis, the molecule returns to the initial state only when this operation is applied three times. Therefore, a distinction is made between the operations C_3 and C_3^2. In many cases, these operations are identical and will be combined, written as $2C_3$. However, in some groups, the characters of the rotation matrices corresponding to a given operation are complex numbers, and the character of C_3 is different from the character C_3^2. For this reason, in the table of characters, they are

recorded as independent elements of symmetry. The same applies to the axes of the fourth and sixth orders, proper and improper.

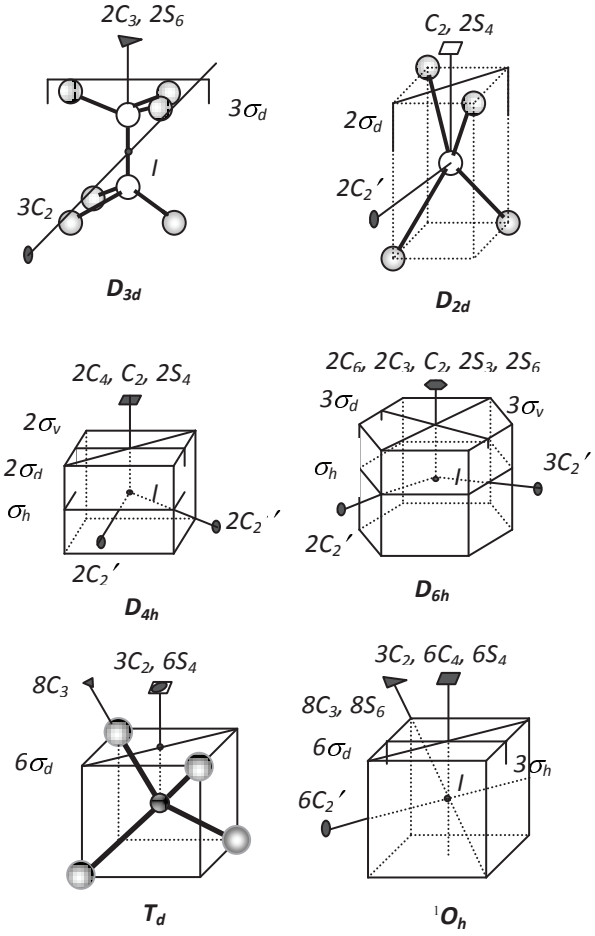

Fig. B.1. Symmetry elements of point groups

Reflection planes are indicated by the symbol σ. Usually, a subscript *h*, *v* or *d* is added to it, denoting the horizontal, vertical and diagonal planes, respectively. The main axis of rotation is perpendicular to σ_h and is aligned with σ_v and σ_d.

The inversion operation is denoted by *I*, and the mirrored axes by S_n. Fig. B.1 shows the symmetry elements of the main point groups.

2. The successive application of two symmetry operations that characterize a certain symmetry group yields the appearance of a third operation from the same group. In other words, symmetry operations within a group must obey the rules of multiplication. Hence it follows that the number and mutual arrangement of the symmetry elements of the group cannot be any, since each operation is linked with other rules of multiplication.

As an example, consider the symmetry operations of the group D_{2h} (Fig. B.2).

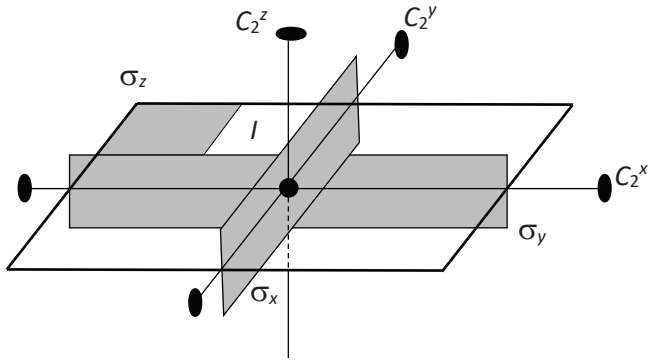

Fig. B.2. Symmetry elements of the group D_{2h}.

Put in the upper left corner of the parallelogram, conventionally depicting a figure of symmetry D_{2h}, a point (Fig. B.3). During the operation, the identity point will not change its position. The C_2^z operation will move it to the lower right corner, the C_2^y operation to the upper right corner, and so on.

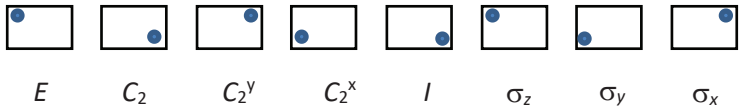

Fig. B.3. Actions of symmetry operations of the D_{2h} group on the position of a point in a parallelogram.

Table B.1. Multiplication table of symmetry elements of group D_{2h}.

D_{2h}	E	C_2^z	C_2^y	C_2^x	I	σ_z	σ_y	σ_x
E	E	C_2^z	C_2^y	C_2^x	I	σ_z	σ_y	σ_x
C_2^z	C_2^z	E	σ_y	σ_x	σ_z	C_2^z	C_2^y	C_2^x
C_2^y	C_2^y	σ_y	E	I	C_2^x	C_2^y	C_2^z	σ_z
C_2^x	C_2^x	σ_x	I	E	C_2^y	σ_y	σ_z	C_2^z
I	I	σ_z	σ_y	σ_x	E	C_2^z	C_2^y	C_2^x
σ_z	σ_z	I	σ_x	σ_y	C_2^z	E	C_2^x	C_2^y
σ_y	σ_y	σ_x	I	σ_z	C_2^y	C_2^x	E	C_2^z
σ_x	σ_x	σ_y	σ_z	I	C_2^x	C_2^y	C_2^z	E

Now, applying symmetry operations to each figure again in the same sequence, we will know what the equivalent of applying two symmetry operations in succession is and compose a multiplication table, in the first line of which the first symmetry operation is given, and in the first column - the second operation (Table B.1).

3. For point symmetry groups in spectroscopy, the Schoenflis designations are usually used, and in crystallography - international symbols (Table B.2).

Table B.2. Point symmetry group notation

System	Schoenflies designations	Short international symbol	Full international symbol
Triclinic	C_1	1	1
	$C_i\,(S_2)$	$\bar{1}$	$\bar{1}$
Monoclinic	C_2	2	2
	$C_s\,(C_{1h})$	m	m
	C_{2h}	$2/m$	$2/m$
Orthorhombic	$D_2\,(V)$	222	222
	C_{2v}	$mm2$	$mm2$
	$D_{2h}\,(V_h)$	mmm	$2/m\ 2/m\ 2/m$
Tetragonal	C_4	4	4
	S_4	$\bar{4}$	$\bar{4}$
	C_{4h}	$4/m$	$4/m$
	D_4	422	422
	C_{4v}	$4mm$	$4mm$
	$D_{2d}\,(V_d)$	$\bar{4}2m$ or $\bar{4}m2$	$\bar{4}2m$ or $\bar{4}m2$
	D_{4h}	$4/mmm$	$4/m\ 2/m\ 2/m$
Trigonal	C_3	3	3
	$C_{3i}\,(S_6)$	$\bar{3}$	$\bar{3}$
	D_3	32 or 321 or 312	32 or 321 or 312
	C_{3v}	$3m$ or $3m1$ or $31m$	$3m$ or $3m1$ or $31m$
	D_{3d}	$\bar{3}m$ or $\bar{3}m1$ or $\bar{3}1m$	$\bar{3}2/m$ or $\bar{3}$ $2/m1$ or $\bar{3}12/m$
Hexagonal	C_6	6	6
	C_{3h}	$\bar{6}$	$\bar{6}$
	C_{6h}	$6/m$	$6/m$
	D_6	622	622
	C_{6v}	$6mm$	$6mm$
	D_{3h}	$\bar{6}m2$ or $\bar{6}2m$	$\bar{6}m2$ or $\bar{6}2m$
	D_{6h}	$6/mmm$	$6/m\ 2/m\ 2/m$
Cubic	T	23	23
	T_h	$m\bar{3}$	$2/m\bar{3}$
	O	432	432
	T_d	$\bar{4}3m$	$\bar{4}3m$
	O_h	$m\bar{3}m$	$4/m\bar{3}2/m$

The simplest point group, triclinic, does not contain rotary axes. In monoclinic and orthorhombic systems, twofold rotational axes and reflection planes appear. The appearance of one threefold axis means a transition to trigonal systems, and the fourfold axis - to tetragonal systems. The presence of a sixthfold axis is characteristic of hexagonal systems, and the presence of four volumetric (diagonal) axes of the third order results in the formation of a cubic system, which is the most symmetric and widespread among molecules.

4. Molecules that do not have a plane of symmetry cannot be combined with their mirror image, just as it is impossible to combine the images of the right and left hands. Such molecules are called chiral. Fig. B.4 shows the amino acid molecules glycine and alanine in their zwitterionic form (see Chapter 14). The glycine molecule has a plane of symmetry, but alanine (and all other amino acids) does not. The first is achiral, the second is chiral. The presence of chirality means that the molecular crystal formed by chiral molecules is optically active, i.e. rotates the plane of polarization of the transmitted light beam.

Fig. B.4.

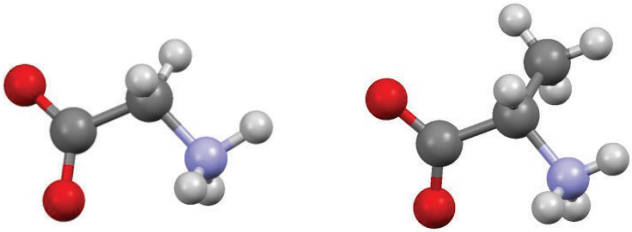

a ***b***

Molecules of glycine (*a*) and alanine (*b*). The plane of the drawing is the mirror plane for glycine. Alanine has no reflection planes and this molecule is chiral.

5. As mentioned in Chapter 4, symmetry operations produce a group in the algebraic sense. The order of a group is the number of all symmetry elements that form a given group. Each group has several elements of symmetry, from which all the rest can be obtained according to the rules of multiplication (i.e., sequential application). Such elements are called *generating* ones. Below is information about the orders of point groups and generating elements (Table B.3.).

Table B.3. Point group order and their generating elements

Triclinic

Group	C_1	C_i
Group Order	1	2
Producing elements		I

Monoclinic

Group	$C_{1h} \equiv C_s$	C_2	C_{2h}
Group Order	2	2	4
Producing elements	σ_h	C_2	C_2, I

Orthorhombic

Group	C_{2v}	D_2	D_{2h}
Group Order	4	4	8
Producing elements	C_2, σ_v	C_2, $C_2^{\perp}$	C_2, $C_2^{\perp}$, I

Trigonal

Group	C_3	$C_{3i} \equiv S_6$	C_{3v}	D_3	D_{3d}
Group Order	3	6	6	6	12
Producing elements	C_3	C_3, I	C_3, σ_v	C_3, $C_2^{\perp}$	C_3, $C_2^{\perp}$, I

Tetragonal

Group	C_4	S_4	C_{4h}	D_4	C_{4v}	D_{2d}	D_{4h}
Group Order	4	4	8	8	8	8	16
Producing elements	C_4	S_4	C_4	C_4, $C_2^{\perp}$	C_4, σ_v	C_2, $C_2^{\perp}$, σ_d	C_4, $C_2^{\perp}$, I

Hexagonal

Group	C_6	C_{3h}	C_{6h}	D_6	C_{6v}	D_{3h}	D_{6h}
Group Order	6	6	12	12	12	12	24
Producing elements	C_6	C_3, σ_h	C_6, I	C_6, $C_2^{\perp}$	C_6, σ_v	C_3, $C_2^{\perp}$, σ_h	C_6, $C_2^{\perp}$, I

Cubic

Group	T	T_h	T_d	O	O_h
Group Order	12	24	24	24	48
Producing elements	C_2, C_3	C_2, C_3, I	S_4, C_3	C_4, C_3	C_4, C_3, I

6. When compiling the symmetry coordinates, it is necessary to know the transformation matrices for all symmetry elements of a given group. Matrices of one-dimensional representations coincide with their character and can, therefore, be taken from tables of characters (Appendix D). Matrices of two- and three-dimensional representations of point groups are given in Table. B.4.

Table. B.4. Transformation matrices of two- and three-dimensional representations for generating symmetry elements

C_3	C_3
E	$\begin{matrix} -\frac{1}{2} & -\frac{\overline{3}}{2} \\ \frac{\overline{3}}{2} & -\frac{1}{2} \end{matrix}$

$C_{3i} \equiv S_6$	S_6
E_g	$\begin{matrix} -\frac{1}{2} & \frac{\overline{3}}{2} \\ -\frac{\overline{3}}{2} & -\frac{1}{2} \end{matrix}$
E_u	$\begin{matrix} \frac{1}{2} & -\frac{\overline{3}}{2} \\ \frac{\overline{3}}{2} & \frac{1}{2} \end{matrix}$

C_{3v} D_3	C_3 C_3	σ_v C_2
E	$\begin{matrix} -\frac{1}{2} & -\frac{\overline{3}}{2} \\ \frac{\overline{3}}{2} & -\frac{1}{2} \end{matrix}$	$\begin{matrix} 1 & 0 \\ 0 & -1 \end{matrix}$

D_{3d}	C_3	C_2	I
E_g	$\begin{matrix} -\frac{1}{2} & -\frac{\sqrt{3}}{2} \\ \frac{\sqrt{3}}{2} & -\frac{1}{2} \end{matrix}$	$\begin{matrix} 1 & 0 \\ 0 & -1 \end{matrix}$	$\begin{matrix} 1 & 0 \\ 0 & 1 \end{matrix}$
E_u	$\begin{matrix} -\frac{1}{2} & -\frac{\sqrt{3}}{2} \\ \frac{\sqrt{3}}{2} & -\frac{1}{2} \end{matrix}$	$\begin{matrix} 1 & 0 \\ 0 & -1 \end{matrix}$	$\begin{matrix} -1 & 0 \\ 0 & -1 \end{matrix}$

C_4 S_4	C_4 S_4
E	$\begin{matrix} 0 & -1 \\ 1 & 0 \end{matrix}$

C_{4h}	C_4	σ_h
E_g	$\begin{matrix} 0 & -1 \\ 1 & 0 \end{matrix}$	$\begin{matrix} -1 & 0 \\ 0 & -1 \end{matrix}$
E_u	$\begin{matrix} 0 & -1 \\ 1 & 0 \end{matrix}$	$\begin{matrix} 1 & 0 \\ 0 & 1 \end{matrix}$

D_4 C_{4v}	C_4 C_4	C_2' σ_v
E	$\begin{matrix} 0 & -1 \\ 1 & 0 \end{matrix}$	$\begin{matrix} 1 & 0 \\ 0 & -1 \end{matrix}$

D_{2d}	S_4	C_2'	σ_d
E	$\begin{matrix} 0 & -1 \\ 1 & 0 \end{matrix}$	$\begin{matrix} 1 & 0 \\ 0 & -1 \end{matrix}$	$\begin{matrix} 0 & 1 \\ 1 & 0 \end{matrix}$

D_{4h}	C_4	C_2'	σ_h
E_g	$\begin{matrix} 0 & -1 \\ 1 & 0 \end{matrix}$	$\begin{matrix} 1 & 0 \\ 0 & -1 \end{matrix}$	$\begin{matrix} -1 & 0 \\ 0 & -1 \end{matrix}$
E_u	$\begin{matrix} 0 & -1 \\ 1 & 0 \end{matrix}$	$\begin{matrix} 1 & 0 \\ 0 & -1 \end{matrix}$	$\begin{matrix} 1 & 0 \\ 0 & 1 \end{matrix}$

C_6	C_6
E_1	$\begin{matrix} \frac{1}{2} & -\frac{\sqrt{3}}{2} \\ \frac{\sqrt{3}}{2} & \frac{1}{2} \end{matrix}$
E_2	$\begin{matrix} -\frac{1}{2} & \frac{\sqrt{3}}{2} \\ -\frac{\sqrt{3}}{2} & -\frac{1}{2} \end{matrix}$

C_{3h}	C_3	σ_h
E'	$\begin{matrix} -\frac{1}{2} & -\frac{\sqrt{3}}{2} \\ \frac{\sqrt{3}}{2} & -\frac{1}{2} \end{matrix}$	$\begin{matrix} 1 & 0 \\ 0 & 1 \end{matrix}$
E''	$\begin{matrix} -\frac{1}{2} & -\frac{\sqrt{3}}{2} \\ \frac{\sqrt{3}}{2} & -\frac{1}{2} \end{matrix}$	$\begin{matrix} -1 & 0 \\ 0 & -1 \end{matrix}$

C_{6h}	C_6	σ_h
E_{1g}	$\begin{matrix} \frac{1}{2} & -\frac{\sqrt{3}}{2} \\ \frac{\sqrt{3}}{2} & \frac{1}{2} \end{matrix}$	$\begin{matrix} -1 & 0 \\ 0 & -1 \end{matrix}$
E_{1u}	$\begin{matrix} \frac{1}{2} & -\frac{\sqrt{3}}{2} \\ \frac{\sqrt{3}}{2} & \frac{1}{2} \end{matrix}$	$\begin{matrix} 1 & 0 \\ 0 & 1 \end{matrix}$
E_{2g}	$\begin{matrix} -\frac{1}{2} & \frac{\sqrt{3}}{2} \\ -\frac{\sqrt{3}}{2} & -\frac{1}{2} \end{matrix}$	$\begin{matrix} 1 & 0 \\ 0 & 1 \end{matrix}$
E_{2u}	$\begin{matrix} -\frac{1}{2} & \frac{\sqrt{3}}{2} \\ -\frac{\sqrt{3}}{2} & -\frac{1}{2} \end{matrix}$	$\begin{matrix} -1 & 0 \\ 0 & -1 \end{matrix}$

D_6 C_{6v}	C_6 C_6	C_2' σ_v
E_1	$\begin{matrix} \frac{1}{2} & -\frac{\sqrt{3}}{2} \\ \frac{\sqrt{3}}{2} & \frac{1}{2} \end{matrix}$	$\begin{matrix} 1 & 0 \\ 0 & -1 \end{matrix}$
E_2	$\begin{matrix} -\frac{1}{2} & \frac{\sqrt{3}}{2} \\ -\frac{\sqrt{3}}{2} & -\frac{1}{2} \end{matrix}$	$\begin{matrix} 1 & 0 \\ 0 & -1 \end{matrix}$

D_{3h}	C_3	C_2	σ_h
E'	$\begin{matrix} -\frac{1}{2} & -\frac{\sqrt{3}}{2} \\ \frac{\sqrt{3}}{2} & -\frac{1}{2} \end{matrix}$	$\begin{matrix} 1 & 0 \\ 0 & -1 \end{matrix}$	$\begin{matrix} 1 & 0 \\ 0 & 1 \end{matrix}$
E''	$\begin{matrix} -\frac{1}{2} & -\frac{\sqrt{3}}{2} \\ \frac{\sqrt{3}}{2} & -\frac{1}{2} \end{matrix}$	$\begin{matrix} 1 & 0 \\ 0 & -1 \end{matrix}$	$\begin{matrix} -1 & 0 \\ 0 & -1 \end{matrix}$

D_{6h}	C_6	C_2'	σ_h
E_{1g}	$\begin{matrix} \frac{1}{2} & -\frac{\sqrt{3}}{2} \\ \frac{\sqrt{3}}{2} & \frac{1}{2} \end{matrix}$	$\begin{matrix} 1 & 0 \\ 0 & -1 \end{matrix}$	$\begin{matrix} -1 & 0 \\ 0 & -1 \end{matrix}$
E_{1u}	$\begin{matrix} \frac{1}{2} & -\frac{\sqrt{3}}{2} \\ \frac{\sqrt{3}}{2} & \frac{1}{2} \end{matrix}$	$\begin{matrix} 1 & 0 \\ 0 & -1 \end{matrix}$	$\begin{matrix} 1 & 0 \\ 0 & 1 \end{matrix}$
E_{2g}	$\begin{matrix} -\frac{1}{2} & \frac{\sqrt{3}}{2} \\ -\frac{\sqrt{3}}{2} & -\frac{1}{2} \end{matrix}$	$\begin{matrix} 1 & 0 \\ 0 & -1 \end{matrix}$	$\begin{matrix} 1 & 0 \\ 0 & 1 \end{matrix}$
E_{2u}	$\begin{matrix} -\frac{1}{2} & \frac{\sqrt{3}}{2} \\ -\frac{\sqrt{3}}{2} & -\frac{1}{2} \end{matrix}$	$\begin{matrix} 1 & 0 \\ 0 & -1 \end{matrix}$	$\begin{matrix} -1 & 0 \\ 0 & -1 \end{matrix}$

T	C_3^{xyz}	C_2^z
E	$\begin{matrix} -\frac{1}{2} & -\frac{\sqrt{3}}{2} \\ \frac{\sqrt{3}}{2} & -\frac{1}{2} \end{matrix}$	$\begin{matrix} 1 & 0 \\ 0 & 1 \end{matrix}$
F	$\begin{matrix} 0 & 0 & 1 \\ 1 & 0 & 0 \\ 0 & 1 & 0 \end{matrix}$	$\begin{matrix} -1 & 0 & 0 \\ 0 & -1 & 0 \\ 0 & 0 & 1 \end{matrix}$

T_d O	$(S_4^z)^{-1}$ C_4^z	C_3^{xyz} C_3^{xyz}
E	$\begin{matrix} 1 & 0 \\ 0 & -1 \end{matrix}$	$\begin{matrix} -\frac{1}{2} & -\frac{\overline{3}}{2} \\ \frac{\overline{3}}{2} & -\frac{1}{2} \end{matrix}$
F_1	$\begin{matrix} 0 & -1 & 0 \\ 1 & 0 & 0 \\ 0 & 0 & 1 \end{matrix}$	$\begin{matrix} 0 & 0 & 1 \\ 1 & 0 & 0 \\ 0 & 1 & 0 \end{matrix}$
F_2	$\begin{matrix} 0 & 1 & 0 \\ -1 & 0 & 0 \\ 0 & 0 & -1 \end{matrix}$	$\begin{matrix} 0 & 0 & 1 \\ 1 & 0 & 0 \\ 0 & 1 & 0 \end{matrix}$

T_h	C_3^{xyz}	C_2^z	I
E_g	$\begin{matrix} -\frac{1}{2} & -\frac{\overline{3}}{2} \\ \frac{\overline{3}}{2} & -\frac{1}{2} \end{matrix}$	$\begin{matrix} 1 & 0 \\ 0 & 1 \end{matrix}$	$\begin{matrix} 1 & 0 \\ 0 & 1 \end{matrix}$
E_u	$\begin{matrix} -\frac{1}{2} & -\frac{\overline{3}}{2} \\ \frac{\overline{3}}{2} & -\frac{1}{2} \end{matrix}$	$\begin{matrix} 1 & 0 \\ 0 & 1 \end{matrix}$	$\begin{matrix} -1 & 0 \\ 0 & -1 \end{matrix}$
F_g	$\begin{matrix} 0 & 0 & 1 \\ 1 & 0 & 0 \\ 0 & 1 & 0 \end{matrix}$	$\begin{matrix} -1 & 0 & 0 \\ 0 & -1 & 0 \\ 0 & 0 & 1 \end{matrix}$	$\begin{matrix} 1 & 0 & 0 \\ 0 & 1 & 0 \\ 0 & 0 & 1 \end{matrix}$
F_u	$\begin{matrix} 0 & 0 & 1 \\ 1 & 0 & 0 \\ 0 & 1 & 0 \end{matrix}$	$\begin{matrix} -1 & 0 & 0 \\ 0 & -1 & 0 \\ 0 & 0 & 1 \end{matrix}$	$\begin{matrix} -1 & 0 & 0 \\ 0 & -1 & 0 \\ 0 & 0 & -1 \end{matrix}$

O_h	C_4^z	C_3^{xyz}	I
E_g	$\begin{matrix} 1 & 0 \\ 0 & -1 \end{matrix}$	$\begin{matrix} -\frac{1}{2} & -\frac{\overline{3}}{2} \\ \frac{\overline{3}}{2} & -\frac{1}{2} \end{matrix}$	$\begin{matrix} 1 & 0 \\ 0 & 1 \end{matrix}$
E_u	$\begin{matrix} 1 & 0 \\ 0 & -1 \end{matrix}$	$\begin{matrix} -\frac{1}{2} & -\frac{\overline{3}}{2} \\ \frac{\overline{3}}{2} & -\frac{1}{2} \end{matrix}$	$\begin{matrix} -1 & 0 \\ 0 & -1 \end{matrix}$
F_{1g}	$\begin{matrix} 0 & -1 & 0 \\ 1 & 0 & 0 \\ 0 & 0 & 1 \end{matrix}$	$\begin{matrix} 0 & 0 & 1 \\ 1 & 0 & 0 \\ 0 & 1 & 0 \end{matrix}$	$\begin{matrix} 1 & 0 & 0 \\ 0 & 1 & 0 \\ 0 & 0 & 1 \end{matrix}$
F_{1u}	$\begin{matrix} 0 & -1 & 0 \\ 1 & 0 & 0 \\ 0 & 0 & 1 \end{matrix}$	$\begin{matrix} 0 & 0 & 1 \\ 1 & 0 & 0 \\ 0 & 1 & 0 \end{matrix}$	$\begin{matrix} -1 & 0 & 0 \\ 0 & -1 & 0 \\ 0 & 0 & -1 \end{matrix}$
F_{2g}	$\begin{matrix} 0 & 1 & 0 \\ -1 & 0 & 0 \\ 0 & 0 & -1 \end{matrix}$	$\begin{matrix} 0 & 0 & 1 \\ 1 & 0 & 0 \\ 0 & 1 & 0 \end{matrix}$	$\begin{matrix} 1 & 0 & 0 \\ 0 & 1 & 0 \\ 0 & 0 & 1 \end{matrix}$
F_{2u}	$\begin{matrix} 0 & 1 & 0 \\ -1 & 0 & 0 \\ 0 & 0 & -1 \end{matrix}$	$\begin{matrix} 0 & 0 & 1 \\ 1 & 0 & 0 \\ 0 & 1 & 0 \end{matrix}$	$\begin{matrix} -1 & 0 & 0 \\ 0 & -1 & 0 \\ 0 & 0 & -1 \end{matrix}$

7. To obtain a complete vibrational representation of a crystal, it is necessary to know the positional symmetry of each atom or molecular ion. Since the positional symmetry group is a subgroup of the crystal space group, the positional symmetry cannot be arbitrary. Possible positional symmetry groups are strictly defined for each space group. All this information is contained in the International Crystallographic Tables (ICT).

Appendix C: Constructing of symmetry coordinates

Despite the fact that the calculation of the vibrational spectrum is currently carried out using well-developed computer programs, to understand the theory of vibrational spectra, it is necessary, however, to have an idea of the algorithm for constructing the symmetry coordinates. Symmetry coordinates are constructed only in a group of equivalent vibrational coordinates that transform into each other under the action of symmetry operations. The order of composing the symmetry coordinates is quite simple and is as follows. Let's enumerate the vibrational coordinates and choose one of them, for example, d_1, as the producing one. Then we will find, in which coordinates d_1 goes when sequentially applying symmetry operations. To now compose the symmetry coordinate for each irreducible representation, it is necessary to take into account the sign and numerical value with which d_1 is transformed in this irreducible representation, i.e. multiply the result of the transformation d_1 by an element of the corresponding transformation matrix. Thus, the expression for the symmetry coordinate $S^{(i)}$ for the i-th irreducible representation is:

$$S^{(i)} = \frac{1}{N} \sum_R \chi^{(i)}(R)\, d_i(R) \qquad \text{(C.1)}$$

where $d_1(R)$ is the record of the coordinate into which the producing d_1 is transformed under the action of the symmetry operation R, $\chi^{(i)}(R)$ is the transformation matrix of the i-th representation, N is the normalizing factor (the square root of the sum of the squares of the coordinate amplitudes in the final expression). As an example, let us compose the symmetry coordinates for the stretching vibrations of AB bonds in the plane of a square AB_4 molecule (Fig. 4.5).

The designations of the vibrational coordinates and the symmetry elements of the D_{4h} group are shown in Fig. C.1. (The figure gives a more detailed designation of the symmetry elements than was done in table of characters of the D_{4h} group (Appendix D), since the result of the transformation d_1 turns out to be different in the case of using symmetry elements relating to the same class, for example, C_2^x or C_2^y, therefore these operations should be considered as independent).

To make up the coordinates of symmetry, it is necessary to know the full form of the transformation matrices of all irreducible representations and for all elements of symmetry. Matrices of one-dimensional representations coincide with their characters and, therefore, can be borrowed from the table of characters of the D_{4h} group. The transformation matrices of doubly degenerate representations are given above (Table B4 of the Appendix B),

but only for the producing symmetry elements of the group, and for all others they are obtained using multiplication operations (Table C.1).

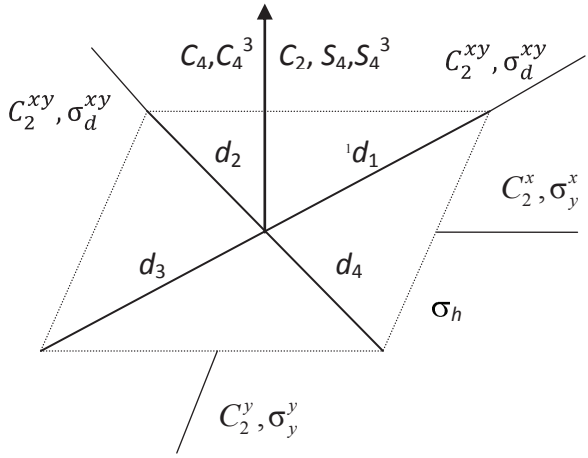

Fig. C.1. Notation of vibrational coordinates of the AB_4 molecule and symmetry elements of the D_{4h} group

Table C1. Transformation matrices of the representations E_g and E_u of the group D_{4h}

R	E_g	E_u	R	E_g	E_u
E	$\begin{matrix}1 & 0\\ 0 & 1\end{matrix}$	$\begin{matrix}1 & 0\\ 0 & 1\end{matrix}$	$I = \sigma_h \cdot C_2$	$\begin{matrix}1 & 0\\ 0 & 1\end{matrix}$	$\begin{matrix}-1 & 0\\ 0 & -1\end{matrix}$
C_4	$\begin{matrix}0 & -1\\ 1 & 0\end{matrix}$	$\begin{matrix}0 & -1\\ 1 & 0\end{matrix}$	$S_4 = \sigma_h \cdot C_4$	$\begin{matrix}0 & 1\\ -1 & 0\end{matrix}$	$\begin{matrix}0 & -1\\ 1 & 0\end{matrix}$
$C_2 = C_4 \cdot C_4$	$\begin{matrix}-1 & 0\\ 0 & -1\end{matrix}$	$\begin{matrix}-1 & 0\\ 0 & -1\end{matrix}$	$S_4^3 = \sigma_h \cdot C_4^3$	$\begin{matrix}0 & -1\\ 1 & 0\end{matrix}$	$\begin{matrix}0 & 1\\ -1 & 0\end{matrix}$
$C_4^3 = C_4 \cdot C_2$	$\begin{matrix}0 & 1\\ -1 & 0\end{matrix}$	$\begin{matrix}0 & 1\\ -1 & 0\end{matrix}$	σ_h	$\begin{matrix}-1 & 0\\ 0 & -1\end{matrix}$	$\begin{matrix}1 & 0\\ 0 & 1\end{matrix}$
C_2^x	$\begin{matrix}1 & 0\\ 0 & -1\end{matrix}$	$\begin{matrix}1 & 0\\ 0 & -1\end{matrix}$	$\sigma_v^x = \sigma_h \cdot C_2^x$	$\begin{matrix}-1 & 0\\ 0 & 1\end{matrix}$	$\begin{matrix}1 & 0\\ 0 & -1\end{matrix}$

$C_2^y = C_2 \cdot C_2^x$	$\begin{matrix}-1 & 0\\ 0 & 1\end{matrix}$	$\begin{matrix}-1 & 0\\ 0 & 1\end{matrix}$	$\sigma_v^y = \sigma_h \cdot C_2^y$	$\begin{matrix}1 & 0\\ 0 & -1\end{matrix}$	$\begin{matrix}-1 & 0\\ 0 & 1\end{matrix}$
$C_2^{xy} = C_4^3 \cdot C_2^y$	$\begin{matrix}0 & 1\\ 1 & 0\end{matrix}$	$\begin{matrix}0 & 1\\ 1 & 0\end{matrix}$	$\sigma_d^{xy} = \sigma_h \cdot C_2^{xy}$	$\begin{matrix}0 & -1\\ -1 & 0\end{matrix}$	$\begin{matrix}0 & 1\\ 1 & 0\end{matrix}$
$C_2^{\bar{x}y} = C_2 \cdot C_2^{xy}$	$\begin{matrix}0 & -1\\ -1 & 0\end{matrix}$	$\begin{matrix}0 & -1\\ -1 & 0\end{matrix}$	$\sigma_d^{\bar{x}y} = \sigma_h \cdot C_2^{\bar{x}y}$	$\begin{matrix}0 & 1\\ 1 & 0\end{matrix}$	$\begin{matrix}0 & -1\\ -1 & 0\end{matrix}$

The result of transformation of the producing coordinate d_1 under the action of the symmetry operation R is shown in the second row of Table C.2 (rotations are made counterclockwise). This line is common for all irreducible representations, since it only shows which coordinate d_1 goes to, regardless of a specific irreducible representation. The characteristic of the individual irreducible representation is laid down in the following lines, where the sign and the numerical coefficient are presented, by which the transformed coordinate in this irreducible representation is multiplied. For two-dimensional representations, each of the components of the transformation matrices shown in Table C.1 are sequentially used.

Table C.2. Transformation of the producing coordinate d_1 under symmetry operations

D_{4h}	E	C_4	C_4^3	C_2	C_2^x	C_2^y	C_2^{xy}	$C_2^{\bar{x}y}$	I	S_4	S_4^3	σ_h	σ_v^x	σ_v^y	σ_d^{xy}	$\sigma_d^{\bar{x}y}$
Rd_1	d_1	d_2	d_4	d_3	d_4	d_2	d_1	d_3	d_3	d_2	d_4	d_1	d_4	d_2	d_1	d_3
A_{1g}	+1	+1	+1	+1	+1	+1	+1	+1	+1	+1	+1	+1	+1	+1	+1	+1
A_{2g}	+1	+1	+1	+1	−1	−1	−1	−1	+1	+1	+1	+1	−1	−1	−1	−1
B_{1g}	+1	−1	−1	+1	+1	+1	−1	−1	+1	−1	−1	+1	+1	+1	−1	−1
B_{2g}	+1	−1	−1	+1	−1	−1	+1	+1	+1	−1	−1	+1	−1	−1	+1	+1
$E_g^{(1,1)}$	+1	0	0	−1	+1	−1	0	0	+1	0	0	−1	−1	+1	0	0
$E_g^{(1,2)}$	0	−1	+1	0	0	0	+1	−1	0	+1	−1	0	0	0	−1	+1
$E_g^{(2,1)}$	0	+1	−1	0	0	0	+1	−1	0	−1	+1	0	0	0	−1	+1
$E_g^{(2,2)}$	+1	0	0	−1	−1	+1	0	0	+1	0	0	−1	+1	−1	0	0
A_{1u}	+1	+1	+1	+1	+1	+1	+1	+1	−1	−1	−1	−1	−1	−1	−1	−1
A_{2u}	+1	+1	+1	+1	−1	−1	−1	−1	−1	−1	−1	−1	+1	+1	+1	+1
B_{1u}	+1	−1	−1	+1	+1	+1	−1	−1	−1	+1	+1	−1	−1	−1	+1	+1
B_{2u}	+1	−1	−1	+1	−1	−1	+1	+1	−1	+1	+1	−1	+1	+1	−1	−1
$E_u^{(1,1)}$	+1	0	0	−1	+1	−1	0	0	−1	0	0	+1	+1	−1	0	0
$E_u^{(1,2)}$	0	−1	+1	0	0	0	+1	−1	0	−1	+1	0	0	0	+1	−1
$E_u^{(2,1)}$	0	+1	−1	0	0	0	+1	−1	0	+1	−1	0	0	0	+1	−1
$E_u^{(2,2)}$	+1	0	0	−1	−1	+1	0	0	−1	0	0	+1	−1	+1	0	0

Finally, summarizing according to expression (C.1) the data presented in each row of table. C.2, find the symmetry coordinates:

$$S^{(A_1g)} = 2(d_1 + d_2 + d_3 + d_4)$$
$$S^{(A_2g)} = 0$$
$$S^{(B_1g)} = 0$$
$$S^{(B_2g)} = 2(d_1 - d_2 + d_3 - d_4)$$
$$S^{(E_g^{(1,1)})} = 0$$
$$S^{(E_g^{(1,2)})} = 0$$
$$S^{(E_g^{(2,1)})} = 0$$
$$S^{(E_g^{(2,2)})} = 0$$
$$S^{(A_1u)} = 0$$
$$S^{(A_2u)} = 0$$
$$S^{(B_1u)} = 0$$
$$S^{(B_2u)} = 0$$
$$S^{(E_u^{(1,1)})} = d_1 - d_2 - d_3 + d_4$$
$$S^{(E_u^{(1,2)})} = d_1 - d_2 - d_3 + d_4$$
$$S^{(E_u^{(2,1)})} = d_1 + d_2 - d_3 - d_4$$
$$S^{(E_u^{(2,2)})} = d_1 + d_2 - d_3 - d_4$$

Appendix D: Tables of characters

D1. Characters of irreducible representations of 32 finite crystallographic groups

The designations of the symmetry elements are given in Appendix B. The symbols most often used in vibrational spectroscopy are used to designate the representations. *A* and *B* are one-dimensional representations, symmetric (*A*), or asymmetric (*B*) relative to the main axis of rotation, *E* - two-dimensional, *F* - three-dimensional. The indices 1 and 2 of the representations denote symmetry or asymmetry with respect to the reflection σ_v in the groups C_{nv} or the twofold rotation axis in the groups D_n. The subscripts *g* (gerade - even) or *u* (ungerade - odd) mean symmetry or asymmetry with respect to the center of inversion, and "dash" and "two dashes" - with respect to the plane of symmetry σ. All this information is contained in the tables themselves. For example, all *g*-type representations are positive for the inversion operation, and *u*-type representations are negative. The last column of each table shows which irreducible representations are translations (*T*) and rotations (*R*) in a given symmetry group.

Tables of characters have properties, the simplest of which are listed below:

1. The table of characters is always "square", i.e. the number of irreducible representations (table rows) is equal to the number of symmetry classes (table columns);
2. The sum of the squares of the dimensions of irreducible representations is equal to the order of the group (that is, the total number of symmetry elements);
3. Each group has one totally symmetric representation, in which the characters are equal to +1 for all elements of symmetry;
4. For any irreducible representation (that is, a row in the table), except for a totally symmetric one, the sum of characters is zero (the sum is taken over all elements of the group, that is, the character is multiplied by the number of symmetry elements in the class).
5. The sum of the squares of the characters for all irreducible representations of any symmetry class (i.e., a table column) is equal to the order of the group divided by the number of symmetry elements in this class.

These rules can be used both to build character tables and to validate them.

Triclinic

C_1	E	
A	1	**T; R**

C_i	E	I	
A_g	1	1	**R**
A_u	1	−1	***T***

Monoclinic

$C_{1h} \equiv C_s$	E	σ_h	
A'	1	1	T_x, T_y; R_z
A''	1	−1	T_z; R_x, R_y

C_2	E	C_2	
A	1	1	T_z; R_z
B	1	−1	T_x, T_y; R_x, R_y

C_{2h}	E	C_2	I	σ_h	
A_g	1	1	1	1	R_z
B_g	1	−1	1	−1	R_x, R_y
A_u	1	1	−1	−1	T_z
B_u	1	−1	−1	1	T_x, T_y

Orthorhombic

C_{2v}	E	C_2	σ_v	σ_x	
A_1	1	1	1	1	T_z
A_2	1	1	−1	−1	R_z
B_1	1	−1	1	−1	T_x; R_y
B_2	1	−1	−1	1	T_y; R_x

$D_2 = V$	E	C_2^z	C_2^y	C_2^x	
A_1	1	1	1	1	
B_1	1	1	−1	−1	T_z; R_z
B_2	1	−1	1	−1	T_y; R_y
B_3	1	−1	−1	1	T_x; R_x

$D_{2h} = V_h$	E	C_2^2	C	C_2^1	I	σ_z	σ_y	σ_x	
A_g	1	1	1	1	1	1	1	1	
B_{1g}	1	1	−1	−1	1	1	−1	−1	R_z
B_{2g}	1	−1	1	−1	1	−1	1	−1	R_y
B_{3g}	1	−1	−1	1	1	−1	−1	1	R_x
A_u	1	1	1	1	−1	−1	−1	−1	
B_{1u}	1	1	−1	−1	−1	−1	1	1	T_z
B_{2u}	1	−1	1	−1	−1	1	−1	1	T_y
B_{3u}	1	−1	−1	1	−1	1	1	−1	T_x

Trigonal ($\varepsilon = e^{2\pi i/3}$)

C_3	E	C_3	C_3^2		
A	1	1	1		T_z; R_z
E { $E(1)$	1	ε	ε^*	(T_x, T_y);	(R_x, R_y)
E { $E(2)$	1	ε^*	ε		

$C_{3i} = S_6$	E	C_3	C_3^2	I	S_6^5	S_6	
A_g	1	1	1	1	1	1	R_z
E_g { $E_g(1)$	1	ε	ε^*	1	ε	ε^*	(R_x, R_y)
E_g { $E_g(2)$	1	ε^*	ε	1	ε^*	ε	
A_u	1	1	1	−1	−1	−1	T_z
E_u { $E_u(1)$	1	ε	ε^*	−1	$-\varepsilon$	$-\varepsilon^*$	(T_x, T_y)
E_u { $E_u(2)$	1	ε^*	ε	−1	$-\varepsilon^*$	$-\varepsilon$	

C_{3v}	E	$2C_3$	$3\sigma_v$		
A_1	1	1	1		T_z
A_2	1	1	−1		R_z
E	2	−1	0	(T_x, T_y);	(R_x, R_y)

D_3	E	$2C_3$	$3C_2$		
A_1	1	1	1		
A_2	1	1	−1		T_z; Rz
E	2	−1	0	(T_x, T_y);	(R_x, R_y)

D_{3d}	E	$2C_3$	$3C_2$	I	$2S_6$	$3\sigma_d$	
A_{1g}	1	1	1	1	1	1	
A_{2g}	1	1	−1	1	1	−1	R_z
E_g	2	−1	0	2	−1	0	(R_x, R_y)
A_{1u}	1	1	1	−1	−1	−1	
A_{2u}	1	1	−1	−1	1	1	T_z
E_u	2	−1	0	−2	1	0	(T_x, T_y)

Tetragonal

C_4	E	C_4	C_2	C_4^3	
A	1	1	1	1	T_z; R_z
B	1	−1	1	−1	
$E\{E(1)$	1	i	−1	$-i$	(T_x, T_y); (R_x, R_y)
$E\{E(2)$	1	$-i$	−1	i	

S_4	E	S_4	C_2	S_4^3	
A	1	1	1	1	R_z
B	1	−1	1	−1	T_z
$E\{E(1)$	1	i	−1	$-i$	(T_x, T_y); (R_x, R_y)
$E\{E(2)$	1	$-i$	−1	i	

C_{4h}	E	C_4	C_2	C_4^3	I	S_4^3	σ_h	S_4	
A_g	1	1	1	1	1	1	1	1	R_z
B_g	1	−1	1	−1	1	−1	1	−1	
$E_g\{E_g(1)$	1	i	−1	$-i$	1	i	−1	$-i$	$(R_x,$
$E_g\{E_g(2)$	1	$-i$	−1	i	1	$-i$	−1	i	$R_y)$
A_u	1	1	1	1	−1	−1	−1	−1	T_z
B_u	1	−1	1	−1	−1	1	−1	1	
$E_u\{E_u(1)$	1	i	−1	$-i$	−1	$-i$	1	i	$(T_x,$
$E_u\{E_u(2)$	1	$-i$	−1	i	1	i	1	$-i$	$T_y)$

D_4	E	$2C_4$	C_2	$2C_2'$	$2C_2''$	
A_1	1	1	1	1	1	
A_2	1	1	1	−1	−1	T_z; R_z
B_1	1	−1	1	1	−1	
B_2	1	−1	1	−1	1	
E	2	0	−2	0	0	(T_x, T_y); (R_x, R_y)

C_{4v}	E	$2C_4$	C_2	$2\sigma_v$	$2\sigma_d$		
A_1	1	1	1	1	1		T_z
A_2	1	1	1	–1	–1		R_z
B_1	1	–1	1	1	–1		
B_2	1	–1	1	–1	1		
E	2	0	–2	0	0	(T_x, T_y);	(R_x, R_y)

$D_{2d} = V_d = S_{4u}$	E	$2S_4$	C_2	$2C_2'$	$2\sigma_d$		
A_1	1	1	1	1	1		
A_2	1	1	1	–1	–1		R_z
B_1	1	–1	1	1	–1		
B_2	1	–1	1	–1	1		T_z
E	2	0	–2	0	0	(T_x, T_y);	(R_x, R_y)

D_{4h}	E	$2C_4$	C_2	$2C_2'$	$2C_2''$	I	$2S_4$	σ_h	$2\sigma_v$	$2\sigma_d$	
A_{1g}	1	1	1	1	1	1	1	1	1	1	
A_{2g}	1	1	1	–1	–1	1	1	1	–1	–1	R_z
B_{1g}	1	–1	1	1	–1	1	–1	1	1	–1	
B_{2g}	1	–1	1	–1	1	1	–1	1	–1	1	
E_g	2	0	–2	0	0	2	0	–2	0	0	(R_x, R_y)
A_{1u}	1	1	1	1	1	–1	–1	–1	–1	–1	
A_{2u}	1	1	1	–1	–1	–1	–1	–1	1	1	T_z
B_{1u}	1	–1	1	1	–1	–1	1	–1	–1	1	
B_{2u}	1	–1	1	–1	1	–1	1	–1	1	–1	
E_u	2	0	–2	0	0	–2	0	2	0	0	(T_x, T_y)

Hexagonal ($\varepsilon = e^{2\pi i/3}$, $\omega = e^{2\pi i/6}$)

C_6	E	C_6	C_3	C_2	C_3^2	C_6^5	
A	1	1	1	1	1	1	T_z; R_z
B	1	1	1	–1	1	–1	
E_1 $E_1(1)$	1	ω	$-\omega^*$	–1	$-\omega$	ω^*	T_x, T_y;
E_1 $E_1(2)$	1	ω^*	$-\omega$	–1	$-\omega^*$	ω	R_x, R_y
E_2 $E_2(1)$	1	$-\omega^*$	$-\omega$	1	$-\omega^*$	$-\omega$	
E_2 $E_2(2)$	1	$-\omega$	$-\omega^*$	1	$-\omega$	$-\omega^*$	

C_{3h}		E	C_3	C_3^2	σ_h	S_3	S_3^2	
A'		1	1	1	1	1	1	R_z
E'	$E'(1)$	1	ε	ε^*	1	ε	ε^*	T_x, T_y
	$E'(2)$	1	ε^*	ε	1	ε^*	ε	
A''		1	1	1	−1	−1	−1	T_z
E''	$E''(1)$	1	ε	ε^*	−1	$-\varepsilon$	$-\varepsilon^*$	R_x, R_y
	$E''(2)$	1	ε^*	ε	−1	$-\varepsilon^*$	$-\varepsilon$	

C_{6h}		E	C_6	C_3	C_2	C_3^2	C_6^5	I	S_3^2	S_6^5	σ_h	S_6	S_3	
A_g		1	1	1	1	1	1	1	1	1	1	1	1	R_z
B_g		1	−1	1	−1	1	−1	1	−1	1	−1	1	−1	
E_{1g}	$E_{1g}(1)$	1	ω	$-\omega^*$	−1	$-\omega$	ω^*	1	ω	$-\omega^*$	−1	$-\omega$	ω^*	R_x, R_y
	$E_{1g}(2)$	1	ω^*	$-\omega$	−1	$-\omega^*$	ω	1	ω^*	$-\omega$	−1	$-\omega^*$	ω	
E_{2g}	$E_{2g}(1)$	1	$-\omega^*$	$-\omega$	1	$-\omega^*$	$-\omega$	1	$-\omega^*$	$-\omega$	1	$-\omega^*$	$-\omega$	
	$E_{2g}(2)$	1	$-\omega$	$-\omega^*$	1	$-\omega$	$-\omega^*$	1	$-\omega$	$-\omega^*$	1	$-\omega$	$-\omega^*$	
A_u		1	1	1	1	1	1	−1	−1	−1	−1	−1	−1	T_z
B_u		1	−1	1	−1	1	−1	−1	1	−1	1	1	1	
E_{1u}	$E_{1u}(1)$	1	ω	−1	−1	$-\omega$	ω^*	−1	$-\omega$	ω^*	1	ω	$-\omega^*$	T_x, T_y
	$E_{1u}(2)$	1	ω^*	−1	−1	ω^*	ω	−1	$-\omega^*$	ω	1	ω^*	$-\omega$	
E_{2u}	$E_{2u}(1)$	1	$-\omega^*$	$-\omega$	1	ω^*	$-\omega$	−1	ω^*	ω	−1	ω^*	ω	
	$E_{2u}(2)$	1	$-\omega$	$-\omega^*$	1	$-\omega$	$-\omega^*$	−1	ω	ω^*	−1	ω	ω^*	

D_6	E	$2C_6$	$2C_3$	C_2	$3C_2'$	$3C_2''$		
A_1	1	1	1	1	1	1		
A_2	1	1	1	1	−1	−1	T_z;	R_z
B_1	1	−1	1	−1	1	−1		
B_2	1	−1	1	−1	−1	1		
E_1	2	1	−1	−2	0	0	T_x, T_y;	R_x, R_y
E_2	2	−1	−1	2	0	0		

C_{6v}	E	$2C_6$	$2C_3$	C_2	$3\sigma_v$	$3\sigma_d$		
A_1	1	1	1	1	1	1		T_z
A_2	1	1	1	1	−1	−1		R_z
B_1	1	−1	1	−1	1	−1		
B_2	1	−1	1	−1	−1	1		
E_1	2	1	−1	−2	0	0	T_x, T_y;	R_x, R_y
E_2	2	−1	−1	2	0	0		

D_{3h}	E	$2C_3$	$3C_2$	σ_h	$2S_3$	$3\sigma_v$	
A_1'	1	1	1	1	1	1	
A_2'	1	1	−1	1	1	−1	R_z
E'	2	−1	0	2	−1	0	T_x, T_y
A_1''	1	1	1	−1	−1	−1	
A_2''	1	1	−1	−1	−1	1	T_z
E''	2	−1	0	−2	1	0	R_x, R_y

D_{6h}	E	$2C_6$	$2C_3$	C_2	$3C_2'$	$3C_2''$	I	$2S_3$	$2S_6$	σ_h	$3\sigma_d$	$3\sigma_v$	
A_{1g}	1	1	1	1	1	1	1	1	1	1	1	1	
A_{2g}	1	1	1	1	−1	−1	1	1	1	1	−1	−1	R_z
B_{1g}	1	−1	1	−1	1	−1	1	−1	1	−1	1	−1	
B_{2g}	1	−1	1	−1	−1	1	1	−1	1	−1	−1	1	
E_{1g}	2	1	−1	−2	0	0	2	1	−1	−2	0	0	R_x, R_y
E_{2g}	2	−1	−1	2	0	0	2	−1	−1	2	0	0	
A_{1u}	1	1	1	1	1	1	−1	−1	−1	−1	−1	−1	
A_{2u}	1	1	1	1	−1	−1	−1	−1	−1	−1	1	1	T_z
B_{1u}	1	−1	1	−1	1	−1	−1	1	−1	1	−1	1	
B_{2u}	1	−1	1	−1	−1	1	−1	1	−1	1	1	−1	
E_{1u}	2	1	−1	−2	0	0	−2	−1	1	2	0	0	T_x, T_y
B_{2u}	2	−1	−1	2	0	0	−2	1	1	−2	0	0	

Cubic ($\varepsilon = e^{2\pi i/3}$)

T		E	$4C_3$	$4C_3^2$	$3C_2$	
A_g		1	1	1	1	
$E\{$	$E(1)$	1	ε	ε^*	1	
	$E(2)$	1	ε^*	ε	1	
F		3	0	0	−1	***T, R***

T_h		E	$4C_3$	$4C_3^2$	$3C_2$	I	$4S_6$	$4S_6^2$	$3\sigma_h$	
A_g		1	1	1	1	1	1	1	1	
$E_g\{$	$E_g(1)$	1	ε	ε^*	1	1	ε	ε^*	1	
	$E_g(2)$	1	ε^*	ε	1	1	ε^*	ε	1	
F_g		3	0	0	−1	3	0	0	−1	***R***
A_u		1	1	1	1	−1	−1	−1	−1	
$E_u\{$	$E_u(1)$	1	ε	ε^*	1	−1	$-\varepsilon$	$-\varepsilon^*$	−1	
	$E_u(2)$	1	ε^*	ε	1	−1	$-\varepsilon^*$	$-\varepsilon$	−1	
F_u		3	0	0	−1	−3	0	0	1	***T***

T_d	E	$8C_3$	$3C_2$	$6S_4$	$6\sigma_d$	
A_1	1	1	1	1	1	
A_2	1	1	1	−1	−1	
E	2	−1	2	0	0	
F_1	3	0	−1	1	−1	***R***
F_2	3	0	−1	−1	1	***T***

O	E	$8C_3$	$3C_2$	$6C_4$	$6C_2'$	
A_1	1	1	1	1	1	
A_2	1	1	1	−1	−1	
E	2	−1	2	0	0	
F_1	3	0	−1	1	−1	***T, R***
F_2	3	0	−1	−1	1	

O_h	E	$8C_3$	$3C_2$	$6C_4$	$6C_2'$	I	$8S_6$	$3\sigma_h$	$6S_4$	$6\sigma_d$	
A_{1g}	1	1	1	1	1	1	1	1	1	1	
A_{2g}	1	1	1	−1	−1	1	1	1	−1	−1	
E_g	2	−1	2	0	0	2	−1	2	0	0	
F_{1g}	3	0	−1	1	−1	3	0	−1	1	−1	***R***
F_{2g}	3	0	−1	−1	1	3	0	−1	−1	1	
A_{1u}	1	1	1	1	1	−1	−1	−1	−1	−1	
A_{2u}	1	1	1	−1	−1	−1	−1	−1	1	1	
E_u	2	−1	2	0	0	−2	1	−2	0	0	
F_{1u}	3	0	−1	1	−1	−3	0	1	−1	1	***T***
F_{2u}	3	0	−1	−1	1	−3	0	1	1	−1	

D2. Characters of irreducible representations of finite molecular groups with the 5th order principal axis of rotation. ($\varepsilon = e^{2\pi i/5}$).

C_5		E	C_5	C_5^2	C_5^3	C_5^4	
A		1	1	1	1	1	T_z, R_z
E_1	$E_1(1)$	1	ε	ε^2	ε^{2*}	ε^*	(T_x, T_y); (R_x, R_y)
	$E_1(2)$	1	ε^*	ε^{2*}	ε^2	ε	
E_2	$E_2(1)$	1	ε^2	ε^*	ε	ε^{2*}	
	$E_2(2)$	1	ε^{2*}	ε	ε^*	ε^2	

	C_{5h}	E	C_5	C_5^2	C_5^3	C_5^4	σ_h	S_5	S_5^7	S_5^3	S_5^9	
	A'	1	1	1	1	1	1	1	1	1	1	R_z
E_1	$E_1'(1)$	1	ε	ε^2	ε^{2*}	ε^*	1	ε	ε^2	ε^{*2}	ε^*	(T_x, T_y)
	$E_1'(2)$	1	ε^*	ε^{2*}	ε^2	ε	1	ε^*	ε^{*2}	ε^2	ε	
E_2	$E_2'(1)$	1	ε^2	ε^*	ε	ε^{2*}	1	ε^2	ε^*	ε	ε^{*2}	
	$E_2'(2)$	1	ε^{2*}	ε	ε^*	ε^2	1	ε^{*2}	ε	ε^*	ε^2	
	A''	1	1	1	1	1	−1	−1	−1	−1	−1	T_z
E_1''	$E_1''(1)$	1	ε	ε^2	ε^{2*}	ε^*	−1	$-\varepsilon$	$-\varepsilon^2$	$-\varepsilon^{*2}$	$-\varepsilon^*$	(R_x, R_y)
	$E_1''(2)$	1	ε^*	ε^{2*}	ε^2	ε	−1	$-\varepsilon^*$	$-\varepsilon^{*2}$	$-\varepsilon^2$	$-\varepsilon$	
E_2''	$E_2''(1)$	1	ε^2	ε^*	ε	ε^{2*}	−1	$-\varepsilon^2$	$-\varepsilon^*$	$-\varepsilon$	$-\varepsilon^{*2}$	
	$E_2''(2)$	1	ε^{2*}	ε	ε^*	ε^2	−1	$-\varepsilon^{*2}$	$-\varepsilon$	$-\varepsilon^*$	$-\varepsilon^2$	

D_5	E	$2C_5$	$2C_5^2$	$5C_2$	
A_1	1	1	1	1	
A_2	1	1	1	−1	T_z; R_z
E_1	2	2 cos 72°	2 cos 144°	0	T_x, T_y; R_x, R_y
E_2	2	2 cos 144°	2 cos 72°	0	

C_{5v}	E	$2C_5$	$2C_5^2$	$5\sigma_v$	
A_1	1	1	1	1	T_z
A_2	1	1	1	−1	R_z
E_1	2	2 cos 72°	2 cos 144°	0	T_x, T_y; R_x, R_y
E_2	2	2 cos 144°	2 cos 72°	0	

D_{5h}	E	$2C_5$	$2C_5^2$	$5C_2$	σ_h	$2S_5$	$2S_5^3$	$5\sigma_v$	
A_1'	1	1	1	1	1	1	1	1	
A_2'	1	1	1	−1	1	1	1	−1	R_z
E_1'	2	2 cos 72°	2 cos 144°	0	2	2 cos 72°	2 cos 144°	0	T_x, T_y
E_2'	2	2 cos 144°	2 cos 72°	0	2	2 cos 144°	2 cos 72°	0	
A_1''	1	1	1	1	−1	−1	−1	−1	
A_2''	1	1	1	−1	−1	−1	−1	1	T_z
E_1''	2	2 cos 72°	2 cos 144°	0	−2	−2 cos 72°	−2 cos 144°	0	R_x, R_y
E_2''	2	2 cos 144°	2 cos 72°	0	−2	−2 cos 144°	−2 cos 72°	0	

D_{5d}	E	$2C_5$	$2C_5^2$	$5C_2$	I	$2S_{10}^3$	$2S_{10}$	$5\sigma_d$	
A_{1g}	1	1	1	1	1	1	1	1	
A_{2g}	1	1	1	−1	1	1	1	−1	R_z
E_{1g}	2	2 cos 72°	2 cos 144°	0	2	2 cos 72°	2 cos 144°	0	R_x, R_y
E_{2g}	2	2 cos 144°	2 cos 72°	0	2	2 cos 144°	2 cos 72°	0	
A_{1u}	1	1	1	1	−1	−1	−1	−1	
A_{2u}	1	1	1	−1	−1	−1	−1	1	T_z
E_{1u}	2	2 cos 72°	2 cos 144°	0	−2	−2 cos 72°	−2 cos 144°	0	T_x, T_y
E_{2u}	2	2 cos 144°	2 cos 72°	0	−2	−2 cos 144°	−2 cos 72°	0	

I	E	$12C_5$	$12C_5^2$	$20C_3$	$15C_2$	
A	1	1	1	1	1	
F_1	3	−2 cos 144°	−2 cos 72°	0	−1	***T; R***
F_2	3	−2 cos 72°	−2 cos 144°	0	−1	
G	4	−1	−1	1	0	
H	5	0	0	−1	1	

I_h	E	$12C_5$	$12C_5^2$	$20C_3$	$15C_2$	I	$12S_{10}$	$12S_{10}^3$	$20S_6$	$15\sigma_h$	
A_g	1	1	1	1	1	1	1	1	1	1	
F_{1g}	3	−2cos 144°	−2cos 72°	0	−1	3	−2cos 72°	−2cos 144°	0	−1	***R***
F_{2g}	3	−2cos 72°	−2cos 144°	0	−1	3	−2cos 144°	−2cos 72°	0	−1	
G_g	4	−1	−1	1	0	4	−1	−1	1	0	
H_g	5	0	0	−1	1	5	0	0	−1	1	
A_u	1	1	1	1	1	−1	−1	−1	−1	−1	
F_{1u}	3	−2cos 144°	−2cos 72°	0	−1	−3	2cos 72°	2cos 144°	0	1	***T***
F_{2u}	3	−2cos 72°	−2cos 144°	0	−1	−3	2cos 144°	2cos 72°	0	1	
G_u	4	−1	−1	1	0	−4	1	1	−1	0	
H_u	5	0	0	−1	1	−5	0	0	1	−1	

D3. Characters of irreducible representations of the infinite groups $C_{\infty v}$ and $D_{\infty v}$ of linear molecules

To designate representations, both spectroscopic symbols and electronic states symbols (in brackets) of linear molecules are used. In the presence of an axis of symmetry of infinite order, the number of states of type E is also infinite; however, only types A_1 and E_1 are realized in normal vibrations of molecules, while the other types are possible only for overtones of bending vibrations.

$C_{\infty v}$	E	$2C_\infty^\varphi$	$\infty\sigma_v$	
A_1 (Σ^+)	1	1	1	T_z
A_2 (Σ^-)	1	1	−1	R_z
E_1 (Π)	2	2 cos φ	0	(T_x, T_y), (R_x, R_y)
E_2 (Δ)	2	2 cos 2φ	0	
E_3 (Φ)	2	2 cos 3φ	0	
...	...	...	...	

$D_{\infty h}$	E	$2C_\infty^\varphi$	σ_h	∞C_2	$\infty\sigma_v$	$2S_\infty^\varphi$	$I \equiv S_2$	
A_{1g} (Σ_g^+)	1	1	1	1	1	1	1	
A_{1u} (Σ_u^+)	1	1	−1	−1	1	−1	−1	T_z
A_{2g} (Σ_g^-)	1	1	1	−1	−1	1	1	R_z
A_{2u} (Σ_u^-)	1	1	−1	1	−1	−1	−1	
E_{1g} (Π_g)	2	2 cos φ	−2	0	0	−2 cos φ	2	R_x, R_y
E_{1u} (Π_u)	2	2 cos φ	2	0	0	2 cos φ	−1	T_x, T_y
E_{2g} (Δ_g)	2	2 cos 2φ	2	0	0	2 cos 2φ	2	
E_{2u} (Δ_u)	2	2 cos 2φ	−2	0	0	−2 cos 2φ	−1	
E_{3g} (Φ_g)	2	2 cos 3φ	2	0	0	−2 cos 3φ	2	
E_{3u} (Φ_u)	2	2 cos 3φ	2	0	0	2 cos 3φ	−2	
...	..	...	...	...	...	...	...	

Appendix E: Correlation tables

Since the positional symmetry group of an atom or molecular group in the crystal lattice is a subgroup of the factor group of the crystal, there are always correlations between the irreducible representations of both groups that establish which irreducible representations of the site group are generated by the irreducible representations of the crystal group. The difficulty, however, lies in the fact that some groups of the crystal allow several variants of correlations (see the "correlation tree" in Fig. 5.6). In the correlation tables, these variants are represented by different columns of irreducible representations relating to the same group of positional symmetry. The top row of the table indicates the symmetry elements that are common to both symmetry groups, positional and crystal. It is the correct choice of the common element of symmetry that guarantees finding the necessary correlations and subsequent analysis of oscillations by symmetry.

Monoclinic

C_{2h}	C_2	C_s	C_i
A_g	A	A'	A_g
B_g	B	A''	A_g
A_u	A	A''	A_u
B_u	B	A'	A_u

Rhombic

		$\sigma(zx)$	$\sigma(yz)$
C_{2v}	C_2	C_s	C_s
A_1	A	A'	A'
A_2	A	A''	A''
B_1	B	A'	A''
B_2	B	A''	A'

D_2	$C_2(z)$	$C_2(y)$	$C_2(x)$
A	A	A	A
B_1	A	B	B
B_2	B	A	B
B_3	B	B	A

D_{2h}	D_2	$C_2(z)$ C_{2v}	$C_2(y)$ C_{2v}	$C_2(x)$ C_{2v}	$C_2(z)$ C_{2h}	$C_2(y)$ C_{2h}	$C_2(x)$ C_{2h}
A_g	A	A_1	A_1	A_1	A_g	A_g	A_g
B_{1g}	B_1	A_2	B_2	B_1	A_g	B_g	B_g
B_{2g}	B_2	B_1	A_2	B_2	B_g	A_g	B_g
B_{3g}	B_3	B_2	B_1	A_2	B_g	B_g	A_g
A_u	A	A_2	A_2	A_2	A_u	A_u	A_u
B_{1u}	B_1	A_1	B_1	B_2	A_u	B_u	B_u
B_{2u}	B_2	B_2	A_1	B_1	B_u	A_u	B_u
B_{3u}	B_3	B_1	B_2	A_1	B_u	B_u	A_u

D_{2h}	$C_2(z)$ C_2	$C_2(y)$ C_2	$C_2(x)$ C_2	$\sigma(xy)$ C_s	$\sigma(zx)$ C_s	$\sigma(yz)$ C_s
A_g	A	A	A	A'	A'	A'
B_{1g}	A	B	B	A'	A''	A''
B_{2g}	B	A	B	A''	A'	A''
B_{3g}	B	B	A	A''	A''	A'
A_u	A	A	A	A''	A''	A''
B_{1u}	A	B	B	A''	A'	A'
B_{2u}	B	A	B	A'	A''	A'
B_{3u}	B	B	A	A'	A'	A''

Trigonal

C_{3v}	C_3	C_s
A_1	A	A'
A_2	A	A''
E	$E(1) + E(2)$	$A' + A''$

D_3	C_3	C_2
A_1	A	A
A_2	A	B
E	$E(1) + E(2)$	$A + B$

S_6	C_3	C_i
A_g	A	A_g
$E_g(1)$	$E(1)$	A_g
$E_g(2)$	$E(2)$	A_g
A_u	A	A_u
$E_u(1)$	$E(1)$	A_u
$E_u(2)$	$E(2)$	A_u

D_{3d}	D_3	C_{3v}	S_6	C_3	C_{2h}	C_2	C_s	C_i
A_{1g}	A_1	A_1	A_g	A	A_g	A	A'	A_g
A_{2g}	A_2	A_2	A_g	A	B_g	B	A''	A_g
E_g	E	E	$E_g(1)+E_g(2)$	$E(1)+E(2)$	A_g+B_g	$A+B$	$A'+A''$	$2A_g$
A_{1u}	A_1	A_2	A_u	A	A_u	A	A''	A_u
A_{2u}	A_2	A_1	A_u	A	B_u	B	A'	A_u
E_u	E	E	$E_u(1)+E_u(2)$	$E(1)+E(2)$	A_u+B_u	$A+B$	$A'+A''$	$2A_u$

Tetragonal

C_4	C_2
A	A
B	A
$E(1)$	B
$E(2)$	B

S_4	C_2
A	A
B	A
$E(1)$	B
$E(2)$	B

C_{4h}	S_4	C_4	C_{2h}	C_2	C_s	C_i
A_g	A	A	A_g	A	A'	A_g
B_g	B	B	A_g	A	A'	A_g
$E_g(1)$	$E(1)$	$E(1)$	B_g	B	A''	A_g
$E_g(2)$	$E(2)$	$E(2)$	B_g	B	A''	A_g
A_u	B	A	A_u	A	A''	A_u
B_u	A	B	A_u	A	A''	A_u
$E_u(1)$	$E(1)$	$E(1)$	B_u	B	A'	A_u
$E_u(2)$	$E(2)$	$E(2)$	B_u	B	A'	A_u

D_4	C_4	C_2	$\frac{C_2'}{C_2}$	$\frac{C_2''}{C_2}$
A_1	A	A	A	A
A_2	A	A	B	B
B_1		A	A	B
B_2	B	A	B	A
E	$E(1)+E(2)$	$2B$	$A+B$	$A+B$

C_{4v}	C_4	σ_v C_{2v}	σ_d C_{2v}	C_2	σ_v C_s	σ_d C_s
A_1	A	A_1	A_1	A	A'	A'
A_2	A	A_2	A_2	A	A''	A''
B_1	B	A_1	A_2	A	A'	A''
B_2	B	A_2	A_1	A	A''	A'
E	$E(1)+E(2)$	$B_1 + B_2$	$B_1 + B_2$	$2B$	$A'+A''$	$A'+A''$

D_{2d}	S_4	$C_2 \rightarrow C_2(z)$ D_2	C_{2v}	C_2	C_2' C_2	C_s
A_1	A	A	A_1	A	A	A'
A_2	A	B_1	A_2	A	B	A''
B_1	B	A	A_2	A	A	A''
B_2	B	B_1	A_1	A	B	A'
E	$E(1)+E(2)$	$B_2 + B_3$	$B_1 + B_2$	$2B$	$A + B$	$A'+A''$

D_{4h}	$C_2' \rightarrow C_2'$ D_{2d}	$C_2'' \rightarrow C_2'$ D_{2d}	C_{4v}	D_4	C_{4h}	S_4	C_4
A_{1g}	A_1	A_1	A_1	A_1	A_g	A	A
A_{2g}	A_2	A_2	A_2	A_2	A_g	A	A
B_{1g}	B_1	B_2	B_1	B_1	B_g	B	B
B_{2g}	B_2	B_1	B_2	B_2	B_g	B	B
E_g	E	E	E	E	$E_g(1)+E_g(2)$	$E(1)+E(2)$	$E(1)+E(2)$
A_{1u}	B_1	B_1	A_2	A_1	A_u	B	A
A_{2u}	B_2	B_2	A_1	A_2	A_u	B	A
B_{1u}	A_1	A_2	B_2	B_1	B_u	A	B
B_{2u}	A_2	A_1	B_1	B_2	B_u	A	B
E_u	E	E	E	E	$E_u(1)+E_u(2)$	$E(1)+E(2)$	$E(1)+E(2)$

	C_2'	C_2''	C_2'	C_2''	C_2, σ_v	C_2, σ_d	C_2'	C_2''
D_{4h}	D_{2h}	D_{2h}	D_2	D_2	C_{2v}	C_{2v}	C_{2v}	C_{2v}
A_{1g}	A_g	A_g	A	A	A_1	A_1	A_1	A_1
A_{2g}	B_{1g}	B_{1g}	B_1	B_1	A_2	A_2	B_1	B_1
B_{1g}	A_g	B_{1g}	A	B_1	A_1	A_2	A_1	B_1
B_{2g}	B_{1g}	A_g	B_1	A	A_2	A_1	B_1	A_1
E_g	$B_{2g}+B_{3g}$	$B_{2g}+B_{3g}$	B_2+B_3	B_2+B_3	B_1+B_2	B_1+B_2	A_2+B_2	A_2+B_2
A_{1u}	A_u	A_u	A	A	A_2	A_2	A_2	A_2
A_{2u}	B_{1u}	B_{1u}	B_1	B_1	A_1	A_1	B_2	B_2
B_{1u}	A_u	B_{1u}	A	B_1	A_2	A_1	A_2	B_2
B_{2u}	B_{1u}	A_u	B_1	A	A_1	A_2	B_2	A_2
E_u	$B_{2u}+B_{3u}$	$B_{2u}+B_{3u}$	B_2+B_3	B_2+B_3	B_1+B_2	B_1+B_2	A_1+B_1	A_1+B_1

	C_2	C_2'	C_2''	C_2	C_2'	C_2''	σ_h	σ_v	σ_d	
D_{4h}	C_{2h}	C_{2h}	C_{2h}	C_2	C_2	C_2	C_s	C_s	C_s	C_i
A_{1g}	A_g	A_g	A_g	A	A	A	A'	A'	A'	A_g
A_{2g}	A_g	B_g	B_g	A	B	B	A'	A''	A''	A_g
B_{1g}	A_g	A_g	B_g	A	A	B	A'	A'	A''	A_g
B_{2g}	A_g	B_g	A_g	A	B	A	A'	A''	A'	A_g
E_g	$2B_g$	A_g+B_g	A_g+B_g	$2B$	$A+B$	$A+B$	$2A''$	$A'+A''$	$A'+A''$	$2A_g$
A_{1u}	A_u	A_u	A_u	A	A	A	A''	A''	A''	A_u
A_{2u}	A_u	B_u	B_u	A	B	B	A''	A'	A'	A_u
B_{1u}	A_u	A_u	B_u	A	A	B	A''	A''	A'	A_u
B_{2u}	A_u	B_u	A_u	A	B	A	A''	A'	A''	A_u
E_u	$2B_u$	A_u+B_u	A_u+B_u	$2B$	$A+B$	$A+B$	$2A'$	$A'+A''$	$A'+A''$	$2A_u$

Hexagonal

C_6	C_3	C_2
A	A	A
B	A	B
$E_1(1)$	$E(1)$	B
$E_1(2)$	$E(2)$	B
$E_2(1)$	$E(1)$	A
$E_2(2)$	$E(2)$	A

C_{3h}	C_3	C_s
A'	A	A'
E'	$E(1)+E(2)$	$2A'$
A''	A	A''
E''	$E(1)+E(2)$	$2A''$

C_{6h}	C_{3h}	C_6	C_{3i}	C_3	C_{2h}	C_2	C_s	C_i
A_g	A'	A	A_g	A	A_g	A	A'	A_g
B_g	A''	B	A_g	A	B_g	B	A''	A_g
$E_{1g}(1)$	$E''(1)$	$E_1(1)$	$E_g(1)$	$E(1)$	B_g	B	A''	A_g
$E_{1g}(2)$	$E''(2)$	$E_1(2)$	$E_g(2)$	$E(2)$	B_g	B	A''	A_g
$E_{2g}(1)$	$E'(1)$	$E_2(1)$	$E_g(1)$	$E(1)$	A_g	A	A'	A_g
$E_{2g}(2)$	$E'(2)$	$E_2(2)$	$E_g(2)$	$E(2)$	A_g	A	A'	A_g
A_u	A''	A	A_u	A	A_u	A	A''	A_u
B_u	A'	B	A_u	A	B_u	B	A'	A_u
$E_{1u}(1)$	$E'(1)$	$E_1(1)$	$E_u(1)$	$E(1)$	B_u	B	A'	A_u
$E_{1u}(2)$	$E'(2)$	$E_1(2)$	$E_u(2)$	$E(2)$	B_u	B	A'	A_u
$E_{2u}(1)$	$E''(1)$	$E_2(1)$	$E_u(1)$	$E(1)$	A_u	A	A''	A_u
$E_{2u}(2)$	$E''(2)$	$E_2(2)$	$E_u(2)$	$E(2)$	A_u	A	A''	A_u

D_6	C_6	C_2' D_3	C_2'' D_3	C_3	D_2	C_2 C_2	C_2' C_2	C_2'' C_2
A_1	A	A_1	A_1	A	A	A	A	A
A_2	A	A_2	A_2	A	B_1	A	B	B
B_1	B	A_1	A_2	A	B_2	B	A	B
B_2	B	A_2	A_1	A	B_3	B	B	A
E_1	$E_1(1) + E_1(2)$	E	E	$E(1) + E(2)$	$B_2 + B_3$	$2B$	$A + B$	$A + B$
E_2	$E_2(1) + E_2(2)$	E	E	$E(1) + E(2)$	$A + B_1$	$2A$	$A + B$	$A + B$

C_{6v}	C_6	σ_v C_{3v}	σ_d C_{3v}	C_3	$\sigma_v \to \sigma(zx)$ C_{2v}	C_2	σ_v C_s	σ_d C_s
A_1	A	A_1	A_1	A	A_1	A	A'	A'
A_2	A	A_2	A_2	A	A_2	A	A''	A''
B_1	B	A_1	A_2	A	B_1	B	A'	A''
B_2	B	A_2	A_1	A	B_2	B	A''	A'
E_1	$E_1(1)+E_1(2)$	E	E	$E(1)+E(2)$	$B_1 + B_2$	$2B$	$A'+A''$	$A'+A''$
E_2	$E_2(1)+E_2(2)$	E	E	$E(1)+E(2)$	$A_1 + A_2$	$2A$	$A'+A''$	$A'+A''$

					$\sigma_h \rightarrow \sigma_v(zy)$		σ_h	σ_v
D_{3h}	C_{3h}	D_3	C_{3v}	C_3	C_{2v}	C_2	C_s	C_s
A_1'	A'	A_1	A_1	A	A_1	A	A'	A'
A_2'	A'	A_2	A_2	A	B_2	B	A'	A''
E'	$E'(1)+E'(2)$	E	E	$E(1)+E(2)$	$A_1 + B_2$	$A + B$	$2A'$	$A'+A''$
A_1''	A''	A_1	A_2	A	A_2	A	A''	A''
A_2''	A''	A_2	A_1	A	B_1	B	A''	A'
E''	$E''(1)+E''(2)$	E	E	$E(1)+E(2)$	$A_2 + B_1$	$A + B$	$2A''$	$A'+A''$

								$\sigma_h \rightarrow \sigma(xy)$
		C_2'	C_2''			C_2''	C_2'	$\sigma_v \rightarrow \sigma(yz)$
D_{6h}	D_6	D_{3h}	D_{3h}	C_{6v}	C_{6h}	D_{3d}	D_{3d}	D_{2h}
A_{1g}	A_1	A_1'	A_1'	A_1	A_g	A_{1g}	A_{1g}	A_{1g}
A_{2g}	A_2	A_2'	A_2'	A_2	A_g	A_{2g}	A_{2g}	B_{1g}
B_{1g}	B_1	A_1''	A_2''	B_2	B_g	A_{2g}	A_{1g}	B_{2g}
B_{2g}	B_2	A_2''	A_1''	B_1	B_g	A_{1g}	A_{2g}	B_{3g}
E_{1g}	E_1	E''	E''	E_1	$E_{1g}(1)+E_{1g}(2)$	E_g	E_g	$B_{2g}+B_{3g}$
E_{2g}	E_2	E'	E'	E_2	$E_{2g}(1)+E_{2g}(2)$	E_g	E_g	A_g+B_{1g}
A_{1u}	A_1	A_1''	A_1''	A_2	A_u	A_{1u}	A_{1u}	A_u
A_{2u}	A_2	A_2''	A_2''	A_1	A_u	A_{2u}	A_{2u}	B_{1u}
B_{1u}	B_1	A_1'	A_2'	B_1	B_u	A_{2u}	A_{1u}	B_{2u}
B_{2u}	B_2	A_2'	A_1'	B_2	B_u	A_{1u}	A_{2u}	B_{3u}
E_{1u}	E_1	E'	E'	E_1	$E_{1u}(1)+E_{1u}(2)$	E_u	E_u	$B_{2u}+B_{3u}$
E_{2u}	E_2	E''	E''	E_2	$E_{2u}(1)+E_{2u}(2)$	E_u	E_u	A_u+B_{1u}

			C_2'	C_2''	σ_v	σ_d	
D_{6h}	C_6	C_{3h}	D_3	D_3	C_{3v}	C_{3v}	C_{3i}
A_{1g}	A	A'	A_1	A_1	A_1	A_1	A_g
A_{2g}	A	A'	A_2	A_2	A_2	A_2	A_g
B_{1g}	B	A''	A_1	A_2	A_2	A_1	A_g
B_{2g}	B	A''	A_2	A_1	A_1	A_2	A_g
E_{1g}	$E_1(1)+E_1(2)$	$E'(1)+E''(2)$	E	E	E	E	$E_g(1)+E_g(2)$
E_{2g}	$E_2(1)+E_2(2)$	$E'(1)+E'(2)$	E	E	E	E	$E_g(1)+E_g(2)$
A_{1u}	A		A_1	A_1	A_2	A_2	A_u
A_{2u}	A		A_2	A_2	A_1	A_1	A_u
B_{1u}	B		A_1	A_2	A_1	A_2	A_u
B_{2u}	B		A_2	A_1	A_2	A_1	A_u
E_{1u}	$E_1(1)+E_1(2)$	$E'(1)+E'(2)$	E	E	E	E	$E_u(1)+E_u(2)$
E_{2u}	$E_2(1)+E_2(2)$	$E''(1)+E''(2)$	E	E	E	E	$E_u(1)+E_u(2)$

D_{6h}	C_3	D_2	C_2 C_{2v}	C_2' C_{2v}	C_2'' C_{2v}	C_2 C_{2h}	C_2' C_{2h}	C_2'' C_{2h}
A_{1g}	A	A	A_1	A_1	A_1	A_g	A_g	A_g
A_{2g}	A	B_1	A_2	B_1	B_1	A_g	B_g	B_g
B_{1g}	A	B_2	B_1	A_2	B_2	B_g	A_g	B_g
B_{2g}	A	B_3	B_2	B_2	A_2	B_g	B_g	A_g
E_{1g}	$E(1)+E(2)$	B_2+B_3	B_1+B_2	A_2+B_2	A_2+B_2	$2B_g$	A_g+B_g	A_g+B_g
E_{2g}	$E(1)+E(2)$	$A+B_1$	A_1+A_2	A_1+B_1	A_1+B_1	$2A_g$	A_g+B_g	A_g+B_g
A_{1u}	A	A	A_2	A_2	A_2	A_u	A_u	A_u
A_{2u}	A	B_1	A_1	B_2	B_2	A_u	B_u	B_u
B_{1u}	A	B_2	B_2	A_1	B_1	B_u	A_u	B_u
B_{2u}	A	B_3	B_1	B_1	A_1	B_u	B_u	A_u
E_{1u}	$E(1)+E(2)$	B_2+B_3	B_1+B_2	A_1+B_1	A_1+B_1	$2B_u$	A_u+B_u	A_u+B_u
E_{2u}	$E(1)+E(2)$	$A+B_1$	A_1+A_2	A_2+B_2	A_2+B_2	$2A_u$	A_u+B_u	A_u+B_u

D_{6h}	C_2 C_2	C_2' C_2	C_2'' C_2	σ_h C_s	σ_d C_s	σ_v C_s	C_i
A_{1g}	A	A	A	A'	A'	A'	A_g
A_{2g}	A	B	B	A'	A''	A''	A_g
B_{1g}	B	A	B	A''	A'	A''	A_g
B_{2g}	B	B	A	A''	A''	A'	A_g
E_{1g}	$2B$	$A+B$	$A+B$	$2A''$	$A'+A''$	$A'+A''$	$2A_g$
E_{2g}	$2A$	$A+B$	$A+B$	$2A'$	$A'+A''$	$A'+A''$	$2A_g$
A_{1u}	A	A	A	A''	A''	A''	A_u
A_{2u}	A	B	B	A''	A'	A'	A_u
B_{1u}	B	A	B	A'	A''	A'	A_u
B_{2u}	B	B	A	A'	A'	A''	A_u
E_{1u}	$2B$	$A+B$	$A+B$	$2A'$	$A'+A''$	$A'+A''$	$2A_u$
E_{2u}	$2A$	$A+B$	$A+B$	$2A''$	$A'+A''$	$A'+A''$	$2A_u$

Cubic

T	C_3	D_2	C_2
A	A	A	A
$E(1)$	$E(1)$	A	A
$E(2)$	$E(2)$	A	A
F	$A+E(1)+E(2)$	$B_1+B_2+B_3$	$A+2B$

T_h	T	C_{3i}	C_3	D_{2h}
A_g	A	A_g	A	A_g
$E_g(1)$	$E(1)$	$E_g(1)$	$E(1)$	A_g
$E_g(2)$	$E(2)$	$E_g(2)$	$E(2)$	A_g
F_g	F	$A_g + E_g(1) + E_g(2)$	$A + E(1) + E(2)$	$B_{1g} + B_{2g} + B_{3g}$
A_u	A	A_u	A	A_u
$E_u(1)$	$E(1)$	$E_u(1)$	$E(1)$	A_u
$E_u(2)$	$E(2)$	$E_u(2)$	$E(2)$	A_u
F_u	F	$A_u + E_u(1) + E_u(2)$	$A + E(1) + E(2)$	$B_{1u} + B_{2u} + B_{3u}$

T_h	D_2	C_{2v}	C_{2h}	C_2	C_s	C_1
A_g	A	A_1	A_g	A	A'	A_g
$E_g(1)$	A	A_1	A_g	A	A'	A_g
$E_g(2)$	A	A_1	A_g	A	A'	A_g
F_g	$B_1 + B_2 + B_3$	$A_2 + B_1 + B_2$	$A_g + 2B_g$	$A + 2B$	$A' + 2A''$	$3A_g$
A_u	A	A_2	A_u	A	A''	A_u
$E_u(1)$	A	A_2	A_u	A	A''	A_u
$E_u(2)$	A	A_2	A_u	A	A''	A_u
F_u	$B_1 + B_2 + B_3$	$A_1 + B_1 + B_2$	$A_u + 2B_u$	$A + 2B$	$2A' + A''$	$3A_u$

T_d	T	C_{3v}	C_3	D_{2d}
A_1	A	A_1	A	A_1
A_2	A	A_2	A	B_1
E	$E(1) + E(2)$	E	$E(1) + E(2)$	$A_1 + B_1$
F_1	F	$A_2 + E$	$A + E(1) + E(2)$	$A_2 + E$
F_2	F	$A_1 + E$	$A + E(1) + E(2)$	$B_2 + E$

T_d	S_4	D_2	C_{2v}	C_2	C_s
A_1	A	A	A_1	A	A'
A_2	B	A	A_2	A	A''
E	$A + B$	$2A$	$A_1 + A_2$	$2A$	$A' + A''$
F_1	$A + E(1) + E(2)$	$B_1 + B_2 + B_3$	$A_2 + B_1 + B_2$	$A + 2B$	$A' + 2A''$
F_2	$B + E(1) + E(2)$	$B_1 + B_2 + B_3$	$A_1 + B_1 + B_2$	$A + 2B$	$2A' + A''$

O	T	D_4	D_3	C_4	C_3
A_1	A	A_1	A_1	A	A
A_2	A	B_1	A_2	B	A
E	$E(1) + E(2)$	$A_1 + B_1$	E	$A + B$	$E(1) + E(2)$
F_1	F	$A_2 + E$	$A_2 + E$	$A + E(1) + E(2)$	$A + E(1) + E(2)$
F_2	F	$B_2 + E$	$A_1 + E$	$B + E(1) + E(2)$	$A + E(1) + E(2)$

O	$3C_2$ D_2	C_2, $2C_2'$ D_2	C_2 C_2	C_2' C_2
A_1	A	A	A	A
A_2	A	B_1	A	B
E	$2A$	$A + B_1$	$2A$	$A + B$
F_1	$B_1 + B_2 + B_3$	$B_1 + B_2 + B_3$	$A + 2B$	$A + 2B$
F_2	$B_1 + B_2 + B_3$	$A + B_2 + B_3$	$A + 2B$	$2A + B$

O_h	O	T_d	T_h	D_{4h}	D_{3d}
A_{1g}	A_1	A_1	A_g	A_{1g}	A_{1g}
A_{2g}	A_2	A_2	A_g	B_{1g}	A_{2g}
E_g	E	E	$E_g(1)+E_g(2)$	$A_{1g} + B_{1g}$	E_g
F_{1g}	F_1	F_1	F_g	$A_{2g} + E_g$	$A_{2g} + E_g$
F_{2g}	F_2	F_2	F_g	$B_{2g} + E_g$	$A_{1g} + E_g$
A_{1u}	A_1	A_2	A_u	A_{1u}	A_{1u}
A_{2u}	A_2	A_1	A_u	B_{1u}	A_{2u}
E_u	$\boldsymbol{E}$	E	$E_u(1)+E_u(2)$	$A_{1u} + B_{1u}$	E_u
F_{1u}	F_1	F_2	F_u	$A_{2u} + E_u$	$A_{2u} + E_u$
F_{2u}	F_2	F_1	F_u	$B_{2u} + E_u$	$A_{1u} + E_u$

Appendix F: Selection Rules for Raman Scattering and Infrared Absorption

System	Class		Raman Tensor				Dipole moment		
Monoclinic			$\begin{vmatrix} a & d & \cdot \\ d & b & \cdot \\ \cdot & \cdot & c \end{vmatrix}$		$\begin{vmatrix} \cdot & \cdot & e \\ \cdot & \cdot & f \\ e & f & \cdot \end{vmatrix}$		M_x	M_y	M_z
$z \parallel C_2$	2	C_2	A, z		B, x,y			B	A
$z \perp \sigma_h$	m	C_{1h}	A', x,y		A'', z			A'	A''
$z \parallel C_2$	$2/m$	C_{2h}	A_g		B_g			B_u	A_u
Rhombic			$\begin{vmatrix} a & \cdot & \cdot \\ \cdot & b & \cdot \\ \cdot & \cdot & c \end{vmatrix}$	$\begin{vmatrix} \cdot & d & \cdot \\ d & \cdot & \cdot \\ \cdot & \cdot & \cdot \end{vmatrix}$	$\begin{vmatrix} \cdot & \cdot & e \\ \cdot & \cdot & \cdot \\ e & \cdot & \cdot \end{vmatrix}$	$\begin{vmatrix} \cdot & \cdot & \cdot \\ \cdot & \cdot & f \\ \cdot & f & \cdot \end{vmatrix}$			
$x, y, z \parallel C_2^x, C_2^y, C_2^z$	222	D_2	A	B_1, z	B_2, y	B_3, x	B_3	B_2	B_1
$z \parallel C_2^z,\ x \parallel \sigma_y$	$mm2$	C_{2v}	A_1, z	A_2	B_1, x	B_2, y	B_1	B_2	A_1
$z \parallel C_2^z,\ x \parallel \sigma_y$	mmm	D_{2h}	A_g	B_{1g}	B_{2g}	B_{3g}	B_{3u}	B_{2u}	B_{1u}
Trigonal			$\begin{vmatrix} a & \cdot & \cdot \\ \cdot & a & \cdot \\ \cdot & \cdot & b \end{vmatrix}$	$\begin{vmatrix} c & d & e \\ d & -c & f \\ e & f & \cdot \end{vmatrix}$	$\begin{vmatrix} d & -c & -f \\ -c & -d & e \\ -f & e & \cdot \end{vmatrix}$				
$z \parallel C_3$	3	C_3	A, z	E, x	E, y			E	A
	$\bar{3}$	C_{3i}	A_g	$E_g, 1$	$E_g, 2$			E_u	A_u
			↓	$\begin{vmatrix} c & \cdot & \cdot \\ \cdot & -c & d \\ \cdot & d & \cdot \end{vmatrix}$	$\begin{vmatrix} \cdot & -c & -d \\ -c & \cdot & \cdot \\ -d & \cdot & \cdot \end{vmatrix}$				

$z \parallel C_3$, $x \parallel C_2$	32	D_3	A_1		E, x	E, y	E	A_2
	$\bar{3}\,m$	D_{3d}	A_{1g}		E_g, 1	E_g, 2	E_u	A_{2u}
			↓		$\begin{vmatrix} c & \cdot & d \\ \cdot & -c & \cdot \\ d & \cdot & \cdot \end{vmatrix}$	$\begin{vmatrix} \cdot & -c & \cdot \\ -c & \cdot & d \\ \cdot & d & \cdot \end{vmatrix}$		
$z \parallel C_3$, $x \parallel \sigma_v$	3m	C_{3v}	A_1, z		E, x	E, y	E	A_1
			$\begin{vmatrix} a & \cdot & \cdot \\ \cdot & a & \cdot \\ \cdot & \cdot & b \end{vmatrix}$		$\begin{vmatrix} c & d & \cdot \\ d & -c & \cdot \\ \cdot & \cdot & \cdot \end{vmatrix}$ $\begin{vmatrix} \cdot & \cdot & e \\ \cdot & \cdot & f \\ e & f & \cdot \end{vmatrix}$	$\begin{vmatrix} \cdot & \cdot & -f \\ \cdot & \cdot & e \\ -f & e & \cdot \end{vmatrix}$		
Tetragonal								
$z \parallel C_4$	4	C_4	A, z	B	E, x	E, y	E	A
	$4/m$	C_{4h}	A_g	B_g	E_g, 1	E_g, 2	E_u	A_u
			↓	↓	↓	$\begin{vmatrix} \cdot & \cdot & f \\ \cdot & \cdot & -e \\ f & -e & \cdot \end{vmatrix}$		
$z \parallel S_4$	$\bar{4}$	S_4	A	B, z	E, x	E, y	E	B
			↓	$\begin{vmatrix} c & \cdot & \cdot \\ \cdot & -c & \cdot \\ \cdot & \cdot & \cdot \end{vmatrix}$ $\begin{vmatrix} \cdot & d & \cdot \\ d & \cdot & \cdot \\ \cdot & \cdot & \cdot \end{vmatrix}$	$\begin{vmatrix} \cdot & \cdot & e \\ \cdot & \cdot & \cdot \\ e & \cdot & \cdot \end{vmatrix}$	$\begin{vmatrix} \cdot & \cdot & \cdot \\ \cdot & \cdot & e \\ \cdot & e & \cdot \end{vmatrix}$	
$z \parallel C_4$, $x \parallel \sigma_v$	4*mm*	C_{4v}	A, z	B_1	B_2	E, x	E, y	E	A_1
			↓	↓	↓	$\begin{vmatrix} \cdot & \cdot & \cdot \\ \cdot & \cdot & e \\ \cdot & e & \cdot \end{vmatrix}$	$\begin{vmatrix} \cdot & \cdot & -e \\ \cdot & \cdot & \cdot \\ -e & \cdot & \cdot \end{vmatrix}$		
$z \parallel C_4$, $x \parallel C_2'$	422	D_4	A_1	B_1	B_2	E, x	E, y	E	A_2
	$4/mmm$	D_{4h}	A_{1g}	B_{1g}	B_{2g}	E_g, 1	E_g, 2	E_u	A_{2u}
			↓	↓	↓	↓	$\begin{vmatrix} \cdot & \cdot & e \\ \cdot & \cdot & \cdot \\ e & \cdot & \cdot \end{vmatrix}$		

$z \parallel S_4,\ x \parallel C_2'$	$\bar{4}2m$	D_{2d}	A_1	B_1	B_2, z	E, x	E, y	E	B_2
Hexagonal			$\begin{vmatrix} a & \cdot & \cdot \\ \cdot & a & \cdot \\ \cdot & \cdot & b \end{vmatrix}$	$\begin{vmatrix} \cdot & \cdot & c \\ \cdot & \cdot & d \\ c & d & \cdot \end{vmatrix}$	$\begin{vmatrix} \cdot & \cdot & -d \\ \cdot & \cdot & c \\ -d & c & \cdot \end{vmatrix}$	$\begin{vmatrix} e & f & \cdot \\ f & -e & \cdot \\ \cdot & \cdot & \cdot \end{vmatrix}$	$\begin{vmatrix} f & -e & \cdot \\ -e & -f & \cdot \\ \cdot & \cdot & \cdot \end{vmatrix}$		
$z \parallel C_6$	6	C_6	A, z	E_1, x	E_1, y	$E_2, 1$	$E_2, 2$	E_1	A
$z \parallel C_3$	$\bar{6}$	C_{3h}	A''	$E'', 1$	$E'', 2$	E'', x	E'', y	E''	A''
$z \parallel C_6$	$6/m$	C_{6h}	A_g	$E_{1g}, 1$	$E_{1g}, 2$	$E_{2g}, 1$	$E_{2g}, 2$	E_{1u}	A_u
			↓	$\begin{vmatrix} \cdot & \cdot & \cdot \\ \cdot & \cdot & c \\ \cdot & c & \cdot \end{vmatrix}$	$\begin{vmatrix} \cdot & \cdot & -c \\ \cdot & \cdot & \cdot \\ -c & \cdot & \cdot \end{vmatrix}$	$\begin{vmatrix} d & \cdot & \cdot \\ \cdot & -d & \cdot \\ \cdot & \cdot & \cdot \end{vmatrix}$	$\begin{vmatrix} \cdot & -d & \cdot \\ -d & \cdot & \cdot \\ \cdot & \cdot & \cdot \end{vmatrix}$		
$z \parallel C_6, x \parallel C_2'$	622	D_6	A_1	E_1, x	E_1, y	$E_2, 1$	$E_2, 2$	E_1	A_2
$z \parallel C_6, x \parallel C_2'$	$6/mmm$	D_{6h}	A_{1g}	$E_{1g}, 1$	$E_{1g}, 2$	$E_{2g}, 1$	$E_{2g}, 2$	E_{1u}	A_{2u}
$z \parallel C_3, x \parallel C_2$	$\bar{6}m2$	D_{3h}	A_1''	$E'', 1$	$E'', 2$	E'', x	E'', y	E''	A_2''
			↓	$\begin{vmatrix} \cdot & \cdot & c \\ \cdot & \cdot & \cdot \\ c & \cdot & \cdot \end{vmatrix}$	$\begin{vmatrix} \cdot & \cdot & \cdot \\ \cdot & \cdot & c \\ \cdot & c & \cdot \end{vmatrix}$	↓	↓		
$z \parallel C_6, x \parallel \sigma_v$	$6mm$	C_{6v}	A_1, z	E_1, x	E_1, y	$E_2, 1$	$E_2, 2$	E_1	A_1
Cubic	$\begin{vmatrix} a & \cdot & \cdot \\ \cdot & a & \cdot \\ \cdot & \cdot & a \end{vmatrix}$	$\begin{vmatrix} b+1/2c & \cdot & \cdot \\ \cdot & b-1/2c & \cdot \\ \cdot & \cdot & -b \end{vmatrix}$		$\begin{vmatrix} c-1/2b & \cdot & \cdot \\ \cdot & c+1/2b & \cdot \\ \cdot & \cdot & -c \end{vmatrix}$		$\begin{vmatrix} \cdot & \cdot & \cdot \\ \cdot & \cdot & d \\ \cdot & d & \cdot \end{vmatrix}$	$\begin{vmatrix} \cdot & \cdot & d \\ \cdot & \cdot & \cdot \\ d & \cdot & \cdot \end{vmatrix}$	$\begin{vmatrix} \cdot & d & \cdot \\ d & \cdot & \cdot \\ \cdot & \cdot & \cdot \end{vmatrix}$	M
$x, y, z \parallel C_2^x, C_2^y, C_2^z$	23	T	A	$E, 1$	$E, 2$	F, x	F, y	F, z	F
	$m3$	T_h	A_g	$E_g, 1$	$E_g, 2$	$F_g, 1$	$F_g, 2$	$F_g, 3$	F_u
			↓	$\begin{vmatrix} b & \cdot & \cdot \\ \cdot & b & \cdot \\ \cdot & \cdot & -b \end{vmatrix}$	$\begin{vmatrix} -\sqrt{3}b & \cdot & \cdot \\ \cdot & \sqrt{3}b & \cdot \\ \cdot & \cdot & 0 \end{vmatrix}$	↓	↓	↓	
$x, y, z \parallel C_4$ axes	432	O	A_1	$E, 1$	$E, 2$	$F_2, 1$	$F_2, 2$	$F_2, 3$	F_1
$x, y, z \parallel S_4$ axes	$\bar{4}3m$	T_d	A_1	$E, 1$	$E, 2$	F_2, x	F_2, y	F_2, z	F_2
$x, y, z \parallel C_4$ *axes*	$m3m$	O_h	A_{1g}	$E_g, 1$	$E_g, 2$	$F_{2g}, 1$	$F_{2g}, 2$	$F_{2g}, 3$	F_{1u}

All components of the Raman tensors of A type vibrations, class C_1, and A_g type, class C_i, are nonzero. In those classes where vibrations that are active in IR and RS are encountered, the directions of the polarization vector in the vibration are indicated next to the designation of the irreducible representation in RS, for example: $F_{2,x}$.

Appendix G: Transformation of Raman tensor

The Raman tensor is defined in a coordinate system rigidly related to the crystallographic or molecular axes in a given point group. Very often in practical spectroscopy, the problem arises of obtaining and interpreting the Raman spectrum of a crystal rotated with respect to the position in which the Raman tensor is known. In addition, in some groups in the same scattering geometry, two different types of vibration symmetry can be recorded simultaneously, so it is necessary to separate them. Both of these problems are solved in the same way: by finding the RS tensor in a rotated coordinate system (i.e., determining the Raman tensor for a rotated crystal). In order to find the form of Raman tensor in the new coordinate system, it is necessary to "rotate" the original tensor by the angle θ. However, we will start with a simpler procedure - the transformation of the coordinates of the polar vector $\boldsymbol{w}$ when it is rotated through an arbitrary angle θ as shown in Fig. G.1 (or, which is the same, when the coordinate system is rotated by an angle θ in the opposite direction).

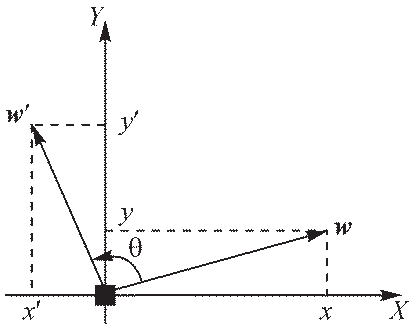

Fig. G.1. Rotation of the vector $\boldsymbol{w}$ around the z-axis by an angle θ

In this case, the new components x', y' will be written as

$$x' = x\cos\theta - y\sin\theta,$$
$$y' = x\sin\theta + y\cos\theta,$$
$$z' = z,$$

or, in matrix form,

$$\begin{matrix} x' \\ y' \\ z' \end{matrix} = \begin{matrix} cos\theta & -sin\theta & 0 \\ sin\theta & cos\theta & 0 \\ 0 & 0 & 1 \end{matrix} \begin{matrix} x \\ y \\ z \end{matrix} . \quad \text{(G.1)}$$

So, the matrix

$$R = \begin{matrix} cos\theta & -sin\theta & 0 \\ sin\theta & cos\theta & 0 \\ 0 & 0 & 1 \end{matrix} \quad \text{(G.2)}$$

is the transformation matrix of the polar vector components when the coordinate system is rotated by an angle θ around the z axis. It is easy to make sure that the transformation matrices when rotated around the x or y axes will be, respectively

$$R_x = \begin{matrix} 1 & 0 & 0 \\ 0 & cos\theta & -sin\theta \\ 0 & sin\theta & cos\theta \end{matrix} \quad \text{and} \quad R_y = \begin{matrix} cos\theta & 0 & -sin\theta \\ 0 & 1 & 0 \\ sin\theta & 0 & cos\theta \end{matrix} \quad \text{(G.3)}$$

The inverse transformation matrix, i.e. from x', y', z' to x, y, z, there is a matrix R^{-1}, the inverse of the matrix R. By the definition of the inverse, $R^{-1}R = E$, where E is the identity matrix. The elements of these two matrices are related by the equality $(R^{-1})_{\alpha\beta} = R_{\beta\alpha}$, which is easy to verify by changing θ to (–θ) in the matrix R, since the inverse transformation is a rotation by (–θ). Thus, in the transition from the new coordinate system to the old transformation matrix is

$$R_z^{-1} = \begin{matrix} cos\theta & sin\theta & 0 \\ -sin\theta & cos\theta & 0 \\ 0 & 0 & 1 \end{matrix} \quad \text{(G.4)}$$

If two polar vectors, $\boldsymbol{v}$ and $\boldsymbol{w}$, are linked by the relation $\boldsymbol{v} = \boldsymbol{Tw}$, where $\boldsymbol{T}$ is a tensor quantity, then upon rotation of the coordinate system we have

$$\boldsymbol{v'} = \boldsymbol{T'w'}.$$

Since $\boldsymbol{v'} = \boldsymbol{Rv}$, $\boldsymbol{w'} = \boldsymbol{Rw}$, then

$$\boldsymbol{Rv} = \boldsymbol{T'Rw},$$

or, multiplying both sides of the equality on the left by $\boldsymbol{R}^{-1}$,

$$\boldsymbol{v} = \boldsymbol{R}^{-1}\boldsymbol{T'Rw}$$

and

$$\boldsymbol{T} = \boldsymbol{R}^{-1}\boldsymbol{T'}\boldsymbol{R}.$$

Having performed two more times the procedure of multiplying both parts of the last relation by $\boldsymbol{R}$, $\boldsymbol{R}^{-1}$, we obtain the law of transformation of tensor quantities:

$$\boldsymbol{T'} = \boldsymbol{R}\boldsymbol{T}\boldsymbol{R}^{-1}, \tag{G.5}$$

where matrices $\boldsymbol{R}$ and $\boldsymbol{R}^{-1}$ are written above. Relationship (G.5) determines the transformation law for the Raman tensor.

In the cubic symmetry group O_h, when the laboratory axes x, y, z are parallel to the C_4 axes of the crystal, the Raman tensor of the totally symmetric vibration A_{1g} has the form

$$\begin{matrix} a & \cdot & \cdot \\ \cdot & a & \cdot \\ \cdot & \cdot & a \end{matrix},$$

components of the twofold degenerate vibration E_g

$$\begin{matrix} b & \cdot & \cdot \\ \cdot & b & \cdot \\ \cdot & \cdot & -2b \end{matrix} \qquad \begin{matrix} -3^{1/2}b & \cdot & \cdot \\ \cdot & 3^{1/2}b & \cdot \\ \cdot & \cdot & 0 \end{matrix},$$

and the components of the threefold degenerate vibration F_{2g}

$$\begin{matrix} \cdot & \cdot & \cdot \\ \cdot & \cdot & d \\ \cdot & d & \cdot \end{matrix} \qquad \begin{matrix} \cdot & \cdot & d \\ \cdot & \cdot & \cdot \\ d & \cdot & \cdot \end{matrix} \qquad \begin{matrix} \cdot & d & \cdot \\ d & \cdot & \cdot \\ \cdot & \cdot & \cdot \end{matrix}.$$

The complete tensor describing the scattering intensity can be represented as follows:

$$\begin{matrix} A_{1g} + 4E_g & F_{2g} & F_{2g} \\ F_{2g} & A_{1g} + 4E_g & F_{2g} \\ F_{2g} & F_{2g} & A_{1g} + 4E_g \end{matrix}.$$

We see that totally symmetric and twofold degenerate vibrations are characterized only by the diagonal terms of the Raman tensor and therefore will be recorded (or not recorded) simultaneously in the Raman

spectrum (see Fig. 5.10). Now let's rotate the crystal 45° around its z-axis. In this case, the Raman tensor of the totally symmetric vibration will not change, and the tensors of twofold and threefold degenerate vibrations are transformed to the form:

$$\boldsymbol{T'}(E_g,1) = \boldsymbol{RTR}^{-1} =$$

$$= \begin{matrix} cos\theta & -sin\theta & 0 \\ sin\theta & cos\theta & 0 \\ 0 & 0 & 1 \end{matrix} \begin{matrix} b & \cdot & \cdot \\ \cdot & b & \cdot \\ \cdot & \cdot & -2b \end{matrix} \begin{matrix} cos\theta & sin\theta & 0 \\ -sin\theta & cos\theta & 0 \\ 0 & 0 & 1 \end{matrix} =$$

$$\begin{matrix} b & \cdot & \cdot \\ \cdot & b & \cdot \\ \cdot & \cdot & -2b \end{matrix}$$

$$\boldsymbol{T'}(E_g,2) = \boldsymbol{RTR}^{-1} =$$

$$= \begin{matrix} cos\theta & -sin\theta & 0 \\ sin\theta & cos\theta & 0 \\ 0 & 0 & 1 \end{matrix} \begin{matrix} -3^{1/2}b & \cdot & \cdot \\ \cdot & 3^{1/2}b & \cdot \\ \cdot & \cdot & 0 \end{matrix} \begin{matrix} cos\theta & sin\theta & 0 \\ -sin\theta & cos\theta & 0 \\ 0 & 0 & 1 \end{matrix} =$$

$$\begin{matrix} \cdot & -\overline{3}b & \cdot \\ -\overline{3}b & \cdot & \cdot \\ \cdot & \cdot & \cdot \end{matrix}$$

$$F_{2g},1 \rightarrow \begin{matrix} \cdot & \cdot & -\frac{\overline{2}}{2}d \\ \cdot & \cdot & \frac{\overline{2}}{2}d \\ -\frac{\overline{2}}{2}d & \frac{\overline{2}}{2}d & \cdot \end{matrix} \qquad F_{2g},2 \rightarrow \begin{matrix} \cdot & \cdot & \frac{\overline{2}}{2}d \\ \cdot & \cdot & \frac{\overline{2}}{2}d \\ \frac{\overline{2}}{2}d & \frac{\overline{2}}{2}d & \cdot \end{matrix}$$

$$F_{2g},3 \rightarrow \begin{matrix} -d & \cdot & \cdot \\ \cdot & d & \cdot \\ \cdot & \cdot & \cdot \end{matrix}$$

And in this case, the total intensity tensor will be written as

$$\begin{matrix} A_{1g} + E_g + F_{2g} & 3E_g & F_{2g} \\ 3E_g & A_{1g} + E_g + F_{2g} & F_{2g} \\ F_{2g} & F_{2g} & A_{1g} + 4E_g \end{matrix}.$$

It is the last "rotated" tensor that allows one to determine the symmetry of vibrations in a garnet crystal of cubic symmetry and to make the assignment of vibrational modes in the Raman spectrum (see Fig. 8.10, Chapter 8).

Appendix H: Frequency of characteristic vibrations

Vibration frequency of diatomic molecules in the gas phase (except for Cl_2)

Molecule	Wavenumber, cm^{-1}
H_2	4157 (*ortho*) 4162 (*para*)
HD	3630
D_2	2993
HF	2907
HCl	2886
HBr	2558
HI	2233
Cl_2	556 (liquid)
Br_2	319
I_2	213
O_2	1555
CO	2140
NO	1877
N_2	2330

Vibrations of common triatomic molecules, linear and angular

		ν_1 Symmetrical stretching	ν_2 bending	ν_3 Asymmetrical stretching
CO_2	lin.	1286, 1388*	667	2349
SO_2	ang.	1147	517	1351
CS_2	lin.	658	397	1533
NO_2	ang.	1325	752	1610
NO_2^-	ang.	1327	806	1286
SH_2	ang.	2615	1183	2627
SiH_2	ang.	1995	999	1993

* Fermi-components $2\nu_2$ and ν_1

Vibrations of tetrahedral five-atomic molecules*

	ν_1	ν_2	ν_3	ν_4	References
CH_4	2915	1520	3072	1304	[1]
CD_4	2085	1075	2258	985	[1]
CF_4 (Liq.)	907	434	1257	630	[2,3]
CCl_4 (Liq.)	459	217	789	313	[4]
CBr_4	269	128	673	182	[5,6]
CI_4	180	89	560,570	122,130	[7,8]
SiH_4	2187	978	2183	910	[1]
SiF_4 (77K)	797	261	991	374	[9]
$SiCl_4$ (Liq.)	423	150	608,628,655	221	[10]
$SiBr_4$ (Liq.)	249	92	485	139	[6]
SiI_4	168	62	405	90	[7]
GeH_4	1989	820	2110	934	[1]
GeF_4	738	205	800	260	[11]
$GeCl_4$ (Liq.)	395	131	456	172	[6]
$GeBr_4$ (Liq.)	235	79	327	111	[6]
GeI_4	159	60	264	79	[7]
SnF_4	621	230	-	-	[12]
$SnCl_4$ (Sol.)	368	105	403	128	[6]
$SnBr_4$ (Liq.)	220	64	278	88	[6]
SnI_4	151	43	220	63	[7]
$PbCl_4$ (Liq)	327	93	349	110	[13]
$PbBr_4$	207	59	231	73	[14]
PbI_4	137	37	168	48	[15]
NH_4^+	3033	1685	3134	1397	[16]
SO_4^{2-}	981	451	1104	613	[16]

* For the numbering of vibrational modes and the corresponding eigen vectors, see Appendix I.

[1] *Kohlrausch K.W.E.* Ramanspektren. Leipzig, 1943.

[2] *Fournier R.P., Savoie R., Bessette F., Cabana A. J.* Chem. Phys. 1968. V. 49. P. 1159-1164.
[3] *Daly F.P., Hopkins A.G., Brown C.W.* Spectrochim. Acta. 1974. V. 30A. P. 2159-2163.
[4] *Chumaevskii N.A.* Russian J. Inorg. Chem., 1989. V. 34. P. 1416-1420.
[5] *Bahnick D.A., Bennett W.E., Person W.B.* J. Phys. Chem. 1969. V. 73. P. 2309-2316.
[6] *Dernova V.S., Kovalev I.F., Kozlova N.V. Voronkov M.G.* Doklady Academii Nayk. 1973. V. 211. P. 137-140.
[7] *Clark R.J.H., Dines T.J.* Inorg. Chem. 1980. V. 19. P. 1681-1686.
[8] *Stammreich H., Tavares Y., Bassist D.* Spectrochim. Acta. 1961. V. 17. P. 661-664.
[9] *Schettino V.* Chem. Phys. Lett. 1973. V. 18. P. 535-539.
[10] *Griffiths J.E.* Spectrochim. Acta. 1974. Vol. 30A, P. 169-180.
[11] *Schulz A., Klapötke T.M.* Spectrochim. Acta. 1995. V. 51A. P. 905-908.
[12] *Beattie R., Cheetham N., Gilson R., Livingston K.M.S., Reynolds D.J.* J. Chem. Soc. A: Inorg. Phys. Theor. 1971. P. 1910-1913.
[13] *Clark R.J.H., Hunter B.K.* J. Mol. Struct. 1971. V. 9. P. 354-356.
[14] *Delwaulle M.L.* Compt. Rend. 1955. V. 240. P. 2132.
[15] *Aleksandrovskaya A.M., Rigina I.V., Godnev I.N.* Optica and Spektroskopiya, 1959 V. 7. P. 844.
[16] *Gerzberg G.*, Infrared and Raman Spectra of Polyatomic Molecules. New York, 1945.

Frequency of stretching and bending vibrations of free (non-interacting) C-H, CH_2 and CH_3 groups

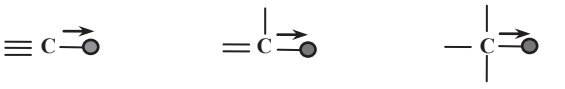

~3300 cm^{-1} 3000-3100 cm^{-1} 2800-2975 cm^{-}

Symmetrical, 2840 – 2860 cm^{-1}

Asymmetrical 2915 – 2935 cm^{-1}

Scissoring, δ 1450 cm^{-1}

Roking, ρ_r 720 cm^{-1}

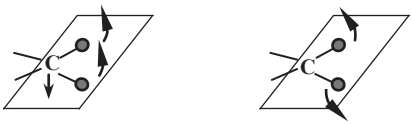

Wagging, ρ_w 1305 cm^{-}

Twisting, ρ_t 1300 cm^{-1}

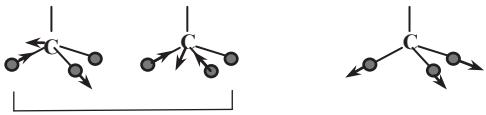

Components of one twofold degenerate stretching vibration 2950 – 2970 cm^{-1}

Symmetrical Stretching 2860 – 2880 cm^{-1}

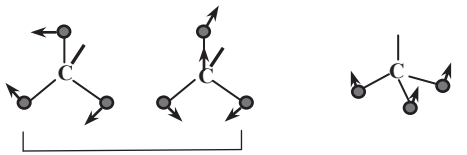

Components of one twofold degenerate bending vibration 1450 – 1470 cm^{-1}

Symmetrical bending (umbrella) 1365 – 1385 cm^{-1}

The probable vibrations of the carboxylate ion, $(-CO_2^-)$

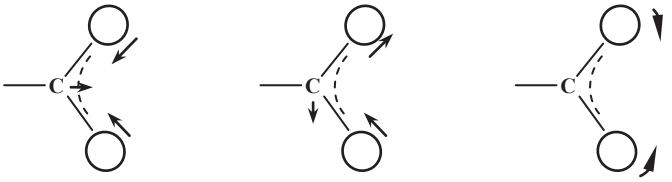

Symmetrical stretching, 1300-1420 cm^{-1}

Asymmetrical stretching, 1550-1610 cm^{-1}

Planar scissoring, δ 650-770 cm^{-1}

Frequency of stretching and bending vibrations of free (non-interacting) NH, NH_2 and NH_3 groups

R_2NH	Stretching 3350-3450 cm^{-1}	Bending in plane ~1600 cm^{-1}

RNH_2	ν_s 3270-3420 cm^{-1}	ν_{as} 3350-3500 cm^{-1}	δ 1590-1650 cm^{-1}

RNH_3	Symmetrical stretching 3150–3250 cm^{-1}	Twofold degenerated stretching 3250 – 3350 cm^{-1}	Symmetrical bending 1200 – 1300 cm^{-1}	Twofold degenerated bending 1450 – 1470 cm^{-1}

Frequency of stretching and bending vibrations of free (non-interacting) SiH_2 and SiH_3 groups

R_2SiH_2	Symmetrical and asymmetrical stretching 2110-2150 cm^{-1}	Scissoring δ 930-950 cm^{-1}	Rocking ρ_r 480-540 cm^{-1}	Wagging ρ_w 800-870 cm^{-1}	Torsional ρ_t 560-690 cm^{-1}

$RSiH_3$	Symmetrical and asymmetrical stretching 2140-2190 cm^{-1}	Symmetrical bending (umbrella) 910-930 cm^{-1}	Asymmetrical bending (umbrella) 930-950 cm^{-1}	Twofold Degenerated bending 680-720 cm^{-1}

Frequency of characteristic vibrations of organic compounds*

Wavenumber, cm^{-1}	Vibration	Compound
480-510	S-S stretch	dialkyl disulfides
615-630	ring deformation	monosubstituted benzenes
650-660	CCl stretch	primery chloroalkanes
620-715	CS stretch	dialkyl disulfides
585-740	CS stretch	alkyl disulfides
820-825	C_3O skeletal stretch	secondary alcohols
720-830	ring vibration	para-disubstituted benzenes
749-835	skeletal stretch	isopropyl group
877	OO stretch	hydrogen peroxide
850-900	symmetric CNC stretch	secondary amines
837-905	CC skeletal stretch	n-alkanes
830-930	symmetric COC stretch	aliphatic ethers
990-1010	trigonal ring breathing	meta-substituted benzenes
990-1010	trigonal ring breathing	mono-substituted benzenes
1015-1030	in-plain CH deformation	mono-substituted benzenes
1020-1060	ring vibration	ortho-disubstituted benzenes
950-1150	CC stretches	n-alkanes
1188-1196	symmetric CO_2 stretch	alkyl sulfates
1205	C_6H_5-C vibration	alkyl benzenes
1200-1230	ring vibration	para-disubstituted benzenes
1251-1270	in-plain CH deformation	*cis*-dialkyl ethylenes
1295-1305	CH_2 in-phase twist	n-alkanes
1175-1310	CH_2 twist and rock	n-alkanes
1290-1314	in-plain CH deformation	*trans*-dialkyl ethylenes
1330-1350	CH deformation	isopropyl group
1368-1385	CH_2 symmetric deformation	n-alkanes
1370-1390	ring stretch	naphthalenes
1385-1415	ring stretch	anthracenes
1465-1466	CH_2 deformation	n-alkanes
1446-1473	CH_3, CH_2 deformation	n-alkanes
1550-1630	ring stretches (doublet)	benzene derivatives
1590-1650	NH_2 scissors	primary amines
1649-1654	symmetric C=O stretch	carboxylic acids (cyclic dimmer)
1700-1725	C=O stretch	aliphatic ketones
1720-1740	C=O stretch	aliphatic aldehydes
2100-2160	C≡C stretch	alkyl acetylenes
2232-2251	C≡N stretch	aliphatic nitrides
2231-2301	C≡C stretch	dialkyl acetylenes
2560-2590	SH stretch	thiols
2849-2861	symmetric CH_2 stretch	n-alkanes
2883-2884	symmetric CH_3 stretch	n-alkanes
2912-2929	anti-symmetric CH_2 stretch	n-alkanes
2965-2969	anti-symmetric CH_3 stretch	n-alkanes
3000-3100	aromatic CH-stretch	benzene derivatives
3330-3400	Bonded anti-symmetric NH_2 stretch	primary amines

**Lin-Vien D., Colthup N.B., Fateley W.B., Graselli J.G.* The Handbook of Infrared and Raman Characteristic Frequencies of Organic Molecules. Academic Press: Boston. 1991.

Characteristic vibrational frequencies of common bonds

Bond	Wavenumber, cm^{-1}	Comment
R-C≡C-R′	2190-2260	Very strong in Raman
H-C≡C-R′	2100-2140	
R-C≡N	2210-2260	Strong in Raman
H-C≡N	2060-2090	
$[C≡N]^-$	2080	
C=C, C=N	1600-1700	
R>C=C=C<R′	1060-1130 (sym)	Weak in IR, strong in Raman
	1900-2000 (asym)	Strong in IR, weak in Raman
–N=C=O	1400-1450 (in phase)	Weak in IR, strong in Raman
	2250-2300 (out of phase)	Strong in IR, weak in Raman
–N=C=S	925-1090 (in phase)	Weak in IR, strong in Raman
	2000-2300(out of phase)	Strong in IR, weak in Raman
–N=C=N–	2100-2160	Strong in IR
H–N=S=O	1090 (in phase)	
	1261 (out of phase)	
Ph–N=S=O	1155 (in phase)	
	1306 (out of phase.)	
Me–N=C=S	CN: 2050-2109	
	CS: 718-837	
Me–S–C≡N	CN: 2080-2130	
	CS: 693-820	
=C=O	1715	This is the average. In compounds with electro-negative substituents, it rises to 1928 cm^{-1} (F–CO–F), with the formation of an H-bond it decreases to ~ 1640 cm^{-1}. Very useful for H-bond diagnostics. In conjugated systems, it also decreases to 1670 cm^{-1}.
–N=O	1580	This is the average. The frequency changes in the same way as in the case of = C = O
$-NO_2$	1350 (sym.)	
	1550 (asym)	
$–O–NO_2$	1250-1300 (sym)	
	1610-1650 (asym)	
Si–O–Si	1000-1100	Asymmetrical mode, weak in Raman
Si-OH	830-920	Si-O stretching
Si-Cl	470-550	
Si-F	800-1000	
P=O	1250-1350	The same tendencies as for =C=O and –N=O.
–S=O	1020-1060	
$–SO_2–$	1140-1160 (in phase)	
	1300-1350 (out of phase)	
C=S	1050-1400	
–S–S–	400-500	Strong in Raman
C–F	1000-1400	

C–Cl	600-800	Strong in Raman
C–Br	500-600	Strong in Raman
C–I	480-600	Strong in Raman
-Me-O-Me-	450-600	bridging oxygen in oxides

Frequency of X-H vibrations*

Bond**	Wavenumber, cm-1	Comment
Li-H	1360	
Be-H	1960	
B-H	2400	
F-H	3950-	This is the maximum value. The frequency greatly decreases with the formation of a hydrogen bond (up to 1450 cm^{-1} for a strong symmetric hydrogen bond $[F\cdots H\cdots F]^-$)
Na-H	1133	
Mg-H	1433	
Al-H	1700-1900	
Si-H	2050-2280	
P-H	2350-2440	Strong in Raman
S-H	2550-2600	Strong in Raman
Cl-H	2886-	This is the maximum value. The frequency greatly decreases with the formation of a hydrogen bond
K-H	956	
Ca-H	1260	
Ga-H	1830	
$(CH_3)_2GaH$	1869	
Ge-H	2120	
$(CH_3)_3GeH$	2049	
CH_3GeH_3	2085	
As-H	2150	
$(CH_3)_2AsH$	2080	
Se-H	2300	
Br-H	2560	
Rb-H	908	
Sr-H	1172	
In-H	1425	
Sn-H	1580	
Sb-H	1890	
Te-H	2070	
I-H	2230	
$(CH_3)_3PbH$	1709	

**F.A. Miller*, Spectra of X-H Systems. In: Course notes on the interpretation of infrared and Raman spectra. D.W Mayo, F.A. Miller, R.W. Hannah. New Jersey, Wiley-Interscience, 2003

K. Nakamoto, Infrared and Raman Spectra of Inorganic and Coordination Compounds, John Wiley & Sons, New Jersey, 2009

** About vibrations of C–H, N–H, O–H bonds see Chapter 11.

Vibrations of the benzene molecule C_6H_6 (group D_{6h}) (the Herzberg system was used for the numbering of modes)

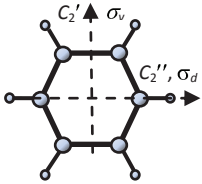

$\Gamma = 2A_{1g}$ (RS) + A_{2g} + $2B_{1g}$ + E_{1g} (RS) + $4E_{2g}$ (RS) + A_{2u} (IR) + $2B_{1u}$ + $2B_{2u}$ + $3E_{1u}$ (IR) + $2E_{2u}$

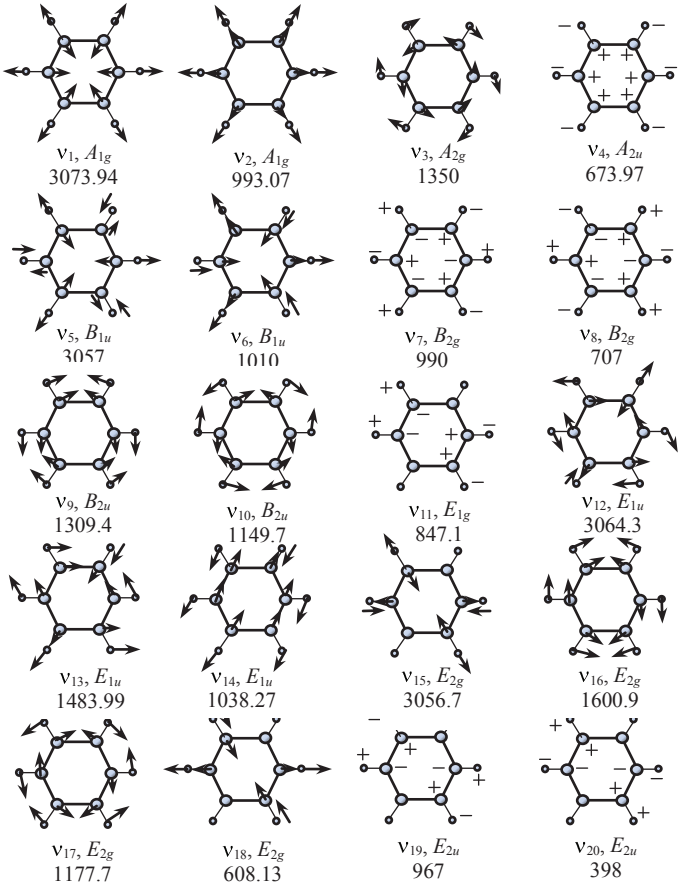

Gerzberg G., Infrared and Raman Spectra of Polyatomic Molecules. New York, 1945.
Callegari A., Merker U., Engels P., Srivastava H.K., Lehmann K.K., Scoles G. J. Chem. Phys. 2000. V. 113. P. 10583-10596.

Vibrations of Me-chalcogen, Me-halogen, and S-S bonds in metal-cluster compounds (Me - Mo, W, Re)*

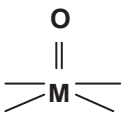

–Me=O, 920-960 cm^{-1}

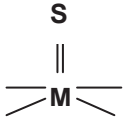

–Me=S, 510-530 cm^{-1}

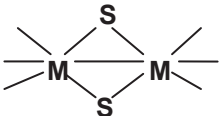

–Me–S_{br}, 360-450 cm^{-1}

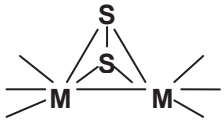

–Me–$(S_2)_{br}$, 230-340 cm^{-1}

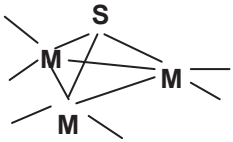

Me_3–S, 450-460 cm^{-1}

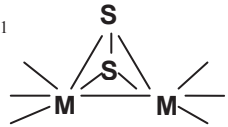

$(S–S)_{br}$, 540-600 cm^{-1}

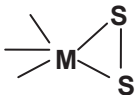

$(S–S)_{term}$, 500-520 cm^{-1}

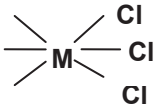

–Me–Cl, 300-340 cm^{-1}

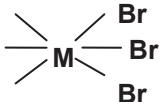

–Me–Br, 180-250 cm^{-1}

Fedin V. P., Kolesov B. A., Mironov Yu. V., Fedorov V. E., Polyhedron, 1989, V.8, P.2419-2423.

Fedin V.P., Sokolov M. N., Mironov Yu. V., Kolesov B.A., Tkachev S. V., Fedorov V. E., Inorg. Chim. Acta, 1990, V.167, p. 39-45.

Fedin V.P., Mironov Yu. V., Sokolov M. N., Kolesov B.A., Fedorov V. E., Yufit D. S., Struchkov Yu. T., Inorg. Chim. Acta, 1990, V.174, P. 275-282.

Fedin V.P., Sokolov M. N., Geras'ko O. A., Kolesov B.A., Fedorov V. E., Mironov A. V., Yufit D. S., Slovohotov Yu. L., Struchkov Yu. T., Inorg. Chim. Acta, 1990, v.175, p.217-229.

Fedin V.P., Kolesov B.A., Mironov Yu. V., Geras'ko O. A., Fedorov V. E., Polyhedron, 1991, V.10, p. 997- 1005.

Vibration frequencies of isotope substitutions of H_2O molecules (gas), cm^{-1} *

	v_1	v_2	v_3
$H_2{}^{16}O$	3657.05	1594.75	3755.93
$H_2{}^{17}O$	3653.15	1591.32	3748.32
$H_2{}^{18}O$	3649.69	1588.26	3741.57
$HD^{16}O$	2723.68	1403.48	3707.47
$D_2{}^{16}O$	2669.40	1178.38	2787.92
$T_2{}^{16}O$	2233.9	995.37	2366.61

* *L. Halonen, T. Carrington Jr.*, J. Chem. Phys. 88 (1988) 4171–4185.

Vibration frequency of monatomic semiconductor crystals, cm^{-1}

C, cubic diamond	1332
C, hexagonal diamond (Lonsdaleite)	1324*
Si	521
Ge	301

Misra A, Tyagi P.K., Yadav B.S., Rai, P. and Misra D. S. Appl. Phys. Lett. **89**, 071911 (2006).

Frequencies of optical phonons of diatom semiconductor crystals with a zinc blende-type structure T_d^2 .

	TO, cm^{-1}	*LO*, cm^{-1}
SiC[a]	783-796	829
ZnS[b]	274	349
ZnSe[b]	206	252
ZnTe[b]	179	206
CdTe[b]	140	171
BN[c]	1055	1285
BP[b]	829	829
AlP[b]	440	501
AlSb[b]	319	340
GaN[d]	562	748
GaP	367	403
GaAs	269	292
GaSb		229
InP	307	343
InAs	215	234
InSb[e]	185	197

[a]*Karch, K., P. Pavone, W. Windl, O. Schutt, D. Strauch*. Phys. Rev. B 50, 23 (1994), 17054-17063. *Nakashima, S, K. Tahara*. Phys. Rev. B 40, 9 (1989), 6339-6344. *Feldman, D.W., Parker, J.H., Choyke, W.J., Patrick, L.* Phys. Rev. 173, 3 (1968) 787. *Olego, D, Cardona, M.* Phys. Rev. B 25, 2 (1982), 1151-1160.

[b]*Wilkinson, G.R.* Raman spectra of ionic, covalent and metallic crystals. In: The Raman Effect, V.2, Marcel Dekker, Inc., New York, 1973

[c]*Shimada, K., T. Sota, K. Suzuku*. J. Appl. Phys. 84, 9 (1998), 4951 4958.

[d]*Zi, J., X. Wan, G. Wei, K. Zhang, X. Xie*, J. Phys. *Condens. Matter* 8 (1996), 6323-6328.

[e]*Price, D. L., J. M. Rowe, and R. M. Nickov*, Phys. Rev. B3, 4 (1971) 1268-1279.

Frequencies of optical phonons of diatom semiconductor crystals with a wurtzite-type structure (C_{6v}^4)

	A_1		E_1		E_2	
	LO	*TO*	*LO*	*TO*	1	2
BN[a]	1258	1006-1053	1281	1053-1085	476	989
AlN[b]	663	514	821	614	303	426
GaN[c]	710-735	533	741	558	145	560-579
InN[d]	586	447	593	476	87	488
BeO[e,f]	1085	678	1095	722	684	340
ZnO[f]	574		583			
ZnS[f]	352	274	352	274	55	
CdS[f]	305	234	307	243	43	256

[a] *Shimada, K., T. Sota, K. Suzuku*. J. Appl. Phys. 84, 9 (1998), 4951-4958.
[b] *Carlone, C, Lakin, K.M., Shanks, H.R*., J. Appl. Phys. 55 (1984) 4010.
[c] *Akasaki, I., H. Amano*, in Properties of Group III Nitrides, ed. Edgar J.H., EMIS Datareviews Series, N11, (1994), an INSPEC publication, 30-34.
Siegle, H., G. Kaczmarczyk, L. Filippidis, L. Litvinchuk, A. Hoffmann, C. Thornsen, Phys. Rev. B 55, 11 (1997), 7000-7004. *Zi, J., X. Wan, G. Wei, K. Zhang, X. Xie,* J. Phys. Condens. Matter 8 (1996), 6323-6328.
[d] *Davydov, V.Yu., Emtsev V.V., Goncharuk A.N., Smirnov A.N., Petrikov V.D., Mamutin V.V., Vekshin V.A., Ivanov S.V., Smirnov M.B. and Inushima T*., Appl. Phys. Lett 75 (1999), 3297-3299.
[e] *Loh E.* Phys. Rev. (1968), 166, 673.
[f] *Arguello C A, Rousseau D L and Porto S P S*. Phys. Rev. (1968) 181, 1351.

Vibrations of mineral crystals

The entire spectrum of vibrations of silicates (50-1200 cm^{-1}) can be conditionally divided into the following areas: 50-300 cm^{-1} – mixed translations of cations and anions SiO_4; 300-400 cm^{-1} – librational vibrations of SiO_4; 400-600 cm^{-1} – bending vibrations of SiO_4; 700-1200 cm^{-1} – stretching vibrations of SiO_4.

Characteristic vibrational frequencies of molecular fragments in mineral crystals, cm^{-1} (see also Appendix I)

$[CO_3]^{2-}$	1080-1090 (calcite, $CaCO_3$, smithsonite, $ZnCO_3$)
$[SO_4]^{2-}$	1000 (barite, $BaSO_4$, celestine, $SrSO_4$)
$[PO_4]^{3-}$	965 (apatite, $Ca_5(Fe, Cl,OH)[PO_4]_3$)

Frequency of totally symmetric stretching vibrations of SiO_4 anions in silicates depending on the number of oxygen atoms common to neighboring tetrahedra

0 - ortho-, 1- diortho-, 2 - ring- and chain-, 3 – ribbon-, 4 - frame silicates.

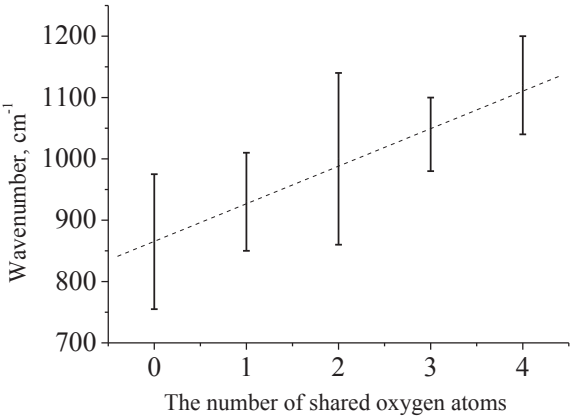

Appendix I: Vibrations of molecular ions in the structure of inorganic crystals

The structure of most of inorganic crystals is based on a mixed ionic-covalent bond, where the ionic component is produced from the interaction of cations and anions in the lattice, and the covalent one describes the bond within a molecular fragment that plays the role of one of the lattice ions (most often an anion). Molecular ions, as a rule, have a relatively simple geometry, and, moreover, weakly interact with neighboring cations in the lattice. For this reason, their vibration frequencies vary relatively little from compound to compound and are well known. The difficulty, however, lies in the fact that the positional symmetry of a molecular ion in the crystal lattice, as a rule, is lower than the symmetry of a free ion, which causes a partial change in its vibrational spectrum due to the splitting of degenerate modes. For example, the symmetry group of the free carbonate ion CO_3^{2-} D_{3h}, while in the aragonite crystal $CaCO_3$, it decreases to C_s, and in the crystal the observed spectrum of molecular ion vibrations is represented by a larger number of bands than in the spectrum of the free ion. In this case, however, the frequencies of its vibrations in the crystal remain in the same regions as the frequencies of the free ion and the knowledge of the latter greatly facilitates the task of interpreting the spectrum. To determine the vibration frequencies of an ion, one usually tries to obtain its vibrational spectrum either in the gas phase or in a frozen gas matrix. In some cases, the spectra of molecular ions in aqueous solutions are given. The latter case, despite its attractiveness, is fraught with the danger of obtaining distorted information, since water molecules, being strong donors of a hydrogen bond, can form it with the peripheral atoms of the ion, or coordinate the central atom. In both cases, the spectrum can differ markedly from the spectrum of an unperturbed molecular ion. Therefore, most often the spectrum of the ion in the crystalline phase is given, bearing in mind that it can vary somewhat from one composition of the crystal to another. In order to have initial information about possible vibrations of a molecular ion in a crystal, below are the eigen vectors of vibrations of free molecular ions of various geometries that are active in IR and Raman, which are common in inorganic chemistry. Usually, the frequencies of vibrations of the same type of symmetry, for example, totally symmetric stretching ones, change monotonically in a chemical series, for example, in a series of halides of elements of the third group. However, the ratio between the vibration frequencies of different types of symmetry of molecular ions of the same geometry, especially for molecules with an inversion center, can change in

the series when the ratio of the masses of the central atom and ligands changes. In order to take this circumstance into account, in each case the frequencies of the observed vibrations are given for ions of the same type with different ratios of the masses of their constituent atoms.

The information presented below also establishes a relation between the spectroscopic designation of the mode (ν_1, ν_2, ν_3, etc.) and the eigen vector (type of symmetry) of the corresponding vibration. Of course, these designations can be arbitrary, but usually they try to adhere to the same order to facilitate understanding of the text of the articles. For simple cases, this order is well known and is used in most of the work. However, for molecules where there are two or more vibrations of the same type of symmetry, the order of designation of vibrations by different authors may be violated, which, of course, must be borne in mind. This turned out to be especially critical for the benzene molecule and its derivatives, where, thanks to the large number of vibrational modes and the numerous works devoted to this topic, two notation systems were established: the Herzberg and Wilson system.

For degenerate vibrations of molecules, for which two or three main axes of symmetry are physically equivalent, the directions of displacements of atoms are given for only one component of the vibration. Other components correspond to offsets along the remaining axes of the coordinate system. The real vibration is a superposition of components (two for twofold degenerate mode, and three for threefold degenerate mode). Since the vibrational phases of each component are not determined, the total vibration in the general case is the displacement of an atom along the contour of an ellipse for twofold and an ellipsoid of rotation for threefold degenerate vibrations.

1. Linear triatomic molecules XY_2 of the $D_{\infty h}$ group

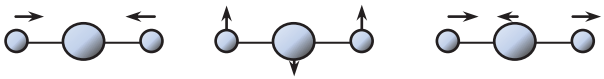

ν_1, $A_{1g}(\Sigma_g^+)$ ν_2, $E_{1u}(\Pi_u)$ ν_3, $A_{1u}(\Sigma_u^+)$

$$\Gamma = A_{1g}\,(\mathrm{RS}) + A_{1u}\,(\mathrm{IR}) + E_{1u}\,(\mathrm{IR})$$

Anions of metal halides XY_2

Anion	ν_1	ν_2	ν_3	References
$CuCl_2^-$	302	108	407	[1]
$CuBr_2^-$	194	81	326	[1]
CuI_2^-	148	65	279	[1]
ZnF_2	596	150	754	[2]
$ZnCl_2$	352	100-103	503	[3]
$ZnBr_2$	223	71	404	[3]
ZnI_2	163	68	337	[4]

[1] *Person I., Sandstrom M., Steel A.T., Zapetero M.J., Aakesson R.* Inorg. Chem. 1991. V. 30. P. 4075.
[2] *Givan A., Loewenschuss A.* J. Chem. Phys. 1980. V. 72. P. 3809.
[3] *Givan A., Loewenschuss A.* J. Chem. Phys. 1978. V. 68. P. 2228.
[4] *Konings R.J., Fearon J.E.* Chem. Phys. Lett. 1993 V. 206. P. 57.

2. Planar trigonal ions XY_3 (CO_3^{2-}, NO_3^-) of the D_{3h} group

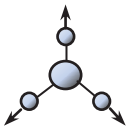

ν_1, A_1'

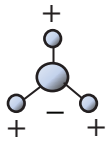

$\nu_2,$

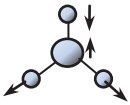

ν_3, E'

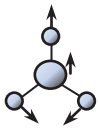

ν_4, E'

$$\Gamma = A_1' \text{ (RS)} + A_2'' \text{ (IR)} + 2E' \text{ (IR, RS)}$$

Vibrations of CO_3^{2-}, NO_3^- anions in the structure of crystals

Compound		ν_1 (A_1')	ν_2 (A_2'')	ν_3 (E')	ν_4 (E')	References
$Ca(CO_3)$	IR	-	879	1429-1492	706	[1]
calcite	RS	1087	-	1432	714	
$Ca(CO_3)$	IR	1080	866	1504,1492	711,706	[1]
aragonite	RS	1084	852	1460	704	
$Na(NO_3)$	IR	-	831	1405	692	[2]
	RS	1068	-	1385	724	
$K(NO_3)$	IR	-	828	1370	695	[2]
	RS	1049	-	1390	716	
SO_3 (gas)		1069	499	1392	530	[3]

[1] *Bhagavantam S., Venkatarayudu T.* Proc. Indian. Acad. Sci. 1939. V. 9A. P. 224.
[2] *Nakagawa I., Walter J.L.* J. Chem. Phys. 1969. V. 51. P. 1389.
[3] *Brassington N.J., Edwards H.G.M., Farwell D.W., Long D.A., Mansour H.R.* J. Raman Spectroscopy, 1978. V. 7. P. 154-157.

The vibrations of the CO_3^{2-} and NO_3^{2-} anions are given in the table as they were presented by the authors in relation to the spectrum of a free molecule of the D_{3h} group. In a crystal, both the symmetry of the modes and their number differ from what should be in a free molecule. The correspondence between the intramolecular vibrations of the free CO_3^{2-} ion and its vibrations in the aragonite crystal is shown in the figure below, and the vibration frequencies taking into account the crystal symmetry are shown in the table below.

Molecule D_{3h}	Site symmetry C_s	Crystal D_{2h}
$1\,A_1'$	A'	A_g, B_{1g}, B_{2g}, B_{3g}
$1\,A_2''$	A''	A_u, B_{1u}, B_{2u}, B_{3u}
$2E'$		

Correlations between intramolecular vibrations of a free CO_3^{2-} ion and its vibrations in an aragonite crystal

Vibrations of CO_3^{2-} anions in aragonite taking into account the crystal symmetry [3]

$\nu_1 (A_1')$		$\nu_2 (A_2'')$		$\nu_3 (E')$		$\nu_4 (E')$			
A_g	B_{3g}	A_g	B_{2g}	A_g	B_{1g} *or* B_{2g}	A_g	B_{1g}	B_{2g}	B_{3g}
1085		853	907	1462	1574	705	721	717	701

[3] *Frech R., Wang E.C., Bates J.B.* Spectrochim. Acta. 1980. V. 36A. P. 915-919.

3. Flat square molecules XY_4 of the D_{4h} group

Planar square ions of D_{4h} symmetry are not widespread in inorganic chemistry. However, coordination compounds often contain structural fragments that are not formally related to square ions, but the vibrations of which are well described precisely by the vibrations of square molecules. For example, if such a fragment is part of a polymer chain. Therefore, there is a need to refer to the theoretical spectrum of square molecules, and we present it here.

$\Gamma =$ 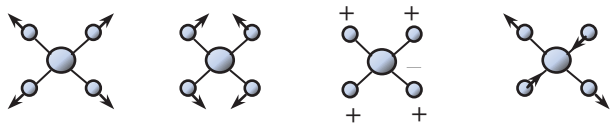

ν_1, A_{1g} ν_2, B_{1g} ν_3, A_{2u} ν_4, B_{2g}

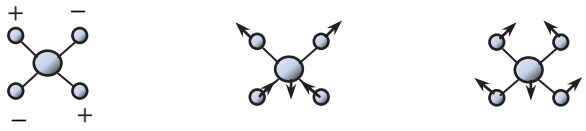

$\nu_5,$ ν_6, E_u ν_7, E_u

$$A_{1g}\,(\mathrm{RS}) + B_{1g}\,(\mathrm{RS}) + B_{2g}\,(\mathrm{RS}) + B_{1u} + A_{2u}\,(\mathrm{IR}) + 2E_u\,(\mathrm{IR})$$

Vibrations of planar square anions XY_4 transition metal halides

Anion	ν_1	ν_2	ν_3	ν_4	ν_6	ν_7	References
$[AuCl_4]^-$	347	171	151	324	356	173	[1,2]
$[AuBr_4]^-$	212	102	-	196	252	~110	[2-3]
$[AuI_4]^-$	148	75	-	110	192	113	[1]
$[PdCl_4]^{2-}$	303	164	150	275	321	161	[2,4]
$[PdBr_4]^{2-}$	188	103	114	172	243	104	[1,4]
$[PtCl_4]^{2-}$	330	171	147	312	313	165	[2,4]
$[PtBr_4]^{2-}$	208	106	105	194	227	112	[2,4]
$[PtI_4]^{2-}$	155	85	105	142	180	127	[1,4]

[1] *Ferraro, J. R.* "Low Frequency Vibrations of Inorganic and Coordination Compounds", Plenum Press, New York, 1971.
[2] *Degen L.A., Rowlands A.J.* Spectrochim. Acta. 1991. V. 47A. P. 1263.
[3] *Bosworth Y.M., Clark R.J.H.* J. Chem. Soc., Dalton Trans. 1975. P. 381.
[4] *Goggin P.L., Mink J.* J. Chem. Soc., Dalton Trans. 1974. P. 1479.

4. Tetrahedral ions XY_4 (T_d group)

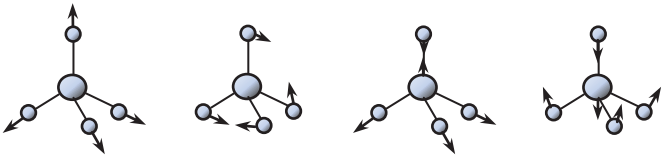

ν_1, ν_2, E ν_3, F_2 ν_4, F_2

$$\Gamma = A_1\,(\mathrm{RS}) + E\,(\mathrm{RS}) + 2F_2\,(\mathrm{IR, RS})$$

Tetrahedral (T_d) oxy-anions of transition elements (aqueous solutions)

Anion	ν_1	ν_2	ν_3	ν_4	References
RuO_4 (liquid)	822	323	914	334	[1]
OsO_4 (gas)	965	333	960	322	[2,3]
MnO_4^-	839	360	914	430	[4]
TcO_4^-	912	325	912	336	[4]
ReO_4^-	971	331	920	332	[4]
CrO_4^{2-}	846	349	890	368	[4]
MoO_4^{2-}	897	317	837	-	[4]
WO_4^{2-}	931	325	838	-	[4]
FeO_4^{2-}	778	-	800	320	[5]
RuO_4^{2-}	856	-	807	330	[5]
VO_4^{3-}	826	336	804	-	[4]

[1] *Griffith W.P.* J. Chem. Soc., Sect. A. 1968. P. 1663.
[2] *McDowell R.S., Goldblatt M.* Inorg. Chem. 1971. V. 10. P. 625.
[3] *Huston J.L., Claassen H. H.* J. Chem. Phys. 1970. V. 52. P. 5646.
[4] *Weinstock N., Schulze H., Muller A.* J. Chem. Phys. 1973. V. 59. P. 5063.
[5] *Griffith W.P.* J. Chem. Soc., Sect. A. 1966. P. 1467.

Tetrahedral (T_d) oxy-anions of transition elements in various crystal matrices

Anion	Matrice	ν_1	ν_2	ν_3	ν_4	References
MnO_4^-	$K[MnO_4]$	845	353	906,914,919	395,400,403	[1]
TcO_4^-	$K[TcO_4]$	910	385	885,917	327	[2]
ReO_4^-	$K[ReO_4]$	969	339	898,926	352	[2]
CrO_4^{2-}	$Na_2[CrO_4]$	851	351	900,933	391	[3]
MoO_4^{2-}	$Th[MoO_4]_2$	955	467	783,795	340-355	[4]
WO_4^{2-}	$Th[WO_4]_2$	990	440	820,915	342,350	[4]
MnO_4^{2-}	$K_2[MnO_4]$	813	325	836,841	339	[5]
FeO_4^{2-}	$K_2[FeO_4]$	830	336	786,796	307,312,318	[5]
VO_4^{3-}	$Na_3[VO_4]$	741,771	333,346	835	333,346	[6]
CrO_4^{3-}	$Ba_2[CrO_4]_2$	828	276		319	[5]
MnO_4^{3-}	$K_3[MnO_4]$	810	324	839	349	[5]
ReO_4^{3-}	$Li_3[ReO_4]$	808	264	848,863	317,320,333	[5]
FeO_4^{3-}	$K_3[FeO_4]$	776	265	818	335,347	[5]
RuO_4^-	$K[RuO_4]$	830	339	840	312,317	[5]
TiO_4^{4-}	$Ba_2[TiO_4]$	761	306,315	775	765,770,780	[5]
ZrO_4^{4-}	$Li_4[ZrO_4]$	792	332,342	835,831	380,389	[5]
HfO_4^{4-}	$Li_4[HfO_4]$	796	325,332	-	366,384	[5]
VO_4^{4-}	$Ba_2[VO_4]$	818	319	762,776,788	361,368,379	[5]
CrO_4^{4-}	$Ba_2[CrO_4]$	806	353,361	825,855,873	390,416,419	[5]
MoO_4^{4-}	$Ba_2[MoO_4]$	792	328	-	352,398	[5]
WO_4^{4-}	$Ba_2[WO_4]$	821	323	-	367,398	[5]
FeO_4^{4-}	$Ba_2[FeO_4]$	762	257	846	320,324	[5]
CoO_4^{4-}	$Ba_2[CoO_4]$	790	296,303	830,850	340	[5]

[1] *Engert C. and Kiefer W.* J. Raman Spectrosc. 1991. V. 22. P. 715-719.
[2] *Gassman P.l., McCloy J.S., Soderquista C.Z., Schweiger M.J.* J. Raman Spectrosc. 2014, V. 45. P. 139–147.
[3] *Doyen L., Frech R.* J. Chem. Phys. 1996. V. 104. P. 7847-7853.
[4] *Augsburger M. S. Pedregosa J. C.* J. Phys. Chem. Sotids. 1995. V. 56. P. 1081-1084.
[5] *Gonzalez-Vilchez F., Griffith W.P.* J. Chem. Soc., Dalton Trans. 1972. P. 1416.
[6] *Kerp O., Möller A.* Z. Anorg. Allg. Chem. 2006. V. 632. P. 1187-1194.

Vibrations of tetrahedral (T_d) cations of halide *p*-elements in the structure of inorganic crystals

Cation	ν_1	ν_2	ν_3	ν_4	References
BF_4^-	774	355	1060	526,530	[1]
BCl_4^-	406	189,194	690,722	278	[2]
BBr_4^-	248	116	605,630,642	170	[2,3]
BI_4^-	169	83	515,543	117	[2]
AlF_4^-	622	210	760	322	[4]
$AlCl_4^-$	348	119	498	182	[5,6]
$AlBr_4^-$	212	98	394	114	[6,7]
AlI_4^-	143,149	51	321-336	82	[6,8]
$GaCl_4^-$	343	120	370	153	[9]
$GaBr_4^-$	207	74	263	105	[6]
GaI_4^-	147	52	211	73	[6,10]
$InCl_4^-$	320	89	335	112-115	[11]
$InBr_4^-$	198	55-64	229-239	79	[3,12]
InI_4^-	139	42	185	58	[10]
$TlCl_4^-$	303-312	60-90	281-297	78-90	[13]
$TlBr_4^-$	184	58	201	69	[14]
TlI_4^-	130	-	146	60	[15]
NF_4^+	846	445,448	1150,1180,1187	610,612	[1]
NCl_4^+	635	430	283	233	[16]
PF_4^+	906	275	1167	358	[17]
PCl_4^+	455-460	180-195	655,665	252	[18]
PBr_4^+	250-256	104	486-509	150	[3,6]
PI_4^+	151-165	71-77	380-400	90-98	[6]
AsF_4^+	745	213	829	272	[19]
$AsCl_4^+$	420	151	503	186	[20]
$AsBr_4^+$	247	85	353,356	116,120	[20]
AsI_4^+	183	72	319	87	[21]
$SbCl_4^+$	396	121	451	139	[22]
$SbBr_4^+$	234	76	305	92	[22]

[1] *Christe K.O., Lind M.D., Thorup N., Russell D.R., Fawcett J., Bau R.* Inorg. Chem. 1988. V. 27. P. 2450-2454.

[2] *Clark R.J.H., Joss S., Taylor M. J.* Spectrochim. Acta. 1986. V. 42A. P. 927-928.

[3] *Shamir J., Schneider S., van der Veken B.J.* J. Raman Spectroscopy. 1986. Vol. 17. P. 463-466.

[4] *Gilbert B., Mamantov G., Begun G.M.* Inorg. Nucl. Chem. Lett. 1974. V. 10. P. 1123.

[5] *Rytter E., Oye H.A.* J. Inorg. Nucl. Chem. 1973. V. 35. P. 4311.

[6] *Aubauer C., Kaupp M., Klapötke T.M., Nöth H., Piotrowski H., Schnick W., Senker J., Suter M.* J. Chem. Soc., Dalton Trans. 2001. P.1880.

[7] *Brown D.H., Stewart D.T.* Spectrochim. Acta. 1970. V. 26A. P. 1344.

[8] *Begun G.M., Boston C.R., Torsi G., Mamantov G.* Inorg. Chem. 1971. V. 10. P. 886.
[9] *Oye H.A., Bues W.* Inorg. Nucl. Chem. Lett. 1972. V. 8. P. 31.
[10] *Woodward L.A., Singer G.H.* J. Chem. Soc. 1958. P. 716.
[11] *Kloo L., Taylor M.J.* Spectrochimica Acta Part A. 2002. V. 58. P. 953-957.
[12] *Waterworth L., Worral I.J.* Inorg. Nucl. Chem. Lett. 1972. V. 8. P. 123.
[13] *Millikan M.B., James B.D.* Inorg. Chim. Acta. 1984. V. 81. P. 109-115.
[14] *Linden A., Petridis A., James B.D.* Helvetica Chimica Acta. 2003. V. 86. P. 711-725.
[15] *Adams D.M., Morris D.M.* J. Chem. Soc. A. 1968. P. 694.
[16] *Minkwitz R., Bernstein D., Sawodny W.* Angew. Chem. 1990. V. 102. P. 185-186.
[17] *Minkwitz R., Lennhoff D., Sawodny W., Härtner H.Z.* Naturforsch. 1992. V. B47, P. 1661.
[18] *Shamir J., Luski S., Bino A., Cohen Sh., Gibson D.* Inorg. Chim. Acta. 1985. V. 104. P. 91-97.
[19] *Schulz A., Klapötke T.M.* Spectrochim. Acta. 1995. V. 51A. P. 905-908.
[20] *Gerken M., Kolb P., Wegner A., Mercier H.P.A., Borrmann H., Dixon D.A., Schrobilgen G.J.* Inorg. Chem. 2000. V. 39. P. 2813-2824.
[21] *Tornieporth-Oetting I., Klapotke Th.* Angen Chcm. 101 (1989). 1742-1744.
[22] *Casteel W.J., KolbJ.P., LeBlond N., Mercier H.P.A., Schrobilgen G.J.* Inorg. Chem. 1996. V. 35. P. 929-942.

Tetrahedral (T_d) halide complexes of *s*- and *d*-elements

Anion	ν_1	ν_2	ν_3	ν_4	References
BeF_4^{2-}	547	255	800	385	[1]
$MgCl_4^{2-}$	252	100	330	142	[2]
$MgBr_4^{2-}$	150	60	290	90	[2]
MgI_4^{2-}	107	42	259	60	[2]
TiF_4 (газ)	712	185	772	209	[3]
$TiCl_4$ (газ)	389	114	498	136	[4]
$TiBr_4$ (газ)	231	68	393	88	[4]
TiI_4	162	51	324	67	[5]
ZrF_4 (4 K)	668	166	672	173	[6]
$ZrCl_4$ (газ)	377	98	418	113	[4]
$ZrBr_4$ (газ)	222	60	315	72	[4]
ZrI_4 (газ)	158	43	254	55	[4]
HfF_4 (4 K)	680	175	655	167	[6]
$HfCl_4$ (газ)	382	101	390	112	[4]
$HfBr_4$ (газ)	235	63	273	71	[4]
HfI_4 (газ)	158	55	224	63	[4]
VCl_4	383	128	475	150	[7]
CrF_4	717		790	201	[8]
$CrCl_4$	373	116	486	126	[9]
$CrBr_4$	224	60	368	71	[9]
$MnCl_4^{2-}$	256	-	278,301	120	[10,11]
$MnBr_4^{2-}$	195	65	209,221	89	[10,11]
MnI_4^{2-}	108	46	188,193	56	[10,11]
$FeCl_4^{-}$	330	106	385	133	[12]
$FeBr_4^{-}$	203	74	297	91	[13]
FeI_4^{-}	142	60	235,252	73	[14]
$FeCl_4^{2-}$	266	82	286	119	[10]
$FeBr_4^{2-}$	162	-	219	84	[10]
$CoCl_4^{2-}$	287	92	320	126,143	[15]
$CoBr_4^{2-}$	179	74	243,249	90,101	[15]
CoI_4^{2-}	118	-	194,202	56	[16]

$NiCl_4^{2-}$	264	-	280,294	119	[16]
$NiBr_4^{2-}$	-	-	228	81	[16]
NiI_4^{2-}	105	-	191	-	[16]
$ZnCl_4^{2-}$	276	80	277	126	[10]
$ZnBr_4^{2-}$	171	-	204	91	[10]
ZnI_4^{2-}	118	-	164	-	[10]

[1] *Quist A.S., Bates J.B., Boyd G.E.* J. Phys. Chem. 1972. V. 76. P. 78
[2] *Maroni V.A.* J. Chem. Phys. 1971. V. 55. P. 4789
[3] *DeVore T.C., Gallaher T.N.* J. Chem. Phys. 1985. V. 82. P. 2512-2514.
[4] *Clark R.J.H., Hunter B.K., Rippon D.M.* Inorg. Chem. 1972. V. 11. P. 56.
[5] *Clark R.J.H., Willis C.J.* J. Chem. Soc. A. 1971. P. 838.
[6] *Bukhmarina V.N., Dobychin S.L., Predtechinskii Yu.B., Shklyarik V.G.* Zhurnal Phyz. Chimii (Russian) 1986. V. 60. P. 1775-1777.
[7] *Dove M.F.A., Creighton J.A., Woodward L.A.* Spectrochim. Acta. 1962. V. 18. P. 267-270.
[8] *Jacobs J., Müller H. S. P., Willner H., Jacob E., Bürger H.* Inorg. Chem. 1992. V. 31. P. 5357-5363.
[9] *Cuoni B., Emmenegger F.P., Rohrbasser C., Schläpfer C.W., Studer P.* Spectrochim. Acta. V. 34A. P. 247-251.
[10] *Avery J.S., Burbridge C.D., Goodgame D.M.L.* Spectrochim. Acta. 1968. V. 24A. P. 1721.
[11] *Edwards H.J.M., Ware M.J., Woodward L.A.* Chem. Commun. 1968. P. 540.
[12] *Kloo L., Taylor M.J.* Spectrochimica Acta Part A. 2002. V. 58. P. 953
[13] *ClarkR.J.H., Dines T.J.* Chemical Physics. 1982. V. 70. P. 269-273.
[14] *Armbruster A., Rotter H.W., Thiele G.* Z.Anorg. Allg. 1996. V. 622. P. 795.
[15] *Schmidtke H.-H., Nover J.* Inog. Chim. Acta 1995. V. 240. P. 231.
[16] *Sabatini A., Sacconi L.* J. Am. Chem. Soc. 1964. V. 86. P. 17.

5. Octahedral ions

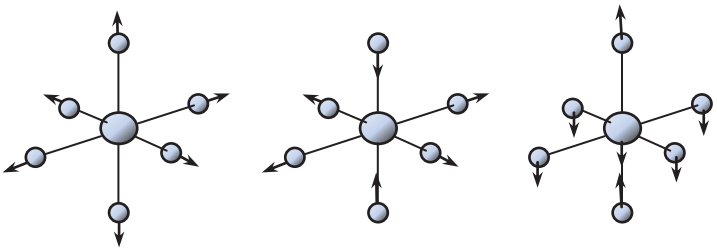

ν_1, A_{1g} ν_2, E_g ν_3, F_{1u}

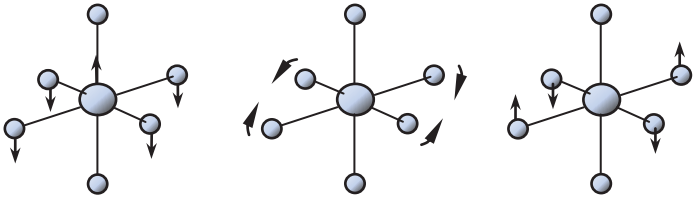

ν_4, F_{1u} ν_5, F_{2g} ν_6, F_{2u}

$$\Gamma = A_{1g}\,(\mathrm{RS}) + E_g\,(\mathrm{RS}) + F_{2g}\,(\mathrm{RS}) + 2F_{1u}\,(\mathrm{IR}) + F_{2u}$$

Vibrations of octahedral (O_h) halide anions *p*-elements in the crystal structure

Anion	ν_1 (A_{1g})	ν_2 (E_g)	ν_3 (F_{1u})	ν_4 (F_{1u})	ν_5 (F_{2g})	References
AlF_6^{3-}	541	400	568	387	322	[1,2]
GaF_6^{3-}	535	398	481	298	281	[2.3]
InF_6^{3-}	497	395	447	226	229	[1,2]
$InCl_6^{3-}$	277	193	250	157	(149)	[4]
TlF_6^{3-}	478	387	412	202	209	[1,2]
$TlCl_6^{3-}$	280	362	294	222,246	155	[5]
$TlBr_6^{3-}$	161	153	190,195	134,156	95	[5]
SiF_6^{2-}	663	477	741	483	408	[10]
GeF_6^{2-}	627	454	600	350	318	[6]
$GeCl_6^{2-}$	309	211	310	213	198	[11]
SnF_6^{2-}	573	460	555		249	[7]
$SnCl_6^{2-}$	323	244	315,341	166,189	171	[8,26,29]
$SnBr_6^{2-}$	182	135	203	111	101	[27,29]
$PbCl_6^{2-}$	285	215	-	-	137	[9]
PF_6^-	741	567	864	560	470	[12,28]
PCl_6^-	360	283	444	285	238	[11,13]
AsF_6^-	689	573	700	385	375	[10,14,28]
$AsCl_6^-$	337	289	333	220	202	[11]
SbF_6^-	668	558	669	350	294	[10,15,28]
$SbCl_6^-$	330	282	353	180	175	[16,21,26]
$SbCl_6^{3-}$	327	274	-	-	137	[17]
$SbBr_6^-$	192	169	224,239	119	78,103	[18]
$SbBr_6^{3-}$	180	153	180	107	73	[19,20]
SbI_6^-	107	96	108	82	54	[19,20]
BiF_6^-	590	547	585	-	231,247	[15,22,23,28]
$BiCl_6^{3-}$	259	215	172	130	115	[19,20]
$BiBr_6^{3-}$	156	130	128	75	62	[19,20]
BiI_6^{3-}	114	103	96	(59)	54	[19,20]
SF_6(Gas)	773.5	641.7	939	614	524	[24]
SeF_6	706.9	658.7	780	437	405	[24]
TeF_6(Gas)	697.1	670.3	752	325	314	[24]

$TeCl_6^{2-}$	287	247	230	158	131	[25]
$TeBr_6^{2-}$	170	148	180	-	96	[25]

[1] *Reisfeld M.J.* Spectrochim. Acta. 1973. V. 29A. P. 1923.
[2] *Baran E.J., Lavat A.E.* Z. Naturforsch. 1981. V. 36A. P. 677.
[3] *Milicev S., Rahten A., Borrmann H.* J. Raman Spectrosc. 1997. V. 28. P. 315.
[4] *Barrowcliffe T., Beattie I.R., Day P., Livingston K.* J. Chem. Soc. A, 1967. P. 1810.
[5] *Spiro T.G.* Inorg. Chem. 1967. V. 6. P. 569.
[6] *Griffiths J.E., Irish D.E.* Inorg. Chem. 1964. V. 3. P. 1134-1137.
[7] *Christe K.O., Schack C.J., Wilson R.D.* Inorg. Chem. 1977. V. 16. P. 849-854.
[8] *Morioka Y., Nakagawa I.* J. Raman Spectrosc. 1987. V. 18, P. 533-536.
[9] *Creighton J.A., Woodward L.A.* Trans. Faraday Soc. 1962. V. 58. P. 1077-1079.
[10] *Naulin C., Bougon R.* J. Chem. Phys. 1976. V. 64. P. 4155.
[11] *Beattie I.R., Gilson T., Livingston K., Fawcett V., Ozin G.A.* J. Chem. Soc. A. 1967. P. 712.
[12] *Grondin J., Lass`egues J-C., Cavagnat D., Buffeteau T., Johansson P., Holomb R.* J. Raman Spectrosc. 2011. V. 42. P. 733-743.
[13] *Muir A.S.* Poluhedron. 1991. V.10. P. 2217.
[14] *Smith G.L., Mercier H.P.A., Schrobilgen G.J.* Inorg. Chem. 2008. V. 47. P. 4173-4184.
[15] *Popov A.I., Shcharabarin A.V., Sukhoverkov V.F., Chumaevsky N.A.* Z. Anorg. Allg. Chem. 1989. V. 576. P. 242.
[16] *Burgard M., MacCordick J.* Inorg. Nucl. Chem. Lett. 1970, V. 6. P. 599.
[17] *Bosworth Y.M., Clark R.J.H.* J. Chem. Soc., Dalton Trans. // 1974. P. 1749.
[18] *Clark R.J.H., Duarte M.L.* J. Chem. Soc., Dalton Trans. // 1977. P. 790.
[19] *Hooper M.A., James D.W.* Aust. J. Chem. 1973. V. 26. P. 1401.
[20] *Hooper M.A., James D.W.* J. Inorg. Nucl. Chem. 1973. V. 35. P. 2335.
[21] *Christian B.H., Collins M.J., Gillespie R.J., Sawyer J.F.* Inorg. Chem. 1986.V. 25. P. 777-788.
[22] *Surles T., Quaterman L.A., Hyman H.H.* J. Inorg. Nucl. Chem. 1973. V. 35. P. 670.
[23] *Gillespie R.J., Martin D., Schrobilgen G.J.* J. Chem. Soc. Dalton Trans. 1980. P. 1898-1903.
[24] *Claassen H.H., Goodman G.L., Holloway J.H., Selig H.* J. Chem. Phys. 1970. V. 53. P. 341-348.
[25] *Baker L.-J., Rickard C.E.F., Taylor M.J.* Polyhedron. 1995. V. 14. P. 401-405.
[26] *Adams D.M., Appleby R.* J. Inorg. Nucl. Chem. 1976. V. 38. P. 1601-1603.
[27] *Clark R.J.H., Maresca L., Puddephatt R.J.* Inorg. Chem. 1968. V. 7. P. 1603-1606.
[28] *Bougon R., Buihuy T., Cadet A., Charpin P., Rousson R.* Inorg. Chem. 1974. V. 13. P. 690-695.
[29] *Woodward L.A., Creighton J.A.* Spectrochim. Acta. 1961. V. 17. P. 594-599.

Vibrations of octahedral (O_h) halide anions *s*- and *d*-elements in the structure of crystals

Anion	ν_1 (A_{1g})	ν_2 (E_g)	ν_3 (F_{1u})	ν_4 (F_{1u})	ν_5 (F_{2g})	References
ScF_6^{3-}	495	375	458	257	235	[1,2,3]
YF_6^{3-}	470	380	419	200	210	[4]
LaF_6^{3-}	443	334	362	130-170	171	[3]
TiF_6^{2-}	630	455	550	315	290,298	[5]
$TiCl_6^{2-}$	320	271	316	183	173	[6,7]
$TiBr_6^{2-}$	192	-	244	119	115	[6]
$GfCl_6^{2-}$	326	257	275	145	156	[8]
VF_6^{-}	663	520	690	304	314	[9]
VF_6^{3-}	504	652	361	335	292	[10]
NbF_6^{-}	704	540	610	244	271	[9]
$NbCl_6^{-}$	367-409	281-295	330-364	162-165	173-185	[11,12]
$NbBr_6^{-}$	219	179	239	112	109	[12]
TaF_6^{-}	707	540	610	244	271	[9]
$TaCl_6^{-}$	378-394	290-300	318-330	156-160	179-195	[11,12]
$TaBr_6^{-}$	230	179	213	106	114	[12]
$CrCl_6^{3-}$	308	255	325	194	182	[13]
MoF_6	741.5	651.6	741.1	264	318	[14]
$MoCl_6^{2-}$	329	-	308	168	154	[15]
$MoCl_6^{3-}$	305	-	302	167	150	[15]
WF_6	771.0	677.2	711	258	320	[14]
WCl_6	437	331	373	160	182	[8]
WCl_6^{-}	382	-	312	157	168	[15]
WCl_6^{2-}	341	-	293	150	-	[15]
TcF_6	712.9	(639)	748	265	(297)	[14]
ReF_6	753.7	(671)	715	257	(295)	[14]
$ReCl_6^{-}$	382	301	322,353	164	186	[16]
$ReCl_6^{2-}$	346	275	313	172	159	[8,17]
$ReBr_6^{2-}$	213	174	217	118	104	[17,18]
ReI_6^{2-}	147	118	164	-	-	[18]
FeF_6^{3-}	511	368	447	268	252	[1,2]
$FeCl_6^{3-}$	290	278	258	-	162	[19]
RuF_6	(675)	(624)	735	275	(283)	[14]
$RuCl_6^{2-}$	331	265	-	-	166	[19-21]
$RuBr_6^{2-}$	204	164	-	-	110	[19-21]
OsF_6	730.7	(668)	720	268	(276)	[14]
$OsCl_6^{2-}$	346	274	314	177	165	[8,17,21]
$OsCl_6^{3-}$	313	-	290,297	185	-	[21]
$OsBr_6^{2-}$	210	173	217	122	107	[21,22,23]
$OsBr_6^{3-}$	189	180	200	116	94	[21]
OsI_6^{2-}	152	121	170	91	80	[21]

OsI_6^{3-}	144	113	140	111	-	[21]
RhF_6	(634)	(595)	724	283	(269)	[14]
$RhCl_6^{2-}$	322	260	330	184	177	[21]
$RhCl_6^{3-}$	308	284	312	(159)	179	[24]
$RhBr_6^{3-}$	190	173	244	(102)	113	[24]
IrF_6	701.7	645	719	276	267	[14,25]
$IrCl_6^{2-}$	352	(225)	333	184	190	[8,23,26]
$IrBr_6^{2-}$	209.6	175.1	-	-	103.2	[23,26]
IrI_6^{3-}	149	133	175	87	88	[27]
PdF_6^{2-}	575	556	-	295	242	[28]
$PdCl_6^{2-}$	317	292	-	-	164	[29]
$PdBr_6^{2-}$	198	176	253	130	100	[30]
PtF_6	656.4	(601)	705	273	(242)	[14]
$PtCl_6^{2-}$	340	320	325	181	160	[8,29]
$PtBr_6^{2-}$	207	190	-	-	97	[29]
PtI_6^{2-}	149	132	181	-	115	[31]
AuF_6^{-}	602	577	653	-	223,242	[32,33]
GdF_6^{3-}	473	380	373	140-190	185	[3]
YbF_6^{3-}	491	(370)	406	191	196	[3]
UF_6	667.1	532.5	624	186.2	202	[14]
NpF_6	654	535	624	198.6	208	[14]
PuF_6	(628)	(523)	616	206.0	(211)	[14]

[1] *Wieghardt K., Siebert H.* J. Mol. Structure. 1971. V. 7 P. 305-313.
[2] *Turrell S., Hafsi S., Conflant P., Barbier P., Drache M., Champarnaud-Mesjard J.-C.* J. Mol. Structure. 1988. V. 174. P. 449-454.
[3] *Von Becker R., Lentz A., Sadowny W.* Z. Anorg. Allg. Chem. 1976. V. 420. P. 210-218.
[4] *Couzi M., Khaïroun S., Tressau A.* Phys. Stat. Sol. (a). 1986. V. 98, P. 423-434.
[5] *Milićev S., Maček J.* J. Chem. Soc. Dalton Trans. 1984. P. 297-299.
[6] *Clark R.J.H., Maresca L., Puddephatt R.J.* Inorg. Chem. 1968. V. 7. P. 1603-1606.
[7] *Adams D.M., Appleby R.* J. Inorg. Nucl. Chem. 1976. V. 38. P. 1601-1603.
[8] *Brown T.L., McDugle W.G., Jr., Kent L.G.* J ACS. 1970. V. 92. P. 3645-3653.
[9] *Bougon R., Buihuy T., Cadet A., Charpin P., Rousson R.* Inorg. Chem. 1974. V. 13. P. 690-695.
[10] *Nagarajan R., Tyagi N., Lofland S., Ramanujachary K.V.* Polyhedron. 2011. V. 30. P. 1425–1429.
[11] *Poulsen F.W., Berg R.W.* J. Inorg. Nucl. Chem. 1978. V. 40. P. 471-476.
[12] *So S.P., Chau F.T.* J. Mol. Structure. 1972. V. 12. P. 113-119
[13] *Von Eysel H.H.* Z. Anorg. Allg. Chem. 1972. V. 390. P. 210-216.
[14] *Claassen H.H., Goodman G.L., Holloway J.H., Selig H.* J. Chem. Phys. 1970. V. 53. P. 341-348.
[15] *Creighton J.A., Sinclair T.J.* Spectrochim. Acta. 1979. V. 35A. P. 507-508.

[16] *Arp O., Preetz W.* Z. Anorg. Allg. Chem. 1994. V. 620 P. 1391-1396.
[17] *Woodward L.A., Ware M.J.* Spectrochim. Acta. 1964. V. 20. P. 711-720.
[18] *Prillwitz P., Preetz, W.* Z. Naturf. B. Chem. Sciences. 1994. V. 49. P. 753-758.
[19] *Witke K., Schlrinitmz K.-D., Eist M., Hass D., Lorenz M.* Z. Anorg. Allg. Chem. 1987. V. 551. P. 215-222.
[19] *von Allwörden H.N., Preetz W.* Z. Naturforsch. 1987. V. 42 a, P. 597-602.
[20] *Clark R.J.H., Dines T.J.* Mol. Phys. 1984. V. 52. P. 859-970.
[21] *Campbell N.J., Davis V.A., Griffith W.P., Townend T.J.* J. Chem. Soc. Dalton Trans. 1985. P. 1673-1675.
[22] *von Homborg H.* Z. Anorg. Allg. Chem. 1980. V. 460. P. 27-36.
[23] *Clark R.J.H., Turtle P.C.* J. Chem. Soc. Faraday Trans. 2: Nucl. Chem. Phys. 1978. V. 74. P. 2063-2076.
[24] *Preetz W., Kuhr W.* Z . Naturforsch. 1989. V. 44b. P. 1221-1227.
[25] *Rotger M., Boudon V., Nguyen A.T. Avignant D.* J. Raman Spectroscopy. 1996. V. 27. P. 145-148.
[26] *von Homborg H.* Z. Anorg. Allg. Chem. 1982. V. 493, P. 104-120.
[27] *Preetz W., Steinebach H.-J.* Z. Naturforsch. 1986. V. 41b. P. 260-262.
[28] *Mazej Z., Lutar K.* J. Fluorine Chem. 2001. V. 107. P. 63-69.
[29] *Woodward L.A., Creighton J.A.* Spectrochim. Acta. 1961. V. 17. P. 594-599.
[30] *Clark R.J.H., Croud V.B., Dawes H.M., Hursthouse M.B.* Polyhedron. 1988.V. 7. P. 261 l-2614.
[31] *Baechle W., Rotter H.W., Thiele G., Clark R.H.J.* Inorg. Chim. Acta. 1992. V. 191. P. 121-129.
[32] *Mazej Z., Goreshnik E.* Solid State Sciences. 2006. V. 8. P. 671–677.
[33] *Griffiths J.E., Sunder W.A.* Spectrochim. Acta. 1979. V. 35A. P. 1329-1331.

Appendix J: Units of measurement and other reference data

Formally, the vibration frequency ν should be measured in Hertz, i.e. the number of oscillations for 1 second. However, the order of this value is $10^{12} – 10^{14}$, which is a certain inconvenience for continuous recording. In the literature, especially the theoretical one, instead of ν, they often use the angular frequency ω, measured in "rad/s". The two frequencies are related by a simple relationship $\omega = 2\pi\nu$, and the order of magnitude of ω is the same as ν. The appearance of the circular frequency ω is due to the fact that when solving the harmonic oscillator equation, it is convenient to use the expression $x(t) = A \cdot \cos(\omega t + \varphi)$ instead of $x(t) = A \cdot \cos(2\pi\nu t + \varphi)$.

In vibrational spectroscopy, information about the frequency of mechanical vibrations is extracted from the characteristics of electromagnetic radiation absorbed in IR spectra and scattered in Raman spectra. Since electromagnetic radiation is usually characterized by a wavelength λ, then it is convenient to somehow associate the frequency of oscillations with this quantity. Therefore, in practical spectroscopy, the so-called spectroscopic frequency was introduced, equal to the number of waves of electromagnetic radiation that fit in a 1 cm segment. This last quantity is called the "wave number" and is measured in inverse centimeters, cm^{-1}. The frequencies of all possible atomic and molecular vibrations, expressed in inverse centimeters, have a range of 10 - 4000 cm^{-1}, with a higher frequency corresponding to a larger value in inverse centimeters. The wave number does not have its own symbol and, therefore, the familiar symbol ω is most often used (incorrectly!). From the definition of the wave number it follows that the true vibration frequency (in Hertz) is related to the spectroscopic frequency ω by a simple relationship:

$$\nu\,(\text{Hz}) = c \cdot \omega(\text{cm}^{-1}) = 3 \cdot 10^{10} \cdot \omega\,(\text{cm}^{-1})$$

In Raman spectroscopy, the wavelength of scattered radiation is also measured, but the physically significant quantity is not the absolute wavelength, but the difference in wavelengths of the incident and scattered light. It turned out to be convenient in this case, too, to characterize the radiation wavelengths by the wavenumber, i.e. the number of wavelengths that fit in a 1 cm interval. In this case, the difference in the wavenumbers of the incident and scattered radiation is also expressed in inverse centimeters, and the obtained values for the position of the vibrational modes correspond to those measured in IR absorption.

The vibrational frequency in Raman spectra published in modern journal articles is commonly referred to as "frequency", "Raman shift" or "wavenumber". As you can see from the previous text, the latter designation is the most accurate. This is what is used in this book.

Formally, the wavenumber is not an energy unit. But due to the fact that the energy of the wave and its wavenumber are related by the proportionality coefficient *hc,* i.e. $E = h\nu = hc \cdot \omega(cm^{-1})$, then there is always a one-to-one correspondence between the wave number and the energy of vibrations. Below are the numerical correspondences between the wavenumber and various commonly used energy quantities.

1 meV $\rightarrow$ 8.06546 cm^{-1}
1 eV $\rightarrow$ 8065.46 cm^{-1}
1 kcal/mole $\rightarrow$ 350 cm^{-1}
1 J $\rightarrow$ $5.041 \cdot 10^{22}$ cm^{-1}
1 erg $\rightarrow$ $5.041 \cdot 10^{15}$ cm^{-1}
1 cm^{-1} $\rightarrow$ $1.9837 \cdot 10^{-16}$ erg
1 THz $\rightarrow$ 33 cm^{-1}
1 Hartree (the atomic unit of energy) $\rightarrow$ $2.19 \cdot 10^{5}$ cm^{-1}

The physical quantities most frequently used in vibrational spectroscopy are given below.

Table of physical quantities (CGS)

Speed of light	c	$2.997925 \cdot 10^{10}$ cm/s
Proton charge	e	$4.80325 \cdot 10^{-10}$ units CGS
Plank constant	h	$6.62620 \cdot 10^{-27}$ erg ·s
	$\hbar = h/2\pi$	$1.05459 \cdot 10^{-27}$ erg ·s
Avogadro constant	N	$6.02217 \cdot 10^{23}$ $mole^{-1}$
Atomic mass unit	amu	$1.66053 \cdot 10^{-24}$ g
Rest mass of electron	m	$9.10956 \cdot 10^{-28}$ g
Rest mass of proton	M_p	$1.67261 \cdot 10^{-24}$ g
M_p/m ratio	M_p/m	1836.11
Mass of hydrogen atom		1.6735×10^{-24} g
Mass of helium atom		6.6464×10^{-24} g
Classical electron radius	r_0	$2.81794 \cdot 10^{-13}$ cm
Bohr radius	a_H	$5.29177 \cdot 10^{-9}$ cm
Bohr magneton	μ_B	$9.27410 \cdot 10^{-21}$ erg/Gs
Boltzmann constant	k_B	$1.38062 \cdot 10^{-16}$ erg /K
Dielectric constant of vacuum	ε_0	1
Magnetic permeability of vacuum	μ_0	1
1 electron-volt	eV	$1.60219 \cdot 10^{-12}$ erg

REFERENCES

Chapter 1

1. Raman C.V., Krishnan K.S. A New Type of Secondary Radiation. *Nature*. 1928. V. 121. p. 501.
2. Landsberg G., Mandelstam L. *Naturwiss*. 1928. V. 16, p. 557, 772.
3. *Light Scattering in Solids II*. Ed. By M. Cardona and G. Guntherodt. Springer-Verlag, 1982.
4. Reissland J.A. *The Physics of Phonons*. Wiley, 1973.
5. Placzek G. *Rayleigh-Streuung und Raman-Effekt*, in Handbuch der Radiologie, E. Marx (ed.), V. 6, 205-374. Academische Verlag: Leipzig, 1934.

Chapter 2

1. Cohen-Tannoudji C., Diu B., Laloe F. *Quantum Mechanics*, Wiley, 2006**.**

Chapter 3

1. Kittel Ch. *Introduction to Solid State Physics*. Willey, 1978.
2. Landau L.D., Lifshitz E.M. *Quantum mechanics, vol 3: course of theoretical physics*, 3rd edn. Pergamon Press, Oxford, 1980

Chapter 5

1. Bhagavantam S., Venkatarayudo T. *Group theory and its application to physical problems.* Waltair: Andhra University. 2nd ed. 1951.
2. Halford R.S. Motions of Molecules in Condensed Systems: I. Selection Rules, Relative Intensities, and Orientation Effects for Raman and Infra-Red Spectra. *J. Chem. Phys*. 1946. V. 14. p. 8-15; Winston H., Halford R.S. Motions of Molecules in Condensed Systems: V. Classification of Motions and Selection Rules for Spectra According to Space Symmetry. *J. Chem. Phys*. 1949. V. 17. p. 607-616.

3. Poulet H., Mathieu J-P. *Spectres de Vibration et Symetrie des Cristaux*. Gordon and Dreach, 1970.

Chapter 6

1. Loudon R. The Raman effect in crystals. *Adv. Phys*. 1964. V. 13. p. 423-482.

Chapter 7

1. Rautian S.G. Real spectral apparatus. *Sov. Phys. Usp.* 1958. V. 1. p. 245–273.

Chapter 8

1. Kolesov B.A., Geiger C.A. A Raman spectroscopic study of Fe–Mg olivines. *Phys. Chem. Miner*. 2004. V. 31. p. 142-154.
2. Alonso M.I., Winer K. Raman spectra of c-Si1-xGex alloys. *Phys. Rev. B*. 1989. V. 39. p. 10056-10062.
3. Kolesov B.A., Geiger C.A., Armbruster T. The dynamical properties of zircon studied by single-crystal X-ray diffraction and Raman spectroscopy. *Eur. J. Mineral*. 2001. V. 13. p. 939-948.
4. Kolesov B. A., Geiger C. A. Raman spectra of silicate garnets. *Phys. Chem. Miner.* 1998. V. 25. p. 142-151.
5. Kolesov B.A., Boldyreva E.V. Difference in the Dynamic Properties of Chiral and Racemic Crystals of Serine Studied by Raman Spectroscopy at 3-295 K. J. Phys. Chem. B. 2007. V. 111. P. 14387—14397.
6. Kolesov B.A. Raman spectra of single H_2O molecules isolated in cavities of crystals. *Journal of Structural Chemistry*. 2006. Vol. 47. No. 1. p. 21-34.
7. Basova T.V., Kolesov B.A. Raman polarization studies of orientation of molecular thin films. *Thin Solid Films*, 1998. V. 325. No 1-2. p. 140-144.

Chapter 9

1. Kolesov B.A. How the vibrational frequency varies with temperature. *J. Raman Spectrosc.*, 2017. V. 48. P. 323–326.
2. Kittel Ch. *Introduction to Solid State Physics*. Willey, 1978.

3. Balkanski M., Wallis R.F., Haro E. Anharmonic effects in light scattering due to optical phonons in silicon. *Phys. Rev B*. 1983. V. 28. p. 1928-1934.
4. Klemens P.G., Anharmonic Decay of Optical Phonons. *Phys. Rev*. 1966. V. 148. p. 845-848.
5. Karpov S.V., *Physics of phonons.* Saint Petersburg State University, Physical department, Saint Petersburg, 2006.
6. Surovtsev N.V. and Kupriyanov I.N., Temperature dependence of the Raman line width in diamond: Revisited. *J. Raman Spectrosc, Supplement*. 2015. V. 46. p. 171–176.
7. Herchen H., Cappelli M.A., Landstrass M.I., Plano M.A., Moyer M.D. First-order Raman scattering in homoepitaxial chemical vapor deposited diamond at elevated temperatures. *Thin Solid Films*. 1992. V. 212. p. 206.
8. Kolesov B.A., Geiger C.A. Low-temperature single-crystal Raman spectrum of pyrope. *Phys. Chem. Minerals*. 2000. V. 27. p. 645-649.

Chapter 10

1. Bloembergen N., The Stimulated Raman Effect, *Amer. J. Phys.* 1967. 35 (11), p. 989.
2. Akhmanov S.A., Kovoteev N.I., *Methods of Nonlinear Optics In Light Scattering Spectroscopy,* Moscow, 1981

Chapter 11

1. Hadzi D, (ed.). *The Hydrogen Bond*. New York and London: Pergamon Press (1957).
2. Pimentel G.C. and McClellan A.L. *The Hydrogen Bond*. San Francisco: Freeman (1960).
3. Hamilton W.C. and Ibers J.A. *Hydrogen Bonding in Solids*. New York: Benjann (1968).
4. Vinogradov S.N. and Linnell R.H. *Hydrogen Bonding*. New York: Van Nostrand Reinhold (1971).
5. Joesten M.D. and Schaad L.J. *Hydrogen Bonding*. New York: Dekker (1974).
6. Kollman P.A. and Allen L.C. The theory of the hydrogen bond. *Chem. Rev*., 1972. **72**, 283-303.
7. Kollman P.A., A general analysis of noncovalent intermolecular interaction. *J. Am. Chem. Soc*., 1977. **99**, 4875-4893.

8. Morokuma K., Why do molecules interact? The origin of electron donor acceptor complexes, hydrogen bonding and proton affinity. *Accts Chem. Res*., 1977. **10**, 294-300.
9. Schuster P., Zundel G. and Sandorfy C. *The Hydrogen Bond. Recent Developments in Theory and Experiment*. Vols. I-III, Amsterdam: North Holland (1976).
10. Jeffrey G.A., *An Introduction to Hydrogen Bonding*. New York and Oxford: Oxford University Press (1997).
11. Arunan E., Desiraju G.R., Klein R.A., Sadlej J., Scheiner S., Alkorta I., Clary D.C., Crabtree R.H., Dannenberg J.J., Hobza P., Kjaergaard H.G., Legon A.C., Mennucci B., Nesbitt D.J. Defining the hydrogen bond: An account (IUPAC Technical Report). *Pure Appl. Chem*., 2011. **83**, 1619–1636.
12. Huggins M.L. *Thesis*, Univ. of California (1919).
13. Latimer W.M., Rodebush W.H. Polarity and ionization from the standpoint of the Lewis theory of valence. *J. Am. Chem. Soc*. 1920. **42**, 1419.
14. Pauling L. The nature of the chemical bond. Application of results obtained from the quantum mechanics and from a theory of paramagnetic susceptibility to the structure of molecules. *J. Am. Chem. Soc*., 1931. **53**, 1367-1400.
15. Bernal J.D., Fowler R.H. Theory of water and ionic solution with particular reference to hydrogen and hydroxyl ions. *J. Chem. Phys*., 1933. **1**. 515.
16. Morokuma K. Molecular orbital studies of hydrogen bonds. *J. Chem. Phys*., 1971. **55**, 1236-1244.
17. Benoit M., Marx D., The Shapes of Protons in Hydrogen Bonds Depend on the Bond Length. *ChemPhysChem*., 2005. **6**, 1738 –1741.
18. Wang L., Fried S.D., Boxer S.G., and Markland T.E., Quantum delocalization of protons in the hydrogen-bond network of an enzyme active site. *PNAS*, 2014. **111**, 18454.
19. Goncharov A.F., Struzhkin V.V., Somayazulu M.S., Hemley R.J., Mao H.K., Compression of Ice to 210 Gigapascals: Infrared Evidence for a Symmetric Hydrogen-Bonded Phase. *Science*, 1996. **273,** 218-220.
20. Aoki K., Yamawaki H., Sakashita M., and Fujihisa H., Infrared absorption study of the hydrogen-bond symmetrization in ice to 110 GPa. *Phys. Rev. B*, 1996. **54**, 15673-15677.
21. Novak A. Hydrogen bonding in solids. Correlation of spectroscopic and crystallographic data. In: *Structure and bonding*. 1974. **18**. 177-216.

22. Kolesov B.A., Raman investigation of H_2O molecule and hydroxyl groups in the channels of hemimorphite. *American Mineralogist*, 2006, **91**, 1355-1362.
23. Galkina Yu.A., Kryuchkova N.A., Vershinin M.A., and Kolesov B.A. Features of strong O–H···O and N–H···O hydrogen bond manifestation in vibrational spectra. *Journal of Structural Chemistry*. 2017, **58**, 911-918.
24. Kolesov B.A., Unusual behavior of benzoic acid at low temperature: Ramanspectroscopic study. *Spectrochimica Acta Part A*, 2015. **142**, 320–323.
25. Averbuch-Pouchot M-T., Structures of Glycinium Phosphite and Glycylglycinium Phosphite. *Acta Cryst*. 1993. **C49**, 815-818.
26. Shikanai F., Komukae M., Czapla Z. and Osaka T., Crystal Structure of $NH_3CH_2COOHH_2PO_3$ in the Ferroelectric Phase. *J. Phys. Soc. of Japan*, 2002. **71**, 498–503.
27. Shikanai F., Yamasaki M., Komukae M. and Osaka T., Structural Study of Partially Deuterated Glycinium Phosphite in the Paraelectric Phase. *J. Phys. Soc. of Japan*, 2003. **72**, 325–329.
28. Machida M., Uchida H., Ishibashi T., Taniguch H., Komukae M., Osaka T. and Koyano N., Neutron Diffraction Study of Crystal Structures of Deuterated Glycinium Phosphite in Paraelectric and Ferroelectric Phases. *J. Phys. Soc. of Japan*, 2004. **73**, 107–115.
29. Perumal R., Senthil Kumar K., Moorthy Babu S., Bhagavannarayana G. Optical characterization of ferroelectric glycinium phosphite single crystals. *Journal of Alloys and Compounds,* 2010. **490**, 342–349.
30. Kolesov B.A., Chupina A.V., Berezin A.S., Kompankov N.B., Abramov P.A., Sokolov M.N., Proton motion inside $[(DMF)_2H]_2[W_6Cl_{14}]$: structural, Raman and luminescence studies. *Phys.Chem.Chem.Phys*., 2020. **22**, 25344-25352.
31. Foces-Foces, C.; Echevarría, A.; Jagerovic, N.; Alkorta, I.; Elguero, J.; Langer, U.; Klein, O.; Minguet-Bonveh M. and Limbach, H-H. A Solid-State NMR, X-ray Diffraction, and ab Initio Computational Study of Hydrogen-Bond Structure and Dynamics of Pyrazole-4-Carboxylic Acid Chains. *J. Am. Chem. Soc*., 2001. **123**, 7898-7906.
32. Nagaoka, S.; Terao, T.; Imashiro, F.; Saika, A.; Hirota, N.; Hayashi, S. A study on the proton transfer in the benzoic acid dimer by ^{13}C high-resolution solid-state NMR and proton T_1 measurements. *Chem. Phys. Letters*, 1981. **80**, 580-584.

33. Meier, B.H.; Graf, F. and Ernst, R.R. Structure and dynamics of intramolecular hydrogen bonds in carboxylic acid dimers: A solid state NMR study, *J. Chem. Phys*., 1982, **76**, 767-774.
34. Meier, B.H.; Meyer, R.; Ernst, R.R.; Zolliker, P.; Furrer A. and W. Hälg, Furrer and W. Hälg, Neutron scattering study of dynamically disordered hydrogen bonds: terephthalic acid. *Chem. Phys. Lett*, 1983. **103**, 169-174.
35. Nagaoka, S., Terao, T., Imashiro, F., Saika, A., Hirota, N., Hayashi, S. An NMR relaxation study on the proton transfer in the hydrogen bonded carboxylic acid dimers. *J. Chem. Phys.*, 1983. **79**, 4694-4703.
36. Skinner J.L. and Trommsdorff H.P. Proton transfer in benzoic acid crystals: A chemical spin–boson problem. Theoretical analysis of nuclear magnetic resonance, neutron scattering, and optical experiments. *J. Chem. Phys*., 1988. **89**, 897-907.
37. Horsewill A.J. and Aibout A. The dynamics of hydrogen atoms in the hydrogen bonds of carboxylic acid dimers. *J. Phys.: Condens. Matter*, 1989. **1**, 9609-9622.
38. Horsewill, A.J.; Ikram A. and Tomsah, I.B.I. Hydrogen bond dynamics in tetrafluoroterephthalic acid studied by NMR and INS. *Mol. Phys*., 1995. **84**, 1257-1272.
39. Brougham, D.F.; Horsewill, A.J.; Ikram, A.; Ibberson, R. M.; McDonald P.J. and Pinter-Krainer M. The correlation between hydrogen bond tunneling dynamics and the structure of benzoic acid dimers. *J. Chem. Phys*., 1996. **105**, 979-982.
40. Brougham, D.F.; Horsewill, A.J. and Jenkinson, R.I. Proton transfer dynamics in the hydrogen bond: a direct measurement of the incoherent tunnelling rate by NMR and the quantum-to-classical transition. *Chem. Phys. Letters*, 1997. **272**, 69-74.
41. Neumann, M.; Brougham, F.; McGloin, C.J.; Johnson, M.R.; Horsewill A.J. and Trommsdorff, H.P. Proton tunneling in benzoic acid crystals at intermediate temperatures: Nuclear magnetic resonance and neutron scattering studies. *J. Chem. Phys*. 1998. **109**, 7300-7311.
42. Horsewill, A.J.; McGloin, C.J.; Trommsdorff, H.P. and Johnson, M.R. Proton tunnelling in the hydrogen bonds of halogen-substituted derivatives of benzoic acid studied by NMR relaxometry: the case of large energy asymmetry. *Chem. Phys*., 2003. **291**, 41-52.
43. Demkin, A.G. and Kolesov, B.A. Tautomeric hydrogen bond in ibuprofen crystals. *Phys. Chem. A*, 2019. **123**, 5537-5541.

44. Pritchina, E.A. and Kolesov, B.A. Raman spectra of terephthalic acid crystals in the temperature range 5 K–300 K. *Spectrochim. Acta Part A: Molecular and Biomolecular Spectroscopy*, 2018, **202**, 319-323.
45. Fischer, P.; Zolliker, P.; Meier, B. H.; Ernst, R. R.; Hewat, A.W.; Jorgensen, J. D. and Rotella, F. J. Structure and Dynamics of Terephthalic Acid from 2 to 300 K. *J. Solid State Chem*., 1986. **61**, 109-125.
46. Wilson, C.C.; Shankland, N. and Florence, A.J. Direct determination of the temperature dependence of proton transfer in the benzoic acid dimer by single crystal neutron diffraction. *Chem. Phys. Lett*. 1996. **253**, 103-107.
47. Ostrowska, K.; Kropidłowska, M. and Katrusiak, A. High-Pressure Crystallization and Structural Transformations in Compressed R,S-Ibuprofen. *Cryst. Growth Des*., 2015. **15**, 1512-1517.
48. Kolesov, B.A., How the vibrational frequency varies with temperature. *J. Raman Spectrosc*., 2017. **48**, 323-326.
49. Kolesov, B.A. Proton Delocalization and Tunneling in Terephthalic Acid: Raman Spectroscopic Study. *J. Phys. Chem. Solids*, 2020. **138**, 1092888.
50. Nakamoto K., Margoshes M., Rundle R. E., Stretching Frequencies as a Function of Distances in Hydrogen Bonds *J. Am. Chem. Soc*., 1955. **77**, 6480-6486.
51. Gilli P., Bertolasi V., Ferretti V., Gilli G., Evidence for Intramolecular N-H···O Resonance-Assisted Hydrogen Bonding in β-Enaminones and Related Heterodienes. A Combined Crystal-Structural, IR and NMR Spectroscopic, and Quantum-Mechanical Investigation. *J. Am. Chem. Soc.*, 2000. **122**, 10405-10417.
52. Alabugin I.V., Manoharan M., Peabody S. and Weinhold F., Electronic Basis of Improper Hydrogen Bonding: A Subtle Balance of Hyperconjugation and Rehybridization. *J. Am. Chem. Soc*., 2003. **125**, 5973-5987.
53. Bent H.A. An Appraisal of Valence-bond Structures and Hybridization in Compounds of the First-row elements. *Chem. Rev*., 1961. **61**, 275-311.

Chapter 12

1. Landau L.D., Lifshitz E.M. Quantum mechanics, vol 3: course of theoretical *physics, 3rd edn.* Pergamon Press, Oxford, 1980
2. Cohen-Tannoudji C., Diu B., Laloe F. *Quantum Mechanics*, Wiley, 2006**.**

3. Veber S.L., Bagryanskaya E.G., and Chapovsky P.L. On the Possibility of Enrichment of H_2O Nuclear Spin Isomers by Adsorption. *JETP*, 2006. **102**, No 1, p. 76.
4. Kolesov, B.A. and Geiger, C.A. Behavior of H2O molecules in the channels of natrolite and scolecite: A Raman and IR spectroscopic investigation of hydrous microporous silicates. *American Mineralogist,* 2006, 91(7), 1039-1048.
5. Kolesov B., Lager G., Schultz A. Behaviour of H_2O and OH in lawsonite: a single-crystal neutron diffraction and Raman spectroscopic investigation. *European J. Mineralogy*. 2008, 20, 63-72.

Chapter 13

1. Kolesov B.A., Boldyreva E.V. An Interpretation of the "Anomalous" Changes in the Low-Wavenumber Range of the Raman Spectra of L-Alanine Crystals. *Chem. Phys. Chem*. 2013. v. 14. 2525–2528.
2. Migliori A., Maxton P.M., Clogston A.M., Zirngiebl E., Lowe M. Anomalous temperature dependence in the Raman spectra of l-alanine: Evidence for dynamic localization. *Phys. Rev. B*. 1988. V. 38. P. 13464.
3. A.S. Davydov, N.I. Kislukha Solitons in one-dimensional molecular chains. *JETP,* 1976. Vol. 44, No. 3, p. 571.
4. Careri G., Buontempo U., Carta F., Gratton E., Scott A.C. *Phys. Rev. Lett*. 1983. V. 51. P. 304.
5. Careri G., Buontempo U., Galluzzi F., Scott A.C., Gratton E., Shyamsunder E. *Phys. Rev. B*. 1984. V. 30. P. 4689.

Chapter 14

1. Rani C., Tanwar M., Kandpal S.,; Ghosh T., Pathak DK., Chaudhary A., Kumar R., Predicting Raman line shapes from amorphous silicon clusters for estimating short-range order. *J. Raman Spectrosc*., DOI: 10.1002/jrs.6117
2. Campbell L.H., Fauchet P.M. The effects of microcrystal size and shape on the one phonon Raman spectra of crystalline semiconductors. *Solid State Commun*. 1986. V. 58. p. 739-741.
3. Kamei T., Stradins P., Matsuda A. Effects of embedded crystallites in amorphous silicon on light-induced defect creation. *Appl. Phys. Lett*. 1999. V. 74. p. 1707-1709.

4. Gaisler S. V., Semenova O. I., Sharafutdinov R.G., and Kolesov B.A. Analysis of Raman Spectra of Amorphous–Nanocrystalline Silicon Films. *Physics of the Solid State*, 2004. Vol. 46, No. 8, p. 1528–1532.
5. Golubev V.G., Davydov V.Yu.,Medvedev A.V., Pevtsov A.B., Feoktistov N.A., *Physics of the Solid State*. 1997. V. 39. p. 1348-1353.
6. Ledoux G., Gong J., Huisken F., Guillois O., Reynaud C. Photoluminescence of size-separated silicon nanocrystals: Confirmation of quantum confinement. *Appl. Phys. Lett*. 2002. V. 80. P. 4834-4836.

Chapter 15

1. Ferrari A.C., Robertson J. Interpretation of Raman spectra of disordered and amorphous carbon. *Phys. Rev. B*. 2000. V. 61. p. 14095-14107; Resonant Raman spectroscopy of disordered, amorphous, and diamondlike carbon. *Phys. Rev. B*. 2001. V. 64. p. 075414-1-13; Raman spectroscopy of amorphous, nanostructured, diamond-like carbon, and nanodiamond**,** *Phil. Trans. R. Soc. Lond. A*. 2004. V. 362. p. 2477–2512.
2. Maultzsch J., Reich S., Thomsen C., Requardt H., Ordejon P. Phonon dispersion in graphite. *Phys. Rev. Letters*. 2004. V. 92. P. 075501.
3. Heller E.J., Yang Y., Kocia L., Chen W., Fang Sh., Borunda M., Kaxiras E. Theory of Graphene Raman Scattering. *ACS Nano*. 2016. V. 10. p. 2803−2818.
4. Jorio A, Pimental M.A., Souza Filho A.G., Saito R., Dresselhaus G., Dresselhaus M.S. Characterizing carbon nanotube samples with resonance Raman scattering. *New Journal of Physics*. 2003. V. 5. p. 139.1–139.17.
5. Hodkiewicz J., *Thermo Fisher Scientific*, Madison, WI USA

Chapter 16

1. Kittel Ch. *Introduction to Solid State Physics.* Willey, 1978.
2. Morosin B., Exchange Striction Effects in MnO and MnS. *Phys. Rev. B*. 1970, V. 1. p. 236-243.
3. Goodenough J., *Magnetism and the Chemical Bond*. Interscience Publishers. New York, London 1963.
4. Chou H-h., Fan H.Y., Light scattering by magnons in CoO, MnO, and α-MnS. *Phys. Rev. B*., 1976, v. 13, p. 3924-3938.

5. Milutinović A., Tomić N., Dević S., Milutinović P., Popović Z.V., Raman scattering by spin excitations in α-MnSe. *Phys. Rev. B*, 2002, v. 66, p. 012302.